METABOLIC REGULATION BY p107 (Rbl1) INFLUENCES MUSCLE STEM CELL FATE DECISIONS

DEBASMITA BHATTACHARYA

A DISSERTATION SUBMITTED TO THE FACULTY OF GRADUATE STUDIES
IN PARTIAL FULFILLMENT OF THE REQUIREMENTS FOR THE DEGREE OF
DOCTOR OF PHILOSOPHY

GRADUATE PROGRAM IN
KINESIOLOGY AND HEALTH SCIENCE

YORK UNIVERSITY
TORONTO, ONTARIO
JANUARY, 2021

Abstract

Skeletal muscle has a remarkable property of effective muscle fiber regeneration that maintain their normal physiology due to the presence of the adult muscle stem cells known as the satellite cells (SCs). The role of SCs is crucial, as myofiber turnover is an ongoing process during the lifetime of an individual to maintain proper muscle tissue viability. However, muscle wasting found in diseases such as muscular dystrophy and disorders that occur during the ageing process are associated with impaired SC function. Indeed, these complications are linked to compromised SC fate decisions for activation, self-renewal and commitment to muscle progenitor cells (MPs), which are characterized by diminished numbers. Thus, understanding the control pathways that impact SC fates is essential to improve their integrity for health and to benefit muscle diseases and disorders. Central to sustaining different SC fates is the regulation of energy generation between glycolysis in the cytoplasm and oxidative phosphorylation (Oxphos) in the mitochondria. However, the mechanisms that connect these energy provisioning centers to control cell behaviour remain obscure. Herein, our results reveal a mechanism by which mitochondrial-localized transcriptional co-repressor p107 governs MP proliferative rate, under the control of NAD^+/NADH ratio. We found p107 directly interacts at the mitochondrial DNA promoter repressing mitochondrial-encoded genes. This reduces the mitochondrial ATP generation capacity, by limiting the electron transport chain complex formation. Importantly, the amount of ATP generated by the mitochondrial function of p107 is directly associated to the cell cycle rate in vivo and in vitro. This is exemplified by absence of p107 that drastically increased cell cycle progression and MP proliferation capacity through enhancement of ATP generation. Oppositely, forced expression of p107 in the mitochondria blocked cell cycle progression in vitro as a consequence of dampened ATP generation. Notably, Sirt1, whose activity is dependent on the

cytoplasmic by-product of glycolysis, NAD^+, directly interacts with p107 impeding its mitochondrial localization and function. Deletion of Sirt1 increased p107 mitochondrial localization, decreased MP mitochondrial Oxphos generation concomitant with attenuated cell cycle progression. Increasing the activity of Sirt1 had the converse effect on p107 function. In addition, we also showed that p107 genetically deleted skeletal muscle contained significantly more quiescent SCs, indicative of a better self-renewal ability. As a first step to test the physiological role of p107 on SCs and MPs, we assessed exercise in humans. We found p107 protein levels were inversely correlated with enhanced mitochondrial Oxphos following endurance exercise in skeletal muscle that might also occur in SCs. These novel results establish a new paradigm to manipulate muscle stem cell fate decisions that are impaired in many diseases and disorders.

Acknowledgements

I would first like to thank my supervisor, **Dr. Anthony Scimè**, for believing in a fresher 7 years ago, who emigrated from India with lots of hope but no direction. If you would not have given me a chance at that time, this would have never been possible. I cannot thank you enough for your immense help, constant motivation and advice through all these years. I sincerely extend my gratitude and appreciation for molding an inexperienced student to a confident researcher. How can I forget the countless number of hours you have put to revise my papers and teach me different techniques? Indeed, I have been extremely lucky to have a supervisor who cared so much about my work and provided me with patient guidance. Thank you for giving me the opportunity to attend conferences, extend my knowledge and making me prepared to face the professional world.

I would like to express my gratitude to **Dr. David Hood** and **Dr. Christopher Perry** for being in my supervisory Committee. Thank you for your mentorship and showing interest in my research work and always providing me with your valuable suggestions, motivation and ideas. I am immensely thankful to **Dr. John C. McDermott**, **Dr. Tara Haas** and **Dr. Mireille Khacho** for providing me with valuable insights and suggestions for improvement in all aspects. I am grateful to Dr. Haas for going over my manuscript and providing insights for improving it. I am really grateful to have such advisors and mentors.

I would also take this opportunity to express my gratitude to **Dr. David Hood** and **Dr. Ali Abdul-Sater**, for allowing me to use Seahorse and Flow cytometer machines. I am obliged to **Dr. Emanuel Rosonina** for letting me use his sonicator. Last but not the least I am indebted to **Dr. Magdalena Jaklewicz**, who was always there to teach and troubleshoot any problems related to confocal microscopy.

I would also like to thank my past and present lab members **Deanna**, **Maryam**, **Nareh**, **Nina**, **Joy**, **Vicky, Kyra** and all the undergrads and volunteers with whom I had the pleasure to work with. Here I would like to extend my special thanks to Joy, who has thoroughly helped me in last two years with experiments, checking on cells and most importantly replenishing the lab stocks and reagents, to ensure smooth running of the lab. I would like to thank each and every one for your invaluable help and support and rendering a fun and learning environment in the lab. I cannot forget the limitless times I have asked **Emmanuel** for help and reagents. He was always there to help and motivate me. I am also beyond thankful to **Geetika** for teaching me how to use the Seahorse machine and the software, and **Jyoti** for helping me in all possible ways. My list is endless. I am forever grateful to each and every one who helped me sail in this journey.

I am indebted to my loving daughter, **Purbita** and husband, **Rick** who have sacrificed immensely throughout these years to make my dreams come true. The journey was equally hard for all three of us, but we made it. It is a huge source of comfort to know how much I am genuinely supported and loved by my family. I am extremely grateful to God for making me a part of such a wonderful family.

Finally, I would like to thank my **parents**, **brother** and **extended family (grandma, uncles, aunts and cousins)** back home in India who have always encouraged me and taught me to fight even in stressful situations. I thank my parents for inculcating in me the mindset of hard work, discipline, perseverance and living on to achieving dream.

Table of Contents

List of Tables

List of Figures

Chapter 1:

Literature Review:

Chapter 4:

p107 regulates mitochondrial ATP generation via mitochondrial gene expression

Chapter 5:

Sirt1 governs p107 mitochondrial function

Chapter 6:

p107 regulates myogenic progenitor proliferation through management of Oxphos

Chapter 7:

Decreased transcriptional co-repressor p107 is associated with exercise-induced mitochondrial biogenesis in human skeletal muscle

Chapter 8:

Discussion

List of Publications:

1. **Bhattacharya, D**., Oresajo, O., Scimè, A. (2020). p107 mediated mitochondrial function controls muscle stem cell proliferative fates. (In revision *Nature Communications*).

2. **Bhattacharya, D**., Scimè, A. (2020). Mitochondrial Function in Muscle Stem Cell Fates. *Frontiers in Cell and Developmental Biology*, *2020*(8), 480.

3. **Bhattacharya, D**., Scimè, A. (2019). Metabolic Regulation of Epithelial to Mesenchymal Transition: Implications for Endocrine Cancer. *Frontiers in endocrinology*, 10, 773.

4. **Bhattacharya, D**., Ydfors, M., Hughes, M.C., Norrbom, J., Perry, C.G., and Scime, A. (2017). Decreased transcriptional corepressor p107 is associated with exercise-induced mitochondrial biogenesis in human skeletal muscle. *Physiol Rep*, 5(5), e13155.

5. Porras, D.P., Abbaszadeh, M., **Bhattacharya, D**., D'Souza, N.C., Edjiu, N.R., Perry, C.G.R., and Scime, A. (2017). p107 Determines a Metabolic Checkpoint Required for Adipocyte Lineage Fates. Stem Cells. *Stem Cells*, *35*(5), 1378-1391.

List of Abbreviations

Acetyl CoA	Acetyl Coenzyme A
ADP	Adenosine di-phosphate
AICAR	5-aminoimidazole-4-carboxamide-1-β-D-ribofuranoside
AMP	Adenosine mono-phosphate
AMPK	AMP-activated protein kinase
ant/rot	Antimycin/Rotenone
ATP	Adenosine tri-phosphate
ATP5A	ATP synthase F1 subunit alpha
Atp6	Mitochondrially encoded ATP synthase membrane subunit 6
Atp8	Mitochondrially encoded ATP synthase membrane subunit 8
ATTC	American Tissue Type Culture
BAX	BCL2 associated X, apoptosis regulator
bFGF	Basic fibroblast growth factor
BJ-HTERT	Immortalized foreskin fibroblast cell line
BMyb	Myb-related protein B
Brdu	Bromodeoxyuridine / 5-bromo-2'-deoxyuridine
BSA	Bovine serum albumin
C	Cytoplasmic fraction
C33A	Cervical carcinoma cell line
$CaCl_2$	Calcium chloride
Cas9	CRISPR associated protein 9
Cdk	Cyclin dependent kinase
Cdk1	Cyclin dependent kinase 1
Cdk2	Cyclin dependent kinase 2
Cdk4	Cyclin dependent kinase 4
Cdk6	Cyclin dependent kinase 6
CH310T1/2	Murine embryo fibroblast cell line
Cip/Kip	Cdk-interacting protein/kinase inhibitory proteins
c-Myc	Myc proto-oncogene protein
CO_2	Carbon dioxide
CoxI	Mitochondrially encoded cytochrome c oxidase I
CoxII	Mitochondrially encoded cytochrome c oxidase II
CoxIII	Mitochondrially encoded cytochrome c oxidase III
Crispr	Clustered regularly interspaced short palindromic repeats
Ct	Threshold cycle
Ctl	Control
Ctx	Cardiotoxin
CytB	Mitochondrially encoded cytochrome B
Dapi	4′,6-diamidino-2-phenylindole
DCA	Dichloroacetic acid
DHAP	Dihydroxyacetone phosphate
DHR123	Dihydrorhodamine 123
DMEM	Dulbecco’s Modified Eagle Medium
DNA	Deoxyribonucleic acid
DREAM	Dimerization partner, RB-like, E2F and multi vulval class B complex

Drp1	Dynamin related protein 1
DTT	Dithiothreitol
DYRK1A	Dual-specificity tyrosine phosphorylation-regulated protein kinase 1A
E2f1	E2f transcription factor 1
E2f2	E2f transcription factor 2
E2f4	E2f transcription factor 4
E2f5	E2f transcription factor 5
ECM	Extracellular matrix
EDL	Extensor digitorum longus
EDTA	Ethylenediaminetetraacetic acid
EGTA	Ethylene glycol tetraacetic acid
EMMA	European Mutant Mouse Archive
ERK1/2	Extracellular signal-regulated kinase 1⁄2
ERRγ	Estrogen-related receptor gamma
ETC	Electron transport chain
$FADH_2$	Reduced flavin adenine dinucleotide
FBS	Fetal bovine serum
FGF	Fibroblast growth factor
FGF2	Fibroblast growth factor 2
FoxM1	Forkhead box protein M1
FoxO1	Forkhead box protein O1
FoxO3	Forkhead Box O3
Fsn1	Fission protein 1
Fzd7	Frizzled 7
g	Relative centrifugal force (RCF)
G0	Quiescent/resting phase
G1	Gap 1 phase,
G2	Gap 2 phase
G6P	Glucose 6-phosphate
gal	Galactose
GCN5	General control non-derepressible 5
GFP	Green fluorescent protein
GPx	Glutathione peroxidases
H19	H19 imprinted maternally expressed transcript
HDAC1	Histone deacetylase 1
HEBS	HEPES-buffered saline
HEK293	Embryonic human kidney cell line
HeLa	Cervical cancer cell line
HEPES	4-(2-hydroxyethyl)-1-piperazineethanesulfonic acid
HGF	Hepatocyte growth factor
Hif1α	Hypoxia inducible factor 1α
HiGlu	High glucose
HIIT	High-intensity interval training
Hsp70	Heat shock protein 70
Hsp90	Heat shock protein 90
HSP1	Heavy strand promoter 1

HSP2	Heavy strand promoter 2
IGF1	Insulin growth factor 1
IgG	Immunoglobulin G
IM	Mitochondrial inner membrane
IP	Immunoprecipitation
Ink	Inhibitor of Cdk4
JNK	c-Jun N-terminal kinase
KCl	Potassium chloride
$KHCO_3$	Potassium bi-carbonate
Ldha	Lactate dehydrogenase a
LHON	Leber hereditary optic neuropathy
LiCl	Lithium chloride
LoGlu	Low glucose
LSP	Light strand promoter
M phase	Mitotic phase
M	Mitochondrial matrix
MAPK	Mitogen activated protein kinase
MCF7	Breast carcinoma cell line
MfnI	Mitofusin I
MfnII	Mitofusin II
MG63	Human osteosarcoma cell line
$MgCl_2$	Magnesium chloride
MIQE	Minimum Information for Publication of Quantitative Real-Time PCR Experiments
MN	Myonuclei
MPs	Myogenic progenitor cells
mRNA	Messenger RNA
Mt-Co1	Mitochondrially encoded cytochrome c oxidase I
mtDNA	Mitochondrial DNA
MTERF1	Transcription termination factor 1, mitochondrial
MTERF3	Transcription termination factor 3, mitochondrial
mTORC1	Mammalian target of rapamycin 1
MuvB	Multi vulval class B complex
Myf5	Myogenic factor 5
MyHC	Myosin heavy chain
MyoD	Myogenic determining factor 1
N	Nuclear fraction
N.D	Not determined
Na_2HPO4	Dibasic sodium phosphate
Na_3VO4	Sodium orthovanadate
NaCl	Sodium chloride
NAD	Nicotinamide adenine dinucleotide
NADH	Reduced nicotinamide adenine dinucleotide
NADPH	Reduced nicotinamide adenine dinucleotide phosphate
NaF	Sodium flouride
$NaHCO_3$	Sodium bi-carbonate

Nam	Nicotinamide
Nd1	Mitochondrially encoded NADH: ubiquinone oxidoreductase core subunit 1/ NADH dehydrogenase 1
Nd2	Mitochondrially encoded NADH: ubiquinone oxidoreductase core subunit 2/ NADH dehydrogenase 2
Nd3	Mitochondrially encoded NADH: ubiquinone oxidoreductase core subunit 3/ NADH dehydrogenase 3
Nd4/Nd4L	Mitochondrially encoded NADH: ubiquinone oxidoreductase core subunit 4/4L/ NADH dehydrogenase 4/4L
Nd5	Mitochondrially encoded NADH: ubiquinone oxidoreductase core subunit 5/ NADH dehydrogenase 5
Nd6	Mitochondrially encoded NADH: ubiquinone oxidoreductase core subunit 6/ NADH dehydrogenase 6
nDNA	Nuclear DNA
NDUFB8	NADH:ubiquinone oxidoreductase subunit B8
NF-κB	Nuclear factor kappa beta
NO•	Nitric oxide radical
NP-40	Nonidet P-40
Nrf1	Nuclear respiratory factor 1
Nrf2	Nuclear factor erythroid 2-related factor 2
OAA	Oxaloacetate
OCR	Oxygen consumption rate
OD	Optical density
olig	Oligomycin
OM	Mitochondrial outer membrane
OpaI	Optic Atrophy 1
Ox	Oxamate
Oxphos	Oxidative phosphorylation
p38α/β MAPK	p38 mitogen-activated protein kinases
p107fl	p107 full length
p107HA	Hemagglutinin tagged p107
p107KD	p107 knocked down
p107mls	p107 with a mitochondrial localization sequence
p15	Cyclin-dependent kinase 4 inhibitor B
p16	Cyclin-dependent kinase inhibitor 2A
p21	Cyclin-dependent kinase inhibitor 1A
p27	Cyclin-dependent kinase inhibitor 1B
p53	Tumour suppressor protein
p57	Cyclin-dependent kinase inhibitor 1C
PAIL	Prediction of Acetylation on Internal Lysines
Pax7- DTA	Paired homeobox transcription factor 7-diphtheria toxin fragment A
Pax7	Paired homeobox transcription factor 7
PBS	Phosphate-buffered saline
PBST	PBS with Tween 20
Pdh	Pyruvate dehydrogenase
Pdk	Pyruvate dehydrogenase kinase

PFA	Paraformaldehyde
PFKFB3	6 phosphofructo-2-kinase/fructose 2,6-biphosphatase 3
Pgc1α	Peroxisome proliferator activated receptor gamma co-activator 1 alpha
Ant1	Adenine nucleotide translocase type 1
Pgc1β	Peroxisome proliferator-activated receptor gamma coactivator 1-beta
PI	Propidium iodide
PK	Pyruvate kinase
PKM	Pyruvate kinase isoenzyme
PKM2	Pyruvate kinase isoenzyme 2
Pmp22	Peripheral myelin protein 22
POLRMT	DNA directed RNA polymerase, mitochondrial
PPP	Pentose phosphate pathway
prMPs	Primary myogenic progenitor cells
PVDF	Polyvinylidene difluoride
qChIP	Quantitative chromatin immunoprecipitation assay
qPCR	Quantitative polymerase chain reaction
R123	Rhodamine 123
Rb	Retinoblastoma associated protein 1
Rbl1	Retinoblastoma like protein 1 (p107)
Rbl2	Retinoblastoma like protein 2 (p130)
RelB	Proto-Oncogene, NF-KB Subunit
Res	Resveratrol
RET	Reverse electron transfer
RGB	Red green blue signal
Rgs2	Regulator of G-protein signaling 2
Rgs5	Regulator of G-protein signaling 5
RIP140	Receptor interacting protein 140
RNA	Ribonucleic acid
RNS	Reactive nitrogen species
ROS	Reactive oxygen species
Rpm	Revolutions per minute
rRNA	Ribosomal RNA
S	Serine
S phase	Synthetic phase
SaOS-2	Osteosarcoma cell line
SC	Satellite cells
SD	Standard deviation
SDHB	Succinate dehydrogenase complex iron sulfur subunit B
SDS	Sodium dodecyl sulfate
SEM	Standard error of the mean
sgRNA	Single guide RNA
Sirt1	Sirtuin 1
Sirt1dn	Sirtuin 1 dominant negative
Sirt1fl	Sirtuin 1 full length
Sirt1KO	Sirtuin 1 knockout
Skp2	S-phase kinase associated protein 2

SOD	Superoxide dismutase
SP	Saponin in PBS
Spry1	Sprouty 1
SUV39H1	Histone-lysine N-methyltransferase
T	Threonine
T98G	Glioblastoma cell line
TA muscle	Tibialis anterior muscle
TBS	Tris-buffered saline
TBST	Tris-buffered saline with Tween-20
TCA	Tri-carboxylic acid cycle
TE	Tris-EDTA
TEFM	Transcription elongation factor, mitochondrial
TFAM	Transcription factor A, mitochondrial
TFB2M	Transcription factor B2, mitochondrial
TGFß	Transforming growth factor beta
Tim	Translocase of the inner membrane
TNF-α	Tumour necrosis factor α
Tom	Translocase of the outer membrane
Tris HCl	Tris-hydrochloride
tRNA	Transfer RNA
U2-OS	Human osteosarcoma cell line
Unt	Untreated
UQ	Ubiquinone
UQCRC2	Ubiquinol-cytochrome C reductase core protein 2
W	Whole cell fraction
Wnt7A	Wingless-type MMTV integration site 7A
Wt	Wild type
YY1	Yin Yang 1

CHAPTER 1
LITERATURE REVIEW

1.1 Introduction

Skeletal muscle constitutes a significant percentage of total body mass and is indispensable to physical movements, maintaining postures and in vital actions (Díaz-Vegas et al., 2019; Hood et al., 2019). It is also a primary peripheral tissue important for utilizing glucose and fatty acid for energy generation essential for the prevention of obesity and type 2 diabetes (Dumont et al., 2015a; Nguyen et al., 2019). Skeletal muscle shows remarkable plasticity as it has an inherent ability to adapt to external stimuli including contractile activity, substrate availability and environmental conditions (Gundersen, 2011; Hood et al., 2006; Zierath & Hawley, 2004). Contraction of skeletal muscle is made possible due to the presence of thousands of long and cylindrical multinucleated muscle fibers. Each of the fibers are surrounded by layers of complex extracellular matrix (ECM) consisting of outermost endomysium and the basement membrane that is in close proximity to the plasmalemma of the myofiber known as sarcolemma (Csapo et al., 2020). The fibers are categorized into myosin heavy chain (MyHC) isoforms with respect to their mitochondrial content, contractile properties and fatigue resistance (Hood et al., 2019; Schiaffino & Reggiani, 2011). They consist of slow contracting oxidative type I, fast contracting oxidative type IIa and glycolytic type IIx fibers (as well as type IIb in rodents) (Pette & Staron, 2001; Schiaffino & Reggiani, 2011).

Besides plasticity, skeletal muscle has a remarkable property of effective muscle fiber regeneration to maintain their normal physiology. Myofiber turnover is an ongoing process during the lifetime of an individual to maintain proper muscle tissue viability (Dumont et al., 2015a; Yin et al., 2013). This is especially important during ageing, diseases such as Duchenne muscular dystrophy and disuse where skeletal muscle fibers are frequently damaged (Dumont et al., 2015a; Yin et al., 2013). Successful regeneration of skeletal muscle is made possible by the adult

myogenic stem cell population known as satellite cells (SCs) that constitute 2% to 10% of total myonuclei (Yin et al., 2013). These are located between the basal lamina and muscle fiber sarcolemma, where they are well positioned to receive signals from the surrounding environment (Dumont et al., 2015a). Inefficient muscle regeneration replaces muscle with fibrotic tissues that cause poor contraction and lead to progressive loss of muscle strength (Mann et al., 2011). Thus, an understanding of the control mechanisms that dictate SC fate decisions is crucial to improve skeletal muscle regeneration potential.

Recently, there has been an increasing realization regarding the importance of cellular metabolism in the regulation of SC functional outcomes to remain quiescent, become activated as myogenic progenitor cells (MPs), self-renew or differentiate (Bhattacharya & Scimè, 2020). Key to understanding how metabolism affects these fate decisions in SCs and MPs is the mitochondria. However, unlike for terminally differentiated myofibers (Díaz-Vegas et al., 2019; Hood et al., 2019), there is a paucity of data for how the mitochondria influences SCs and MPs. Now this thesis reveals how a transcriptional co-repressor and a member of retinoblastoma family of proteins, p107, governs SC and MP behaviour through a newly discovered mitochondrial mechanism.

1.2 Satellite cell fates

Over half a century has passed since a population of mononucleated cells was discovered between the basal lamina and plasma membrane of skeletal muscle fibers (Atz & Katz, 1961; Mauro, 1961) representing 2-10% of the total myonuclei (White et al., 2010). Due to their peripheral localization they were termed satellite cells. At that time their close proximity to the myofiber raised the hypothesis that they might be involved in regeneration and growth. A

possibility proved correct with advances over many years that showed SCs as the primary myogenic stem cells necessary for the regeneration and maintenance of skeletal muscle fibers.

As with other stem cells, SCs have the ability to self-renew and give rise to functional progeny. Usually, SCs are quiescent within their niche and enter the cell cycle when activated by external cues such as injury or trauma. Their ideal positioning enable them to receive local signals from muscle fibers, fibroblasts, endothelial cells and systemic factors from blood vessels with which they co-localize (Yin et al., 2013). After activation some SCs become committed to enter the myogenic lineage as MPs, whereas others self-renew to replenish their pool. In turn the MPs either proliferate and exit the cell cycle to differentiate into myocytes or they become quiescent SCs, repopulating the stem cell pool **(Figure 1.1)** (Dumont et al., 2015a; Yin et al., 2013; Zammit et al., 2006).

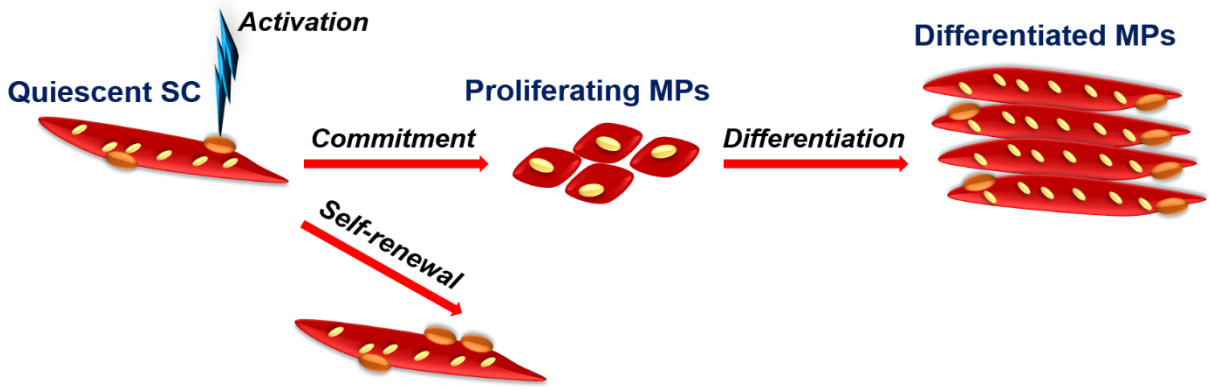

Figure 1.1: Schematic of satellite cell fates: Satellite cells (SCs) remain quiescence in their niche. After activation some SCs become committed to enter the myogenic lineage as myogenic progenitors (MPs), whereas others self-renew to replenish their pool. In turn the MPs either proliferate and exit the cell cycle to differentiate into myocytes or they become quiescent SCs, repopulating the stem cell pool.

Quiescent SCs are characterized by the expression of paired homeobox transcription factor 7 (Pax7). Stimuli from damaged, diseased or developing muscle induce the quiescent SCs to activate, expand and give rise to new muscle fibers. Following activation, all SCs express the myogenic determining factor 1 (MyoD) protein (Zammit et al., 2006) and also might express myogenic factor 5 (Myf5) (Kuang et al., 2007; McKinnell et al., 2008). These are required for MPs to proliferate and instigate proper differentiation (Kuang et al., 2007). The MyoD gene expression is rapidly induced both in vivo and in vitro and is detectable before any sign of cellular division (Grounds et al., 1992; Yablonka-Reuveni, 2011; Yablonka-Reuveni & Rivera, 1994; Zammit et al., 2004). Most proliferating $Pax7^{+}MyoD^{+}$ MPs, downregulate Pax7, sustain MyoD expression and differentiate. This coincides with upregulated expression of another muscle specific transcription factor, myogenin. which marks the entry of MPs into the differentiation phase accompanied by cessation of proliferation (Olguin et al., 2007; Yin et al., 2013; Zammit et al., 2006) **(Figure 1.2)**. The differentiating MPs initiate expression of various muscle specific genes encoding structural proteins resulting in their fusion (Przewoźniak et al., 2013). A few $Pax7^{+}MyoD^{+}$ MPs lose MyoD protein expression, but continue to maintain Pax7 expression, and eventually withdraw from cell cycle re-expressing markers that characterize SC quiescence (Zammit et al., 2004, 2006) **(Figure 1.2)**. Thus, MyoD is initially expressed in all activated SCs, before it is lost from some cells when the decision is made to self–renew (Zammit et al., 2004, 2006). Thus, orchestrated regulation of SC activation, self-renewal, proliferation and differentiation are necessary for skeletal muscle regeneration, repair and maintenance.

Quiescent SCs constitute a heterogeneous population, with most representing a committed population that had expressed Myf5 (during their development or after their activation and returned to quiescence), ($Pax7^{pos}Myf5^{pos}$), and a small uncommitted number (10%) that had never expressed

Myf5, ($Pax7^{pos}Myf5^{neg}$) (Kuang et al., 2007). The later population can undergo asymmetric or apical basal division producing $Pax7^{pos}Myf5^{neg}$ and $Pax7^{pos}Myf5^{pos}$ cells. Apart from asymmetric divisions, both SC populations also maintain and expand their population by symmetric division (Dumont et al, 2015a; Kuang et al., 2007; Yin et al., 2013). The equilibrium between symmetric and asymmetric division to maintain the homeostatic population of SCs is preserved by Wingless-type MMTV integration site 7A (Wnt7A) signaling with its receptor Frizzled 7 (Fzd7) (Le Grand et al., 2009). Their signaling pathway dictates the polarity, parallel or perpendicular, of mitotic division with respect to the basal lamina. Wnt7A by binding Fzd7 induces symmetric division by causing the SC to divide in a parallel orientation producing two identical daughter cells. On the other hand, the absence of Wnt7A favours cellular division perpendicular to the basal lamina resulting in asymmetric division. This produces one daughter cell retaining SC characteristics and another daughter cell that is committed to myogenic program (Le Grand et al., 2009).

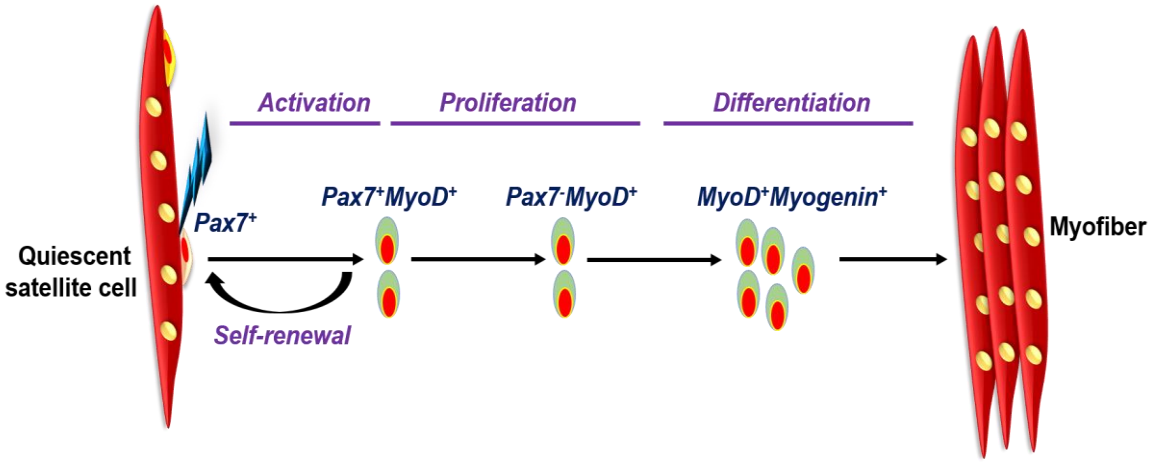

Figure 1.2: Role of Pax7 and MyoD in satellite cell fate decisions: All satellite cells upregulate MyoD protein when activated. Some $Pax7^{+}MyoD^{+}$ satellite cells (SCs) downregulate Pax7, maintain MyoD expression and differentiate to form myofibers by upregulating myogenin. For self-renewal, some activated SCs downregulate MyoD and return to quiescence.

1.3 Cell cycle regulation of satellite cells and myogenic progenitors

The cell cycle is the sequential order of events resulting in cell growth and division giving rise to two daughter cells (Bertoli et al., 2013). It is a tightly regulated process which can be divided into various phases. Sequentially, it consists of a G1 (gap 1) phase, S (synthetic) phase, G2 (gap 2) phase and M (mitotic) phase. During G1, the cells are metabolically active and prepare for synthesizing DNA that leads into S phase when DNA is replicated. The completion of DNA synthesis is followed by the G2 phase, during which cell growth continues and proteins are synthesized in preparation for M phase. At M phase, the nucleus divides (karyokinesis) and cytoplasmic division (cytokinesis) occurs to produce two daughter cells.

Apart from these cell cycle stages, there is a G0 or quiescent phase when the cells leave the cell cycle in response to environmental changes such as depletion of nutrients or growth factors, changes in cell adhesion and increased cell density during early G1 phase (Legesse-Miller et al., 2012; Lemons et al., 2010). The cells in G0 maintain their quiescent state, by reducing nucleotide synthesis and oxidative damage to prevent entrance back into the cell cycle (Legesse-Miller et al., 2012; Lemons et al., 2010). However, on receiving a stimulus, the cells exit from G0 and return to G1 to resume their growth and division.

Crucial to cell cycle progression are the cyclin dependent kinases (Cdks) which are serine/threonine protein kinases, and their regulatory subunits cyclins that modify various cell cycle regulators (Lim & Kaldis, 2013). Cyclin/Cdk complexes are activated during specific periods of the cell cycle facilitating the progression of cell division. Of most importance are the cyclin D family of proteins that pair with Cdk4 and Cdk6 in G1, cyclins A and E coupled with Cdk2 during the G1/S transition and cyclin B1 together with Cdk1 that operates at the G2/M transition (Lim & Kaldis, 2013). Cell cycle progression can be interrupted when Cdks are inactivated by Cdk

inhibitors (Bertoli et al., 2013; Lubischer, 2007). These are represented by two distinct families; the inhibitor of Cdk4 (Ink) protein family and Cdk-interacting protein/kinase inhibitory proteins (Cip/Kip) family (Lim & Kaldis, 2013). The Ink family which includes p15, p16, p18 and p19 can bind specifically to Cdk4 and Cdk6 and inhibit their kinase activity by interfering their interaction with cyclin D family (Sherr & Roberts, 1999). In contrast, the Cip/Kip family, which includes p21, p27 and p57, can bind to both Cdks and cyclin subunits and thus modulate the activities of cyclins D, E, A and B-Cdk complexes (Polyak et al., 1994; Sherr & Roberts, 1999; Wade Harper et al., 1993).

During cell cycle progression, cell cycle checkpoints are important to ensure proper division, determining whether a cell would proceed to the next phase of the cell cycle (Bertoli et al., 2013). If the DNA damage is too critical to repair, the cells activate apoptotic signaling cascades to prevent transmission of damaged DNA to the daughter cells (De Zio et al., 2013). The checkpoints also ensure that the cells have accumulated enough growth factors before transitioning to the next phase (Barnum & O'Connell, 2014). There are four well-known known checkpoints that regulate cell cycle progression. The G0 restriction point, G1 checkpoint, G2 checkpoint and the metaphase checkpoint, also known as the spindle checkpoint (Barnum & O'Connell, 2014). During G0 restriction point, the cells in G1 decide whether to enter a reversible quiescent state if there is not enough growth factors, or to proceed into the S phase of the cell cycle by up-regulating cyclin D/Cdk4/6 followed by cyclin E/Cdk2 (Bertoli et al., 2013; Foster et al., 2010). This restriction point is largely controlled by the retinoblastoma susceptibility protein (Rb) and transcription factor E2f signaling pathway. Release of E2f due to Rb phosphorylation by cyclin D/Cdk4/6 and cyclin E/Cdk2 (Lundberg & Weinberg, 1998), allows transcription of genes that promotes the initiation of DNA replication and S phase entry (Barnum & O'Connell, 2014). The

G1 DNA damage checkpoint, hinders the initiation of DNA replication in the presence of DNA damage and is largely controlled by the tumour suppressor protein p53 and Cdk inhibitor, p21 (Barnum & O'Connell, 2014). The G2 restriction point ensures proper cellular growth and synthesis of necessary proteins for division that are made during the S and G2 phases (Barnum & O'Connell, 2014). This restriction point also prevents cells from undergoing mitosis if they encountered any DNA damage during G2, sequestering inactive cyclin B/Cdk1. Finally, the spindle checkpoint is crucial to chromosome segregation during mitosis and meiosis (Barnum & O'Connell, 2014). Its function is to ensure that the chromosomes have aligned at the mitotic plate during metaphase and prevent premature anaphase onset (Gorbsky, 2015).

The ability of cells to enter the cell cycle also critically depends on the availability of metabolites (Foster et al., 2010). Regulation of cell proliferation by metabolism evolved in part from cellular ability to cope with nutritional deprivation by reducing growth and cell cycle progression (Kalucka et al., 2015). During mid to late G1, a nutrient-sensitive cell growth checkpoint enables cell to progress to S phase and complete cell division, only in presence of adequate nutrients (Foster et al., 2010). Importantly, cells primed for mitotic division upregulate glycolytic activator, 6 phosphofructo-2-kinase/fructose 2,6-biphosphatase 3 (PFKFB3), at the nutrient sensitive checkpoint, and blocking glycolysis or reducing glucose availability impairs cells' ability to pass through this metabolic checkpoint (Almeida et al., 2010; Tudzarova et al., 2011). Moreover, overexpression of PFKFB3, stimulates cell proliferation by upregulating cyclin D3/Cdk1 and inhibiting p27 (Yalcin et al., 2009). Another glycolytic enzyme, glyceraldehyde 3-phosphate dehydrogenase that converts glyceraldehyde 3-phosphate to 1,3-bisphosphoglycerate also promotes G2/M progression by upregulating cyclin B/Cdk1 activity (Carujo et al., 2006). Muscle specific pyruvate kinase isoenzyme (PKM) is a rate limiting enzyme of glycolysis that aids

in transfer of a phosphate group from phosphoenolpyruvate to ADP to produce pyruvate and ATP. Its alternative splice form, PKM2, depending on its activity, decides whether glucose should be converted to lactate or shuttle to PPP to produce building blocks for cell division (Mazurek, 2011). Furthermore, in response to mitogenic stimuli, it acts as a transcriptional activator and kinase phosphorylating and eventually acetylating histones triggering G1/S transition and cell proliferation (Yang et al., 2012). Similar to glycolysis, glutaminolysis also favours G1/S phase and in addition promotes S to G2/M progression (Colombo et al., 2011).

Apart from the metabolic intermediates, cellular energy and redox status are also determining factors for cell cycle progression (Kaplon et al., 2015). In this regard, a crucial factor that regulates cell proliferation by sensing cellular energy status is AMP-activated protein kinase (AMPK). During cellular energy stress such as glucose deprivation that reduces ATP levels, AMPK becomes activated to cause cell cycle arrest (Kaplon et al., 2015). AMPK mediates cell cycle arrest at G1 by phosphorylating p53 and upregulating p21 (Imamura et al., 2001; Jones et al., 2005a). Furthermore, AMPK can inhibit mammalian target of rapamycin 1 (mTORC1), an important cell growth checkpoint factor (Foster et al., 2010; Gwinn et al., 2008). In presence of sufficient nutrients, mTORC1 blocks p27 and promotes stabilization of the cyclin D/Cdk4/6 and cyclin E/Cdk2 complexes promoting G1/S transition (Romero-Pozuelo et al., 2020). mTORC1 is shown to be important for mitotic entry after DNA damage checkpoint (Hsieh et al., 2018). Another pivotal cell cycle metabolic checkpoint factor is NAD^+ dependent deacetylase Sirtuin 1 (Sirt1), which is activated when cellular NAD^+/ NADH ratio is high (Boutant & Cantó, 2014). Under genotoxis stress, Sirt1 prevents p53 mediated trancriptional activation of p21, thereby hindering cell cycle arrest (Vaziri et al., 2001). Therefore, the cell cycle machinary is profoundly

influenced by changes in cellular metabolism. Yet the molecular basis that connects nutrient availability, energy status to the core cell cycle machinary is not well understood.

Similar to other stem and progenitor cell types, proper regulation of cell cycle is important for SC and MP fate decisions **(Figure 1.3)** (Almeida et al., 2016; Cliff & Dalton, 2017; Soufi & Dalton, 2016). Microarray analysis revealed that there are 500 genes that are upregulated in quiescent SCs, but not in cycling MPs (Fukada et al., 2007; Liu et al., 2013). Some of the important quiescence markers are the negative regulators of cell cycle including Cdk inhibitors, p27 and p57, Rb, regulator of G-protein signaling 2 and 5 (Rgs2, Rgs5), peripheral myelin protein 22 (Pmp22) and the negative regulator of fibroblast growth factor (FGF) signaling sprouty 1 (Spry1). All these quiescent genes have a role in maintaining SC quiescence and prevent activation. For example, when activated SCs return to quiescence, they express Spry1, that promotes cell cycle exit by inhibiting the extracellular signal-regulated kinase (ERK) pathway (Shea et al., 2010). SCs from Spry1 null mouse showed impaired SC self-renewal after muscle injury (Shea et al., 2010). Moreover, conditional genetic deletion of p27 or Rb results in aberrant SC activation and proliferation (Chakkalakal et al., 2014; Hosoyama et al., 2011; Huh et al., 2004). Importantly, SC quiescence is also maintained by Notch signaling pathway (Bjornson et al., 2012; Buas & Kadesch, 2010; Conboy & Rando, 2002; Philippos et al., 2012). Notch activity is highest in quiescence and progressively decreases during activation and differentiation (Bröhl et al., 2012; Wen et al., 2012). Indeed, an interruption in Notch activity leads to SC precocious differentiation bypassing S phase (Philippos et al., 2012). Another transcriptional factor which is important for maintenance of quiescence is Forkhead Box O3 (FoxO3). FoxO3 mRNA and protein levels are higher in quiescent compared to activated SCs. FoxO3 genetically deleted SCs proliferate and differentiate faster, where as its overexpression inhibits cell cycle entry into S phase and terminal differentiation

(Gopinath et al., 2014). In addition, FoxO3 also promotes expression of Notch receptors that maintains quiescence (Gopinath et al., 2014).

On receiving mitogenic signals upon muscle injury, SCs exit the quiescent stage to enter the cell cycle in G1 as proliferating MPs (Almeida et al., 2016). However, recent evidence suggests that there is an intermediary stage between SC quiescence and activation, called the "G Alert" stage that primes the SCs to become activated. Rodgers et al showed that following muscle injury, quiescent SCs from an uninjured distant site exhibited a different cell cycle gene expression profile from those of mice that had never been injured. They expressed many cell cycle genes found in activated SCs, despite not entering the cell cycle (Rodgers et al., 2014), which is indicative of an intermediate stage between quiescence and activation.

Following injury induced activation, a vast majority of SCs and MPs proliferate in a concerted manner. A peak in MP proliferation is evident between second and fifth day after injury (Murphy et al., 2014; Rodgers et al., 2014). Damaged fibers release various cytokines and growth factors such as tumour necrosis factor α (TNF-α), hepatocyte growth factor (HGF), insulin growth factor 1 (IGF1) and fibroblast growth factor (FGF) which are important for activation of signaling pathways related to SC cell cycle entry (Almeida et al., 2016). IGF1 inactivate the transcription factor FoxO1, leading to downregulation of p27 thereby promoting cell cycle entry (Dumont et al., 2015). Furthermore, FGF2 is expressed in regenerating muscle and activates several mitogen activated protein kinase (MAPK) pathways such as p38α/β and extracellular signal-regulated kinase ½ (ERK1/2) pathway, which are crucial for G1/S phase transition (Jones et al., 2005b; Kondoh et al., 2007). Importantly, p38α/β MAPK activates *MyoD* gene expression that is thought to promote cell cycle entry (Jones et al., 2005b). Conversely, its expression is suppressed by Notch during quiescence to prevent premature SC activation (Jones et al., 2005a; Kondoh et al., 2007).

Another MAPK, c-Jun N-terminal kinase (JNK) triggers the expression of cyclin D1, promoting SC cell cycle progression (Perdiguero et al., 2007). Proliferating MPs express activated Cdk4 that inactivate Rb by phosphorylation, thus ensuring cell division. Furthermore, global gene expression analysis has shown that a number of cell cycle regulators such as cyclin A, B, D and E are enriched in cultured MPs to potentiate cell proliferation (Fukada et al., 2007). In contrast to proliferating MPs, differentiating myotubes contain high levels of Cdk inhibitor p21 and hypophosphorylated Rb (active repressor form) (Chakkalakal et al., 2014). Importantly, differentiation requires concerted up-regulation of p21, p19 and p57 (Cao et al., 2003; Chakkalakal et al., 2014; Pajcini et al., 2010).

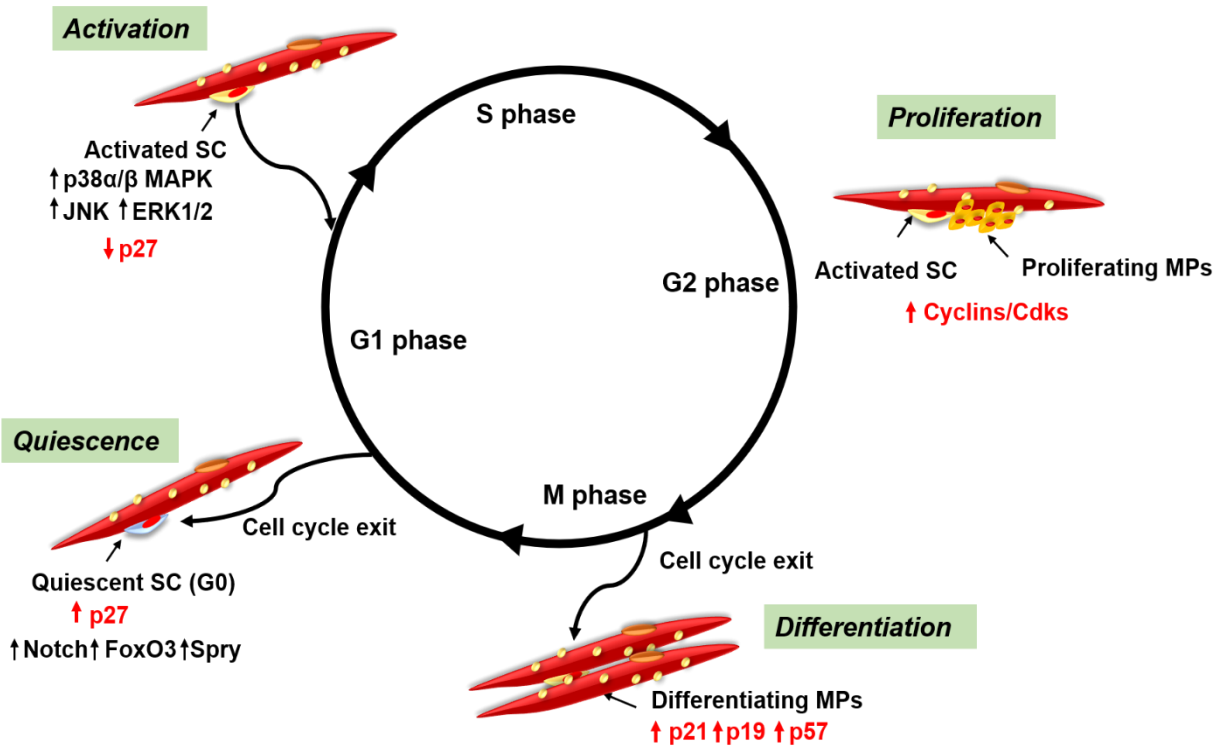

Figure 1.3: Cell cycle control of satellite cell fates: Proper regulation of cell cycle is important for SC and MP fate decisions. In resting condition, Forkhead box O3 (FoxO3) transcription factor that activates Notch signaling pathway, help to maintain quiescent state (G0) of the SCs. Cyclin kinase inhibitor, p27 is upregulated to prevent cell cycle entry. After activation, SCs can either enter quiescence by upregulating Spry1 or enter cell cycle and progress to S phase. The activated SCs that are primed for differentiation upregulate p38α/β mitogen activated protein kinase (p38α/βMAPK), extracellular signal-regulated kinase 1⁄2 (ERK1/2) and c-Jun N-terminal kinase (JNK) with simultaneous downregulation of p27 to promote cell cycle entry into G1/S phase. The MPs undergo rounds of proliferation, stimulated by cyclins/Cdks, in S/G2/M phase. Following proliferation, the MPs exit cell cycle by upregulating p21, p19 and p57 to differentiate into myofibers.

1.4 Mitochondria and oxidative phosphorylation

Mitochondria are double membranous organelles that consist of outer and inner membranes, the latter forming numerous folds called cristae (Hood et al., 2019). The area between the outer and inner membranes is called the inter-membrane space, whereas the matrix is the space encompassed by the inner membrane. Mitochondria are considered bioenergetic hubs where ATP

is produced via oxidative phosphorylation (Oxphos) by catabolism of different fuel sources such as glucose, fatty acids and glutamine (Chandel, 2018).

The process of mitochondrial ATP generation via Oxphos occurs in the inner mitochondrial membrane where electron transport chain (ETC) accepts electrons from reducing agents. The ETC comprises of five multi-subunit complexes, as well as a lipid soluble electron carrier between complexes I/II and III called ubiquinone (UQ) and the water soluble carrier between complexes III and IV called cytochrome c **(Figure 1.4)** (Martínez-Reyes & Chandel, 2020). The reducing equivalents that include reduced nicotinamide adenine dinucleotide (NADH) and reduced flavin adenine dinucleotide ($FADH_2$) might be produced by the tri-carboxylic acid (TCA) cycle, from intermediates of different metabolic pathways. For this process, the TCA cycle, housed in the mitochondrial matrix, performs a series of interconnecting reactions. NADH and $FADH_2$ enter the ETC, through complexes I and II respectively where they become oxidized (Martínez-Reyes & Chandel, 2020). The electrons formed from oxidation of the reducing equivalents migrate through ETC complexes to the final electron acceptor oxygen that is reduced to water in complex IV (Martínez-Reyes & Chandel, 2020). This passing of electrons through ETC is accompanied by pumping of protons from the mitochondrial matrix to the inter-membrane space (Martínez-Reyes & Chandel, 2020). Complexes I, III and IV are responsible for this proton pump resulting in the creation of mitochondrial membrane potential (ψ) in the inter-mitochondrial membrane (Sena & Chandel, 2012). This results in flowback of protons into the matrix through complex V (ATP synthase), which produces ATP from ADP (Martínez-Reyes & Chandel, 2020).

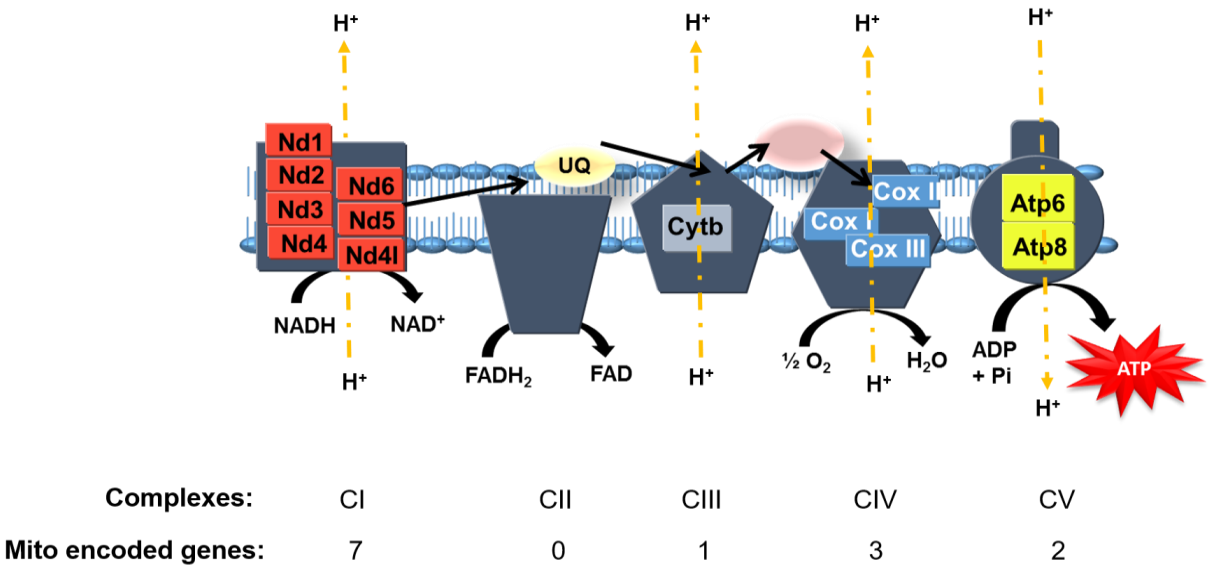

Figure 1.4: Schematic of electron transport chain (ETC): The ETC is made up of 5 complexes (C), CI, CII, CIII, CIV, and CV. The complexes contain subunits from 13 mitochondrial (mito) encoded genes including seven for CI, one for CIII, three for CIV and two for CV. The electrons formed from oxidation of the reducing equivalents NADH and $FADH_2$ migrate through ETC complexes to the final electron acceptor oxygen that is reduced to water by complex IV. The passing of electrons through the ETC is accompanied by pumping of protons from the mitochondrial matrix to the inter-membrane space. The flowback of protons into the matrix through complex V produces ATP from ADP.

1.5 Glycolysis and Oxphos

The production of ATP through Oxphos is tightly coupled to glycolysis **(Figure 1.5)**. Glycolysis is the process of intracellular biochemical conversion of glucose into two molecules of pyruvate with generation of two molecules each of ATP and NADH in the cytosol. This occurs through ten enzymatic reactions. NADH produced from glycolysis in the cytosol might be transported by the malate-aspartate shuttle into the mitochondria to be oxidised by ETC (Kane, 2014). Furthermore, in proliferating cells, the enzymatic reactions produce glycolytic intermediates that are incorporated into various metabolic pathways to generate macromolecules

such as nucleotides, lipids, amino acids and NADPH, which are necessary for cell division (Lunt & Vander Heiden, 2011; Ryall, 2013; Shyh-Chang et al., 2013) **(Figure 1.5)**. For example, glycolytic intermediate glucose 6-phosphate, shuttles into the pentose phosphate pathway (PPP), resulting in production of NADPH and Ribose-5-phosphate (Yu et al., 2016). NADPH acts as a reducing agent in lipid, nucleotide and amino acid biosynthesis whereas ribose-5-phosphate aids in nucleic acids biosynthesis (Vander Heiden & Deberardinis, 2017; Yu et al., 2016). Additionally, the intermediate dihydroxyacetone phosphate (DHAP) produced during glycolysis is converted to glycerol-3-phosphate, which helps in biosynthesis of the integral components of cell membranes, phospholipids and tri-acylglycerols (Yu et al., 2016).

The glycolytic end product pyruvate, has several potential fates. In the presence of oxygen, pyruvate usually enters the TCA cycle either as acetyl CoA through the action of pyruvate dehydrogenase (Pdh) or as oxaloacetate via pyruvate carboxylase **(Figure 1.5)**. Another potential fate of pyruvate is its conversion to lactate in the cytosol by lactate dehydrogenase a (Ldha) that usually occurs in the absence of oxygen. In the anaerobic condition, NADH, which would normally enter the mitochondria, instead is oxidised to NAD^+ in the reaction that forms lactate from pyruvate. In this way, glycolysis is sustained by NAD^+ driving the first biochemical reaction in the glycolytic pathway (DeBerardinis et al., 2008). In response to acute energy demand, compared to Oxphos, glycolysis enables a faster rate of ATP generation (Pfeiffer et al., 2001).

The generation of ATP through glycolysis, despite the presence of oxygen is called the aerobic glycolysis or Warburg effect (Lunt & Vander Heiden, 2011). In tumours, the most prevalent explanation for the Warburg effect is a strategy to deal with immense anabolic demands of the proliferating cells. Many of the metabolites from energy producing pathways are shunted to biosynthetic pathways to support macromolecular synthesis needed for cell division (Lunt et al.,

2015; Vander Heiden & Deberardinis, 2017). In fact, for cancer cells, despite aerobic conditions, under an abundant supply of glucose, the percentage of ATP generated from glycolysis alone exceeds the amount produced by the mitochondria (DeBerardinis et al., 2008; Locasale & Cantley, 2010).

As energy generation is in response to energy demand of the cells, ATP production varies in different microenvironments and cellular conditions. Mammalian cells rely primarily on both glycolysis and Oxphos to produce ATP. However, the decision to use ATP from glycolysis or Oxphos is dependent on cell types, substrate availability, stages of cellular proliferation or differentiation (Pfeiffer et al., 2001). In this regard, glycolysis and Oxphos mutually collaborate to generate ATP, although the control mechanism is not properly understood. Cells devise their own mechanism for energy generation, if either of the ATP generating hubs fail to comply with the demand of the cells. For example, synthesizing ATP from glucose through glycolysis is the optimal ATP-producing tactic, when cells are restricted by their inability to maintain enough mitochondrial function to perpetuate sufficient flux through ETC (Locasale & Cantley, 2010; Vazquez et al., 2010). Indeed, in rapidly proliferating cancer cells, glycolysis is ramped up as Oxphos is not sufficient to fuel the cell division (Vander Heiden & Deberardinis, 2017). Furthermore, if glucose availability is perturbed, cancer cells switch their reliance on mitochondrial Oxphos (de Padua et al., 2017; Shiratori et al., 2019). An important parameter that measures cellular energy status and its reliance on glycolysis or Oxphos is NAD^+/NADH ratio (Menzies & Auwerx, 2015). Increased reliance on ATP derived from glycolysis is associated with low NAD^+/NADH ratio (Heiden et al., 2009), a phenomenon also observed in cancer cells (Vander Heiden & Deberardinis, 2017). In hypoxic environment, where glycolysis is enhanced to compensate for the weakened Oxphos production in the mitochondria, there is low NAD^+/NADH ratio (Eales et al., 2016). Similarly, in

certain pathological conditions such as hyperglycemia and diabetes, reduced Oxphos activity might be a consequence of low NAD/NADH ratio, indicative of their inclination towards glycolysis for ATP (Xiao et al., 2018). Contrarily, glucose starvation or caloric restriction that elevates cellular NAD^+/NADH stimulates ATP production through Oxphos in lieu of glycolysis (Xiao et al., 2018). Therefore, a critical factor coordinating ATP produced by glycolysis or Oxphos is NAD+/NADH ratio which in turn depends on cellular condition and substrate availability.

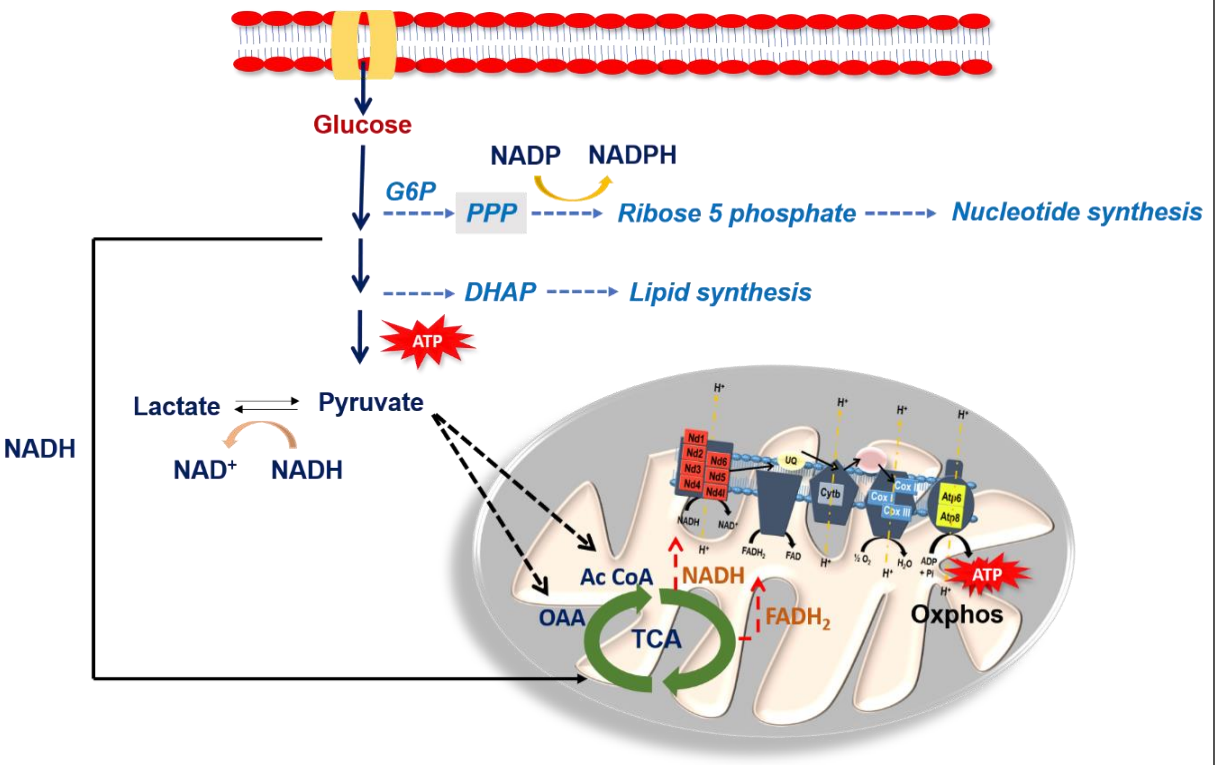

Figure 1.5: Diagrammatic representation of glycolysis and Oxphos: In the cytosol, glucose is oxidised to pyruvate by glycolysis, which enters the Tri-carboxylic (TCA) cycle via acetyl CoA or oxaloacetate (OAA). NADH and $FADH_2$ produced by TCA cycle enters electron transport chain complex and is oxidised by donating electrons. The electrons move through the complexes to produce ATP by a process called oxidative phosphorylation (Oxphos). Pyruvate on the other hand might also form lactate and NAD^+ by utilizing NADH. The glycolytic intermediates glucose 6-phosphate (G6P) shuttles into the pentose phosphate pathway (PPP), resulting in production of NADPH and Ribose-5-phosphate and dihydroxyacetone phosphate (DHAP) that forms lipid.

1.6 Mitochondrial DNA

The mitochondrial matrix maintains distinct genomic DNA that is not present in the nucleus. In mammals, the mitochondrial DNA (mtDNA) is approximately 16,600 base pairs of double stranded DNA having a non-coding D-loop regulatory region and encoding 13 mRNAs, which are translated to form critical components of ETC complexes, along with 2 rRNAs and 22 transfer tRNAs (D'Souza & Minczuk, 2018) **(Figure 1.6)**. The remaining components of the ETC are encoded by nuclear genes, which are imported into the mitochondria usually via specialized import machineries (Mokranjac & Neupert, 2005).

There are two strands of mtDNA based on different buoyant densities in a cesium chloride gradient, designated as heavy (H) strand and light (L) strand. The individual L strand transcription is initiated from a single promoter (LSP), whereas H strand transcription initiates at two different promoters (HSP1) and (HSP2) (D'Souza & Minczuk, 2018; Montoya et al., 1982). HSP2 transcription initiation site is located in the 5' end of 12s rRNA gene and produces a polycistronic RNA molecule covering almost the entire H strand encoding 12 mRNAs and 12 tRNAs. On the other hand, the HSP1 transcription initiation site is located 100 base pairs upstream of HSP2 causes transcription of 16S and 12S ribosomal (r) RNA. LSP drives the expression of *Nd6,* a complex 1 subunit of the ETC, as well as 8 tRNAs (Clayton, 2000; Guja & Garcia-Diaz, 2012). These polycistronic precursors are processed to produce individual mRNA, tRNAs and rRNAs. In addition to the most accepted structure of mtDNA, a 75 base pair open reading frame has been identified within the 16S rRNA, that yields a 24-oligopeptide designated as Humanin, that might have some neuroprotective function (Barshad et al., 2018).

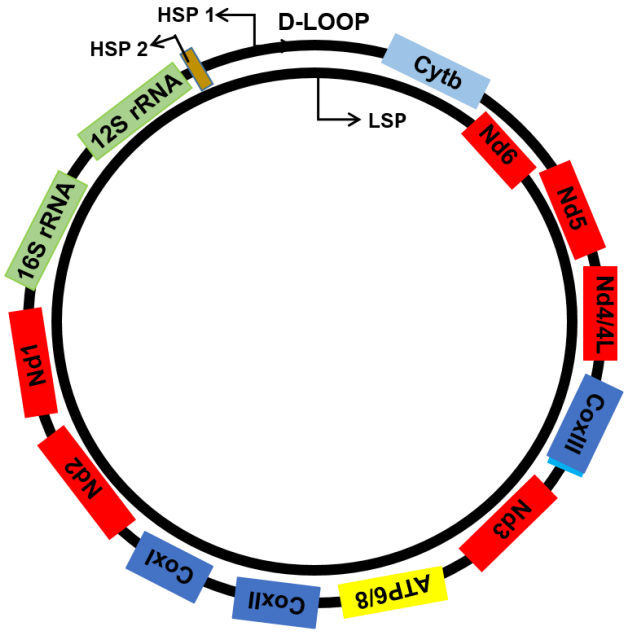

Figure 1.6: Schematic of mitochondrial DNA. Representation of mitochondrial DNA with D-loop regulatory region, two heavy strand promoters (HSP1 and HSP2) and one light strand promoter (LSP). The ETC subunit genes encoded are for complex I, *Nd1*, *Nd2*, *Nd3*, *Nd4/Nd4L*, *Nd5* and *Nd6* (red), complex III, *Cytb* (light blue), complex IV, *CoxI*, *CoxII* and *CoxIII* (dark blue) and complex V, *Atp6* and *Atp8* (yellow).

1.7 Transcriptional regulation of mitochondrial DNA

The human mtDNA transcription initiation requires mitochondrial DNA-directed RNA polymerase (POLRMT), transcription factor A of mitochondria (TFAM) and transcription factor B2 of mitochondria (TFB2M) (Falkenberg et al., 2002; Gaspari et al., 2004). TFAM is a 29kDa protein, which can bind, unwind and bend mitochondrial DNA to facilitate transcriptional initiation (Farge & Falkenberg, 2019). It also packages mtDNA into nucleoprotein structures called nucleoids, that perhaps maintains mtDNA integrity and influence mitochondrial gene expression (Bouda et al., 2019; Farge & Falkenberg, 2019; Gustafsson et al., 2016; Kukat et al., 2015). Structurally, TFAM contains a mitochondrial matrix targeting sequence, two tandem high mobility group box domains separated by a linker region (Ngo et al., 2014). It also has a 30 amino

acid C terminal tail, which has been characterized as a DNA binding region essential for transcriptional activation and interaction with TFB2M (Cotney & Shadel, 2006; Falkenberg et al., 2002; McCulloch & Shadel, 2003; Rubio-Cosials et al., 2011).

TFB2M, structurally homologous to bacterial RNA methyltransferase (Cotney & Shadel, 2006), also aids in mitochondrial transcription initiation (Morozov et al., 2015). Through its interaction with POLRMT, TFB2M facilitates transition from a closed to open promoter confirmation required for transcription initiation by inducing promoter melting (Gaspari et al., 2004; Litonin et al., 2010; Lodeiro et al., 2010; Ramachandran et al., 2017).

It is uncertain if TFAM is an actual component of a transcription complex with POLRMT and TFB2M (Falkenberg et al., 2002; Litonin et al., 2010; Shi et al., 2012; Yakubovskaya et al., 2014) or the transcriptional machinery might comprise a two component system made up of TFB2M and POLRMT with TFAM acting as a transcriptional activator (Lodeiro et al., 2012; Shutt et al., 2010; Zollo et al., 2012). According to the former mechanism, transcription initiation starts with TFAM binding to 10–15 base pairs upstream of the start site for transcription (Gustafsson et al., 2016). Here it interacts with POLRMT recruiting it to the promoter (Hillen et al., 2017) that creates a structural change facilitating POLRMT-DNA interaction (Morozov et al., 2014; Posse et al., 2014; Yakubovskaya et al., 2014). Following, TFB2M is also incorporated in the transcription complex, thereby forming the initiation complex conducive for transcription (Morozov et al., 2014; Yakubovskaya et al., 2014).

For the latter mode of transcription, TFAM levels differentially regulate the different promoters (Clayton, 2000; Gaspari et al., 2004; Ngo et al., 2014; Shutt et al., 2010). In the absence of TFAM, POLRMT and TFB2M bind to both LSP and HSP1 in-vitro, but direct HSP1 promoter specific transcription initiation more efficiently. However, in the presence of TFAM, transcription

from LSP is more proficient compared to HSP1. This can be attributed to differential DNA bending by TFAM (Ngo et al., 2011), and/or the TFAM binding sites for these two promoters are on opposite directions relative to the transcription initiation site (Ngo et al., 2014). For HSP2, promoter specific transcription initiation was achievable only by POLRMT and TFB2M (Lodeiro et al., 2012; Zollo et al., 2012), whereas, in-vitro transcription initiation from HSP2 was inhibited by TFAM (Lodeiro et al., 2012; Zollo et al., 2012). Based on TFAM's ability to differentially activate HSP1 and LSP and to repress HSP2 promoter (Shokolenko & Alexeyev, 2017), it can be speculated that it differentially activates the different promoters to balance the need of gene expression and ribosomal biogenesis, in response to different physiological or environmental changes.

Besides the initiation factors, the transcription machinery also includes the mitochondrial transcription elongation factor (TEFM), that ensures processivity and stabilization of the elongation complex (Agaronyan et al., 2015; Hillen et al., 2017; Minczuk et al., 2011). Finally, the termination of mtDNA transcription originating from LSP and HSP1 is performed by mitochondrial transcription termination factor 1 (MTERF1) (Asin-Cayuela et al., 2005; Barshad et al., 2018). However, not much is known about MTERF1 mediated transcriptional termination from HSP2 (Yakubovskaya et al., 2010).

1.8 Mitochondrial DNA and Oxphos

mtDNA are limiting and crucial for ATP synthesis, as it encodes 13 mitochondrial genes which are the functional components of 4 out of 5 ETC complexes (Gustafsson et al., 2016; Taylor & Turnbull, 2007). This is evident in diseases and ageing where mtDNA mutations are characterized by reduction in mitochondrial function and Oxphos (Carelli & Chan, 2014; Gorman et al., 2016; Ryzhkova et al., 2018). Oxphos deficiency due to mtDNA

mutation also causes leakage of electrons from ETC, resulting in oxidative stress, thereby predisposing mitochondrial deregulation (Lee et al., 2017). Indeed, mutation of mtDNA encoded *Atp6* and *Atp8* genes, decreased mitochondrial ATP generation and produced high levels of oxidative stress induced mitochondrial damage (Houštěk et al., 2006). Furthermore, mutation of ETC complex I encoded mitochondrial genes is the predominant cause of impaired ATP synthesis in progression of Leber hereditary optic neuropathy (LHON) disease (Baracca et al., 2005). Additionally, mtDNA mutation might also effect ETC complexes I, III and IV formation and stability, thereby reducing ATP synthesis capacity (Pello et al., 2008).

The significance of mtDNA to ATP generation was further underscored by experiments using a high throughput screen to assess real time ATP concentration in live human cells. These experiments showed that decreased mitochondrial ATP generation was associated with a deficiency in mitochondrial encoded genes (Mendelsohn et al., 2018). Another recent study showed that inducible depletion of mtDNA, reduced mitochondrial transcripts and ETC complex formation (Martínez-Reyes et al., 2016). This caused a reduction in the mitochondrial ATP generation, which attenuated cell proliferation (Martínez-Reyes et al., 2016). This was evident in mtDNA depleted cells that did not survive when grown in galactose only media where ATP generation is completely dependent on mitochondrial Oxphos (Martínez-Reyes et al., 2016).

1.9 Mitochondrial biogenesis and dynamics

Mitochondrial number within a cell is maintained by two opposing forces, biogenesis and mitophagy that create and eliminate mitochondria, respectively to sustain energy (Hood et al., 2019). Mitochondrial biogenesis is a multistep mechanism by which cells increase

the mitochondrial content and function in response to different physiological, metabolic and pathological changes (Handschin & Spiegelman, 2006; Sanchis-Gomar et al., 2014). Crucial to mitochondrial biogenesis is peroxisome proliferator-activated receptor co-activator 1 alpha (Pgc1α). It interacts and co-activates a variety of transcription factors including the nuclear respiratory factors (Nrf) 1 and 2 which promote expression of TFAM that might enhance mitochondrial transcription and gene expression (Gureev et al., 2019).

Proper mitochondrial morphology and organization are maintained by two opposing forces; fusion and fission which are associated with ATP generation capacity (Khacho & Slack, 2017). In this regard, the switch in mitochondrial dynamics caused by fusion or fission are associated with differential energy generation capacities (Khacho et al., 2016). Mitochondrial fusion is a two-stage process where the outer membrane is fused by mitofusin I (MfnI) and II (MfnII), followed by fusion of inner membrane by Optic Atrophy 1 (OpaI). Mitochondrial fusion produces elongated mitochondria that might be associated with mtDNA stability influencing Oxphos (Mishra & Chan, 2016; Mitra et al., 2009; Ramos et al., 2019; Song & Hwang, 2018). Absence of mitochondrial fusion due to genetic deletion of both Mfn1 and Mfn2 in mouse heart resulted in decreased mtDNA content and ETC function (Chen et al., 2011; Papanicolaou et al., 2012). In skeletal muscle, conditional genetic deletion of Mfn1 and Mfn2 also caused instability and mutagenesis of mtDNA (Chen et al., 2010). Moreover, loss of inner mitochondrial membrane fusion due to ablation of Opa1 in skeletal muscle also resulted in severe mtDNA depletion and reduced ETC complex activity (Tezze et al., 2017).

On the other hand, increased Oxphos might be necessary to promote fusion and elongated mitochondria (Mishra & Chan, 2016). This interpretation is via the development of an in vitro fusion assay using isolated mitochondria (Hoppins et al., 2011; Meeusen et al., 2004; Schauss et al., 2010), which enabled more detailed investigation regarding the regulation of mitochondrial fusion by Oxphos

(Mishra & Chan, 2014). The importance of Oxphos to mitochondrial fusion was demonstrated in isolated mitochondria, where addition of respiratory substrates that stimulate Oxphos, resulted in mitochondrial inner membrane fusion (Mishra & Chan, 2014). In skeletal muscle, oxidative fibers that have increased reliance on Oxphos, had more mitochondrial fusion (Mishra et al., 2015). Human cells growing in galactose media that forces cells to rely on Oxphos showed elongated mitochondria (Rossignol et al., 2004). Moreover, in cells from patients with mtDNA mutation, defective Oxphos generation led to impaired mitochondrial fusion (Mishra & Chan, 2014).

Fission is associated with division of mitochondria by dynamin related protein 1 (Drp1) and fission protein 1 (Fsn1). Drp1 is essential to maintain cellular homeostasis by its regulation during differentiation, cell survival, apoptosis and clearance of damaged mitochondria by mitophagy (Inoue-Yamauchi & Oda, 2012; Kim et al., 2013; Lee et al., 2011). Fission results in augmented mitochondrial fragmentation that causes increased oxidative stress and reduced ATP production (Jheng et al., 2012). Transgenic mice overexpressing Drp1 in skeletal muscle exhibited reduced mtDNA, less muscle mass and compromised exercise mediated benefits (Touvier et al., 2015).

1.10 Metabolic transitions in SCs and MPs

SCs are characterized by dynamic metabolic reprogramming during different stages of the differentiation process from predominately Oxphos in quiescence to upregulation of glycolysis during activation and proliferation, back to a reliance on Oxphos during terminal differentiation (Bhattacharya & Scimè, 2020) **(Figure 1.7)**. Quiescent SCs have very few mitochondria, tightly packed around the nucleus, reduced levels of mtDNA and a very low metabolic rate (Latil et al., 2012). This is similar to other adult stem cell populations, such as quiescent long-term hematopoietic stem cells that reside in the bone marrow. These are also characterized by mitochondria with a paucity of mtDNA, reduced mass and poor development (Simsek et al.,

2010). However, unlike long-term hematopoietic stem cells, quiescent SCs barely depend on glycolysis and rely more on the mitochondria to produce ATP through ß-oxidation of fatty acids and Oxphos (Ryall et al., 2015).

Quiescent SCs are thought to consist of two distinct populations based on differences in mitochondrial density, which is inversely associated with Pax7 levels (Rocheteau et al., 2012). The SC population with low levels of Pax7 had more mitochondria and mtDNA with greater ATP generation compared to the other resident SCs and expressed higher levels of myogenic commitment markers (Rocheteau et al., 2012). Moreover, the quiescent SCs with reduced mitochondrial density and lower mitochondrial activity showed increased markers of stemness and decreased markers of myogenic commitment. This population utilized more time before entering the cell cycle for the first round of division after activation, suggesting that they represented a self-renewal population (Rocheteau et al., 2012).

When they become activated, SCs exhibit a metabolic switch from fatty acid oxidation to higher rates of glycolysis (Ryall et al., 2015). In muscle regeneration experiments, activated SCs isolated from skeletal muscle had a high level of glycolysis and oxygen consumption rate following 3 days of injury (Pala et al., 2018). The reliance on glycolysis provides the proliferating MPs with macromolecules to meet their anabolic demands during proliferation and might also act to protect them from ROS produced by mitochondrial Oxphos (Folmes et al., 2012). This is evident in other highly proliferative stem cell types. For the highly proliferative undifferentiated embryonic stem cells, self-renewal is maintained by utilizing a high rate of energy generation and a ready supply of macromolecules for cell division. In this case, relying more on glycolysis producing lactate from pyruvate rather than acetyl CoA for Oxphos (Cliff & Dalton, 2017). Recently, single cell RNA sequencing revealed that expression for mitochondrial genes also

increased substantially in activated SCs after injury and in committed MPs that had been isolated from mouse skeletal muscle and cultured in vitro (Dell'Orso et al., 2019). This was also associated with a progressive increase in transcripts associated with TCA cycle, ETC complexes and fatty acid synthesis (Dell'Orso et al., 2019).

To increase their proliferative rate, committed SCs have devised several methods to actively reduce Oxphos production in favour of glycolysis. MP proliferation is associated with hypoxia inducible factor 1α (Hif1α) activation. This promotes glycolysis to produce lactate, thereby attenuating Oxphos capacity, which is required for differentiation. Indeed, SCs obtained from genetically deleted Hif1α and Hif2α mice had reduced self-renewal and MPs underwent precocious differentiation (Yang et al., 2017). When MPs were pre-conditioned in hypoxic environment and transplanted into *mdx* mice, a mouse model for muscle wasting disease, there was improved regeneration capacity of the pre-conditioned MPs (Liu et al., 2012). Oppositely, Hif1α has also been shown to inhibit differentiation of MPs (Majmundar et al., 2015). This was thought to be mediated through Hif1α mediated inhibition of Wnt signaling that repressed MP differentiation (Majmundar et al., 2015). The discrepancies in their findings for Hif1α might relate to the timing of its activity in SC and MP fate decisions (Majmundar et al., 2015).

Another potential mechanism that might downregulate Oxphos capacity in favour of glycolysis in MPs is activation of pyruvate dehydrogenase kinase (Pdk). In the mitochondria Pdk suppresses Pdh that converts pyruvate to acetyl CoA for the TCA cycle, thereby inhibiting mitochondrial oxidative capacity (Zhang et al., 2014). Pluripotent and some adult stem cells have devised this method to inhibit mitochondrial Oxphos and enhance glycolysis to sustain rapid proliferation (Folmes et al., 2011; Takubo et al., 2013). Although not much is known about regulation of MPs by Pdk, it was shown that in hypoxia or glucose

deprivation, MPs have higher Pdk activity to support enhanced glycolysis (Abbot et al., 2005; Hori et al., 2019).

Reduced Oxphos capacity in human MPs during proliferation is maintained by low levels of ETC complex III, IV and V subunits, mitochondrial proteins and enzymes compared to differentiating cells (Hoffmann et al., 2018). A similar profile is observed in proliferating pluripotent stem cells, which are characterized by decreased complex I and complex IV ETC nuclear encoded genes and a reduction in mitochondrial biogenesis regulators such as peroxisome proliferator-activated receptor co-activator 1 beta (*Pgc1β*) and estrogen-related receptor gamma (*ERRγ*) (Sperber et al., 2015; Zhou et al., 2012)

As MPs begin to differentiate, glycolysis subsides in favour of Oxphos, which is essential for terminal differentiation **(Figure 1.7)**. Recently, a study showed that conditional deletion of Pdh in SCs that resulted in defective MP proliferation, also caused poor terminal differentiation and inefficient skeletal muscle regeneration upon injury. Thus, suggesting the requirement of pyruvate for efficient Oxphos during differentiation (Hori et al., 2019). Indeed, chloramphenicol, an inhibitor of mitochondrial protein synthesis and function, has been shown to inhibit myogenic differentiation (Rochard et al., 2000; Seyer et al., 2006, 2011). Compared to MPs, differentiated myofibers have a higher mitochondrial mass composed of pronounced levels of mtDNA, ETC complex proteins and TCA cycle enzymes (Hoffmann et al., 2018; Kraft et al., 2006; Lyons et al., 2004; Remels et al., 2010). The terminally differentiated myofibers require functional mitochondria to sustain the high energy demand of skeletal muscles. A lack of functional mitochondria in terminally differentiated tissues due to mtDNA mutations is the cause of many diseases of different organs that include skeletal muscle (Chinnery, 2015).

Energy output from mitochondria during MP differentiation is associated with their dynamic reorganization by fission, mitophagy, biogenesis and fusion **(Figure 1.7)**. In metabolic complications such as type 2 diabetes, decreased myogenic differentiation is attributed to impaired mitophagy, which suggests the importance of mitochondrial clearance in facilitating differentiation (Henriksen et al., 2019). Importantly, during early myogenic differentiation, there is upregulation of the fission protein Drp1 mediated mitochondrial fragmentation and subsequent mitophagy by sequestosome 1 (Sin et al., 2016). Drp1 inhibition caused a reduction in differentiation of MPs with reduced mitochondrial elongation, mtDNA content and mitochondrial biogenesis (Kim et al., 2013). However, at later stages of differentiation if Drp1 is not repressed then myogenic differentiation does not proceed (De Palma et al., 2010).

Following mitophagy, the mitochondrial biogenesis activator Pgc1α and the fusion protein Mfn2 rebound mitochondrial dynamics (Sin et al., 2016). As differentiation progresses, Opa1 mediates mitochondrial fusion and Pgc1α amplifies mitochondrial biogenesis that together form the dense elongated mitochondrial network pertaining to increased Oxphos reliance in differentiated myotubes (Sin et al., 2016). Ectopic overexpression of Pgc1α in an MP cell line increased mtDNA, mitochondrial encoded *cytochrome c oxidase* gene expression that enhanced mitochondrial respiration and function (Baldelli et al., 2014; Wu et al., 1999). Importantly, overexpressing Pgc1α in human MPs boosted myofiber formation capacity both in vitro and in vivo with enhanced metabolic activity (Haralampieva et al., 2017).

Intriguingly, MyoD has recently been shown to control mitochondrial function that might be necessary for efficient differentiation. By genome wide ChIP seq analysis of a MP line, it was found that the MyoD interacted with several metabolic genes including those involved in mitochondrial biogenesis, fatty acid oxidation and ETC function (Shintaku et al., 2016).

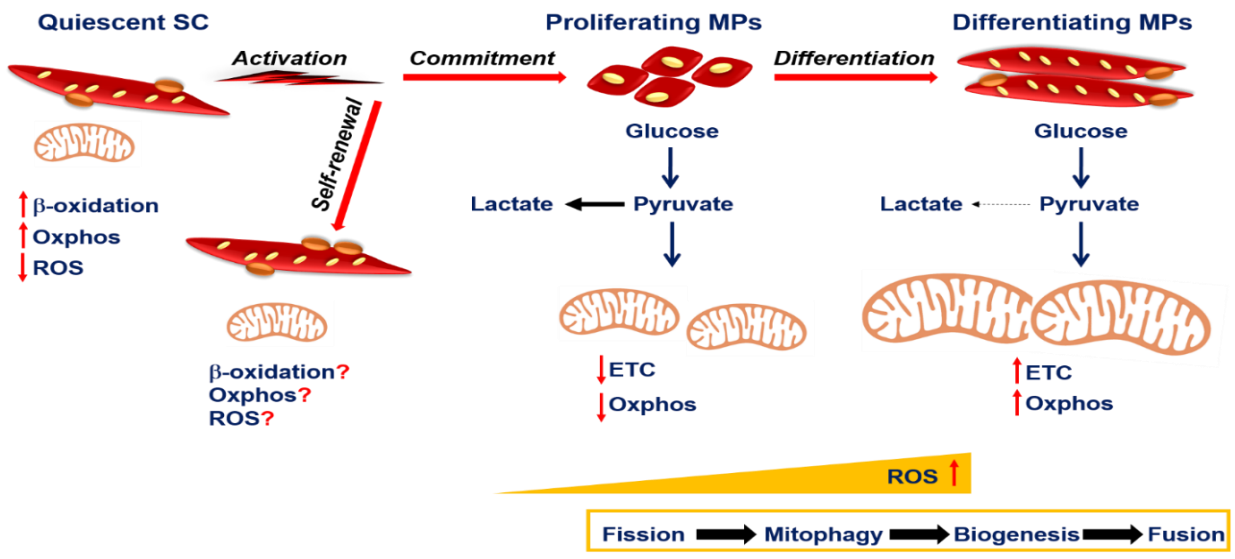

Figure 1.7: Mitochondrial function in satellite cell fates. Quiescent satellite cells (SCs) utilize fatty acids through β-oxidation for Oxphos in the mitochondria. Activation of quiescent SCs might potentiate their self-renewal or formation of myogenic progenitor cells (MP) that undergo proliferation and eventually differentiate as part of myofibers. Mitochondrial metabolism is poorly elucidated in self-renewing SCs, whereas MPs rely on glycolysis to obtain energy for rapid division. As differentiation progresses, there is increased mitochondrial fission, followed by mitophagy, after which the mitochondria are repopulated by mitochondrial biogenesis and fusion. ROS levels increase as MPs begin to differentiate.

1.11 Mitochondrial oxidative stress in SCs and MPs

Reactive oxygen species (ROS) is a by-product of mitochondrial Oxphos, generated as a result of electron transfer reactions in ETC (Sena & Chandel, 2012). Leakage of electrons during their shuttling through the ETC at complexes I and III, might generate ROS that cause oxidative stress to the cells (Martínez-Reyes & Chandel, 2020). ROS can also be produced via an accumulation of excess NADH at complex I known as reductive stress (Pryde & Hirst, 2011; Xiao & Loscalzo, 2020; Yan, 2014). Reductive stress can be caused by an enhanced NADH production by Pdh complex that overwhelms complex 1 (Fisher-Wellman et al., 2015). Additionally, hypoxic or high glucose environment that impedes

mitochondrial ATP generation, might also contribute to reductive stress (Oldham et al., 2015). Alternatively, ROS can be generated by reverse electron transport (RET), whereby electrons backflow from ubiquinone or complex II to complex I (Chouchani et al., 2014; Scialò et al., 2016; Treberg et al., 2011). RET and likely reductive stress can also be induced by blockage of ETC complexes, including complexes III, IV and V that impede ATP generation, which might lead to NADH accumulation at complex I (Mills et al., 2016; Xiao & Loscalzo, 2020).

To protect the cells from the potential harmful effect of ROS, mitochondria have their own antioxidant defense systems (Oyewole & Birch-Machin, 2015). Notable among them are catalase, glutathione peroxidases (GPxs) and superoxide dismutase (SOD) which are able to scavenge ROS to maintain cellular homeostasis (Schieber & Chandel, 2014). Depending on their efficiency, antioxidants can keep the level of ROS at an optimum level, so that it might act as a signaling molecule in facilitating adaptation to hypoxia, regulation of autophagy and stem cell differentiation (Sena & Chandel, 2012; Snezhkina et al., 2020).

In some adult stem and progenitor cells ROS signaling is important for fate decisions. For example, in long-term quiescent HSCs barely any ROS is produced, which protects them from precocious differentiation, which is contrary to activated HSCs that require ROS for successful differentiation (Owusu-Ansah & Banerjee, 2009; Simsek et al., 2010; Tothova et al., 2007). Although not much is known for SCs, ROS generation is associated with their activation and subsequent differentiation (Kozakowska et al., 2015; Le Moal et al., 2017). Furthermore, though the contribution of mitochondrial ROS is substantial, it does not preclude the potential ROS effect from other cellular sources that might affect SC fate (Acharya et al., 2013; Le Moal et al., 2017). Despite a reliance on fatty acid metabolism and Oxphos, quiescent SCs have low ROS levels and

transcriptomic analysis revealed that quiescent SCs express a greater quantity of antioxidants to protect them from potential harmful effects of ROS (Pallafacchina et al., 2010). SCs obtained from genetically deleted antioxidant superoxide dismutase mice showed lower differentiation ability (Manzano et al., 2013). Indeed, quiescent SCs had a better survival rate than their activated counterparts after hydrogen peroxide treatment, which causes accumulation of cellular generated ROS (Pallafacchina et al., 2010).

Both mitochondrial and nicotinamide adenine dinucleotide phosphate (NADPH) oxidase induced ROS are increased during the MP differentiation process (Acharya et al., 2013). NADPH oxidase is thought to instigate more mitochondrial ROS by opening mitochondrial ATP sensitive potassium channels. This allows the surge of potassium ions in the mitochondrial matrix, thereby reducing the mitochondrial membrane potential (Zhang et al., 2001). Attenuated mitochondrial ROS production by inhibiting NADPH oxidase activity, prevented their dysfunction (Doughan et al., 2008). Although important, excessive ROS is detrimental to MPs by targeting mtDNA and mitochondrial function (Sandiford et al., 2014; Sestili et al., 2009) that leads to swelling and disruption of mitochondria (Sestili et al., 2009). Moreover, deletion of mitochondrial antioxidant, GPx, in MPs resulted in lower proliferation and differentiation potential (Lee et al., 2006) and MPs obtained from GPx null mice poorly differentiated with impaired myotube formation (Lee et al., 2006).

Mechanistically, excessive ROS in MPs is thought to increase nuclear factor kappa beta (NF-κB) (Ardite et al., 2004; Catani et al., 2004), which reduces MyoD levels, thereby inhibiting differentiation (Guttridge et al., 2000; Sandiford et al., 2014). Also, NF-κB mediated activation of YY1, which is a myogenic transcriptional repressor might be another target of ROS mediated inhibition of myogenic differentiation in MPs (Wang et al., 2007). Importantly, muscle restricted

inhibition of NF-κB in mice enhanced SC activation and muscle regeneration (Mourkioti et al., 2006).

The inhibitory function of NF-κB is thought to occur through its classical signaling pathway, which operates via the p65/p50 heterodimer mediated transcription of target genes (Dahlman et al., 2010). However, contrary to its role as a negative regulator in undifferentiated MPs, NF-κB also supports differentiating MPs. This role is achieved by the use of its alternative signaling pathway, which relies on RelB/p52 mediated transcription (Dahlman et al., 2010). In this case, NF-κB mediates transcription of genes that are known to stimulate Oxphos and mitochondrial biogenesis, which are required for myogenic differentiation. Some reports have shown that NF-κB can also promote myogenic differentiation through insulin like growth factor II or p38MAPK, which are both known regulators of myogenic differentiation (Baeza-Raja & Muñoz-Cánoves, 2004; Bakkar et al., 2008; Conejo et al., 2001; Ji et al., 2010). Interestingly, ROS was required by MPs to exit cell cycle and initiate the process of differentiation by activating p38αMAPK (L'Honoré et al., 2018). This is similar to neural stem cells where ROS has been shown to act as a signaling molecule to activate a cascade of events that upregulate the transcriptional genes required for differentiation (Khacho et al., 2016). Inhibition of ROS by the antioxidant n-acetyl-cysteine or of p38αMAPK prevented muscle differentiation, but increased the SC pool, suggesting the importance of both the factors in mediating SC differentiation (Brien et al., 2013; Richards et al., 2011). Thus, the negative and positive effects of ROS on SC function might relate to dose and time dependent considerations. An evaluation of other potential factors that influence ROS during SC engagement is important to unravel its bi-faceted role.

In addition to ROS, reactive nitrogen species (RNS) might also be made from the superoxide leakage in mitochondria and reactive nitric oxide (NO•) produced from L-arginine by

nitric oxide synthase (Le Moal et al., 2017). NO• is important for SC activation, self-renewal and MP differentiation (Buono et al., 2012; De Palma et al., 2010; Rigamonti et al., 2013; Tatsumi et al., 2006). NO• might be critical for mitochondrial elongation, required for myogenic differentiation. In primary MPs, inhibition of NO synthesis, prevented mitochondrial elongation and myogenic differentiation (De Palma et al., 2010).

1.12 Environmental influence on SC and MP mitochondrial adaptation

Many studies have showed that skeletal muscle adaptation through modifiable physiological perturbations can in part be attributed to innate changes that occur in the quiescent SC pool (Al-Khalili et al., 2003; Al-Khalili et al., 2014; Bell et al., 2010; Bollinger et al., 2015; Bourlier et al., 2013; Boyle et al., 2012; Lund et al., 2017; Maples et al., 2015). Thus, reflecting a genetic change in specific DNA sequences and/or from changes to the epigenome in quiescent SCs that would influence the transcriptome and the pathways they influence. Caloric availability is one aspect of the external environment that affects mitochondrial function in SCs **(Figure 1.8)**. Caloric restricted post-mortem human and mouse SCs have a remarkable ability to stay dormant owing to their anoxic environment with the ability to become activated up to 17 and 14 days respectively post death. They are characterized by reduced mitochondrial mass and density similar to one of the two quiescent SC subpopulations that showed increased stem cell markers and reduced commitment (Latil et al., 2012; Rocheteau et al., 2012). Contrarily, despite a lack of nutrients as found in post mortem SCs, those from caloric restricted mice have a higher mitochondrial activity and Oxphos capacity (Cerutti et al., 2014). Importantly, metformin, a caloric restriction mimicking drug that increases Oxphos, maintained SC quiescence in vitro and in vivo (Pavlidou et al., 2017).

The age-related micro-environment also influences quiescent SCs, as exemplified by their lower numbers and reduced activation potential (Chakkalakal et al., 2012) **(Figure 1.8)**. Among

several contributing factors, an alteration in mitochondrial function associated with ageing might influence the decreased number and regeneration potential of SCs (García-Prat et al., 2016b; Pala et al., 2018). Importantly, ageing is correlated with reduced mitochondrial content, mtDNA and ATP production (Short et al., 2005). SCs obtained from aged mice showed enhanced ROS mediated irreversible senescence owing to their inability to remove damaged organelles that also include mitochondria (Cosgrove et al., 2014; García-Prat et al., 2016b). In addition, SCs from aged human skeletal muscle displayed decreased expression of genes required for ETC function (Bortoli et al., 2005). Similarly, primary MPs obtained from the aged skeletal muscles showed impaired mitochondrial Oxphos that attenuated myogenic differentiation (Pääsuke et al., 2016).

Severe and progressive skeletal muscle degeneration observed in muscle wasting diseases and complications such as muscular dystrophies and sepsis are also thought to influence SC mitochondria function. Impaired mitochondrial function was revealed in dystrophic mouse models including, the muscular dystrophy (*mdx)* and the double knockout dystrophin (Pant et al., 2015; Vila et al., 2017). In addition, absence of dystrophin in SCs reduced the commitment of MPs by reducing asymmetric division which is thought to exacerbate impaired regeneration in muscular dystrophies (Chang et al., 2018; Dumont et al., 2015b). MPs obtained from dystrophic mice displayed attenuated oxygen consumption, mitochondrial membrane potential and elevated ROS (Onopiuk et al., 2009). The importance of dystrophin to mitochondria and MP function was highlighted by restoration of dystrophin in *mdx* MPs (Matre et al., 2019). This enhanced Oxphos potential to near normal levels, which was associated with improved MP proliferation and differentiation. Furthermore, transplantation of these intrinsically modified MPs in dystrophic mice reinstated their regenerative ability (Matre et al., 2019).

Health complications due to sepsis, which might cause long term myopathy is also associated with reduced SC activation, proliferation and regenerative capacity (Rocheteau et al., 2015). Skeletal muscle that had confronted sepsis was characterized by reduced SC numbers, concomitant with defective mitochondria, degraded mtDNA and antioxidants levels to combat excessive ROS (Rocheteau et al., 2015). Normally, on activation, SCs switch from Oxphos to glycolysis that provides macromolecules required for proliferation. However, in sepsis, SC activation was associated with a higher level of Oxphos that was not conducive for division, hence limiting their regenerative capacity (Rocheteau et al., 2015).

Metabolic complications as observed in obesity are also linked to dysfunctional mitochondria **(Figure 1.8)**. Notably, many reports have showed that cultured MPs from obese individuals differentiate into myotubes retaining the metabolic derangement evident in their skeletal muscles of origin (Lund et al., 2017). Cultured SCs obtained from obese compared to lean human subjects showed reduced mtDNA copy number and function and altered metabolic function (Bollinger et al., 2015; Boyle et al., 2012).

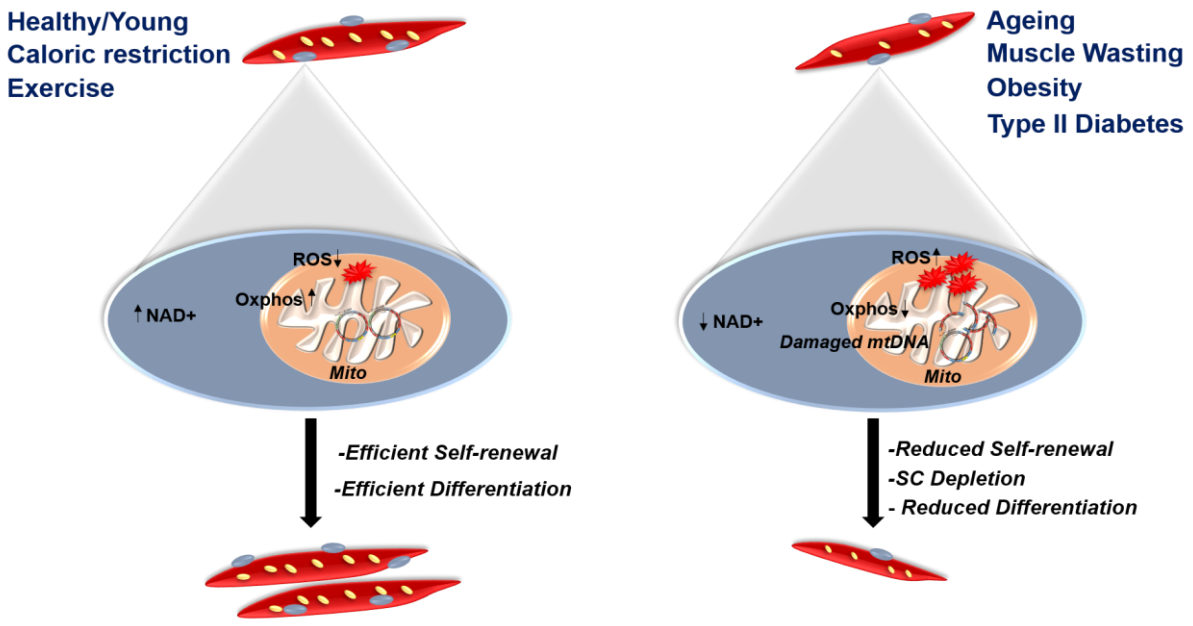

Figure 1.8: Influence of the micro-environment on mitochondria of quiescent satellite cells. In a healthy, calorie restricted or exercise adapted micro-niche, mitochondria from quiescent satellite cells (SCs) operate efficiently, producing Oxphos with very low ROS. This maintains quiescence and effective self-renewal and differentiation. However, mitochondrial adaptations due to metabolic complications as observed in ageing, muscle wasting diseases, obesity and type 2 diabetes, lead to fragmented mtDNA, impairment of Oxphos producing capacity and overproduction of ROS that reduce SC self-renewal and differentiation capacity.

Similar to obesity, SCs from streptozotocin induced diabetic mice showed impaired myotube formation and regeneration following cardiotoxin induced muscle damage (Jeong et al., 2013). SCs obtained from the mouse model of obesity and diabetes (ob/ob and db/db) showed impaired MP proliferation and differentiation (Nguyen et al., 2011). In addition, cultured myotubes from diabetic human skeletal muscle showed mitochondrial dysfunction with reduced mitochondrial content and Oxphos capacity (Minet & Gaster, 2011). Moreover, the SCs from human diabetic skeletal muscles lack metabolic flexibility to adapt to the micro-environment (Aguer et al., 2011). When grown in galactose media, which is known to induce oxidative

metabolism, SCs from healthy human skeletal muscles acclimatized by enhancing their mitochondrial content and Oxphos capacity, unlike the SCs from diabetic subjects, suggesting that they are obstinate to the changed micro-environment (Aguer et al., 2011).

Intriguingly, environmental cues that can potentially influence mitochondrial function in SCs is also highlighted by a change in Oxphos capacity of uninjured muscle that is distant from a site of a muscle injury (Rodgers et al., 2014). Despite originating from uninjured muscle these SCs had higher mitochondrial activity, mtDNA content, transcriptional activity and regeneration potential compared to SCs from a mouse where no muscle injury was induced. Moreover, the SCs obtained from the uninjured muscle where a muscle injury was generated at a distant site were more primed to become activated (Rodgers et al., 2014). The factor(s) that cause the environmental changes to enhance this phenomenon are unknown.

1.13 Influence of exercise on SC and MP adaptation

A notable physiological perturbation that affects SC and MP function is exercise. Indeed, an integral function of skeletal muscle is its ability to undergo remodeling in response to exercise that is known to improve metabolic health and physical fitness (Bassel-Duby & Olson, 2006; Coffey & Hawley, 2007; Hood et al., 2019). At the physiological level, exercise has been shown to increase muscle efficiency and flexibility, higher recruitment of myofibers and vascularization (Cartee et al., 2017; Pagnotti et al., 2019). At the cellular level, exercise has been demonstrated to increase mitochondrial number with increased mtDNA copy number, enhanced expression of proteins that are involved in β oxidation of fatty acid, TCA cycle and the ETC, concomitant with a significant increase in respiratory capacity (Burgomaster et al., 2008; Cao et al., 2012; Hood et al., 2019; Jacobs et al., 2013; Menshikova et al., 2006; Porter et al., 2015; Short et al., 2005).

Another important functional characteristic of exercise is that, it can stimulate SCs that is dependent on different exercise parameters of intensity, duration, modality and frequency (Abreu & Kowaltowski, 2020; Farup et al., 2014; Joanisse et al., 2015; Shefer et al., 2010). In human skeletal muscle, following a single bout of acute eccentric exercise, a significant increase in SC numbers was apparent at 24 hours, and peaking at 72 hours post exercise recovery (Cermak et al., 2013; Farup et al., 2014; Mackey et al., 2009; Mikkelsen et al., 2009; O'Reilly et al., 2008; Toth et al., 2011). Likewise, a single bout of resistance exercise or in combination with endurance exercise also increased SC numbers (Mackey et al., 2007; McKay et al., 2012; Snijders et al., 2014; Walker et al., 2012; Wernbom et al., 2013). In this regard, a number of growth factors and inflammatory cytokines released from muscle fibers and surrounding cells aid in SC activation, proliferation and and/or differentiation to help in muscle repair following exercise induced damage (Chen et al., 2020).

The role of SCs in muscle hypertrophy depends on different parameters including age, genetic mutation, and exercise regimen (Goh et al., 2019; Goh & Millay, 2017; Mccarthy et al., 2011; Murach et al., 2018a). Early studies had shown that SCs are important for exercise induced muscle gain, as their depletion by irradiation resulted in loss of hypertrophy following weight bearing exercises (Adams et al., 2002; Rosenblatt & Parry, 1992). Contrarily some studies showed that SCs were not necessary for hypertrophy. These studies used tamoxifen inducible Cre-Lox system to deplete SCs in Pax7-diphtheria toxin fragment A (DTA) mouse skeletal muscle. One study showed that hypertrophy occurred in spite of SC ablation (Mccarthy et al., 2011). Another study using the same mouse model demonstrated that mechanical overload in the first few weeks of SC ablated muscle showed hypertrophy, but by 8 weeks hypertrophy was attenuated in these SC ablated muscle (Fry et al., 2014a). The lack of hypertrophy might be caused by differential

accumulation of extracellular matrix and fibroblasts in the absence of SCs over time (Fry et al., 2014a). However, SC activation and fusion into myofibers are contributing factors for myofiber growth and accumulation of myonuclei following resistance exercise (Blaauw & Reggiani, 2014; Bruusgaard et al., 2010; Guerci et al., 2012). Many studies have shown that prolonged resistance exercise increased SC numbers that contributed to muscle hypertrophy (Farup et al., 2014; Kadi et al., 2004; Kadi & Thornell, 2000; Leenders et al., 2013; Mackey et al., 2007, 2011a; Menon et al., 2012; Olsen et al., 2006; Petrella et al., 2006; Suetta et al., 2013; Verdijk et al., 2009).

Unlike for resistance training, it is likely that SCs do not have a hypertrophic role in muscle endurance exercise adaptation (Cisterna et al., 2016; Shefer et al., 2010; Jackson et al., 2015; Manzanares et al., 2019; Masschelein et al., 2020). There is an increase in the number of SCs that is directly proportional to the intensity of the endurance exercise (Kurosaka et al., 2009) with no evident hypertrophy. However, applying resistance to the exercise, increased SCs that contributed to muscle hypertrophy (Masschelein et al., 2020; Murach et al., 2018b).

Apart from increasing SC numbers, exercise can also alter SC myogenic regeneration capacity. Recently, it was shown that SCs obtained from endurance-exercised mice had improved regeneration capacity due to prevalence of more self-renewing markers (Abreu & Kowaltowski, 2020). Although ageing is associated with decreased SC activity, endurance exercise in humans was shown to improve SC regeneration ability that might be due to improved mitochondrial function (Joanisse et al., 2016). In addition, biopsy derived SCs obtained from musculus vastus lateralis of exercised obese human subjects committed and differentiated into myotubes with the same enhanced metabolic benefits that were provided in vivo by exercise (Lund et al., 2017). Importantly, the SCs cultured in vitro to form myotubes had enhanced glucose and lipid oxidation, which suggests that the external cue of exercise is capable of altering mitochondrial function

directed by changes in the quiescent SCs (Lund et al., 2017; Bourlier et al., 2013). Four weeks of voluntary wheel running in diabetic mice induced SC activation and myogenic progression. (Fujimaki et al., 2014). Moreover, SCs obtained from hypertrophic muscle, induced by functional overload, mimicking resistance exercise, had increased proliferative potential (Fujimaki et al., 2016). Thus, in response to exercise, SCs undergo an innate change that enhance their myogenic regeneration capacity.

SCs might play a role in exercise induced remodeling of fiber types. Both a single bout of resistance exercise and a combined resistance exercise with high intensity interval training resulted in enhanced SC number in type I specific muscle fibers of sedentary or overweight human subjects (Pugh et al., 2018). Following 6 weeks of high intensity sprint interval or moderate intensity continuous aerobic exercise, there was enhancement in proliferating SCs in type I and type II muscle fibers (Joanisse et al., 2015). Furthermore after high intensity sprint interval training, there was an increase in hybrid fibers expressing both myosin heavy chain type I and II isoforms along with increased SC number (Joanisse et al., 2013). This increase in SCs might be necessary for fiber type remodeling from fast to slow twitch fibers in response to prolonged exercise (Joanisse et al., 2013).

Leading models propose that the greater mitochondrial oxidative capacity following chronic exercise result from continual and coordinated stimulation of transcriptional pathways (Kupr & Handschin, 2015). This process results in a steady state accumulation of mitochondrial proteins manifesting as greater mitochondrial content (Flück & Hoppeler, 2003; Perry et al., 2010; Pilegaard et al., 2000). Indeed, the majority of the literature has focused on the role of transcriptional factors and co-activators required for promoter activation. One such model suggests that exercise activates Pgc1α, which co-activates a variety of transcription factors controlling the

expression of distinct families of mitochondrial proteins, thereby enhancing mitochondrial functions in skeletal muscle (Baar et al., 2002; Gureev et al., 2019; Kupr & Handschin, 2015). It was shown that following every session of high intensity training, Pgc1α mRNA increased 4 h post exercise, but returned to its pre-exercise levels after 24 h (Perry et al., 2010). This repeated transient increase of Pgc1α was believed to cause the sustained increase in its transcription as well as metabolic proteins (Perry et al., 2010). However, it is not known if Pgc1α's influence also affects SCs during exercise. In vitro, adenoviral overexpression of Pgc1α in SCs obtained from human skeletal muscle, resulted in enhanced myofiber forming capacity, with an initial switch to slow twitch oxidative myofibers (Haralampieva et al., 2017). Another study showed that SCs obtained from muscle-specific Pgc1α overexpressing mice had an accelerated response to injury along with higher proliferative capacity (Dinulovic et al., 2016).

1.14 Sirt1

Sirtuins are a family of NAD^+ dependent protein deacetylases that are important regulators of a variety of cellular processes ranging from energy metabolism and stress response, to tumorigenesis and ageing (Boutant & Cantó, 2014; McBurney et al., 2013). The reaction catalyzed by Sirt1 uses NAD^+ as a co-substrate, resulting in the production of the deacetylated substrate, nicotinamide and 2′-O-acetyl-ADP-ribose (Cantó et al., 2012). Structurally, Sirt1 has three major domains: the N-terminal domain that binds acetylated protein substrates (Caito et al., 2010; Ghisays et al., 2016), the catalytic domain that binds acetyl-lysine and NAD^+, and the C-terminal domain (Pan et al., 2012).

In particular, Sirt1 is a master metabolic regulator coupling energy status to transcriptional response by modifying the transcription factors and cofactors involved in metabolic homeostasis (Bordone & Guarente, 2005; Knight & Milner, 2012; Cantó & Auwerx, 2009). Its activity is

modulated by the cytoplasmic NAD^+/NADH ratio. Sirt1 activity increases when NAD^+ levels are high, observed during caloric restriction, exercise and fasting (Cantó et al., 2010; Cantó & Auwerx, 2009; Chabi et al., 2009; Chen et al., 2008; Rodgers et al., 2005). In fact, any condition that stimulates cellular NAD^+/NADH, has been shown to activate Sirt1. This is highlighted by incubation of c2c12 cells and primary MPs with galactose in place of glucose (Ryall et al., 2015). This increased the cells NAD^+/NADH ratio, which increased Sirt1 mediated deacetylation of histones and muscle gene expression. On the contrary, for high energy states observed during soaring glucose and fat availability, NAD^+/NADH decreases that decreases Sirt1 activity (Anderson et al., 2017; Cantó et al., 2015; Li et al, 2013).

Sirt1 enhances mitochondrial activity either directly or indirectly by controlling transcription factors and co-activators (Tang, 2016). During fasting or an acute bout of exercise when NAD^+/NADH ratio is high, Sirt1 mediated Pgc1α deacetylation has been shown to enhance fatty acid oxidation genes and mitochondrial function in skeletal muscle (Cantó & Auwerx, 2009; Gerhart-Hines et al., 2007). Treatment of mice with Sirt1 specific activator, resveratrol that increases NAD^+/NADH ratio, enhanced their running time and the oxygen consumption by their skeletal muscles, protected them from diet induced obesity and insulin resistance (Lagouge et al., 2006; Borra et al., 2005). This was concomitant with induction of genes for oxidative phosphorylation and mitochondrial biogenesis accredited to a decreased acetylation level of Pgc1α (Lagouge et al., 2006).

In addition to controlling metabolism, Sirt1 plays a crucial role in SC fate decisions. However, there are two opposing views concerning Sirt1 mediated SC activation. Rando and his group showed that as SCs exit from quiescence, Sirt1 up-regulates autophagy that provides additional energy required for SC activation and MP proliferation (Tang & Rando, 2014).

Furthermore, using inducible SC-specific Sirt1KO mouse, the authors showed that ablation of Sirt1, delayed SC activation due to inhibition of autophagy and delayed their entry into S phase of the cell cycle (Tang & Rando, 2014). Furthermore, deletion of SC specific Sirt1, prevented muscle regeneration and its overexpression facilitated muscle regeneration in older mice (Myers et al., 2019). Contrarily, Ryall showed that during SC activation, there was decreased NAD^+ due to switch from Oxphos to glycolysis, which in turn attenuated the activity of Sirt1 (Guarente, 2000; Imai et al., 2000; Michan & Sinclair, 2007; Ryall et al., 2015). Furthermore, genetic deletion of Sirt1 led to deregulated activation of SCs promoting premature differentiation with reduced myofiber size and diminished muscle regenerative capacity (Ryall et al., 2015). The divergent role Sirt1 showed by these groups might be attributed to the time point that was considered to observe SC activation. While Ryall's group isolated SCs from extensor digitalis longus (EDL) muscle fiber culture at early time point, Rando's group considered a later time point to observe SC activation (Ryall et al., 2015; Tang & Rando, 2014). Also, to assess the effect of Sirt1KO on SC activation, one group used whole body knockout while the other group used inducible SC-specific Sirt1KO mice, which might have caused the difference in SC functional outcome. Other than SC activation, Sirt1 is also important for proliferation (Pardo & Boriek, 2011; Rathbone et al., 2009) and cell cycle progression of MPs (Rathbone et al., 2009). Overexpression of Sirt1 increased MP proliferation and cell cycle progression concomitant with increased Rb phosphorylation and decreased cell cycle inhibitor p21 (Rathbone et al., 2009). In this context, Sirt1 might act by down-regulating myostatin signaling, which impedes MP proliferation (Wang et al., 2016). The effect of Sirt1 was also studied in the context of myogenic differentiation that showed it can inhibit myogenic differentiation by repressing muscle specific transcription factor MyoD (Fulco et al.,

2003). Increased Sirt1 activity during glucose starvation also impeded myogenic differentiation (Fulco et al., 2008).

Both Sirt1 and SCs have been shown to decline with ageing, suggesting that increasing Sirt1 might rescue age related decline in metabolic functions and muscle regeneration capacity (Myers et al., 2019; Zhang et al., 2016). Indeed, resistance training along with Sirt1 activator resveratrol, increased SC proliferation capacity improving muscle regeneration and function in ageing (Alway et al., 2017). Furthermore, it was shown that NAD^+ repletion in ageing mice enhanced mitochondrial function most likely by elevating Sirt1 activity. In this case, NAD^+ repletion in ageing and *mdx* mice also enhanced SC activation with improved muscle regeneration capacity following injury (Zhang et al., 2016). Notably, SCs with Sirt1 specific deletion, failed to become activated, promote muscle regeneration following injury or enhance mitochondrial function in spite of NAD^+ repletion (Zhang et al., 2016). This suggests that in the presence of appropriate stimulus Sirt1 might rejuvenate mitochondrial function and improve muscle regeneration potential in ageing.

1.15 Retinoblastoma susceptibility protein 1, Rbl1 (p107)

Rbl1 (p107) is a member of the retinoblastoma susceptibility (Rb) gene family of co-transcriptional repressors that also consists of the proteins Rb1 (Rb) and Rbl2 (p130). The Rb gene family are conserved across many species and are known to regulate proliferation by controlling cell cycle, differentiation, senescence and apoptosis (Henley and Dick, 2012; Fisher and Muller, 2017). Rb was first identified as the tumour suppressor gene mutated in retinoblastoma, a rare childhood cancer (Lee et al., 1987; Manning & Dyson, 2011). Subsequent research demonstrated that a variety of human cancers could be caused by mutation of Rb or its functional pathway (Chinnam & Goodrich, 2011). Conversely p107 and p130 are rarely mutated or not directly

inactivated in human cancers, but their function is adversely affected in response to Rb mutation (Burkhart & Sage, 2008).

All three proteins share homology at the N terminal domain, bipartite pocket domain and C terminal domain **(Figure 1.9)**.

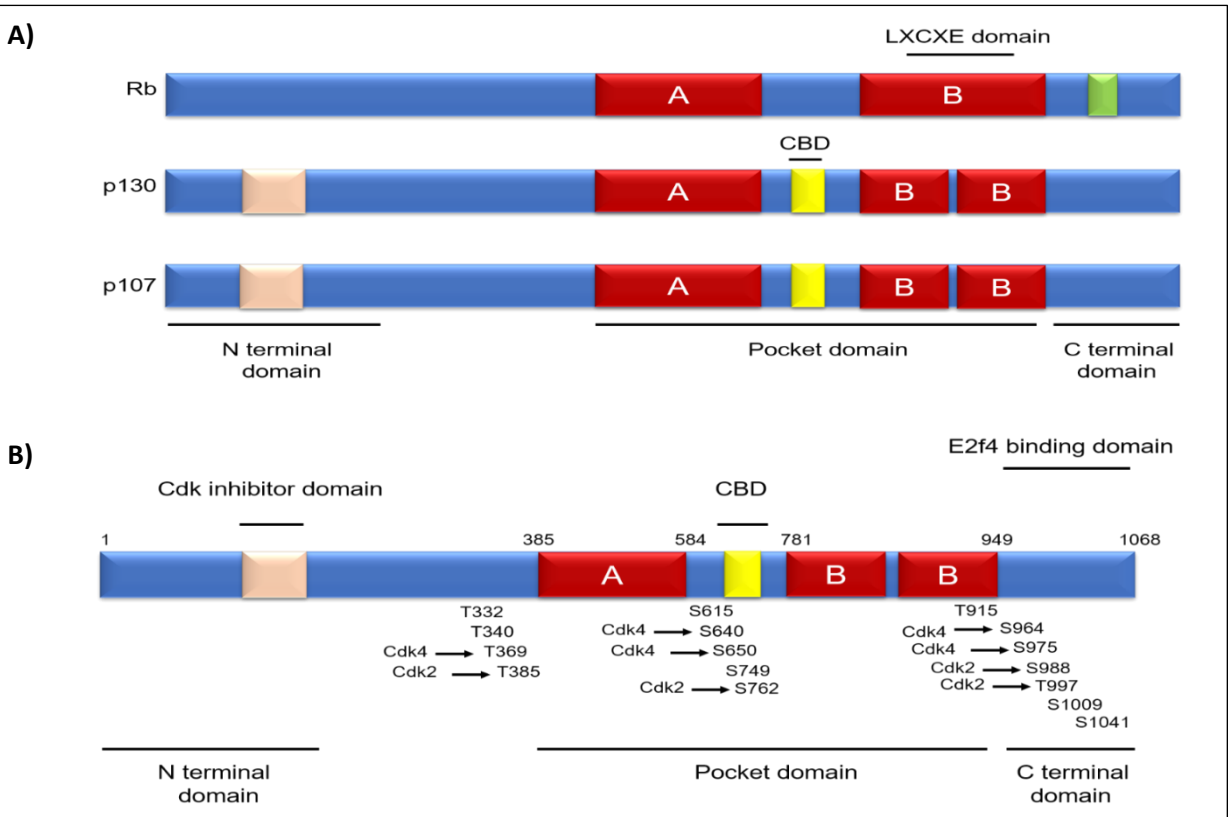

Figure 1.9: Schematic representation of Rb, p130 and p107 structural and functional domains. **(A)** Common structural domains of Rb, p107 and p130 showing N terminal domain, pocket domain containing the LXCXE motif and C terminal domain. **(B)** Representation of p107 structural domains showing N terminal domain that contains cyclin dependent kinase (Cdk) inhibitor domain, A and B pocket domain that has cyclin binding domain (CBD) and a C terminal domain that binds E2f4. Identified Threonine (T) and Serine (S) phosphorylation sites and their respective kinases are noted.

The pocket domain of all three members contain a cleft that binds the LXCXE motif originally identified in viral oncoproteins (Lee et al., 1998; Mulligan & Jacks, 1998). Unlike Rb, p107 and p130 have a long spacer region between the bipartite pocket domain that binds cyclins

and also a cyclin dependent kinase inhibitor domain in the N-terminus (Faha et al., 1992; Hannon et al., 1993; Li et al., 1993; Wirt & Sage, 2010). In addition, p107 and p130 can also bind cyclin A/Cdk2 or cyclin E/Cdk2 and prevent their kinase activity through the spacer region between A and B pocket domain **(Figure 1.9)** (Castaño et al., 1998; Ewen et al., 1992; Lees et al., 1992; Classon & Dyson, 2001; Woo et al., 1997).

As with Rb and p130, p107 does not bind to DNA directly to repress nuclear gene expression, but primarily interacts with the transcription factor E2f4 or E2f5 **(Figure 1.10)** (Attwooll et al., 2004; Müller et al., 2001; Wirt & Sage, 2010; Young et al., 2003a). It has also been shown to interact with E2f1, E2f2 and E2f3 as a compensatory role in repressing transcription of E2f targeted genes in the absence of Rb (Hurford et al., 1997; Lee et al., 2002). The C terminal domain of p107 is important for binding to the transactivation domain of the E2f transcription factor family (Giacinti & Giordano, 2006; Zhu et al., 1995).

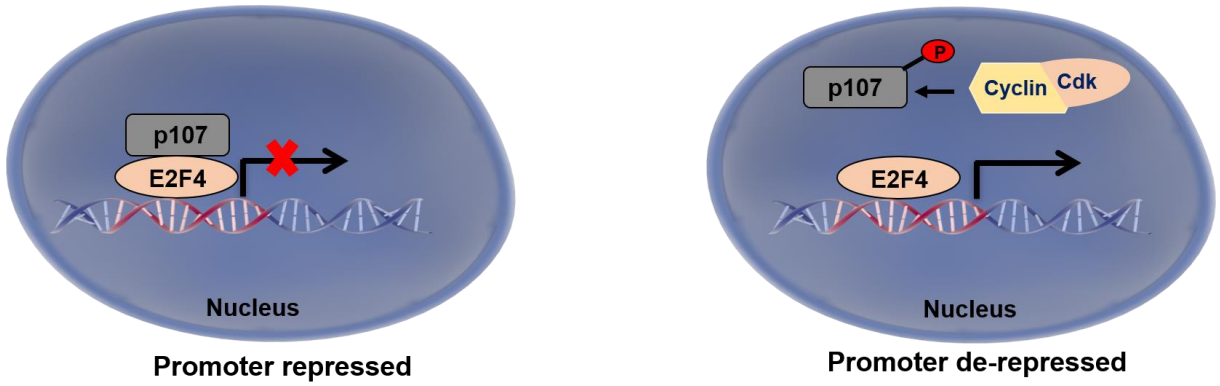

Figure 1.10: Diagram for p107 nuclear function. In the nucleus p107 cannot bind to the DNA directly, but with the E2f4 transcription factor it represses cell cycle genes. Upon phosphorylation by Cyclin/Cdks, p107 gets deactivated that abrogates its binding with E2f4, thereby de-repressing gene transcription.

Phosphorylation by cyclin/Cdks, abrogate p107 binding to E2f4 thereby de-repressing gene expression. In mid G1 of the cell cycle, it is phosphorylated by cyclin D/Cdk4 or Cdk6 in the cytoplasm (Beijersbeigen et al., 1995; Xiao et al., 1996) and eventually by cyclin A or E/Cdk2 in late G1 or G1/S phase when it enters the nucleus (Chittenden et al., 1993; Cobrinik et al., 1993; Lees et al., 1992; Lindeman et al., 1997; Müller et al., 1997; Rodier et al., 2005; Schwarz et al., 1993; Shirodkar et al., 1992; Verona et al., 1997; Zini et al., 2001). p107 remains phosphorylated until dephosphorylation most likely by protein phosphatase 2A (Balciunaite et al., 2005; Garriga et al., 2004; Kolupaeva et al., 2008).

p107 expression is very low or non-existent during quiescence and in most differentiated cells, but is highly expressed in proliferating cells (Beijersbergen et al., 1994; Burkhart & Sage, 2008; Garriga et al., 1998; Wirt & Sage, 2010). It was demonstrated that p107 genetically deleted (p107KO) embryonic fibroblasts and primary MPs showed accelerated cell cycle rate compared to controls (LeCouter et al., 1998). In this context, over expression of p107 in some cell types has been shown to repress cell cycle progression. It arrests cell cycle at G1 in some cell types such as osteosarcoma cell lines (SaOS-2 and U2-OS), cervical carcinoma cell line, C33A (Jiang et al., 2000; Xiao et al., 1996; Zhu et al., 1993) but could not suppress proliferation of osteosarcoma cell line MG63 and the breast carcinoma cell line MCF7 (Zhu et al., 1993). It is not understood why p107 has differential effects on different cell lines, nor if the cell cycle is repressed through its direct interaction with E2f4 in the nucleus.

p107 has also been shown to inhibit cell cycle progression through possible interactions with cytoplasmic factors (Wirt & Sage, 2010). p107 downregulates S-phase kinase associated protein 2 (Skp2), that promotes G1/S phase transition by stabilizing Cdk inhibitor p27 in the cytoplasm of proliferating cells (Rodier et al., 2005). The stabilized p27 inhibit cyclin E/Cdk2

which helps in cell cycle progression (Hwang & Clurman, 2005; Rodier et al., 2005). Also p107 was shown to bind Smad3 in the cytoplasm, in response to the cytokine TGFß and together enter the nucleus, thereby repressing transcription of the cell cycle regulator c-Myc along with E2f4 (Chen et al., 2002).

A number of mechanisms have been proposed to account for Rb family mediated transcriptional repression (Dunaief et al., 1994; Ferreira et al., 2001; Trouche et al., 1997). Active repression by p107 might involve a mechanism by which condensed chromatin structure is enhanced through histone deacetylation and methylation. p107 has been shown to interact with chromatin modifiers histone deacetylase 1 (HDAC1) and histone methyltransferase SUV39H1, to alter chromatin structure thereby repressing transcription of target genes (Ferreira et al., 1998, 2001; Iavarone & Massagué, 1999; Stiegler et al., 1998). In addition, it has been reported that in late G1, pocket protein repressor complexes dissociate from E2f responsive promoters, accommodating histone acetylation for transcriptional activation (Rayman et al., 2002; Taubert et al., 2004).

Recently, an evolutionarily conserved protein complex known as DREAM (dimerization partner,-RB-like,-E2F and multi vulval class B (MuvB)) has been shown to repress cell cycle genes by scaffolding MuvB proteins with E2f transcription factors and Rb family proteins (Guiley et al., 2015; Mages et al., 2017; Pilkinton et al., 2007). MuvB, which is an important component of the DREAM complex contains protein homologues in the form of sub-complex (LIN9, LIN37, LIN52, LIN54 and RBAP48) (Harrison et al., 2006; Korenjak et al., 2004; Lewis et al., 2004; Van Den Heuvel & Dyson, 2008). Less information is known for the role of p107 in the DREAM complex than for p130 and RB. It is well documented that p130 represses cell cycle genes at G0 phase of the cell cycle by binding with DREAM. p107 has been shown to bind with MuvB sub-complex in

some cell lines including HeLa, glioblastoma cell line (T98G), embryonic human kidney cell line (HEK293), fibroblast cell lines (BJ-HTERT) and U2-OS cells, although the control mechanism is not elucidated in regards to specific stage of the cell cycle or cellular condition (Guiley et al., 2015; Litovchick et al., 2011; Schmit et al., 2007). In this case the LXCXE motif of p107 interacts with dual-specificity tyrosine phosphorylation-regulated protein kinase 1A (DYRK1A) mediated phosphorylated LIN52 to form DREAM (Guiley et al., 2015; Litovchick et al., 2011; Schmit et al., 2007). Recently, it was shown that p107 can only repress G1/S phase with DREAM complex in SaOS-2 cells, when both p130 and Rb are absent (Schade et al., 2019b). Additionally, in the absence of p130, it was shown to repress cell cycle genes at G0 phase of cell cycle (Schade et al., 2019a). Also in mice lacking p130 and a p107 mutant allele that is incapable of binding to MuvB a functional DREAM complex was not made and repression of E2f-dependent cell cycle genes was lost (Forristal et al., 2014; Litovchick et al., 2007). Thus, suggesting that it binds with the DREAM complex when providing a compensatory role for Rb and/or p130. Another study showed that, p107 along with p130 can inhibit G2/M genes by interacting with the DREAM complex, following p53 activation in response to DNA damage (Schade et al., 2019) Upon cell cycle entry, p130 releases MuvB and recruits cell cycle regulator, BMyb and FoxM1 to upregulate mitotic gene expression (Sadasivam et al., 2012). However, it is not clear if p107 also releases repression of cell cycle genes by switching its interaction with MuvB to BMyb (Litovchick et al., 2011).

1.16 p107 and metabolic regulation

Several studies have shown that p107 has a profound influence on energy metabolism. Scimè et al., showed that p107 genetically deleted mice (p107KO) developed thermogenic and oxidative “brown-type” instead of white adipocytes (Scimè et al., 2005). Furthermore, p107KO and knockdown (p107KD) stem cells were committed to the thermogenic adipose lineage both in

vitro and in vivo (De Sousa et al., 2014). In addition, p107 has been shown to have a role in determining the metabolic state of adipose progenitors by regulating energy expenditure that in turn governs their lineage fates (Porras et al., 2017). Recently, it has been demonstrated to be involved in mediating the thermogenic program of cancer associated human adipocyte precursors by governing their metabolic function (Cantini et al., 2020).

For skeletal muscle, it was shown that p107 plays a crucial role in determining fiber types. p107 deficient mice have higher levels of oxidative MyHC type I and type IIA fibers (Scimè et al., 2010). Importantly, the differentiation of p107KO primary MPs resulted in more oxidative myotubes (Scimè et al., 2010). Though, it is not known at what level p107 controls fiber type formation, the result suggests that it is SC and/or MP cell autonomous. Thus, p107 might function in either of these cells and be involved in one of the multiple signaling pathways that are reprogrammed during muscle fiber type determination and switching.

CHAPTER 2
RATIONALE, HYPOTHESIS and OBJECTIVES

Rationale

Mounting evidence have shown that Rb and p107, members of the retinoblastoma family of transcriptional nuclear co-repressors, which are associated with regulating cell cycle, also influence the energy status of cells and tissues (Baar et al., 2002; Dali-Youcef et al., 2007; De Sousa et al., 2014; Fajas, 2013; Jones et al., 2016; Petrov et al., 2016; Porras et al., 2017; Scimè et al., 2005, 2010; Zacksenhaus et al., 2017). In particular, our lab has shown that p107 is necessary for the adipocyte progenitor fate decision of white versus beige fat lineages (De Sousa et al., 2014; Porras et al., 2017; Scimè et al., 2005). In this case, p107 governs the adipocyte lineage fate decision by regulating energy expenditure of progenitor cells (Porras et al., 2017). Unexpectedly, p107 depleted progenitors are primed for pro-thermogenic adipocyte commitment owing to their reliance on aerobic glycolysis. Inhibiting aerobic glycolysis convert their differentiation potential from beige to white adipocyte lineages (Porras et al., 2017). Thus, p107 controls adipocyte progenitor fate decision through metabolic control in the nucleus.

For skeletal muscle, p107 has been shown to determine the metabolic phenotype of myofibers (Scimè et al., 2010). p107 deficient mice have higher levels of oxidative type I and type IIA muscle fibers with enhanced metabolism. It is not known how p107 prevalence controls fiber type formation. However, the differentiation of p107KO primary MPs resulted in the formation of oxidative myotubes, suggesting a SC and/or MP intrinsic mechanism (Scimè et al., 2010).

We thus **Hypothesize** that "**p107 has a metabolic role in muscle stem cells that potentially regulates their fate decisions**"

We have undertaken four specific Objectives to answer this question:

Objectives

Objective 1: Establish a p107 metabolic function in MPs (Chapter 4)

We delineated a mitochondrial function of p107 in MPs. First, as p107 is a known nuclear co-repressor, we investigated and determined that it interacted at the mtDNA regulatory D-loop region. We found that this interaction influenced mtDNA gene expression, ETC complex formation and mitochondrial ATP generation.

Objective 2: Determine the upstream regulatory factor(s) that govern p107 metabolic function in MPs (Chapter 5)

We dissected the upstream regulatory factor(s) that control p107 mitochondrial localization, hence its function in this organelle. We deciphered how the glycolytic output, NAD^+/NADH, directed p107 mitochondrial localization and function. In this regard, we highlighted that p107 interacted with Sirt1, a known energy sensor of NAD^+/NADH. We also underscored that Sirt1 regulation of mitochondrial encoded gene expression and ATP generation was dependent on p107.

Objective 3: Determine how p107 metabolic function affects cellular homeostasis (Chapter 6)

We discovered a novel control mechanism for how cell cycle is regulated based on a mechanism that integrates ATP generation from glycolysis and mitochondria, which is linked by p107. Indeed, differential ATP generation due to presence or absence of mitochondrial p107 controlled MP proliferation rate both in vitro and in vivo.

Objective 4: Investigate the effect of exercise on p107 function in MPs (Chapter 7)

We assessed how p107 might function in MPs at the physiological level in skeletal muscle. Physiological stress caused by exercise was used to promote potential impacts on skeletal muscle SCs and/or MPs. We found that p107 protein levels were inversely correlated with the enhanced mitochondrial Oxphos following exercise in skeletal muscle.

CHAPTER 3
MATERIALS AND METHODS

Cells

The c2c12 myogenic progenitor cell line was purchased from the American Tissue Type Culture (ATTC) and grown in Dulbecco's Modified Eagle Medium (DMEM) (Wisent) containing 25mM glucose supplemented with 10% fetal bovine serum (FBS) and 1% penicillin streptomycin. Primary myogenic progenitor cells (prMPs) were grown on rat tail collagen I (ThermoFisher Scientific) coated dishes containing Ham's F10 Nutrient Mix Media (ThermoFisher Scientific) supplemented with 20% FBS, 1% penicillin streptomycin and 2.5ng/ml bFGF (PeproTech).

For the nutrient specific experiments, c2c12 cells or prMPs were grown in stripped DMEM with 10% FBS and 1% penicillin streptomycin for 20 hours supplemented with 1mM, 5.5mM or 25mM glucose; or 4mM or 20mM glutamine; or 4mM glutamine with 25mM glucose or 10mM galactose for 6 hours. For drug specific treatment, c2c12 cells were grown in DMEM with 10% FBS, 1% penicillin streptomycin, supplemented with 2.5mM oxamate (Ox) or 6mM dicholoroacetic acid (DCA) for 40 hours. For Sirt1 inhibition, cells were grown in stripped DMEM with 10% FBS, 1% penicillin streptomycin and 5.5mM glucose with or without 10mM nicotinamide (Nam) for 20 hours. For Sirt1 activation, cells were grown in DMEM with 10% FBS, 1% penicillin streptomycin with or without 10μM resveratrol (Res) and for inactivation with 50μM Res for 18 hours.

Primary myogenic progenitor cell (prMP) isolation

All animal experiments were performed following the guidelines approved by the Animal Care Committee of York University. For derivation of prMPs and tissue immunofluorescence wild type (Wt) and p107KO mice were from M. Rudnicki (LeCouter et al., 1998) maintained on a mixed (NMRI, C57/Bl6, FVB/N) background (Chen et al., 2004b). Extensor digitorum longus muscles

of 3-month aged mice were dissected from tendon to tendon and digested in filter sterilized 0.2% type 1 collagenase (Sigma Aldrich) in serum free DMEM for 30 minutes. Upon unravelling, it was transferred to a pre-warmed petri dish containing DMEM (Wisent) with 1% penicillin, streptomycin. The muscle was then flushed gently with the media until it released the fibers with an intermittent incubation at 37°C every 5 minutes. After 30 minutes, individual fibers were transferred into 24 well tissue culture plates containing pre-warmed Ham's F10 Nutrient Mix Media (ThermoFisher Scientific) supplemented with 20% FBS, 1% penicillin streptomycin and 2.5ng/ml bFGF (PeproTech). After 3 days, the fibers were transferred to rat tail collagen I (ThermoFisher Scientific) coated Ham's F10 Nutrient Mix Media with 20% FBS, 1% penicillin, streptomycin and 2.5ng/ml bFGF (PeproTech). The media was changed every alternate day, until the fibers generated prMPs that were collected by trypsinization and passaging onto collagen coated plates to remove live fibers.

Cloning

The p107mls expression plasmid that expresses p107 only in the mitochondria was made by cloning full length p107 into the pCMV6-OCT-HA-eGFP expression plasmid vector (Newman et al., 2016) that contains a mitochondrial localization signal. We used the following forward 5'-CACCAATTGATGTTCGAGGACAAGCCCCAC-3' and reverse 5'-CACAAGCTTTTAATGATTTGCTCTTTCACT-3' primer sets that contain the restriction sites Mfe1 and HindIII, respectively, to amplify a full length p107 insert from a p107 Ha tagged plasmid (Iwahori & Kalejta, 2017). The restriction enzyme digested full length p107 insert which was then ligated to an EcoRI/HindIII digest of pCMV6-OCT-HA-eGFP, which removed the HA-eGFP sequences but retained the N-terminal mitochondrial localization signal (OCT).

Transfections

The calcium chloride method was used for transfections, whereby a mixture containing a total of 10μg of plasmid DNA, 125mM $CaCl_2$ and H_2O were added dropwise to HEBS buffer (274mM NaCl, 10mM KCl, 1.4mM Na_2HPO_4, 15mM D-glucose and 42mM HEPES), incubated at room temperature for 1 hour and then added to 1×10^5 cells that had been passaged on the previous day. 18 hours post transfection, fresh DMEM containing 25mM glucose supplemented with 10% fetal bovine serum (FBS) and 1% penicillin streptomycin was added, and the cells used the next day. For overexpression studies, at least 4 different p107KO c2c12 cells were transfected as above with GFP mitochondrial localization empty vector pCMV6-OCT-HA-eGFP, (Newman et al., 2016) p107fl expressing full length p107 tagged HA, and p107mls expressing full length p107, which is directed to the mitochondria. For Sirt1 overexpression experiments, c2c12 cells were transfected with p107fl alone expressing full length p107 tagged HA or with full length (Sirt1fl) or dominant negative (Sirt1dn) Sirt1 (Boily et al., 2009).

p107KO and SirtKO cell line derivation

Crispr/Cas9 was used to generate p107 and Sirt1 genetically deleted c2c12 (p107KO and Sirt1KO) cell lines. For p107KO cells, c2c12 cells were simultaneously transfected with 3 pLenti-U6-sgRNA-SFFV-Cas9-2A-Puro plasmids each containing a different sgRNA to target p107 sequences 110 CGTGAAGTCATCCAGGGCTT, 156 GGGAGAAGTTATACACTGGC and 350 AGTTTCGTGAGCGGATAGAA (Applied Biological Materials), and for Sirt1KO with 2 Double Nickase plasmids each containing a different sgRNA to target sequences 148 CGGACGAGCCGCTCCGCAAG and 110 CCATGGCGGCCGCCGCGGAA (Santa Cruz Biotechnology). Following 18 hours of incubation, the media was changed for 6 hours and then passaged into 96 well tissue culture plates. On the next day, the media was aspirated and

replenished with DMEM containing 2mg/ml puromycin for antibiotic selection. Following, the media was changed every 2 days until cell clones were visible. Any surviving clones was grown and tested by Western blotting. For control cells, c2c12 cells were transfected by empty vector, pLenti-U6-sgRNA-SFFV-Cas9-2A-Puro (Applied Biological Materials) and selected as above.

Mitochondrial, nuclear and cytosolic isolation

For nuclear and cytoplasmic isolation, at least 1 million cells were pelleted, washed in PBS, dissolved in 500µl of cytoplasmic buffer (10mM Tris pH 7.4, 10mM NaCl, 3mM $MgCl_2$, 0.5% NP-40 with 1mg/ml of each pepstatin, leupeptin and aprotinin protease inhibitors) and incubated on ice for 5 minutes followed by rocking on ice for 5 minutes. After centrifugation at 2500g for 5 minutes at 4ºC, the supernatant was stored as the "cytoplasmic fraction". The cell pellet that represents the "nuclear fraction" was then washed 8 times with the cytoplasmic buffer and lysed with nuclear lysis buffer containing 50mM Tris pH 7.4, 5mM $MgCl_2$, 0.1mM EDTA, 1mM dithiothreitol (DTT), 40% (wt/vol) glycerol and 0.15 unit/µl benzonase (Novagen).

For mitochondrial and cytosolic isolation, at least 1 million cells were washed in PBS, pelleted, dissolved in 5 times the packed volume with isolation buffer (0.25M sucrose, 0.1% BSA, 0.2mM EDTA, 10mM HEPES, pH 7.4; with 1mg/ml of each pepstatin, leupeptin and aprotinin protease inhibitors), transferred into a prechilled Dounce homogenizer and homogenized loose (5-6 times) and tight (5-6 times) on ice. The homogenate was transferred into an eppendorf tube and centrifuged at 1000g at 4ºC for 10 minutes. The supernatant was then centrifuged at 14000g for 15 min at 4ºC and the resulting supernatant was saved as "cytosolic fraction". The pellet representing the "mitochondrial fraction" was washed twice and dissolved in 50µl of isolation buffer. The mitochondria were lysed by repeated freeze-thaw cycles (3 times each) on dry ice.

Mitochondria fractionation

Mitochondrial fractions were isolated using a hypotonic osmotic shock approach (Lu et al., 2009). For this, cells were collected by centrifugation at 1500 rpm and the cell pellet resuspended in STE buffer (250mM sucrose, 5mM Tris pH 7.4 and 1mM EGTA), Dounce homogenized and centrifuged at 1000g for 3 mins to remove cell debris. The supernatant was then centrifuged at 10,000g for 10 mins to isolate pelleted mitochondria. The mitochondria were resuspended in hypertonic STE buffer containing 250mM sucrose and centrifuged at 16000g for 10 minutes to isolate matrix (M) and inner membrane (IM) proteins from the outer membrane (OM) proteins in the pellet and supernatant, respectively. To obtain a pure mitochondria matrix protein (M) fraction the isolated mitochondria were resuspended in hypotonic STE buffer containing 25mM sucrose and centrifuged at 16000g for 10 mins. After centrifugation, the soluble inner membrane (IMS) and outer membrane (OM) protein fractions were present in the supernatant and the matrix protein fraction (M) in the pellet. To demonstrate mitochondria matrix veracity, 50μg/ml porcine trypsin (Promega) was added for 30 mins followed by 20μg/ml trypsin inhibitor aprotinin (Roche) for 10 minutes before centrifugation at 16000g for 10 mins. Only fractions containing M proteins were unavailable for trypsin digestion. As a control whole cell treatment of c2c12 cells with both buffers showed that trypsin treatment can digest p107.

Western blot analysis

For Western blot analysis, cells were lysed in RIPA buffer (0.5% NP-40, 0.1% sodium deoxycholate, 150mM NaCl, 50mM Tris-Cl, pH 7.5, 5mM EDTA) or mitochondrial isolation buffer (0.25M sucrose, 0.1% BSA, 0.2mM EDTA, 10mM HEPES, pH 7.4) containing protease inhibitors (1mg/ml of each of pepstatin, aprotinin and leupeptin). Protein lysates were loaded on gradient gels (6-15%) or 7.5% gels. Samples to be loaded were first boiled for 3 minutes in loading

buffer containing 4% SDS, 10% 2-mercaptoethanol, 20% glycerol, 0.004% bromophenol blue, 0.125M Tris HCl and 1mM DTT. Gels were run in 1X running buffer (10X running buffer contains 25mM Tris base, 192mM glycine and 0.1% SDS powder and 90% ddH_2O) and the proteins were separated by electrophoresis for 2 hours at 30 milliamps. Proteins were transferred using a wet transfer method onto a 0.45μm pore sized polyvinylidene difluoride (PVDF) membrane (Santa Cruz Biotechnology) at 4ºC for 80 minutes at 100V. The membranes were blocked for an hour at room temperature in 5% non-fat milk in Tris-buffered saline (TBS-150mM NaCl and 50mM Tris base) containing 0.1% Tween-20 (TBST). The PVDF membranes were probed overnight at 4ºC with primary antibodies (listed below) diluted in 5% non-fat milk or 1% BSA in TBST. Next day, the membranes were washed three times with TBST and secondary antibodies conjugated with horseradish peroxidase diluted in 5% non-fat milk in TBST were added for an hour at room temperature with gentle rocking. The membranes were again washed 3 times with TBST followed by a final wash with TBS for 10 minutes and visualized with chemiluminescence on photographic films. Protein levels were evaluated by densitometry using Image J software.

Primary antibodies used

α-tubulin (66031, Proteintech); Cox4 (ab16056, Abcam) and Total OXPHOS rodent WB antibody cocktail (Abcam); p107-C18, p107-SD9, histone H3-C16, Sirt1-B7, IgG-D7, Ha-tag-F7, Brdu-MoBU-1, Pax-7 (EE8) (Santa Cruz Biotech); MyoD (Novus Biologicals) and Sirt1-D1D7 (Cell Signaling). Details is in Table 2.

Co-immunoprecipitation

For Immunoprecipitation (IP), protein lysates were pre-cleared with 50μl protein A/G plus agarose beads (Santa Cruz Biotechnology) by rocking at 4ºC for an hour. The sample was centrifuged at 15000 rpm for a minute. Fresh protein A/G agarose beads along with 5μg of p107-

C18, Sirt1-B7 or IgG-D7 antibody (Santa Cruz Biotechnology) were added to the supernatant and rocked overnight at 4ºC. The next day the pellets were washed 3 times with wash buffer (50mM HEPES pH 7.0, 250mM NaCl and 0.1% Np-40) and loaded onto polyacrylamide gels and Western blotted for p107-SD9 (Santa Cruz Biotechnology) or Sirt1-D1D7 (Cell Signaling). Inputs represent 10% of lysates that were immunoprecipitated.

RNA isolation

Cells were grown in 6cm tissue culture plates, washed in PBS, scraped with 500µl of Qiazol reagent (Qiagen). To this, 100µl of chloroform was added for 3 minutes, mixed vigorously and then centrifuged at 12000g for 15 minutes that separates the samples into 3 phases. The aqueous phase was collected to which 250µl of isopropanol was added and incubated at room temperature for 10 minutes, then centrifuged at 12000g for 10 minutes. The supernatant was discarded and the pellet was washed with 500µl of 75% ethanol by centrifugation at 7600g for 5 minutes and resuspended in DNAse and RNAse free water. The RNA concentration was determined by NanoDrop 2000 (ThermoFisher Scientific).

qPCR

qPCR experiments were performed according to the MIQE (Minimum Information for Publication of Quantitative Real-Time PCR Experiments) guidelines (Bustin et al., 2009). The optical density (OD) of RNA was measured using the NanoDrop 2000 (ThermoFisher Scientific), RNA purity was inferred by the A260/280 ratio (~2.00 is pure). 1µg of RNA was reverse transcribed into cDNA using the All-in-One cDNA Synthesis SuperMix (Bimake) and the cDNA used for qPCR. qPCR assays were performed on Light cycler 96 (Roche) using SYBR green Fast qPCR Master mix (Bimake) with appropriate primer sets and Rplp0 (36B4) as a normalization control was used **(Table 1)**. Relative expression of cDNAs was determined with 36B4 as the

internal control using the ΔΔCt method. For fold change, the ΔΔCt was normalized to the control. Student t-tests, one-way or two-way Anova and Tukey post hoc tests were used for comparison and to obtain statistics.

Mitochondrial and nuclear DNA content

To obtain the mitochondrial to nuclear DNA ratio (mtDNA/nDNA), $1X10^6$ cells grown on a 6cm tissue culture plate were untreated or treated with 1mM 5-aminoimidazole-4-carboxamide-1-β-D-ribofuranoside (AICARFusher) (Toronto Research Chemicals) in presence of 5.5mM or 25mM glucose, or with or without 10mM Nam for 24 hours. The cells were washed in PBS and lysed with 600µl of lysis buffer containing 100mM NaCl, 10mM EDTA, 0.5% SDS solution, 20mM Tris HCl; pH 7.4 and 6µl of 1µg/µl proteinase k (ThermoFisher Scientific). Following incubation in the lysis buffer at 55ºC for 3 hours, 100µg/ml RNase A (ThermoFisher Scientific) was added and incubated at 37ºC for 30 minutes. After, 250µl of 7.5M ammonium acetate and 600µl of isopropanol were added, the cells were centrifuged at 15000g for 10 minutes at 4ºC. The supernatant was discarded and the pellet containing mitochondrial and nuclear DNA was washed with 70% ethanol and resuspended in Tris EDTA buffer (10mM Tris HCl pH 7.4, 1mM EDTA). qPCR assays were performed on 10ng DNA with primer sets to Mt-Co1 and H19 **(Table 1)** representing total mitochondrial and nuclear DNA content, respectively. Ct values were obtained and the ratio mtDNA:nDNA were determined by the formula: nDNA Ct- mtDNA Ct.

Quantitative chromatin immunoprecipitation assay (qChIP)

qChIP was performed on mitochondrial lysates containing only mitochondrial DNA. Mitochondrial fractions were collected as described above, washed twice in PBS by centrifugation at 14000g for 15 minutes at 4°C, resuspended in 200µl of PBS containing 1% formaldehyde and rocked at room temperature for 30 minutes to fix the cells. The fixation reaction was quenched by

adding 125mM of glycine in PBS and rocked for 5 minutes at room temperature. The fixed pellet was washed twice in PBS containing 100mM NaF and 1mM Na_3VO_4 by centrifuging at 14000g for 5 minutes at 4°C. The pellet was the resuspended in 500µl of ChIP lysis buffer (40mM Tris, pH 8.0, 1% Triton X-100, 4mM EDTA, 300mM NaCl) and sonicated at 24% amplitude, 15 seconds on, 15 second off for 3 cycles (Model 120 Sonic Dismembrator, ThermoFisher Scientific). Following sonication, the samples were centrifuged at 13000 rpm for 10 minutes at 4°C and the supernatant was transferred to a new tube containing 100µl of dilution buffer 1 (40mM Tris, pH 8.0, 4mM EDTA) from which the input controls were removed before 150µl of dilution buffer 2 (40mM Tris, pH 8.0, 0.5% Triton X-100, 4mM EDTA, 150mM NaCl) was added. To preclear, 50µl of protein A/G agarose beads (Santa Cruz Biotechnology) was added and rocked for 90 minutes at 4°C. The beads were then pelleted and discarded, and to the supernatant was added 5µg of p107 antibody (p107- C18) (Santa Cruz Biotechnology) or IgG antibody (IgG-D7) (Santa Cruz Biotechnology). This was rocked overnight at 4°C and on the following day, 50µl of protein A/G agarose beads were added and rocked for 90 minutes at 4°C. The beads were collected by centrifugation and were washed sequentially with 5 minutes rocking at 4°C before centrifugation by adding the following: low salt complex wash buffer (0.1% SDS, 1% Triton X-100, 2mM EDTA, 20mM Tris HCl, pH 8.0, 150mM NaCl), high salt complex wash buffer (0.1% SDS, 1% Triton X-100, 2mM EDTA, 20mM Tris HCl, pH 8.0, 500mM NaCl), LiCl wash buffer (0.25M LiCl, 1% NP-40, 1% deoxycholic acid, 1mM EDTA, 10mM Tris, pH 8.0) and 2 washes with TE buffer (10mM Tris HCl, pH 8.0, 1mM EDTA). After the last wash, the mtDNA-protein complexes were isolated by resuspending the beads in 250µl of elution buffer (1% SDS, 0.1M $NaHCO_3$), vortexing, rocking for 15 minutes at room temperature and centrifuging at 2000 rpm in a microcentrifuge for 2 minutes. The supernatant was transferred to a clean tube and to the remaining beads another

250μl of elution buffer was added and the isolation step repeated. For isolation of mtDNA fragments, to the 500μl of mtDNA-protein complexes in elution buffer, 20μl of 5M NaCl was added and incubated at 65°C overnight. The next day, the DNA was isolated using DNA purification kit (Thermo Fisher Scientific), and the concentration determined using the NanoDrop 2000 (ThermoFisher Scientific). Relative occupancy was determined by amplifying isolated DNA fragments using the D-loop primer sets **(Table 1)** analyzed using the ΔΔCt method and the fold changes were normalized to IgG ΔΔCt values.

NAD^+/NADH assay

Cells growing in 6cm tissue culture plates were washed with PBS and scraped into 500μl of 0.5M perchloric acid, vortexed and freeze-thawed on dry ice three times. The cells were then centrifuged at 4°C for 5 minutes at 7,000 rpm in a microfuge and 100μl of 2.2M $KHCO_3$ was added to the supernatant on ice. This was again centrifuged at 7,000 rpm for 15 minutes at 4°C and the supernatant was collected to be analyzed. For the lactate assay; 20μl of the supernatant, 258μl of lactate buffer (1M glycine, 500mM hydrazine sulfate, 5mM EDTA), 20μl of 25mM β-nicotinamide-adenine dinucleotide (NAD) (Roche) and 2μl of porcine heart lactate dehydrogenase (Ldh) (Sigma-Aldrich) were added to each well of an assay plate. For the pyruvate assay; 20μl of the supernatant, 218μl of pyruvate buffer (1.5M Tris, pH 8), 180μl of 6μM β-nicotinamide-adenine dinucleotide, reduced NAD (NADH) (Roche) and 2μl of rabbit skeletal muscle LDH (Sigma-Aldrich) were added for each well. The assay plates were then read by a microplate reader (Glomax, Promega) with excitation at 340nm and emission peak at 450nm and the concentration values were attained by comparing to standard curves. The standard curves were made with 0, 2, 3, 4, 5, 6, 7, and 10mM NADH (Roche) in lactate buffer for the lactate assay and in pyruvate buffer for the pyruvate assay. Estimation of free NAD^+/NADH in cells was based on lactate/pyruvate

(pyruvate + NADH + H^+ = lactate + NAD^+) (Sun et al 2012). The results were normalized to control samples and graphed.

ATP generation capacity and rate assay

The ATP generation capacity assay is based on the requirement of luciferase for ATP in producing light from the reaction:

$$\text{Luciferin} + \text{ATP} + O_2 \xrightarrow{\text{Luciferase}} \text{Oxyluciferin} + \text{AMP} + \text{Pyrophosphate} + CO_2 + \text{Light}$$

It was measured from mitochondrial fractions by using the ATP determination kit (ThermoFisher Scientific). In each well of a 96 well assay plate, 10µl of the isolated mitochondria was added to 4µl of 100mM ADP and 86 µl of reaction mix (1.78µl ddH_2O, 100µl of 20X reaction buffer, 20µl of 0.1M DTT, 100µl of 10mM D-luciferin and 0.5µl firefly luciferase from a 5mg/mL stock solution, all supplied by the kit manufacturer) in room temperature. The plate was then read over a period of 15 minutes every 1 minute for emission peak at 560 nm by a microplate reader (Glomax, Promega). The amount of ATP generated was normalized to the protein content of the mitochondrial fractions determined by Bradford Assay Kit (Biobasic) and graphed over time. The ATP generation rate was calculated from the slope of the graph of ATP that was produced over time up to the point where its production reached a steady state.

Immunocytochemistry and confocal imaging

For confocal microscopy, cells were grown on Nunc Lab-Tek™ II chambered tissue culture plates (ThermoFisher Scientific), fixed for 5 minutes with 95% methanol and permeabilized for 30 minutes at 4ºC with blocking buffer (3% BSA and 0.1% saponin in PBS). Cells were then incubated with primary antibody p107-SD9 or HA-tag-F7 (Santa Cruz Biotechnology) in 1:100 dilution in blocking buffer for 1 hour. After 3 washes with 0.05% saponin

in PBS (SP), cells were incubated with secondary antibody donkey anti-mouse IgG NL493-conjugated (R and D Systems) at a 1:200 dilution in blocking buffer. Cells were then washed 3 times in SP and re-incubated with primary antibody Cox4 (Abcam) at a 1:100 dilution in blocking buffer for 1 hour. After 3 washes in SP, cells were incubated with secondary antibody goat anti rabbit IgG Alexa Fluor 594 (ThermoFisher Scientific) in 1:200 dilution for 1 hour. After, washing 3 times with SP, 4′,6-diamidino-2-phenylindole (Dapi) was added and Vectashield mounting media (Vector) was added before placing the coverslip. Confocal images and Z-stacks were obtained using the Axio Observer.Z1 microscope with alpha Plan-Apochromat 63x/Oil DIC (UV) M27 (Zeiss). Digital images were captured using Axiocam MR R3 (Zeiss). Optical sections were then "stacked" or merged to create high resolution "z-series" images. Z-stack images were also portrayed as orthogonally projected on XY, YZ and XZ plane with maximum intensity using ZEN imaging software (Zeiss). A line was drawn through a representative cell to indicate relative intensity of RGB signals.

Mitochondrial length and area measurement

Live cell imaging was used to measure mitochondrial length and area of **c**ells grown on 35mm high glass-bottom µ-Dish tissue culture plates (MatTek Corp). The cells were washed with PBS and stained with 1µl of MitoView red (Biotium) in 5mls of serum free DMEM for 30 minutes. The cells were then washed with PBS and refed with serum free DMEM and immediately live cell imaged using the Axio Observer.Z1 (Zeiss) microscope with alpha plan-apochromat 40x/Oil DIC (UV) M27 (Zeiss) in an environment chamber (5% CO_2; 37°C). Digital images were captured using Axiocam MR R3 (Zeiss). Mitochondrial length was measured by tracing the mitochondria from one end to the other with a line that was calibrated to the scale bar using Image J software. Area was measured using Image J software. Briefly, threshold was used to select the area of each

mitochondria. The background was eliminated and using analyze particle, the area of each mitochondria was measured by considering the scale bar as the reference point. At least 100 mitochondria were measured for length and area from each of 3 different controls (Ctl) and p107KO c2c12 cells. The measurements were categorized and graphed within different intervals of lengths and areas, respectively.

Cardiotoxin-induced muscle regeneration

Three-month-old anesthetized wild type and p107KO mice were injected intramuscularly in the tibialis anterior (TA) muscle with 40µl of cardiotoxin (Ctx) Latoxan (Sigma) that was prepared by dissolving in water to a final concentration of 10µM. A day after Ctx injury, bromodeoxyuridine (Brdu) at 100mg/kg was injected intraperitonially. TA muscles were collected on day 2 post Ctx injection, immersed in a 1:2 ratio of 30% sucrose:optimal cutting temperature compound (ThermoFisher Scientific) solution and frozen slowly in liquid nitrogen-cooled isopentane. Mice were also untreated or treated with 750mg/kg oxamate (Ox) for four consecutive days, with Ctx on the third day and Brdu on the fourth day, before the TA muscles were dissected on the fifth day for freezing.

Immunohistochemistry

The frozen samples were cross sectioned at 10µm thickness on a cryostat and mounted on positive charged slides (FroggaBio). Muscle tissue sections were washed with PBS and fixed with 4% paraformaldehyde (PFA) for 15 minutes at room temperature. 2N HCl was added for 20 minutes followed by 40mM sodium citrate for 10 minutes at room temperature. After washing in PBS, muscle sections were blocked in blocking buffer (5% goat serum, 0.1% Triton X in PBS) for 30 minutes. Muscle tissue sections were then incubated with primary antibody anti-MyoD (Novus Biologicals) in blocking buffer in 1:100 ratio overnight or p107-SD9 or Pax7-EE8 in blocking

buffer in 1:100 ratio for 90 minutes. After three washes in 0.05% Tween 20 in PBS (PBST), cells were incubated with secondary antibody goat anti rabbit IgG Alexa Fluor 594 (ThermoFisher Scientific) or donkey anti-mouse IgG NL493-conjugated (R and D Systems) for one hour in 1:200 ratio. After three washes in PBST the tissue section was re-incubated with primary antibody Brdu-MoBU-1 (Santa Cruz Biotechnology) or Cox4 (Abcam) in blocking buffer in 1:100 ratio for 1 hour. After washing 3 times in PBST, the tissue section was incubated with secondary antibody donkey anti-mouse IgG NL493-conjugated (R and D Systems) or goat anti rabbit IgG Alexa Fluor 594 (ThermoFisher Scientific) in 1:200 ratio for 1 hour. After washing 3 times in PBST, Dapi was added and Vectashield mounting media (Vector) was added before placement of coverslip. The sample was imaged using confocal microscopy with the Axio Observer.Z1 microscope with alpha Plan-Apochromat 40x/Oil DIC (UV) M27 (Zeiss). Pax7 positive proliferating MPs containing p107 co-localized with Cox4 were identified in successive tissue sections that were cut at 6μm instead of 10μm. Proliferating MPs were determined by enumerating the $MyoD^{+}Brdu^{+}Dapi^{+}$ cells as a percentage of all the $Dapi^{+}$ cells per field. Six fields per muscle section from 4 to 5 different mice for each treatment was used for the analysis.

Growth curve and Proliferation Rate

3000 cells were plated for both control and p107KO c2c12 cells that were untreated or treated with 2.5mM Ox. On each of the following 3 days, the number of cells were counted and graphed. Proliferation rate was calculated from the slope of the cell proliferation over time.

Flow Cytometry

For cell cycle analysis 50000, Ctl and p107KO c2c12 cells were treated or untreated with 2.5mM Ox for 40hrs or Ctl and Sirt1KO c2c12 cells were grown in 5.5mM glucose, to activate Sirt1, for 20 hours or p107KO cells 24 hours post transfection with pCMV6-OCT-HA-eGFP alone

or together with p107fl or p107mls were used. The cells were washed twice with PBS by centrifuging at 1200g for 5 minutes and re-dissolved in 1ml of PBS. Cells were then fixed by adding the cell suspension dropwise to 9ml of 70% ethanol while vortexing and then kept at -20°C overnight. The next day, the fixed cells were pelleted at 4000 rpm for 5 minutes and resuspended with 3ml PBS on ice for 10 minutes to rehydrate the cells. The rehydrated cells were centrifuged at 4000 rpm for 5 minutes and dissolved in 500µl of PBS containing 50µg/ml propidium iodide (ThermoFisher Scientific) and 25µg/ml RNAse (ThermoFisher Scientific). The samples were put in 96 well plates and loaded on the Attune Nxt Flow Cytometer (ThermoFisher Scientific). Forward and side scatter were appropriately adjusted and propidium iodide was excited with the 488-nm laser and detected in the BL2 channel. The excitation was analyzed by the ModFit LT™ software that provided the percentage of cells present in each of G1, S and G2 phases of cell cycle, which were represented graphically. Flow cytometry for cell cycle analysis of transfected cells consisted of cells transfected with empty vector pCMV6-OCT-HA-eGFP expressing GFP alone or along with p107fl expressing full length p107 or with p107mls expressing full length p107, which is directed to the mitochondria. GFP positive cells were first sorted using the BL1 channel of the cytometer by adjusting forward and side scatter, followed by detection of propidium iodide that was excited with the 488-nm laser and detected in the BL2 channel. The excitation was analyzed by the ModFit LT™ software that provided the percentage of cells present in each of G1, S and G2 phases of cell cycle and represented graphically.

Live cell ATP analysis (Seahorse)

3000 proliferating or growth arrested cells, control or p107KO cells were grown for 24 hours in DMEM(Wisent) containing 10% FBS and 1% penicillin streptomycin on microplates (Agilent Technologies). Furthermore, the control cells were treated or untreated with 2.5mM

oxamate in DMEM containing 10% FBS and 1% penicillin streptomycin overnight. For transfection experiments, p107KO cells (3000) were transfected with pCMV6-OCT-HA-eGFP alone or together with p107fl or p107mls in DMEM (Wisent) containing 10% FBS and 1% penicillin streptomycin on microplates (Agilent Technologies) and left for 24 hours before performing the experiments. For analysis, on the same day of assay, the cells were washed in XF assay media supplemented with 10mM glucose, 1mM pyruvate and 2mM glutamine (Agilent Technologies) and incubated in a CO_2 free incubator in the same media at 37°C for 1 hour. The media was then removed and replenished with fresh XF media supplemented with 10mM glucose, 1mM pyruvate and 2mM glutamine and the microplate was assessed using the Seahorse XF real-time ATP rate assay kit (Agilent Technologies) on a previously calibrated Seahorse XFe96 extracellular flux analyzer (Agilent Technologies), with addition of 1.5µM of oligomycin and 0.5µM rotenone + antimycin A as per the manufacturer's direction. The energy flux data in real time was determined using Wave 2.6 software.

Mitochondrial ROS determination

50000 Ctl and p107KO cells were treated or untreated with 2.5mM Ox for 40 hours, or p107KO cells transfected with empty vector alone, p107fl, p107mls or Ctl and Sirt1KO cells were trypsinized and washed twice in PBS by centrifuging at 400g for 5 minutes. The cell pellets were resuspended in 5ml PBS with 20µM of mitochondrial ROS indicator dihydrorhodamine 123 (DHR 123) (ThermoFisher Scientific) and incubated at 37°C for 30 minutes in the dark. DHR123 is an uncharged non-fluorescent ROS indicator and is oxidized to positively charged fluorescent rhodamine 123 (R123) that accumulates in the mitochondria. After staining with DHR123, the stained cells were collected by centrifugation and re-dissolved in 500µl of PBS. ROS was then assessed by measuring the fluorescent R123 levels by flow cytometry using the Attune Nxt flow

cytometer by first adjusting forward and side scatter appropriately. R123 was excited with the 488-nm laser and detected in the BL1 channel. The data was analyzed using FlowJo software.

Statistical analysis

Statistical analysis was performed by GraphPad Prism. Student's t-tests were used unless otherwise stated. Results were considered to be statistically significant when $p < 0.05$. Specific data was analyzed using an appropriate one-way or two-way analysis of variance (ANOVA) with a criterion of $p < 0.05$. All significant differences for ANOVA testing were evaluated using a Tukey post hoc test. All data are mean ± SD.

Table 1: List of primer sets

Gene Name	Sequence Accession Number	Amplicon Length (bp)	Forward primer sequence	Reverse primer sequence
Rplp0 (36B4)	MGI:1927636	29	GAGGAATCAGATGAGGATATGGGA	AAGCAGGCTGACTTGGTTGC
mt-Nd2 (Nd2)	MGI:102500	121	CATAGGGGCATGAGGAGGACT	TGAGTAGAGTGAGGGATGGGTTG
mt-Nd6 (Nd6)	MGI:102495	44	TGTTGCAGTTATGTTGGAAGGAG	CAAAGATCACCCAGCTACTACC
mt-Co2 (Cox2)	MGI:102503	98	AGTTGATAACCGAGTCGTTCTG	CTGTTGCTTGATTTAGTCGGC
mt-Atp6 (Atp6)	MGI:99927	55	TCCCAATCGTTGTAGCCATC	TGTTGGAAAGAATGGAGTCGG
D-loop	MF 133498.1	173	GCGTTATCGCCTCATACGTT	GGTGCGTCTAGACTGTGTG
Nfe2l2 (Nrf2)	MGI:108420	146	AGAGCAACTCCAGAAGGAACAG	TGTGGGCAACCTGGGAGTAG
Mfn2	MGI:2442230	103	AGAGGCAGTTTGAGGAGTGC	ATGATGAGACGAACGGCCTC
Ppargc1a (Pgc-1α)	MGI:1342774	126	TACGCAGGTCGAACGAAACT	ACTTGCTCTTGGTGGAAGCA
Nrf1	MGI:1332235	154	GTTGGTACAGGGGCAACAGT	TCGTCTGGATGGTCATTTCA
H19	MGI:95891	207	GTACCCACCTGTCGTCC	GTCCACGAGACCAATGACTG
Mt-Co1	MGI:102504	342	CCCAATCTCTACCAGCATC	GGCTCATAGTATAGCTGGAG
Slc25a4 (ANT 1)	MGI:1353495	174	GTCTCTGTCCAGGGCATCAT	ACGACGAACAGTGTCAAACG

Table 2: List of antibodies

Target Protein	Antibody name	Host/Class	Company
p107	p107-C18	Rabbit polyclonal	SantaCruz Biotechnology
p107	p107-SD9	Mouse monoclonal	SantaCruz Biotechnology
α-tubulin	α-tubulin	Mouse monoclonal	Proteintech
Cox4	Cox4 (ab16056)	Rabbit polyclonal	Abcam
IgG	IgG-D7	Mouse monoclonal	SantaCruz Biotechnology
MyoD	MyoD	Rabbit polyclonal	Novus Biologicals
Brdu	Brdu-MoBU-1	Mouse monoclonal	SantaCruz Biotechnology
NDUFB8 SDHB UQCRC2 MTCO ATP5A	Total OXPHOS rodent WB antibody cocktail	Total OXPHOS rodent WB antibody cocktail	Abcam
Sirt1	Sirt1- B7	Mouse monoclonal	SantaCruz Biotechnology
HA	HA-tag- F7	Mouse monoclonal	SantaCruz Biotechnology
Pax7	Pax-7 (EE8)	Mouse monoclonal	SantaCruz Biotechnology
		Goat anti-rabbit antibody	Biorad
		Rabbit anti-goat antibody	Biorad
		Goat anti-mouse antibody	Biorad
		Anti-mouse NL493 conjugated donkey IgG (HRP)	R and D Systems
		Alexa Fluor 594 goat anti rabbit IgG (HRP)	Life Technologies

CHAPTER 4

p107 regulates mitochondrial ATP generation via mitochondrial gene expression

Abstract

Advances in the field of bioenergetics have shed light on metabolic regulation of stem cell fates that in particular cast the mitochondria in maintaining and dictating stem cell state outcomes (Shyh-Chang & Ng, 2017). In this regard, mitochondrial contribution in myogenic stem cell fates has also gained consideration (Bhattacharya & Scimè, 2020). Disrupted mitochondrial function is associated with muscle wasting diseases and ageing; wherein impaired SC self-renewal and/or limited number of their proliferating committed progenitors, MPs, is observed (Brack & Muñoz-Cánoves, 2016). In this chapter we have showcased a novel mechanism for regulating mitochondrial ATP generation in MPs, by the transcriptional co-repressor p107. In vivo, we found that p107 localizes in the mitochondria of activated and proliferating MPs. In vitro, using MP primary cells and cell lines, we found that during proliferation p107 acts in the mitochondria, by interacting at the mtDNA D-loop promoter. Here it represses mitochondrial encoded genes, thereby limiting the availability of ETC complex proteins, resulting in reduced ATP generation. Indeed, compared to controls, absence of p107 in p107KO MP cell lines, leads to enhanced mitochondrial gene expression, ETC complex protein formation with consequential significantly increased ATP production capacity.

Results

p107 is localized in the mitochondria of myogenic progenitor cells

p107 is normally present in the cytoplasm during proliferation of different cell types and enters the nucleus in late G1 or G1/S phase of the cell cycle (Lindeman et al., 1997; Heiko Müller et al., 2001; Rodier et al., 2005; Verona et al., 1997; Wirt & Sage, 2010; Zini et al., 2001). We confirmed its cytoplasmic presence in actively proliferating MP cells by assessing the MP cell line c2c12. For this, cytoplasmic and nuclear fractions of proliferating c2c12 cells were Western blotted for p107. As is the case in other cell types, we also found that p107 is present in the cytoplasm of proliferating MPs **(Fig. 4.1A)**. Considering the emergent findings that showed p107 can influence the metabolic state of progenitors (Porras et al., 2017), we assessed its potential metabolic role in the cytoplasm. As mitochondria are crucial in controlling metabolism, we tested for the presence of p107 within this cytoplasmic organelle. We compared the mitochondria to the remainder of the cytoplasmic proteins of proliferating and contact inhibited confluent growth arrested c2c12 cells. We chose to assess contact inhibited cells because in mouse fibroblastic CH310T1/2 cell line, p107 is known to translocate to the nucleus from the cytoplasm when growth arrested in this manner (Porras et al., 2017). Intriguingly, Western blot analysis demonstrated that p107 was in the mitochondria of the cells during proliferation **(Fig. 4.1B)**. On the contrary, when the cells were contact inhibited in growth arrested cultures, p107 was negligible in the mitochondria **(Fig. 4.1B)**.

To further assess for the presence of p107 in the mitochondria, we used a biochemical method utilizing osmotic shock, by varying sucrose concentration to isolate various mitochondria sub-fractions in c2c12 cells (Lu et al., 2009). To accomplish this, the intact mitochondria were dissolved in hypertonic buffer containing 250mM sucrose that separated the outer membrane (OM) from the matrix (M) and inner membrane (IM) proteins. To isolate the pure M proteins,

mitochondria were dissolved in hypotonic buffer containing 25mM sucrose. This caused osmotic shock, swelling the inner membrane and rupturing the outer membrane, thereby separating the soluble inner membrane (IMS) and OM protein fractions from the M protein fraction **(Fig. 4.2A)**. This method enabled us to investigate p107 presence in different mitochondrial fractions. We found that p107 was not located in the OM nor in the IMS protein fractions, but localized within the M fraction of the mitochondria **(Fig. 4.2B)**. To further demonstrate the purity of the M protein fraction, and confirm the rupture of the outer membrane, we treated the fractions with the proteolytic enzyme trypsin. We found that matrix localized p107 is resistant to trypsin digestion unlike, Cox4 in the IMS protein fraction. Additionally, p107 from the whole cell control lysate also showed sensitivity to trypsin digestion **(Fig. 4.2B)**. These data suggest that p107 is localized in the matrix and inaccessible to trypsin digestion.

We corroborated the mitochondrial localization of p107 by using confocal microscopy and subsequent analysis of generated Z-stacks, which showed p107 and the mitochondrial protein Cox4 co-localize in proliferating c2c12 cells **(Fig. 4.3B)**. The specificity of the immunocytochemistry for p107 was confirmed by the absence of immunofluorescence in p107KO c2c12 cells **(Fig. 4.3B)**. These cells were generated with Crispr/Cas9 directing p107 specific gRNAs that resulted in null protein expression that was confirmed by Western blot analysis **(Fig. 4.3A)**. p107 and Cox4 co-localization was suggested by matching fluorescence intensity peaks of a line scanned for red, green and blue (RGB) profile in which the arrows denoted overlapped peaks indicating co-localization **(Fig. 4.3C).** We also performed orthogonal projection that scrutinizes a portion of a Z-stack image in 3 projection planes (XY, YZ and XZ) to confirm p107 co-localization with Cox4. The selected part of the Z-stacked image was dissected into a frontal plane in the XY direction, a sagittal plane in the YZ direction, and a transverse plane in the XZ direction. The

generated projections in 3 different planes, confirmed that p107 and Cox4 co-localized in the mitochondria **(Fig. 4.3D)**.

As p107 was localized in the mitochondria of MP cell line, c2c12 cells, we sought if the mitochondrial localization of p107 was physiologically pertinent. This was accomplished by investigating its localization in MPs in tibialis anterior (TA) muscle of mice. In vivo, proliferating MPs arise from activated SCs that enter cell cycle, during skeletal muscle regeneration following injury (Nguyen et al., 2019; Relaix & Zammit, 2012). Thus, we induced acute skeletal muscle regeneration in mice by an intramuscular injection of cardiotoxin (Ctx) into the TA muscle. Ctx belongs to the family of snake venom toxins that causes myolysis of myofibers, triggering their injury and subsequent regeneration (Guardiola et al., 2017). Two days post injury, we isolated and processed the tissue for immunohistochemistry **(Fig. 4.4A)**. By confocal microscopy, we found that p107 co-localized with Cox4 in MPs derived from activated SCs that expressed Pax7 **(Fig. 4.4B)**. Together, this data showcases that p107 is present in the mitochondria of MPs both in vitro and in vivo.

We next confirmed that p107 also localized in the mitochondria of primary MPs (prMPs) obtained from mouse skeletal muscle. We isolated prMPs from wild type (Wt) and p107KO extensor digitorum longus (EDL) myofibers. Confocal microscopy and subsequent analysis of generated Z-stacks also showed that p107 and the mitochondrial protein Cox4 co-localized in Wt prMPs that was supported by the lack of p107 immunofluorescence in p107KO prMPs **(Fig. 4.5A)**. Also, similar to c2c12 cells, p107 and Cox4 fluorescence intensity peaks were matched on a line scanned RGB profile that showed several overlapping peaks indicative of co-localization in Wt prMPs **(Fig. 4.5B)**. An orthogonal projection of a Z-stack also showed co-localization in 3

projection planes; frontal in the XY direction, sagittal in the YZ direction, and transverse in the XZ direction; thereby corroborating p107 and Cox4 co-localization in prMPs **(Fig. 4.5C)**.

Thus, by Western blotting, confocal immunocytochemistry, confocal immunohistochemistry and biochemical analysis, we confirmed that p107 localized in the mitochondria of MPs from both primary cells and cell lines suggesting that it might have an important function in this organelle.

p107 interacts at the mtDNA

To find the functional consequence of p107 mitochondrial matrix localization, we assessed if it interacted at the mtDNA to repress mitochondrial gene expression, similar to its role as a co-transcriptional repressor on nuclear promoters (Wirt & Sage, 2010). We evaluated this potential by first performing quantitative chromatin immunoprecipitation (qChIP) analysis for the D-loop regulatory region of isolated mitochondria from c2c12 cells. qChIP revealed that p107 interacted at the mtDNA of proliferating cells, when it was present in the mitochondria **(Fig. 4.1B and 4.6B)**. The interaction was not readily discernible in growth arrested cells where p107 levels were deficient in the mitochondria and not detected in p107KO cells **(Fig. 4.6B)**. Immunoglobulin G (IgG) antibody was used as a negative control for non-specific antibody-chromatin interaction in the proliferating and growth arrested cells. We found that unlike differential binding of p107, IgG showed negligible interaction at the D-loop regulatory region of the mtDNA **(Fig. 4.6B)**. This data suggests that the interaction of p107 at the mtDNA regulatory region might repress mitochondrial encoded gene expression.

p107 represses mtDNA encoded gene expression

We next appraised if its promoter occupancy at the mtDNA D-loop might repress mitochondrial encoded gene expression. For this we performed quantitative PCR (qPCR) of 4 of

13 mitochondrial encoded genes that are subunits of 3 of the 5 ETC complexes. qPCR analysis showed that during proliferation when p107 was abundant in the mitochondria, there was significantly less expression of the mitochondrial encoded genes for complex I, *NADH dehydrogenase 2* (*Nd2*) and *NADH dehydrogenase 6* (*Nd6*); complex IV, *cytochrome c oxidase 2* (*Cox2*) and complex V, *ATP synthase 6 (Atp6)*, compared to growth arrested cells where p107 was barely present **(Fig. 4.7)**.

We confirmed the potential of p107 to repress mitochondrial gene expression by assessing p107KO MPs. qPCR analysis showed that p107KO c2c12 cells had significantly increased mitochondrial encoded gene expression for *Nd2, Nd6, Cox2* and *Atp6* compared to control cells during proliferation **(Fig. 4.8A)**. The expressions of these mitochondrial encoded genes were also significantly upregulated in p107KO prMPs compared to Wt prMPs during proliferation **(Fig. 4.8B).** Thus, the absence of p107 on the mtDNA promoter of p107-deleted cells, resulted in de-repression of the mitochondrial encoded genes.

We further tested the mitochondrial function by rescuing the de-repression found in p107KO cells by adding back p107. For this we used transient transfection assays of p107KO cells that were over expressed with empty vector, full length p107 (p107fl) or p107 possessing a mitochondrial localization sequence (p107mls). Western blotting of cytoplasmic and mitochondrial fractions 48 hours post transfection showed that p107fl was present in both the cytoplasmic and mitochondrial fractions and p107mls was solely present in the mitochondria **(Fig. 4.9A)**. To further confirm their localization capacity, we performed confocal microscopy immunofluorescence and Z-stack analysis after transfection with empty vector, p107fl or p107mls. Similar to the Western blot results, p107mls co-localized only in the mitochondria with Cox4, unlike p107fl which was present in both cytoplasm and mitochondria and to a lesser extent in the

nucleus **(Fig. 4.9B)**. As both constructs were shown to be in the mitochondria, we evaluated the functional consequence of adding back p107 to the p107KO cells. qPCR analysis showed significantly decreased mitochondrial gene expression for *Nd2*, *Nd6*, *Cox2* and *Atp6* in p107KO c2c12 cells overexpressing p107fl or p107mls compared to that transfected with empty vector **(Fig. 4.10A, 4.10B, 4.10C and 4.10D)**. Importantly, this suggests that the repression of mitochondrial encoded gene expression is due to a p107 mitochondrial specific function.

p107 limits electron transport chain complex formation

As mitochondrial genes are crucial for ETC complex formation (D'Souza and Minczuk, 2018), we next gauged if p107 promoter occupancy and its control over mtDNA gene expression affected ETC complex formation. For this we assessed the protein expression of key subunits within the five ETC complexes that include complex I subunit NDUFB8, complex II subunit SDHB, complex III subunit UQCRC2, complex IV subunit MTCO and complex V subunit ATP5A. These key proteins become readily labile if not present within their specific complex, thus providing an estimation of ETC complex assembly. By Western blotting, we found that p107KO c2c12 cells had augmented levels of ETC complex subunit proteins compared to normal c2c12 cells during proliferation **(Fig. 4.11A),** which corresponded to the significantly increased mitochondrial encoded gene expression **(Fig. 4.8A).** Similar to the p107KO cells, growth arrested c2c12 cells with barely any p107 in the mitochondria **(Fig. 4.1B)** and increased mitochondrial gene expression **(Fig. 4.7)**, also displayed increased ETC subunit proteins compared to the proliferating cells **(Fig. 4.11B)**. Together, this data showed that the presence of p107 in the mitochondria might limit ETC complex formation through mtDNA promoter binding that repressed the mitochondrial encoded gene expression.

p107 controls mitochondrial ATP synthesis

Mitochondria gene expression is crucial for ETC complex formation, which in turn regulates mitochondrial ATP generation capacity (Reinecke et al., 2009). Thus, we next assessed if p107 mtDNA promoter occupancy and its control over mitochondrial gene expression and ETC complex formation had an impact on the capacity of mitochondria to generate ATP. Using a luminescence assay kit for Oxphos generation, the potential ATP generation capacity and rate were determined from isolated mitochondria in control and p107KO c2c12 cells. The ATP generation capacity and rate, were normalized to their protein content to exclude the potential contribution of mitochondria number. We found that the potential rate and capacity of ATP formation from isolated mitochondria of p107KO cells were significantly higher than control cells **(Fig. 4.12A and 4.12B)**, consistent with the increase in mitochondrial gene expression profile **(Fig. 4.8A)** and increased ETC proteins **(Fig. 4.11A)** linked to the absence of p107. We further evaluated if growth arrested cells that also had increased ETC proteins **(Fig. 4.11B)** and mitochondrial gene expression **(Fig. 4.7B)** due to a lack of p107 in the mitochondria **(Fig. 4.1B)** might also have increased mitochondrial ATP generation. Similar to the p107KO cells, the luminescence assay showed that growth arrested cells exhibited significantly higher ATP generation capacity and rate compared to the proliferating cells **(Fig. 4.13A and 4.13B)**.

We corroborated the ATP generation findings based on the luminescence assay by using live cell metabolic analysis with Seahorse. The analysis showed that p107KO c2c12 cells exhibited significantly higher oxygen consumption rate (OCR), increased Oxphos and glycolysis, as well as mitochondrial/glycolytic ATP ratio compared to the control cells **(Fig. 4.14A, 4.14B and 4.14C).** Furthermore, live cell metabolic analysis by Seahorse, also confirmed that growth arrested cells had significantly enhanced OCR concomitant with increased Oxphos and glycolysis, as well as

mitochondrial/glycolytic ATP ratio compared to the proliferating c2c12 cells **(Fig. 4.15A, 4.15B and 4.15C).** Together, these results suggest that p107 impacts mitochondrial ATP generation through regulation of mitochondrial encoded gene expression that is crucial for ETC complex formation.

Increased Oxphos in p107KO cells is associated with mitochondrial fusion

As elevated mitochondrial energy generation has been shown to increase mitochondrial fusion causing elongation (Hoppins et al., 2011; Meeusen et al., 2004; Mishra & Chan, 2014a, 2016b), we evaluated if the increased mitochondrial ATP generation capacity is associated with enhanced mitochondrial network. We assessed if p107KO cells that had increased ATP generation capacity and rate might also have elongated mitochondrial morphology. To visualize mitochondrial morphology, we stained our cells with MitoView red, which is a fluorogenic mitochondrial stain for live cells. Live cell imaging by confocal microscopy revealed that p107KO c2c12 cells had an elongated mitochondrial network compared to control cells, which is indicative of mitochondrial fusion **(Fig. 4.16).** We quantified the mitochondrial morphology using Image J software. This showed that the p107KO cells had significantly more mitochondria having greater lengths and areas, compared to the controls **(Fig. 4.17A and 17B)**. Thus, this data is in congruence with previous findings that had shown that increased mitochondrial ATP production cause mitochondrial fusion leading to elongated mitochondrial morphology (Mishra & Chan, 2016b).

Figure 4.1

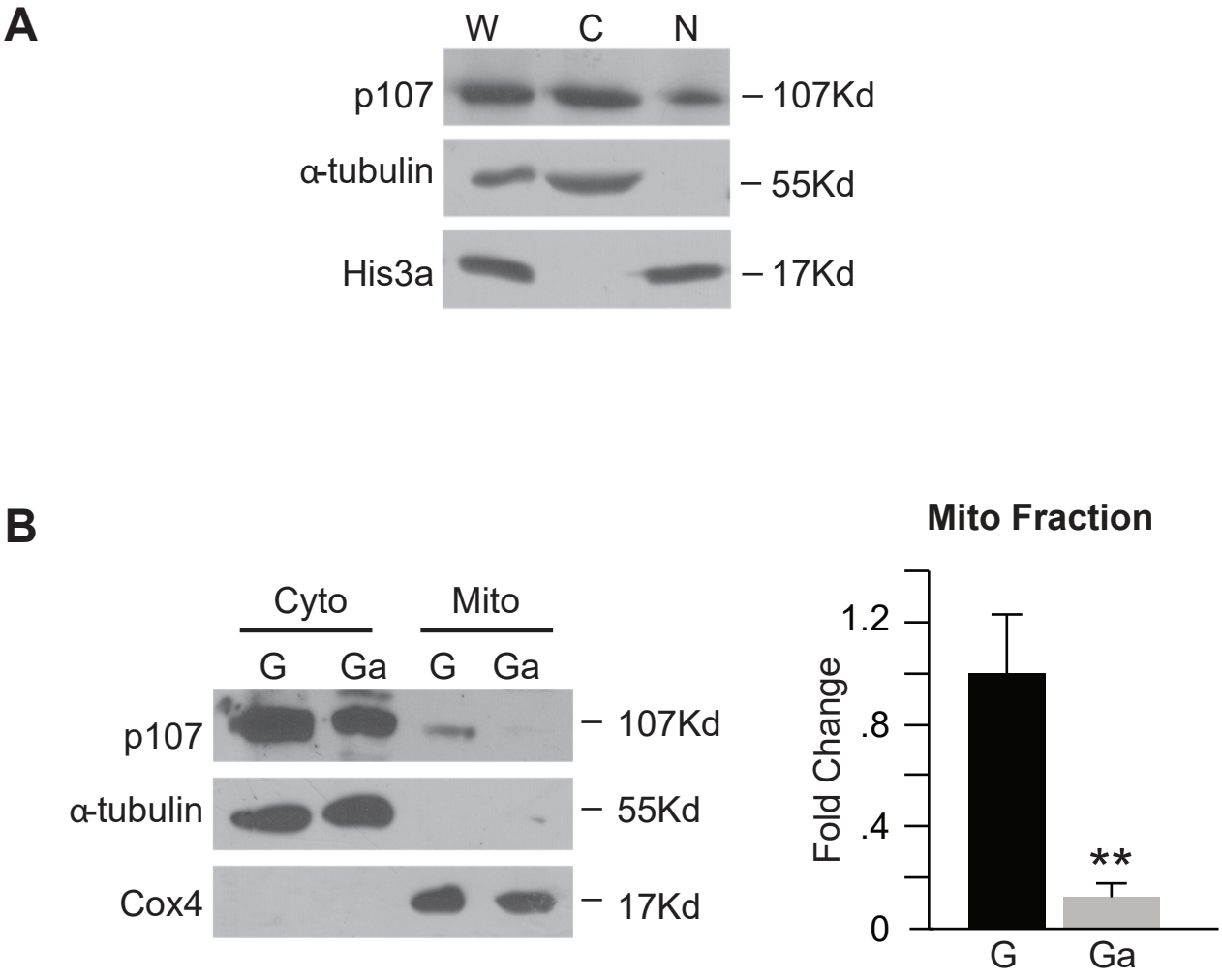

Figure 4.1. p107 is localized in the mitochondria of proliferating myogenic progenitors (MPs). (A) Representative Western blot of whole cell (W), cytoplasmic (C) and nuclear (N) fractions for p107, α-tubulin (cytoplasm loading control) and His3a (nucleus loading control) during proliferation of c2c12 MPs. **(B)** Representative Western blot of cytoplasmic (Cyto) and mitochondrial (Mito) c2c12 fractions for p107, α-tubulin and Cox4 (mitochondria loading control) and graphical enumeration of p107 in the mito fractions during proliferation (G) and growth arrest (Ga), n=3, asterisks denote significance, $^{**}p<0.01$; Student T-test.

Figure 4.1

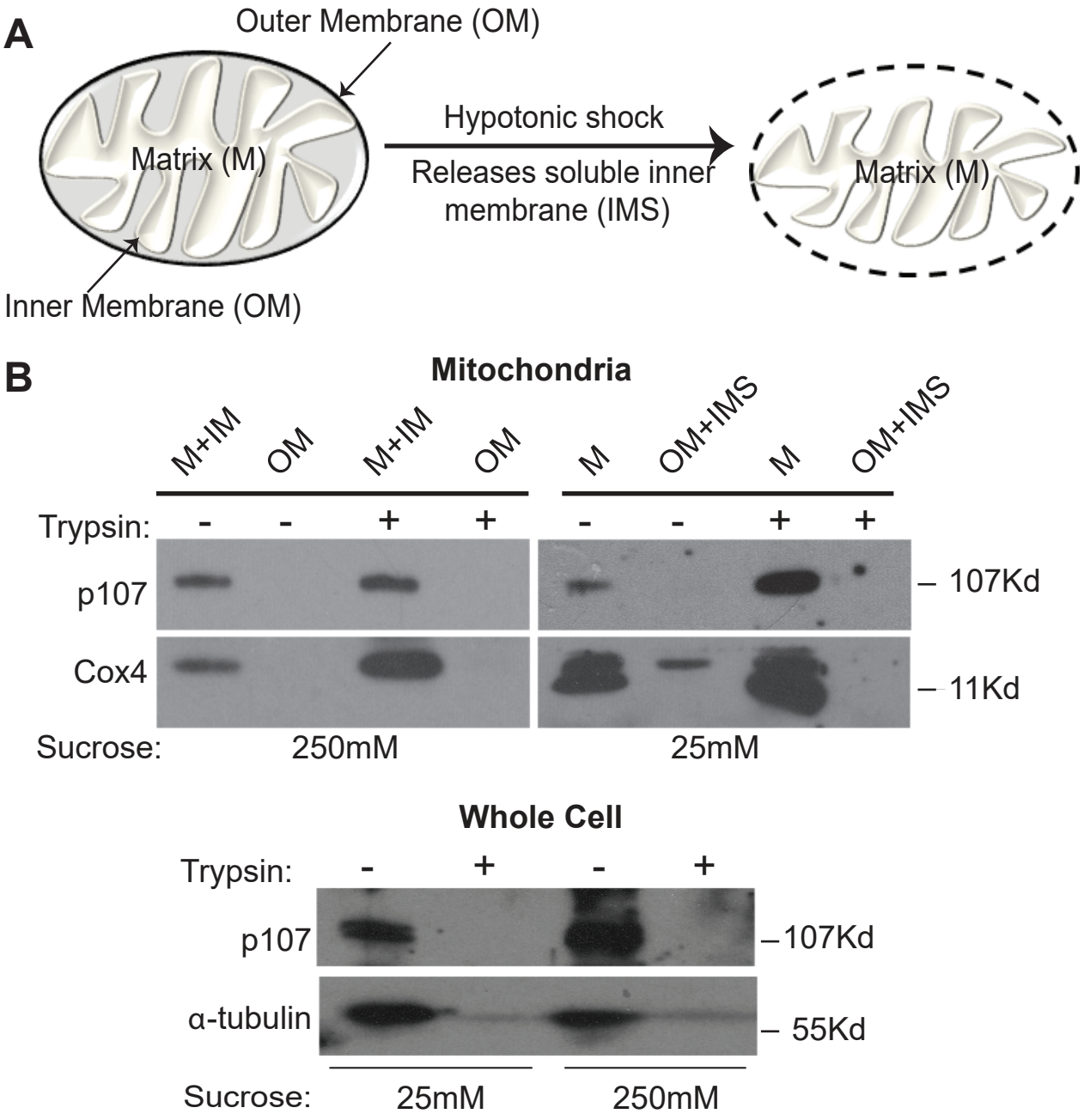

Figure 4.2. p107 is localized in the mitochondrial matrix of proliferating MPs. **(A)** Diagrammatic representation of hypotonic osmotic shock treatment that swells the inner membrane (IM), ruptures the outer membrane (OM), releases soluble inner membrane (IMS) mitochondrial proteins, preserving the mitochondrial matrix (M). **(B)** Representative Western blot for p107, α-tubulin and Cox4, of c2c12 whole cell and mitochondrial fractions including OM, IM, IMS and M that were isolated using 250mM or 25mM sucrose buffer, treated and untreated with trypsin.

Figure 4.3

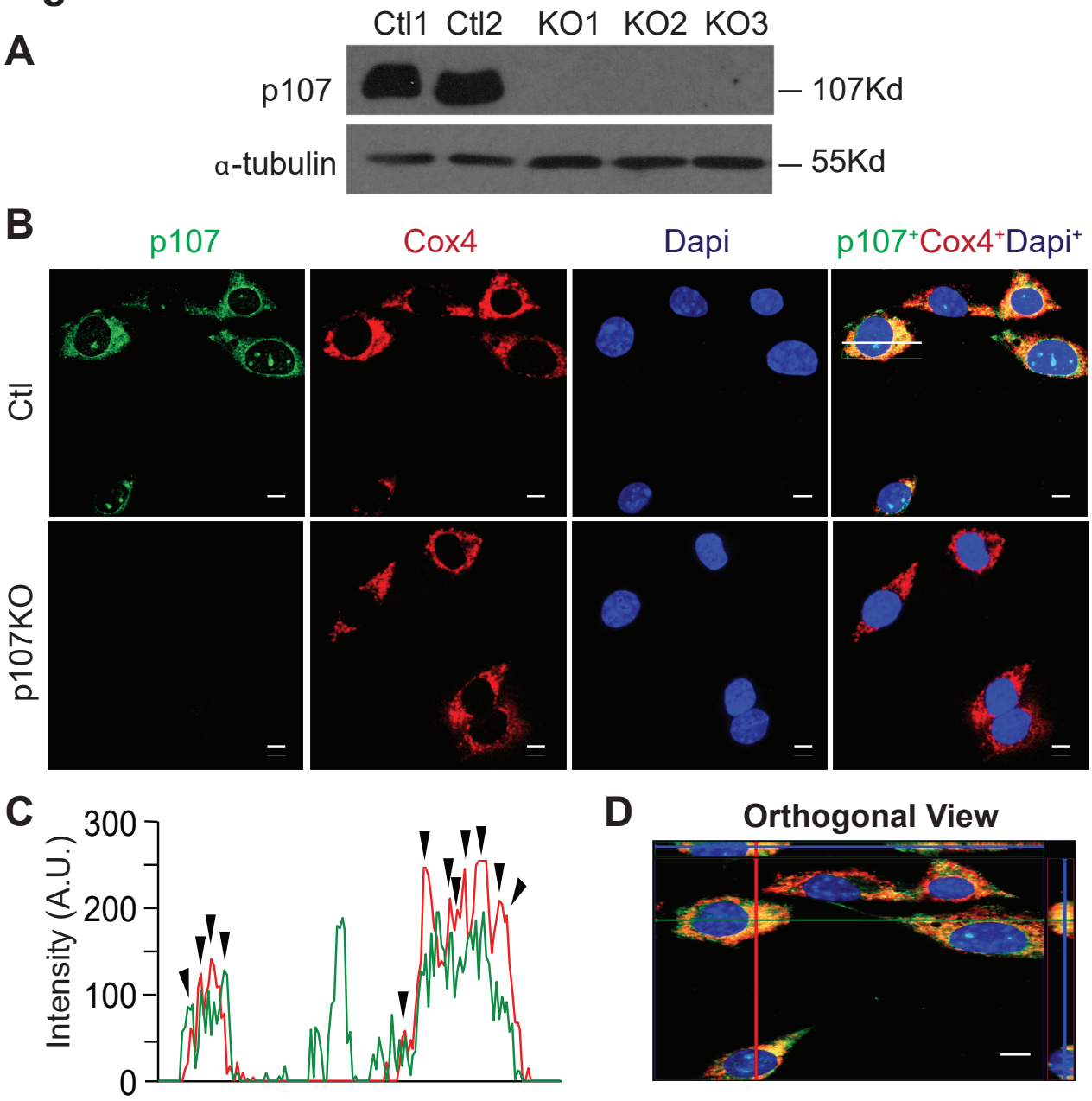

Figure 4.3. Confirmation of p107 localization in the mitochondria of proliferating c2c12 cells by confocal microscopy and Z-stack analysis. (A) Representative Western blot for p107 and α-tubulin of different clones for control (Ctl) c2c12 cells and p107 genetically deleted c2c12 cells (p107KO) generated by Crispr/Cas9. **(B)** Immunofluorescence and confocal microscopic images for p107 (green), Cox4 (red), Dapi (blue) and Merge of proliferating Ctl and p107KO c2c12 cells (scale bar 10um). **(C)** A line was drawn through a representative cell to indicate relative intensity of RGB signals with the arrowheads pointing to areas of concurrent intensities and **(D) a**n orthogonal projection was generated by a Z-stack (100 nm interval) image set using the ZEN program (Zeiss) in the XY, XZ, and YZ planes.

Figure 4.4

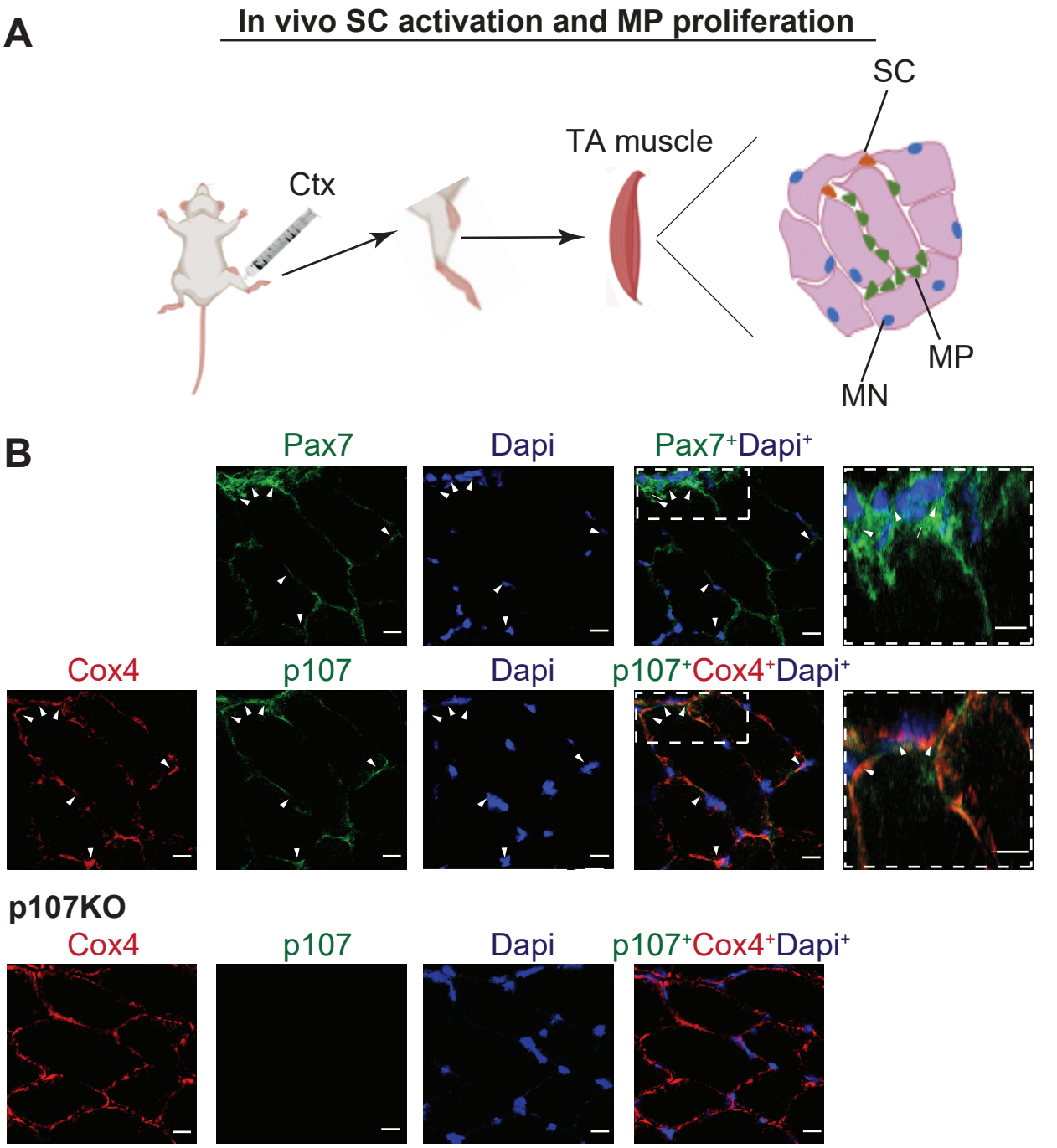

Figure 4.4. In vivo, p107 is present in the mitochondria of MPs. **(A)** Schematic for inducing in vivo satellite (SC) activation and MP proliferation in the tibialis anterior (TA) muscle with cardiotoxin (Ctx) injury (MN is myonuclei). **(B)** Confocal microscopic immunofluorescence of wild type (Wt) TA muscle section 2 days post injury for Pax7 (green), Dapi (blue) and Merge; p107 (green), Cox4 (red), Dapi (blue) and Merge and for p107KO TA muscle section for p107 (green), Cox4 (red), Dapi (blue) and Merge. Arrows denote $Pax7^{+}p107^{+}Cox4^{+}$ cells (scale bar 20μm).

Figure 4.5

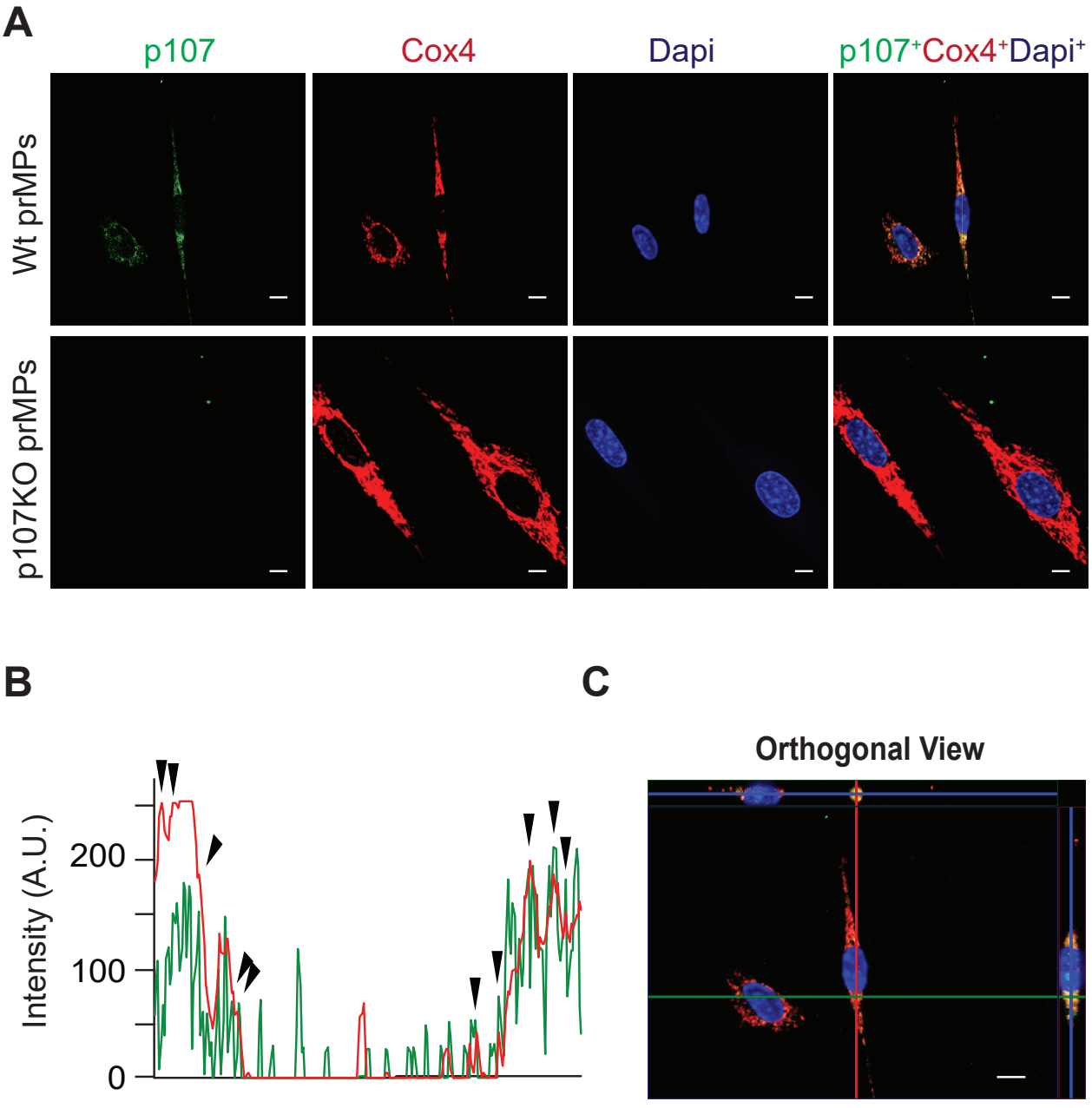

Figure 4.5. p107 is present in the mitochondria of proliferating primary MPs. (A) Confocal immunofluorescence microscopy for p107 (green), Cox4 (red), Dapi (blue) and Merge of wild type (Wt) and p107KO primary (pr) MPs (scale bar 10μm). **(B)** A line was drawn through a representative cell to indicate relative intensity of RGB signals with the arrowheads pointing to areas of concurrent intensities and **(C)** an orthogonal projection was generated by a Z-stack (100 nm interval) image set using the ZEN program (Zeiss) in the XY, XZ, and YZ planes.

Figure 4.6

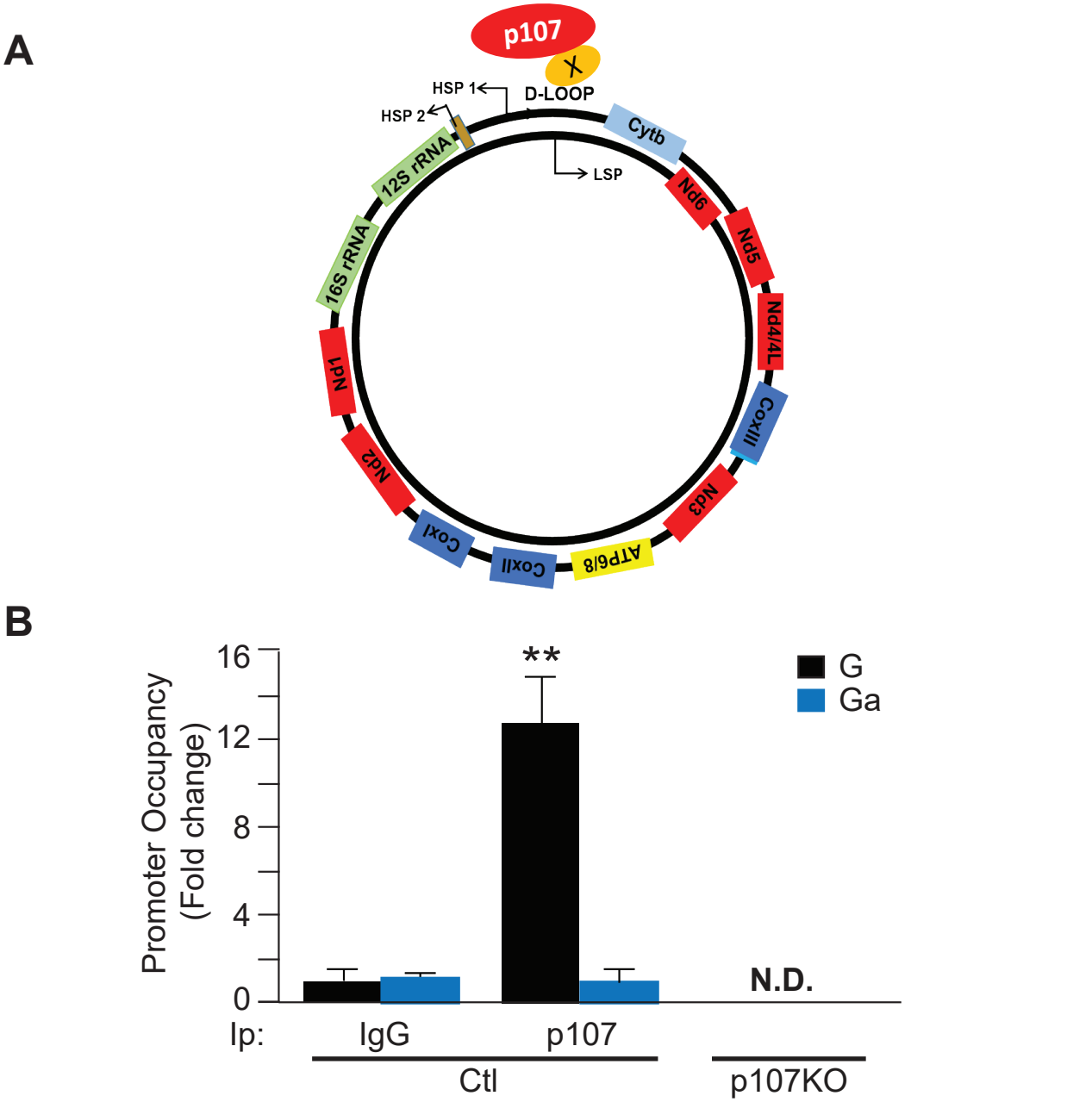

Figure 4.6. p107 interacts at the mitochondrial DNA promoter. (A) Schematic of p107 binding to mitochondrial DNA D-loop regulatory region with a potential transcription factor that binds to the DNA directly (X), that is currently unknown. HSP1 and HSP2 stand for heavy strand promoters 1 and 2 respectively, LSP stands for light strand promoter and genes encoding electron transport chain complexes are shown. **(B)** Graphical representation of relative p107 and IgG mitochondrial DNA promoter occupancy by qChIP analysis during proliferation (G) and growth arrest (Ga) in control (Ctl) and p107KO c2c12 cells, n=3, asterisks denote significance, $^{**}p<0.01$; two-way Anova with post hoc Tukey test. Not detected (N.D.).

Figure 4.7

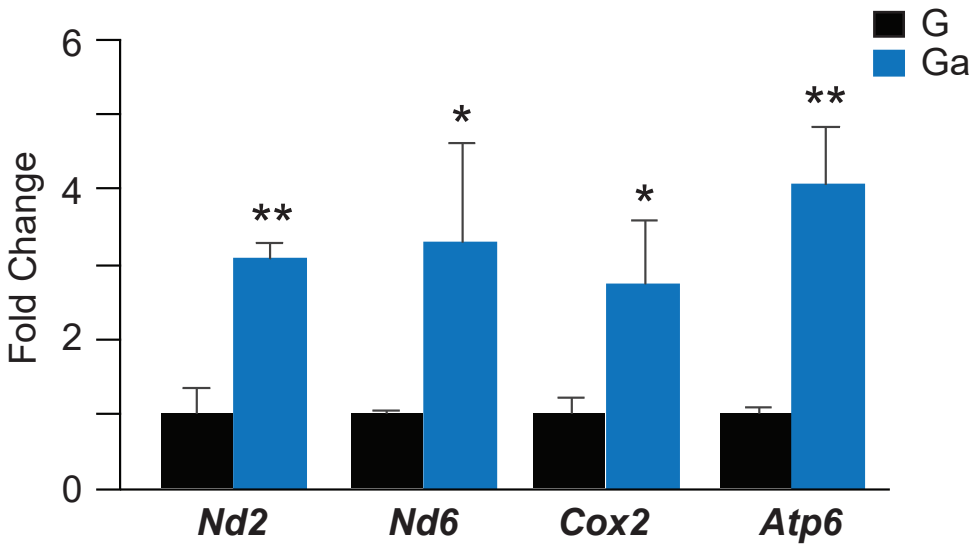

Figure 4.7. p107 represses mitochondrial gene expression. Gene expression analysis by qPCR of mitochondrial encoded genes *Nd2*, *Nd6*, *Cox2* and *Atp6* for c2c12 cells during proliferation (G) and growth arrest (Ga), n=3, asterisks denote significance, **p*<0.05, ***p*<0.01; Student T-test.

Figure 4.8

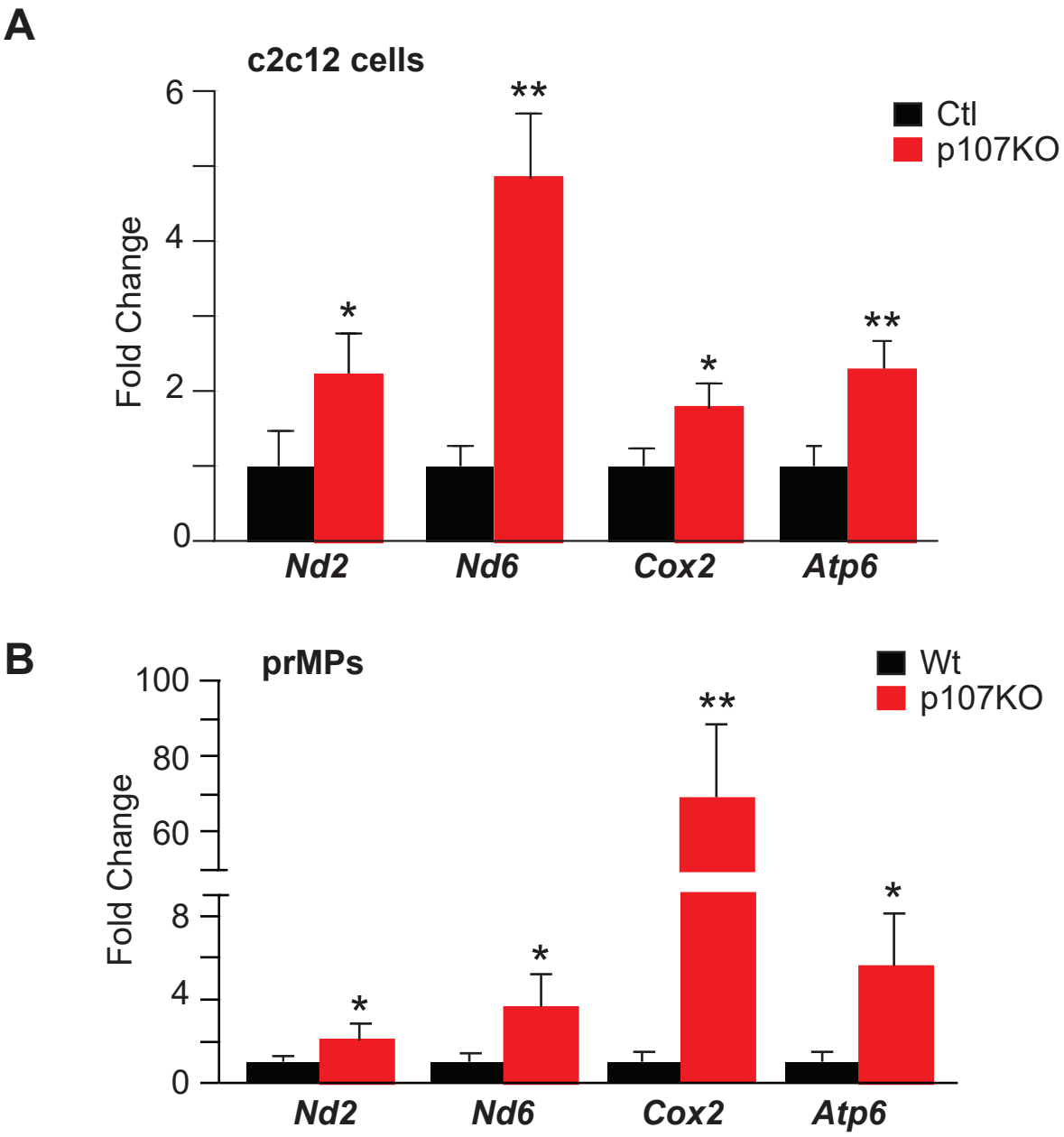

Figure 4.8. Absence of p107 increases mitochondrial gene expression. Gene expression analysis by qPCR of mitochondrial encoded genes *Nd2*, *Nd6*, *Cox2* and *Atp6* for **(A)** control (Ctl) and p107KO c2c12 cells, n=4 and **(B)** Wt and p107KO primary myogenic progenitors (prMPs) during proliferation, n=4, asterisks denote significance, **p*<0.05, ***p*<0.01; Student T-test.

Figure 4.9

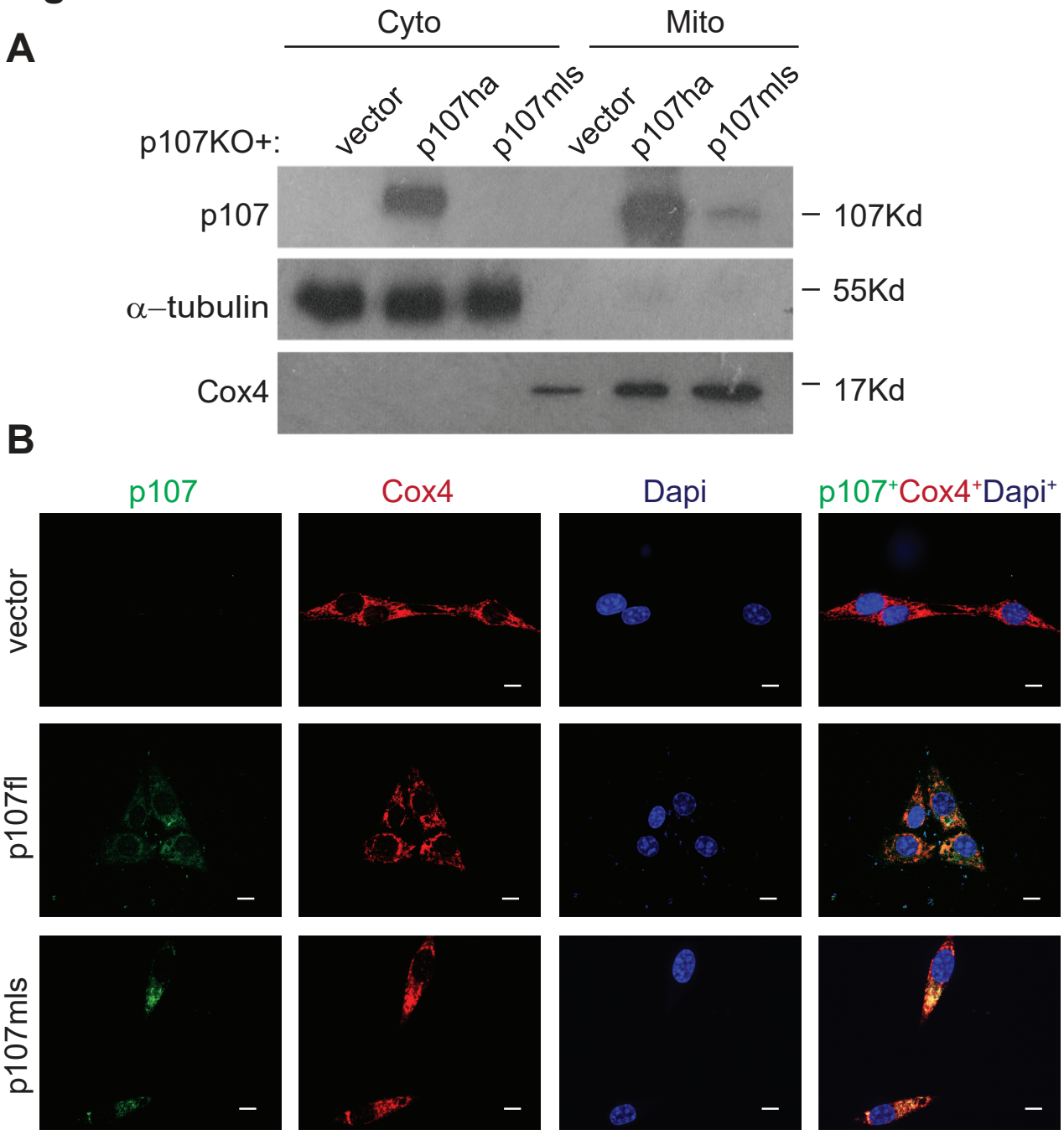

Figure 4.9. Overexpression of p107 with mitochondrial localization sequence (p107mls). (A) Representative Western blot of cytoplasmic (Cyto) and mitochondrial (Mito) fractions for p107, α-tubulin and Cox4 and **(B)** Confocal microscopic immunofluorescence and Z-stack (100 nm interval) image using the ZEN program (Zeiss) for p107 (green), Cox4 (red), Dapi (blue) and Merge (scale bar 10μm) for p107KO c2c12 cells transfected with empty vector or full length p107 (p107fl) or p107 with a mitochondrial localization seuqnece (p107mls).

Figure 4.10

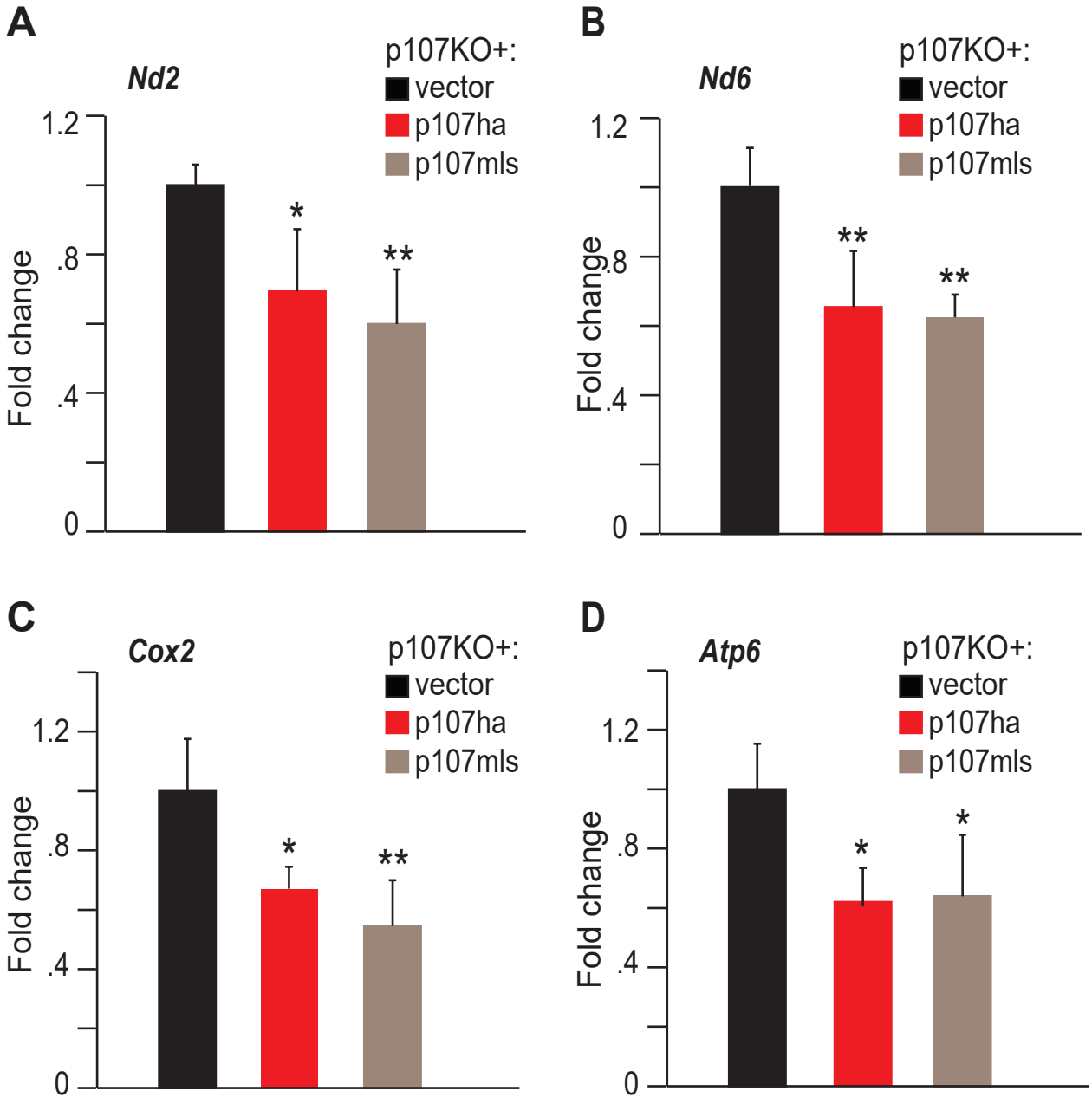

Figure 4.10. Overexpressing p107 decreases mitochondrial gene expression. Gene expression analysis by qPCR of mitochondrial encoded genes **(A)** *Nd2*, **(B)** *Nd6*, **(C)** *Cox2* and **(D)** *Atp6* for p107KO c2c12 cells transfected with empty vector, full length p107 (p107fl) or p107 with a mitochondrial localization sequece (p107mls), n=4, asterisks denote significance, *p<0.05, **p<0.01; one way-Anova and post hoc Tukey test.

Figure 4.11

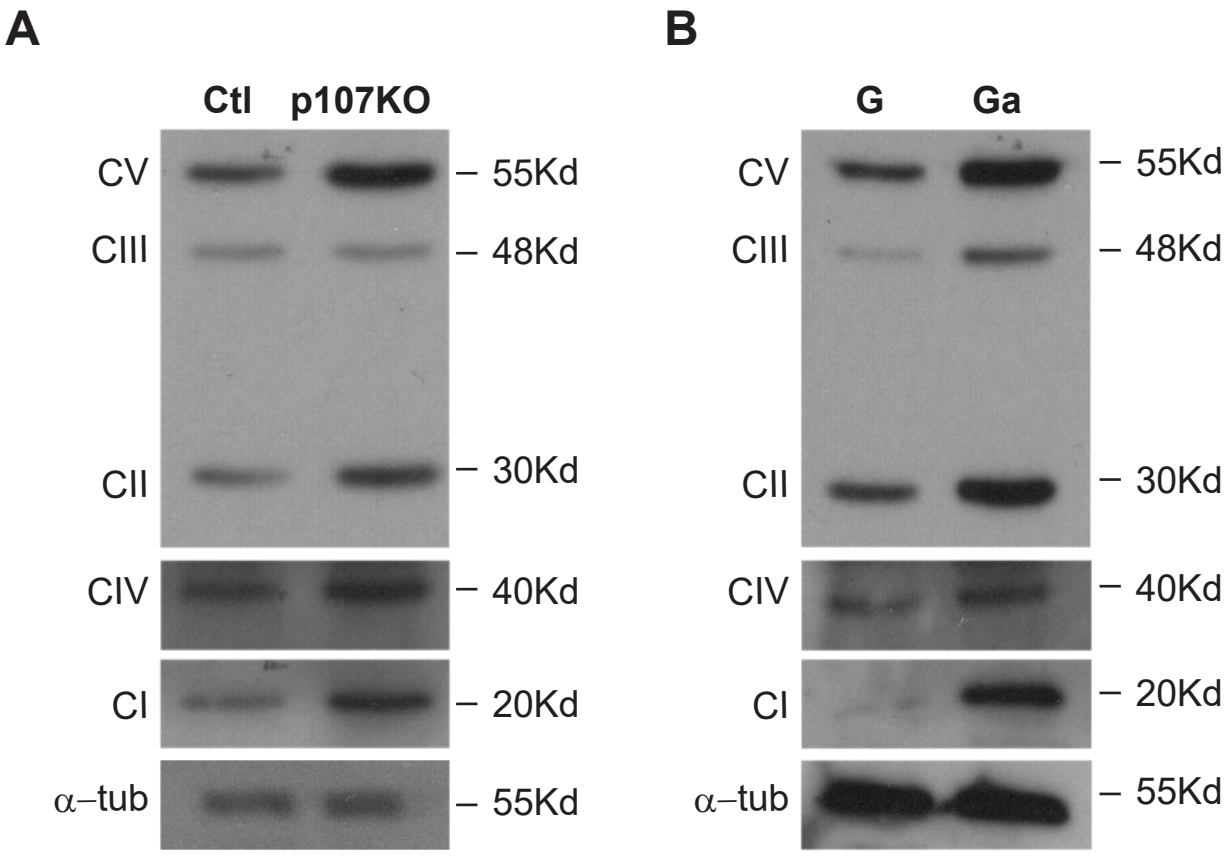

Figure 4.11. p107 influences electron transport chain complex formation. Representative Western blot of **(A)** control (Ctl) compared to p107KO c2c12 cells and **(B)** proliferating (G) compared to growth arrested (Ga) c2c12 cells for a key subunit from each electron transport chain complex (C) including, CI (NDUFB8), CII (SDHB), CIII (UQCRC2), CIV (MTCO) and CV (ATP5A).

Figure 4.12

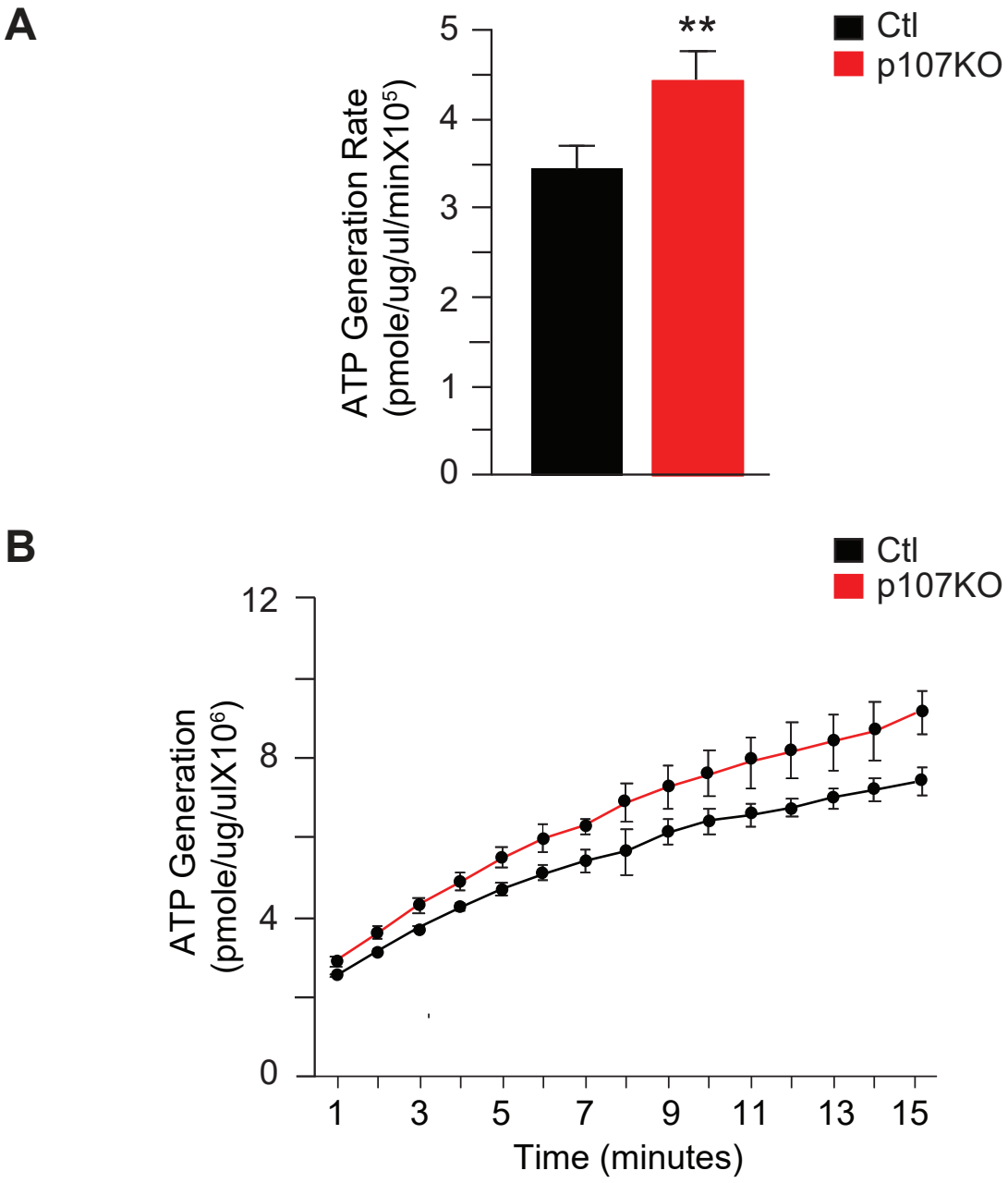

Figure 4.12. Absence of p107 is associated with an increase in mitochondrial ATP generation potential. ATP generation **(A)** rate and **(B)** capacity of isolated mitochondria over time for control (Ctl) and p107KO c2c12 cells, n=4. For rate, asterisks denote significance, ***p*<0.01; Student T-test. For capacity statistics see Table 3.

Figure 4.13

A

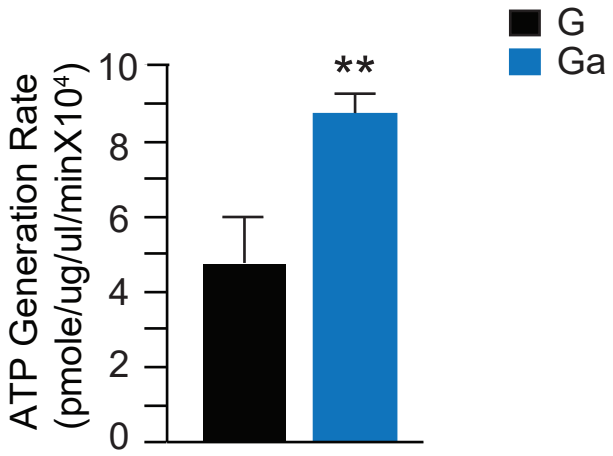

B

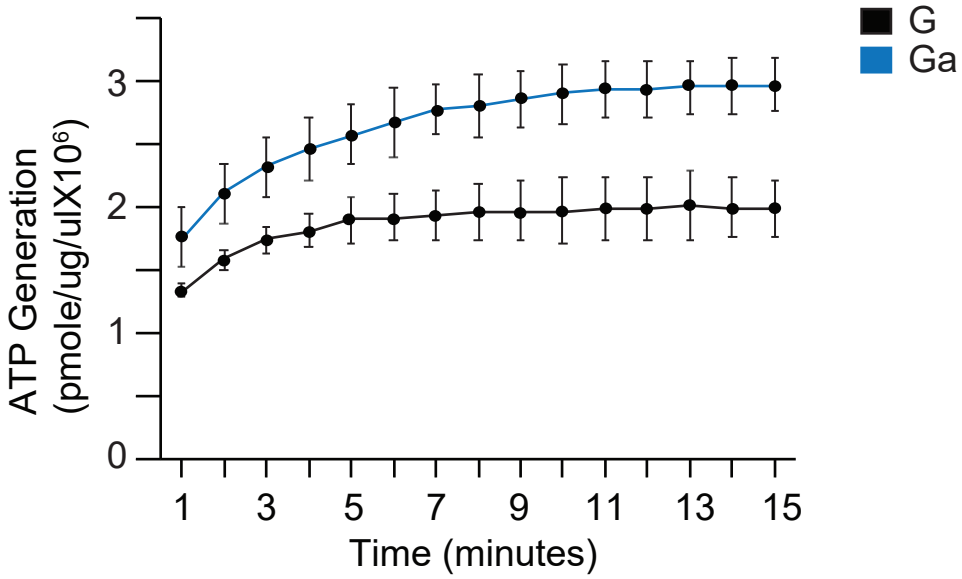

Figure 4.13. p107 decreases mitochondrial ATP generation potential of proliferaing MPs. ATP generation **(A)** rate and **(B)** capacity of isolated mitochondria over time for proliferating (G) and growth arrested (Ga) c2c12 cells. n=4. For rate, asterisks denote significance, ***p*<0.01; Student T-test. For capacity statistics see Table 3.

Figure 4.14

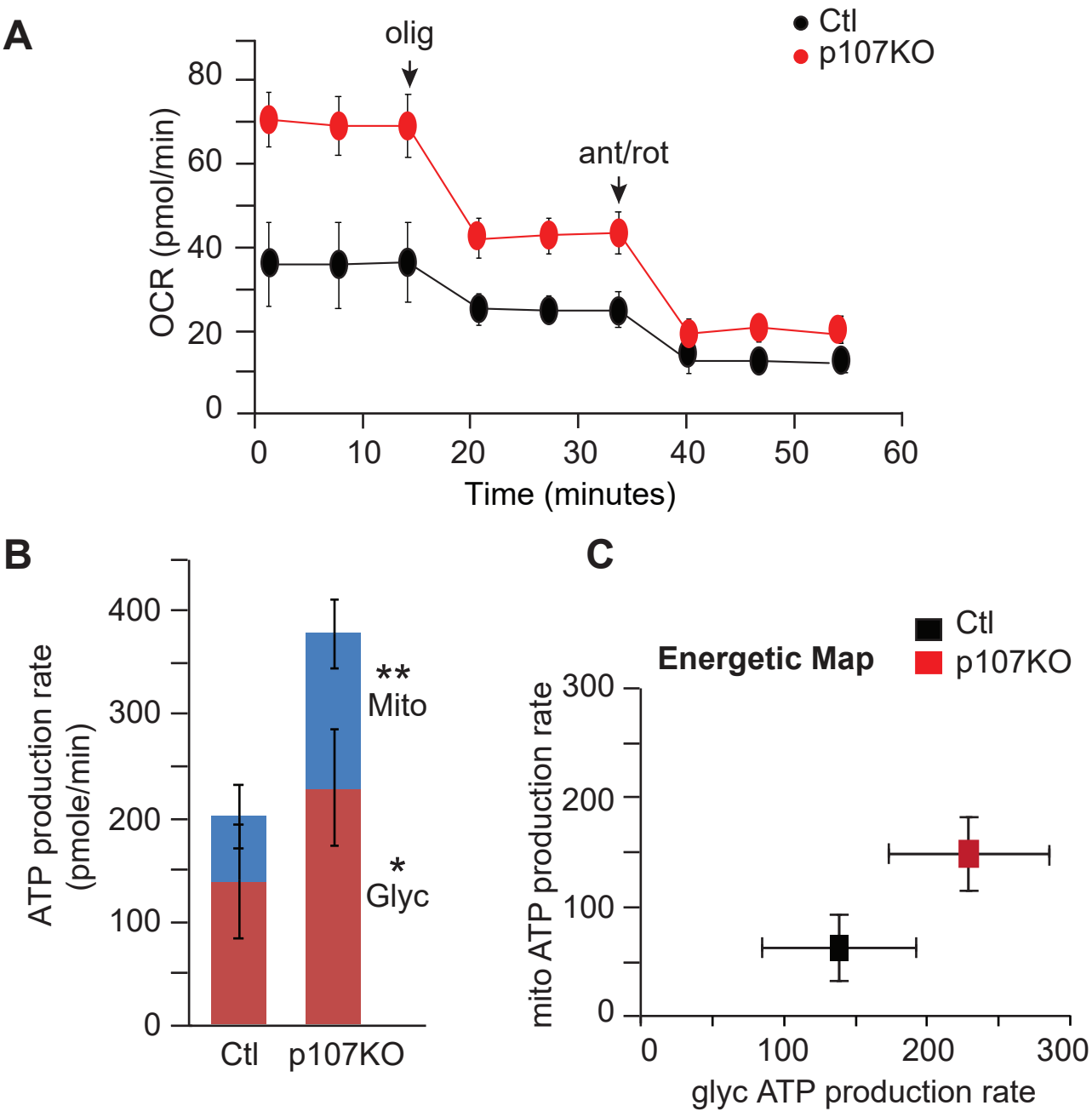

Figure 4.14. p107KO c2c12 cells have higher oxygen consumption rate and mitochondrial to glycolytic ATP production rate. Live cell metabolic analysis by Seahorse for **(A)** oxygen consumption rate (OCR) over time with addition of oligomycin (olig), antimycin A (ant) and rotenone (rot) **(B)** Glycolytic (Glyc) and mitochondrial (Mito) ATP production rate and **(C)** Energetic map for control (Ctl) and p107KO c2c12 cells. n=4-5, asterisks denote significance,*p<0.05, **p<0.01; two-way Anova and post hoc Tukey test.

Figure 4.15

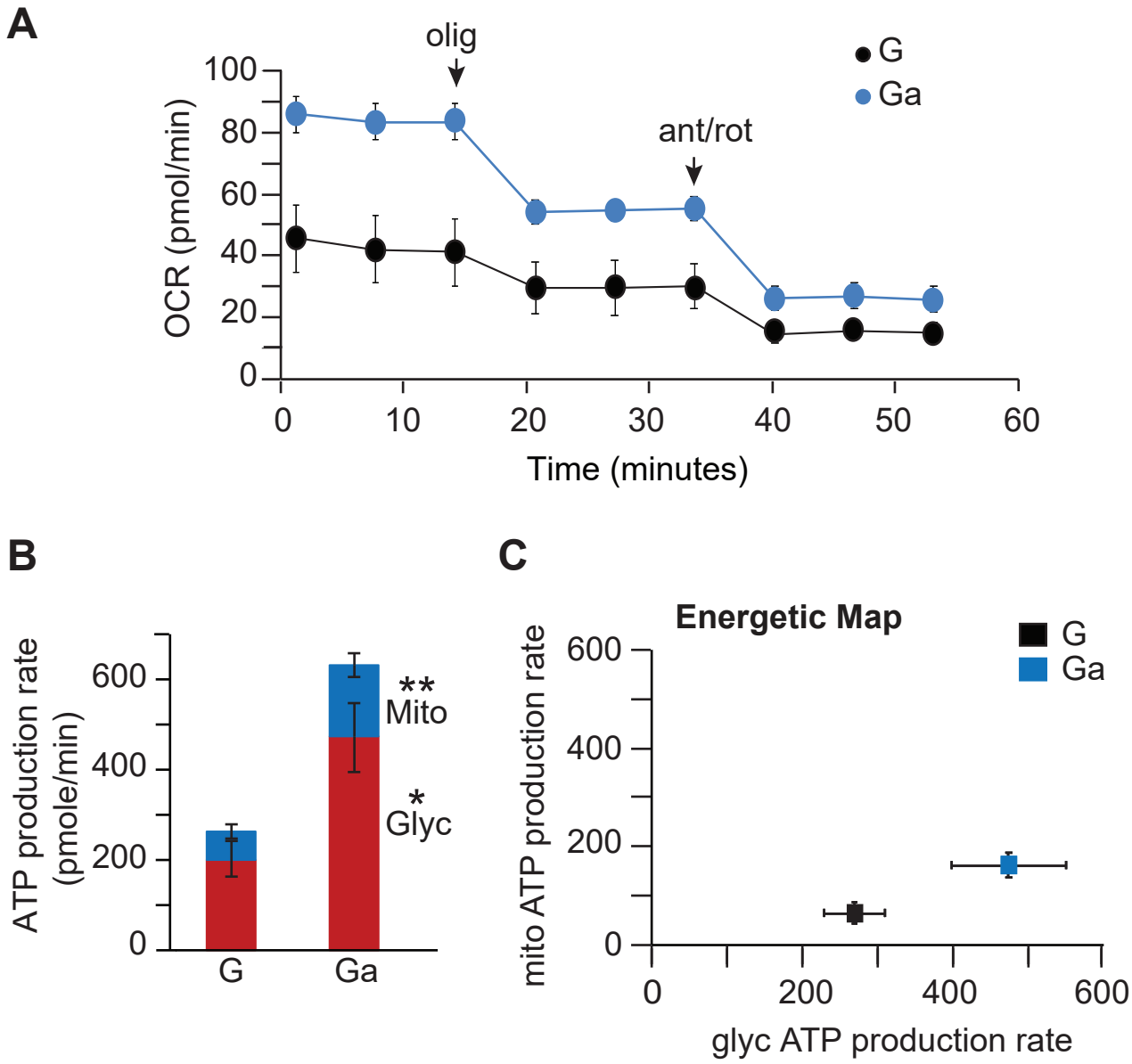

Figure 4.15. p107 reduces oxygen consumption rate and mitochondrial to glycolytic ATP production rate. Live cell metabolic analysis by Seahorse for **(A)** oxygen consumption rate (OCR) over time with addition of oligomycin (olig), antimycin A (ant) and rotenone (rot) **(B)** Glycolytic (Glyc) and mitochondrial (Mito) ATP production rate and **(C)** Energetic map for proliferating (G) and growth arrested (Ga) c2c12 cells. n=7-8, asterisks denote significance, *p<0.05, **p<0.01; Student T-test.

Figure 4.16

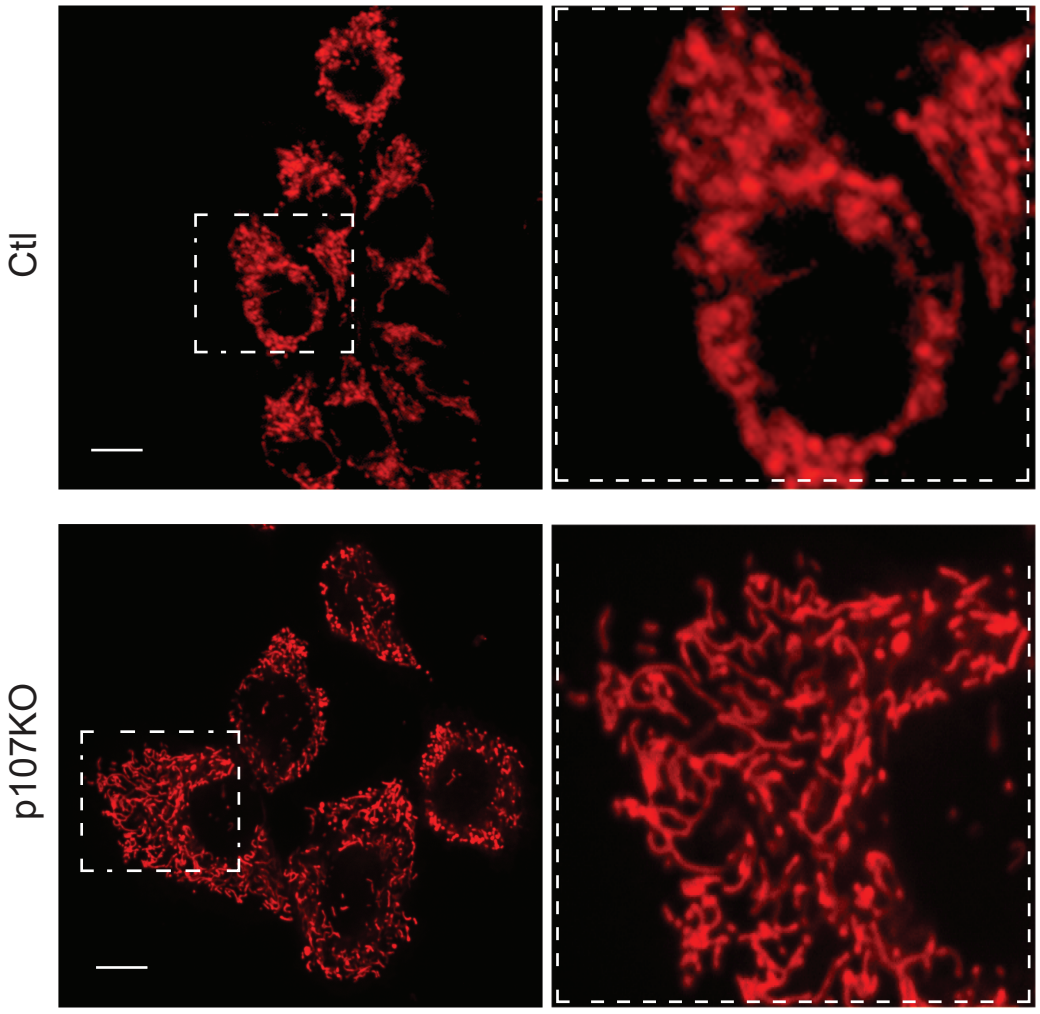

Figure 4.16. p107KO c2c12 cells have elongated mitochondria. Representative live cell confocal microscopy image of stained mitochondria (MitoView Red) for control (Ctl) and p107KO c2c12 cells (scale bar 20um).

Figure 4.17

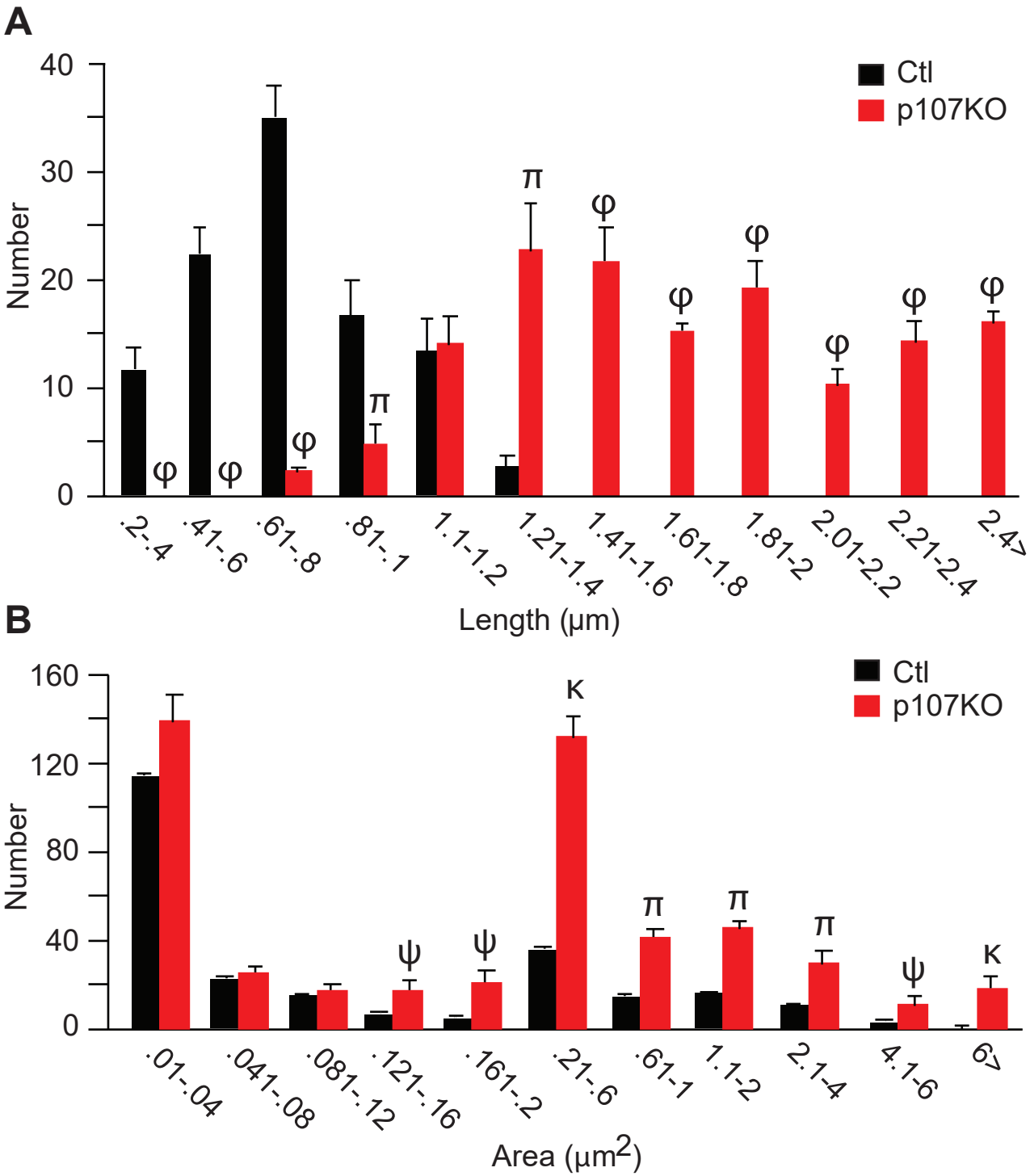

Figure 4.17. p107KO c2c12 cells have increased mitochondrial length and area. Graphical representation of mitochondria number per grouped **(A)** lengths and **(B)** areas for control (Ctl) and p107KO c2c12 cells using image J quantification, n=3, atleast 100 mitochondria were counted per n, significance denoted by ψ=p<0.05, π=p<0.01, κ =p<0.001, ϕ=p<0.0001; Student T-test.

CHAPTER 5

Sirt1 governs p107 mitochondrial function

Abstract

The regulation of glycolysis in the cytoplasm and oxidative phosphorylation (Oxphos) in the mitochondria are integrated into the control mechanisms that govern stem cell fate decisions (Ito & Ito, 2016). However, the control mechanism(s) that synchronize their association remain obscure. In this chapter, we show that during MP proliferation, p107 acts as an indirect energy sensor of the cytoplasmic NAD^+/NADH ratio that affects its mitochondrial function of regulating Oxphos. When the NAD^+/NADH ratio is low, p107 compartmentalizes in the mitochondria, where it interacts at the D-loop promoter region of mitochondrial DNA, repressing mitochondrial gene expression limiting ETC protein formation, thereby suppressing ATP generation. On the contrary, with high NAD^+/NADH, p107 is localized mostly in the cytoplasm with the opposite effects on mitochondrial gene expression and ATP generation. The NAD^+/NADH control of p107 is facilitated by its interaction with the NAD^+ dependent deacetylase and energy sensor Sirt1. Deletion of Sirt1 or inhibition of its activity in MPs increases p107 mitochondrial localization concomitant with decreased mitochondrial gene expression and ATP generation. On the other hand, increasing the activity of Sirt1 has the opposite effect on p107 mitochondrial function.

Results

Glucose levels control p107 mitochondrial localization

As availability of nutrients impact mitochondrial energy generation (Hwang & Song, 2017; Locasale & Cantley, 2010), we evaluated how it would influence p107 sub-cellular localization and function during MP proliferation. Since glucose availability is important for dividing cells, we assessed the effect of glucose metabolism on p107 mitochondrial function. For this purpose, we grew c2c12 cells in low (5.5mM) or high (25mM) glucose as the sole nutrient in stripped media (not supplemented with glucose, glutamine and pyruvate). Western blot analysis of isolated mitochondria revealed that p107 translocation into mitochondria was glucose concentration dependent **(Fig. 5.1A)**. Its presence was negligible in mitochondria when cells were grown in a low concentration (5.5mM) of glucose, but at a higher glucose concentration (25mM) there was a significant increase of p107 localization in mitochondria **(Fig. 5.1A)**.

We next assessed the p107 mitochondrial functional consequence due to varied glucose concentration. First, we evaluated its interaction at the mtDNA D-loop regulatory region, by performing qChIP analysis on isolated mitochondria from c2c12 cells grown in stripped media with 5.5mM or 25mM glucose. As expected, we found that cells grown in higher glucose (25mM) concentration had significantly increased p107 mtDNA interaction at the promoter compared to cells grown in a lower (5.5mM) glucose concentration **(Fig. 5.1B)**. IgG antibody was used as a negative control for non-specific antibody-chromatin interaction. IgG showed negligible interaction at the D-loop regulatory region of the mitochondrial DNA, unlike differential binding of p107. Furthermore, no interaction was detected in p107KO cells **(Fig. 5.1B)**. These results suggest that high glycolytic flux increases p107 interaction at the mtDNA, which might have functional consequences.

Glucose levels regulate p107 repressor function of mitochondrial gene expression

As a higher glucose concentration increased p107 mitochondrial localization and mtDNA interaction, we assumed that this would be associated with a decreased mitochondrial encoded gene expression pattern. We assessed for this possibility by performing qPCR analysis on c2c12 cells grown in stripped media with 25mM compared to a lower (5.5mM) glucose concentration. We found that the higher glucose concentration that increased p107 mitochondrial presence **(Fig. 5.1A)** was indeed associated with a significant decrease in mitochondrial encoded gene expression for *Nd2* and *Nd6* (complex I), *Cox2* (complex IV), and *Atp6* (complex V) **(Fig. 5.2A, 5.2B, 5.2C and 5.2D)**.

We next confirmed that the glucose concentration dependent control of mitochondrial gene expression was due to a p107 mitochondrial function. This was accomplished by evaluating the effect of varying the glucose concentrations in p107KO c2c12 cells. Indeed, we found that the glucose concentration did not affect the mitochondrial encoded gene expression for *Nd2, Nd6, Cox2* and *Atp6*, in p107KO cells compared to control cells **(Fig. 5.2A, 5.2B, 5.2C and 5.2D)**.

We corroborated that the mitochondrial encoded gene expression differences with varying glucose concentration were due to p107, by using prMPs obtained from EDL muscle isolated from Wt and p107KO mice. As with c2c12 cells, qPCR analysis of Wt prMPs showed that mitochondrial encoded genes *Nd2*, *Nd6*, *Cox2* and *Atp6* significantly decreased in cells grown in high (25mM) compared to low concentrations of glucose in stripped media **(Fig. 5.3A, 5.3B, 5.3C and 5.3D)**. Moreover, p107KO prMPs grown in low (5.5mM) or high (25mM) glucose concentrations, had no differences in mitochondrial gene expression **(Fig. 5.3A, 5.3B, 5.3C and 5.3D)** similar to p107KO c2c12 cells **(Fig. 5.2A, 5.2B, 5.2C and 5.2D)**. Together, these data suggest that glucose

concentration affecting mitochondrial encoded gene expression is dependent on p107 interaction at the mtDNA promoter.

Glucose levels do not affect mitochondrial biogenesis

We verified that changes in mitochondrial gene expression in c2c12 cells grown in varying glucose concentrations was not influenced by differences in mitochondrial biogenesis. For this two approaches were used. First, by qPCR in c2c12 cells, we assessed the gene expression of key regulatory factors of mitochondrial biogenesis, including *peroxisome proliferator activated receptor gamma co-activator 1 alpha* (*Pgc1α*), mitofusin 2 *(Mfn2*), adenine nucleotide translocase type 1 (*Ant1*) and *nuclear factor erythroid 2-related factor 2 (Nrf2*) **(Fig. 5.4A)**. We found that *Pgc1α* and *Mfn2* were not detected at all, as they are mostly expressed in differentiated myotubes (Bach et al., 2003; Lin et al., 2014). Though *Ant1* and *Nrf2* were detected by qPCR, there were no significant differences in their expression when the cells were grown in low (5.5mM) compared to high (25mM) glucose concentrations in stripped media **(Fig. 5.4A)**. Second, by determining the mtDNA to nuclear DNA (nDNA) content we evaluated if the mtDNA copy number was different in the divergent glucose concentrations. We found no significant differences in the mtDNA/nDNA ratio in c2c12 cells grown in low (5.5mM) versus high (25mM) glucose concentrations **(Fig. 5.4B)**. To validate our results, mitochondrial biogenesis activator 5-aminoimidazole-4-carboxamide-1-β-D-ribofuranoside (AICAR) was used as a positive control, which increased the mtDNA/nDNA ratio significantly for both concentrations of glucose **(Fig. 5.4B)**. Together, these data show that mitochondrial gene expression might be mediated by glycolytic flux induced p107 mitochondrial localization and not merely a consequence of differences in mitochondrial biogenesis.

NAD^+/NADH ratio regulates p107 mitochondrial function

As glucose metabolism affects the NAD^+/NADH redox balance, we determined if this balance might impact p107 mitochondrial localization and function. We found that c2c12 cells grown in stripped media containing 5.5mM compared to 25mM glucose had significantly increased cytoplasmic NAD^+/NADH **(Fig. 5.5)**. This suggested that redox state of the cells governed by glycolytic flux in the cytoplasm might have a role in controlling p107 sub-cellular localization.

We next evaluated if the cytoplasmic NAD^+/NADH ratio was responsible for p107 function by manipulating the redox potential in a glucose concentration independent manner. We first used oxamate, a structural analog of pyruvate that inhibits lactate dehydrogenase a (Ldha), resulting in the formation of acetyl CoA instead of lactate (Valvona et al., 2016). Treatment of c2c12 cells with 2.5mM oxamate for 40 hours significantly decreased the NAD^+/NADH ratio compared to untreated cells **(Fig. 5.6A)**. Western blot analysis showed that the addition of oxamate, increased p107 mitochondrial localization **(Fig. 5.6B),** and resulted in a significant downregulated mitochondrial encoded gene expression for *Nd2, Nd6, Cox2* and *Atp6* **(Fig. 5.7A, 5.7B, 5.7C and 5.7D)**. To confirm that the functional consequence was driven by p107, we also treated p107KO c2c12 cells with oxamate and found that mitochondrial gene expression for *Nd2, Nd6, Cox2* and *Atp6* were not affected unlike control cells **(Fig. 5.7A, 5.7B, 5.7C and 5.7D)**. This suggests that decreasing the NAD^+/NADH ratio due to oxamate treatment caused significantly decreased mitochondrial gene expression as a result of p107 mitochondrial localization.

As ETC complex formation is partly dependent on the mitochondrial encoded genes, we evaluated if decreased mitochondrial gene expression with reduced NAD^+/NADH and increased p107 mitochondrial localization, would limit ETC complex protein formation. To accomplish this,

we performed Western blot using antibodies against key subunits of the 5 complexes as before including complex I subunit NDUFB8, complex II subunit SDHB, complex III subunit UQCRC2, complex IV subunit MTCO and complex V subunit ATP5A. Our results revealed that oxamate treatment decreased ETC complex protein levels in proliferating c2c12 cells compared to untreated cells **(Fig. 5.8).** This is in line with decreased mitochondrial gene expression **(Fig. 5.7A, 5.7B, 5.7C and 5.7D)** due to increased p107 mitochondria localization with oxamate treatment **(Fig. 5.6B).** We also performed the same experiment in p107KO c2c12 cells that were treated or untreated with oxamate and found there were no differences in the ETC protein levels **(Fig. 5.8)**, corresponding to the unchanged mitochondrial gene expression pattern **(Fig. 5.7A, 5.7B, 5.7C and 5.7D)**. This suggests that NAD^+/NADH might control Oxphos via p107 dependent regulation of mitochondrial gene expression and ETC complex formation.

We substantiated that the NAD^+/NADH ratio promoted p107 mitochondrial function, which was not only reliant on glucose, by treatment of cells with dichloroacetic acid (DCA). DCA is an inhibitor of pyruvate dehydrogenase kinase, which normally inhibits pyruvate dehydrogenase that converts pyruvate to acetyl CoA (Rodrigues et al., 2015). Similar to oxamate, when c2c12 cells were treated with 6mM DCA for 40 hours, there was a significant decrease in NAD^+/NADH ratio compared to untreated cells **(Fig. 5.9A)**. Moreover, Western blot analysis of DCA treated cells showed increased p107 levels in the mitochondria **(Fig. 5.9B)**, as well as significant decreased mitochondrial encoded gene expression for *Nd2*, *Nd6*, *Cox2* and *Atp6* **(Fig. 5.9C)** when compared to untreated controls. Together, these results suggest that in response to lower cytoplasmic NAD^+/NADH, p107 preferentially localizes in the mitochondria, to repress mitochondrial gene expression that impacts ETC complex protein formation.

High NAD^+/NADH levels impede p107 mitochondrial function

We next assessed the p107 functional outcome of increasing the NAD^+/NADH ratio in a glucose independent manner. For this we grew cells in galactose (gal) that is known to increase Oxphos, but also increase the NAD^+/NADH ratio (Ryall et al., 2015). Indeed, growth of c2c12 cells with 10mM gal for 6 hours significantly increased the NAD^+/NADH ratio compared to the cells grown in glucose **(Fig. 5.10A)**. As expected, Western blot analysis showed that treatment of c2c12 cells with gal resulted in significantly less p107 in the mitochondria **(Fig. 5.10B)** and significantly higher mitochondrial gene expression for *Nd2*, *Nd6*, *Cox2* and *Atp6* compared to the cells grown in glucose **(Fig. 5.10C)**. This suggests that a shift to a higher NAD^+/NADH ratio, prevents p107 mitochondrial localization, thereby de-repressing mitochondrial gene expression.

Glutamine has no effect on p107 mitochondrial function

We next tested another nutrient, glutamine that is metabolized via Oxphos for a potential effect on p107 mitochondrial function. We substituted glutamine for glucose as the sole growth nutrient in stripped media. We found that c2c12 cells grown in two different concentrations of glutamine (5mM and 20mM) in stripped media had no effect on the cytoplasmic NAD^+/NADH ratio **(Fig. 5.11A)**. As anticipated, Western blot analysis of c2c12 cells grown in the different glutamine concentrations had no effect on the p107 mitochondrial localization levels, in accordance with unchanged NAD^+/NADH ratio **(Fig. 5.11B)**. Also, there was no significant mitochondrial gene expression changes for *Nd2*, *Cox2* and *Atp6* **(Fig. 5.11C)**. However, the mitochondrial encoded gene expression levels of *Nd6* was significantly increased in c2c12 cells grown in the high (20mM) compared to the low (5mM) glutamine concentration **(Fig. 5.11C)**. A possible explanation is that *Nd6* is the only mitochondrial gene expressed from the L-strand of mtDNA (D'Souza & Minczuk, 2018). Together, these results showcase that p107 acts by sensing

the cytoplasmic NAD^+/NADH ratio to regulate mitochondrial gene expression, which might influence the ATP production in the mitochondria.

Glycolytic flux regulates p107 control of mitochondrial ATP generation

We next investigated if glycolytic flux that controls mitochondrial gene expression in a p107 dependent manner can also affect the mitochondrial ATP synthesis capacity and rate. Using a luminescence assay kit, the potential ATP generation capacity and rate were determined in isolated mitochondria of c2c12 cells under different glucose concentrations that affected NAD^+/NADH ratios. We found that there was a significant decrease in the ATP generation rate and capacity of c2c12 cells at a lower NAD^+/NADH ratio, by comparing cells grown in stripped media containing 25mM to 5.5mM glucose **(Fig. 5.12A and 5.12B)**. The decrease in ATP generation capacity corresponded to the presence of p107 in the mitochondria **(Fig. 5.1A)**. Importantly, in the p107KO c2c12 cells, where mitochondrial gene expression was not influenced by the NAD^+/NADH ratio **(Fig. 5.2A, 5.2B, 5.2C and 5.2D)**, the potential mitochondrial ATP rate and generation capacity were unaffected by varying the glucose concentration **(Fig. 5.12C and 5.12D)**. Together, these data suggest that p107 regulates the potential mitochondrial energy production by recognizing the cytoplasmic NAD^+/NADH ratio.

We substantiated the importance of NAD^+/NADH to p107 control of Oxphos by treating cells with oxamate that decreased the NAD^+/NADH ratio **(Fig. 5.6A)** and increased p107 mitochondrial levels **(Fig. 5.6B)**. Live cell metabolic imaging with Seahorse of oxamate treated c2c12 cells compared to untreated cells, showed a significant decrease in OCR **(Fig. 5.13A)**, as well as ATP generation from both Oxphos and glycolysis **(Fig. 5.13B)** that corresponded to a reduced mitochondrial/glycolytic ATP ratio **(Fig. 5.13C).** Together this data suggests that, in response to a shift to low NAD^+/NADH ratio, p107 locates in the mitochondria to attenuate ATP

generation capacity as a consequence of repressing mitochondrial gene expression and limiting ETC complex formation.

We next considered that enhanced p107 mitochondrial function, by overloading NADH levels might lead to increased ROS generation. In this case, we hypothesized that NADH accretion, due to oxamate, would cause mitochondrial ROS by reductive stress, by overwhelming ETC complex I (Xiao & Loscalzo, 2020) and/or due to drastically reduced number of ETC complexes **(Fig. 5.8)** instigated by p107 repression of mitochondrial gene repression **(Fig. 5.7A, 5.7B, 5.7C and 5.7D)**. To test the possibility, we stained both oxamate treated and untreated c2c12 cells, with dihydrorhodamine 123 (DHR123). DHR123 is an uncharged non-fluorescent ROS indicator that is oxidized to positively charged fluorescent rhodamine 123 (R123) in the mitochondria (O'Connell et al., 2002). By flow cytometry, we found that oxamate treated cells produced significantly higher levels of R123. This might be potentially caused by higher mitochondrial ROS produced in oxamate treated compared to untreated cells **(Fig. 5.14A and 5.14B)**. Moreover, this was a p107 dependent mechanism, as ROS generation was not affected in p107KO cells treated with oxamate compared to untreated cells **(Fig. 5.14A and 5.14B)** where mitochondrial gene expression **(Fig. 5.7A, 5.7B, 5.7C and 5.7D)** and ETC complex formation **(Fig. 5.8)** were unaltered by this treatment. Together, this suggests that p107 mitochondrial localization might increase the potential for mitochondrial ROS generation. We believe this might occur because limiting ETC complex proteins due to repression of mitochondrial gene expression might not sufficiently oxidize augmented NADH levels. On the other hand, in p107KO cells the greater capacity of the ETC for Oxphos, might buffer the increased availability of NADH. Further experiments using mitochondrial targeted ROS fluorophores that are oxidized directly by mitochondrial superoxides such as MitoSOX Red/ Amplax Red shall confirm this function.

To further assess that suppression of mitochondrial genes by p107 might lead to enhanced ROS production, we overexpressed p107KO c2c12 cells with empty vector alone or together with p107fl (full length p107) or with p107mls that contained a mitochondrial localization sequence. We hypothesized that over expression of these p107 constructs that decreased mitochondrial gene expression **(Fig. 4.10A, 4.10B, 4.10C and 4.10D)** would lead to increased ROS production, as was found with oxamate treatment **(Fig. 5.14A and 5.14B)**. Thus, we measured ROS by staining the transfected cells with DHR123 and performing flow cytometry to quantify the amount of fluorescence caused by its oxidation. We found that overexpression of p107fl and p107mls resulted in high ROS levels **(Fig. 5.15A and 5.15B)**. Thus, this result corroborates that elevated p107 levels in the mitochondria might promote mitochondrial ROS generation.

Sirt1 directly interacts with p107

As p107 mitochondrial function is regulated by the NAD^+/NADH ratio and NAD^+ dependent Sirt1 deacetylase is an energy sensor of this ratio (Anderson et al., 2017), we evaluated if Sirt1 potentially controls p107 mitochondrial function. To test this possibility, we first determined if p107 and Sirt1 interact endogenously. Importantly, reciprocal Immunoprecipitation (IP)/Western blot analysis of p107 and Sirt1 on native non over-expressing c2c12 lysates showed that they directly interacted **(Fig. 5.16B and 5.16C)**. $1/10^{th}$ of the lysates that were used in the IP reactions were Western blotted for p107 and Sirt1 to provide an estimate of the input protein lysate that were IPed. We also used two negative controls to bolster the validity of our findings. First, the specificity of the antibodies used were tested using lysates **(Fig. 5.16B and 5.16C)** for p107 on p107KO cells **(Fig. 4.3A)**; and for Sirt1 on genetically deleted Sirt1 (Sirt1KO) cells, which were made using Crispr/Cas9 **(Fig. 5.16A)**. Second, a negative IP control with an IgG antibody did not display a p107 or Sirt1 interaction upon Western blotting **(Fig. 5.16B and 5.16C).** These results

highlight that p107 interacts with Sirt1 in native cellular protein lysates, suggestive of a potential mechanism to regulate p107 mediated mitochondrial function.

Genetic deletion of Sirt1 increases p107 mitochondrial function

We next gauged if Sirt1 activity might affect p107 mitochondrial function. For this, we grew c2c12 and Sirt1KO cells in stripped media with a low glucose concentration (5.5mM) that results in a high NAD^+/NADH ratio, a condition that is known to activate Sirt1 activity. We had demonstrated that 5.5mM glucose concentration significantly decreased p107 sub-cellular localization inside the mitochondria **(Fig. 5.1A)**. However, unlike control cells Western blot analysis of Sirt1KO cells showed that p107 is present in the mitochondria of c2c12 cells grown in stripped media with 5.5mM glucose **(Fig. 5.17A).** This signifies that p107 mitochondrial translocation is dependent on Sirt1 activity. Therefore, we predicted that due to presence of p107 in the mitochondria of Sirt1KO cells, its mitochondrial gene expression would be lower compared to control cells. Indeed, qPCR analysis showed that there were significant reductions of the mitochondrial encoded genes *Nd2, Nd6, Cox2* and *Atp6*, in Sirt1KO cells compared to controls grown in 5.5mM glucose **(Fig. 5.17B)**. Relevantly, these results suggest that p107 mitochondrial function is dependent on Sirt1 activity.

Next, we wanted to compare Sirt1KO cells grown in 5.5mM to 25mM glucose. We had demonstrated a significant lower p107 mitochondrial presence in c2c12 cells grown in 5.5mM compared to 25mM glucose **(Fig. 5.1A)** and it did not relocate from the mitochondria in Sirt1KO cells grown in 5.5mM **(Fig. 5.17A).** Thus, we postulate that p107 mitochondrial localization should not be affected in Sirt1KO cells grown in 25mM versus 5.5mM glucose concentration. To test this, we performed Western blot analysis on Sirt1KO c2c12 cells grown in 5.5mM and 25mM glucose and as expected, we did not find any differences in p107 mitochondrial levels **(Fig. 5.18A)**.

This is in contrast to control cells that showed differences in p107 mitochondrial localization in low versus high glucose concentrations **(Fig. 5.1A)**. This finding corresponded to no changes in the mitochondrial encoded gene expression for *Nd2*, *Nd6*, *Cox2* and *Atp6* for Sirt1KO cells grown in 5.5mM versus 25mM glucose **(Fig. 5.18B),** unlike control cells that displayed decreased mitochondrial gene expression in the higher glucose concentration due to increased p107 levels in the mitochondria **(Fig. 5.2A, 5.2B, 5.2C and 5.2D)**.

These results suggest that Sirt1 activity might also affect the mitochondrial ATP generation function of p107, implied by the decreased mitochondrial gene expression in Sirt1KO cells compared to control c2c12 cells grown in 5.5mM glucose. We tested this notion, by using a luminescence assay for potential ATP generation rate and capacity on isolated mitochondria. The mitochondria were normalized to their protein content to exclude the potential contribution of their number. We found that ATP generation rate and capacity of Sirt1KO cells were drastically reduced **(Fig. 5.19A and 5.19B)** compared to control cells in 5.5mM glucose which aligned with p107 localization **(Fig. 5.17A)** and the mitochondrial encoded gene expression **(Fig. 5.17B)**. Furthermore, there were no differences in ATP generation rate or capacity between Sirt1KO cells grown in 5.5mM or 25mM glucose **(Fig. 5.19C and 5.19D)** corresponding to unaltered p107 mitochondrial levels **(Fig. 5.18A)** and mitochondrial gene expression **(Fig. 5.18B)**. Together, these data suggest that p107 mitochondrial function is dependent on Sirt1 activity.

Sirt1 deacetylase activity affects p107 mitochondrial function

As Sirt1 deletion affected p107 mediated mitochondrial function, we next wanted to evaluate if the deacetylase activity of Sirt1 affected p107 mitochondrial function. To accomplish this, we used expression plasmids for Sirt1 full length (Sirt1fl), that retained its enzymatic function and Sirt1 dominant negative (Sirt1dn), which had a base substitution (H363Y) in the deacetylase

catalytic site rendering it inactive (Ghosh et al., 2007). c2c12 cells were transiently transfected with hemagglutinin (HA) tagged p107fl alone or together with Sirt1fl or Sirt1dn and grown in low (5.5mM) or high (25mM) glucose concentrations in stripped media. Confocal microscopy and Z-stack analysis revealed that overexpression of Sirt1dn grown in 5.5mM glucose was unable to prevent Ha tagged p107 mitochondria localization **(Fig. 5.20),** similar to Sirt1KO cells that had p107 in the mitochondria when grown in the same condition **(Fig. 5.18A)**. Moreover, there were no differences in mitochondrial p107HA levels in the overexpressing Sirt1dn cells grown in 5.5mM and 25mM glucose. However, Sirt1fl over expressing cells grown in 5.5mM glucose and 25mM glucose showed differences in p107 mitochondrial localization **(Fig. 5.21)**, similar to c2c12 cells grown in low and high glucose **(Fig. 5.1A)**. This suggests that Sirt1 deacetylase activity is vital for encumbering p107 mitochondrial localization.

Next, we assessed Sirt1 activity on mitochondrial encoded gene expression, to find a possible association with p107 subcellular localization. c2c12 cells were transiently transfected with Sirt1fl or Sirt1dn, grown in 5.5mM and 25mM glucose in stripped media and analyzed by qPCR for *Nd2*, *Nd6*, *Cox2* and *Atp6* genes. We found that Sirt1dn overexpressing c2c12 cells had no differences in mitochondrial encoded gene expression when grown in 5.5mM or 25mM glucose **(Fig. 5.22A, 5.22B, 5.22C and 5.22D)** which is in accordance with the unchanged p107 mitochondrial localization **(Fig. 5.20 and 5.21)**, However, Sirt1fl overexpressing c2c12 cells showed decreased mitochondrial gene expression when grown in a higher concentration (25mM) compared to lower concentration (5.5mM) of glucose **(Fig. 5.22A, 5.22B, 5.22C and 5.22D)**. This suggests that Sirt1 enzyme activity is important for regulating p107 mediated mitochondrial function.

Inhibition of Sirt1 activity enhances p107 mitochondrial function

To further confirm that Sirt1 catalytic action is important for p107 mitochondrial function, we modulated Sirt1 activity using various factors to appraise its influence on p107 mediated mitochondrial function. First, we tested the effect of inhibiting Sirt1 by treating c2c12 cells with Sirt1 inhibitor nicotinamide (Nam). Western blot analysis showed that inhibition of Sirt1 activity by Nam increased p107 mitochondrial localization compared to untreated cells **(Fig. 5.23A)**. To determine if the inhibition of Sirt1 activity that had promoted p107 mitochondrial localization, increased its interaction with mtDNA promoter, we conducted qChIP assays. The increased mitochondrial presence of p107 with compromised Sirt1 activity was concomitant with increased mtDNA promoter interaction **(Fig. 5.23B)**. IgG antibody was used as a negative control for non-specific immunoglobulin-chromatin interaction in presence or absence of Nam. We found that unlike differential interaction by p107, IgG showed negligible binding at the D-loop regulatory region of the mtDNA with and without Nam **(Fig. 5.23B)**. Moreover, no p107 detection was observed at the D-loop promoter in p107KO cells **(Fig. 5.23B)**.

We appraised if the effect of increased mtDNA interaction of p107 due to inhibition of Sirt1 activity influenced mitochondrial gene expression. Indeed, we found that Nam treatment decreased the expression of *Nd2*, *Nd6*, *Cox2* and *Atp6* genes compared to untreated c2c12 cells **(Fig. 5.24A)**. However, Nam treatment of p107KO and Sirt1KO c2c12 cells had no effect on the mitochondrial gene expression **(Fig. 5.24B and 5.24C)**. Importantly, these data suggest that Sirt1 activity influences mitochondrial gene expression in a p107 dependent manner, as absence of either p107 or Sirt1 failed to impact changes on the mitochondrial gene expression.

Next, we found that both the potential ATP generation rate and capacity of isolated mitochondria were reduced with Sirt1 attenuated activity with Nam in c2c12 cells **(Fig. 5.25A and 5.25B**). On the contrary, Sirt1KO cells showed no differences in ATP generation capacity and rate

with Nam treatment **(Fig. 5.25C and 5.25D)** that corresponded to a lack of changes in mitochondrial gene expression profile **(Fig. 5.24C)**. Finally, we confirmed that the decreased mitochondrial gene expression and ATP generation rate and capacity by inhibiting Sirt1 with Nam was not due to a decrease in mitochondrial biogenesis. This was accomplished by assessing the mtDNA content by quantifying the potential changes in the mtDNA/nDNA ratio. The ratio remained unaltered in Nam treated compared to untreated c2c12 cells **(Fig. 5.25E)**. These results suggest that the functional consequence of inhibiting Sirt1 activity is due to the mitochondrial function of p107 and not a change in mitochondrial content.

We corroborated the effect of inhibiting Sirt1 activity on p107 mitochondrial function by treating c2c12 cells with a high dose (50μM) of resveratrol (Res) that is known to repress Sirt1 activity (Park et al., 2012). By Western blotting, treatment of cells with this concentration of Res showed increased p107 localization in the mitochondria compared to untreated cells **(Fig. 5.26A)**. This was associated with significantly reduced mitochondrial gene expression for *Nd2*, *Nd6*, *Cox2* and *Atp6* **(Fig. 5.26B)** together with significant attenuation of ATP generation rate and capacity **(Fig. 5.26C),** as was the case when using Nam as an inhibitor. Together, these results suggest that inhibition of Sirt1 catalytic activity increases p107 localization within the mitochondria where it interacts at the mtDNA to repress mitochondrial encoded gene expression and decrease ATP generation potential.

Enhancing Sirt1 activity decreases p107 mitochondrial function

We verified that Sirt1 enzymatic activity regulated p107 mitochondrial function by enhancing Sirt1 catalytic activity indirectly using a low concentration of Res (10μM) (Park et al., 2012). Western blot analysis of c2c12 cells treated with this concentration of Res resulted in a decrease for p107 levels in the mitochondria **(Fig. 5.27A)**.

Using qChIP we also found that the enriched Sirt1 activity with low Res treatment reduced p107 mtDNA promoter interaction at the D-loop **(Fig. 5.27B)**. The IgG antibody used as a negative control for non-specific interaction showed negligible binding at the D-loop regulatory region of the mtDNA and no detection was observed in p107KO cells **(Fig. 5.27B)**.

We performed qPCR to determine if decreased p107 mtDNA interaction with activated Sirt1 (low Res treatment) would de-repress mitochondrial gene expression. As expected, heightened Sirt1 activity, enhanced the mitochondrial encoded gene expression for *Nd2*, *Nd6*, *Cox2* and *Atp6* when the cells were treated with 10μM Res **(Fig. 5.28A).** Relevantly, no differences were observed in p107KO and Sirt1KO c2c12 cells untreated or treated with this Res concentration (10μM) **(5.28B and 5.28C),** suggesting that Sirt1 catalytic activity regulates mitochondrial gene expression directly in a p107 dependent manner.

We hypothesized that boosting Sirt1 activity with low (10μM) Res treatment would influence the ATP generation rate and capacity. This idea was tested by performing ATP generation assays. We found that the potential ATP synthesis rate and capacity of isolated mitochondria from c2c12 cells were significantly greater when Sirt1 activity was enriched **(Fig. 5.29A and 5.29B)**. This corresponded to the increased p107 redistribution from the mitochondria to the cytoplasm **(Fig. 5.27A)** and significant elevation of mitochondrial gene expression **(Fig. 5.28A)**. However, no differences in ATP generation rate and capacity were observed in Sirt1KO c2c12 cells **(Fig. 5.29C and 5.29D)**, which was anticipated because 10μM Res had no effect on mitochondrial gene expression **(Fig. 5.28C)**. Together, these results suggest that Sirt1 catalytic activity directly regulates p107 sub-cellular localization that ultimately impacts its repressive function on mitochondrial gene expression and ATP generation capacity.

Figure 5.1

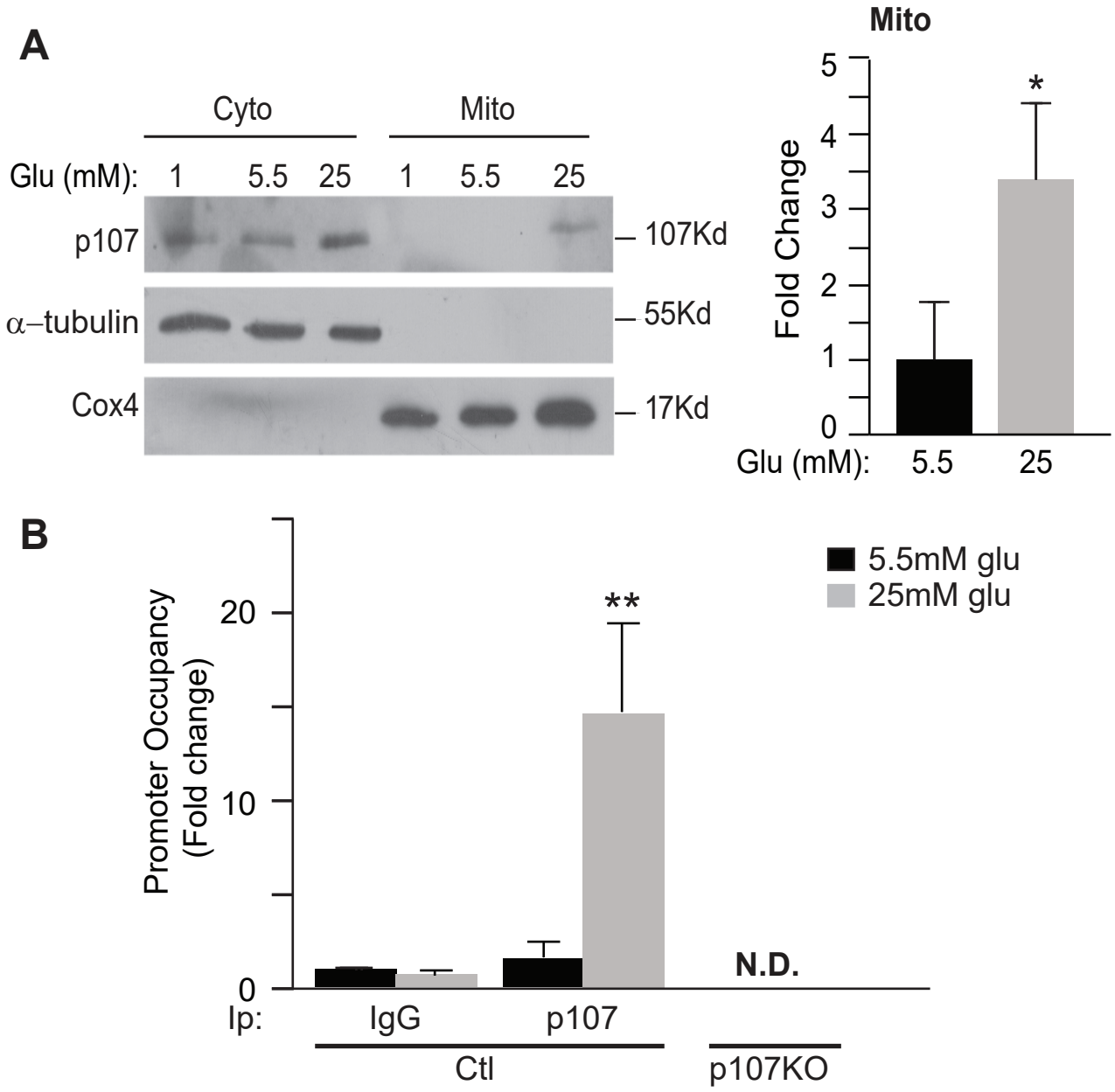

Figure 5.1. Increased glucose availability increases p107 mitochondrial localization and mtDNA promoter binding in c2c12 cells. (A) Representative Western blot and graphical representation of cytoplasmic (Cyto) and mitochondrial (Mito) fractions for p107, α-tubulin and Cox4 of c2c12 cells grown in stripped media (SM) containing only 1.0mM, 5.5mM or 25mM glucose (Glu), n=3, asterisks denote significance, *p<0.05; Student T-test. **(B)** Graphical representation of relative p107 and IgG mitochondrial DNA promoter occupancy by qChIP analysis for control (Ctl) and p107KO c2c12 cells grown in SM containing only 5.5mM (LoGlu) or 25mM (HiGlu) glucose, N.D denotes not detected. n=3, asterisks denote significance, **p<0.01; two-way Anova with post hoc Tukey test.

Figure 5.2

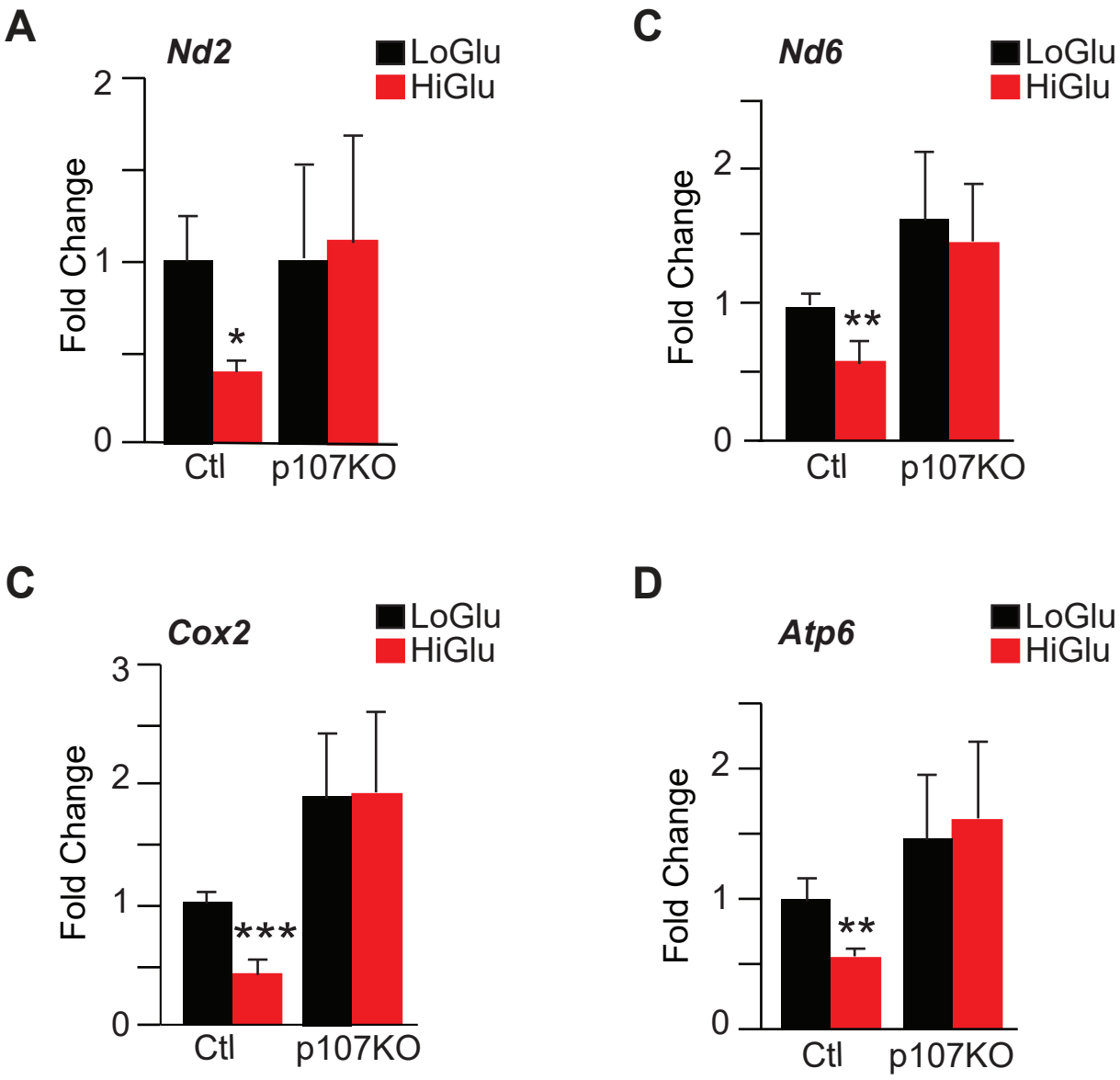

Figure 5.2. p107 reduces mitochondrial gene expression of c2c12 cells in high glucose. Gene expression analysis by qPCR of mitochondrial encoded genes **(A)** *Nd2*, **(B)** *Nd6*, **(C)** *Cox2* and **(D)** *Atp6* for Control (Ctl) and p107KO c2c12 cells grown in stripped media containing only 5.5mM glucose (LoGlu) or 25mM glucose (HiGlu), n=4, asterisks denote significance, *p<0.05, **p<0.01, ***p<0.001; two-way Anova with post hoc Tukey test.

Figure 5.3

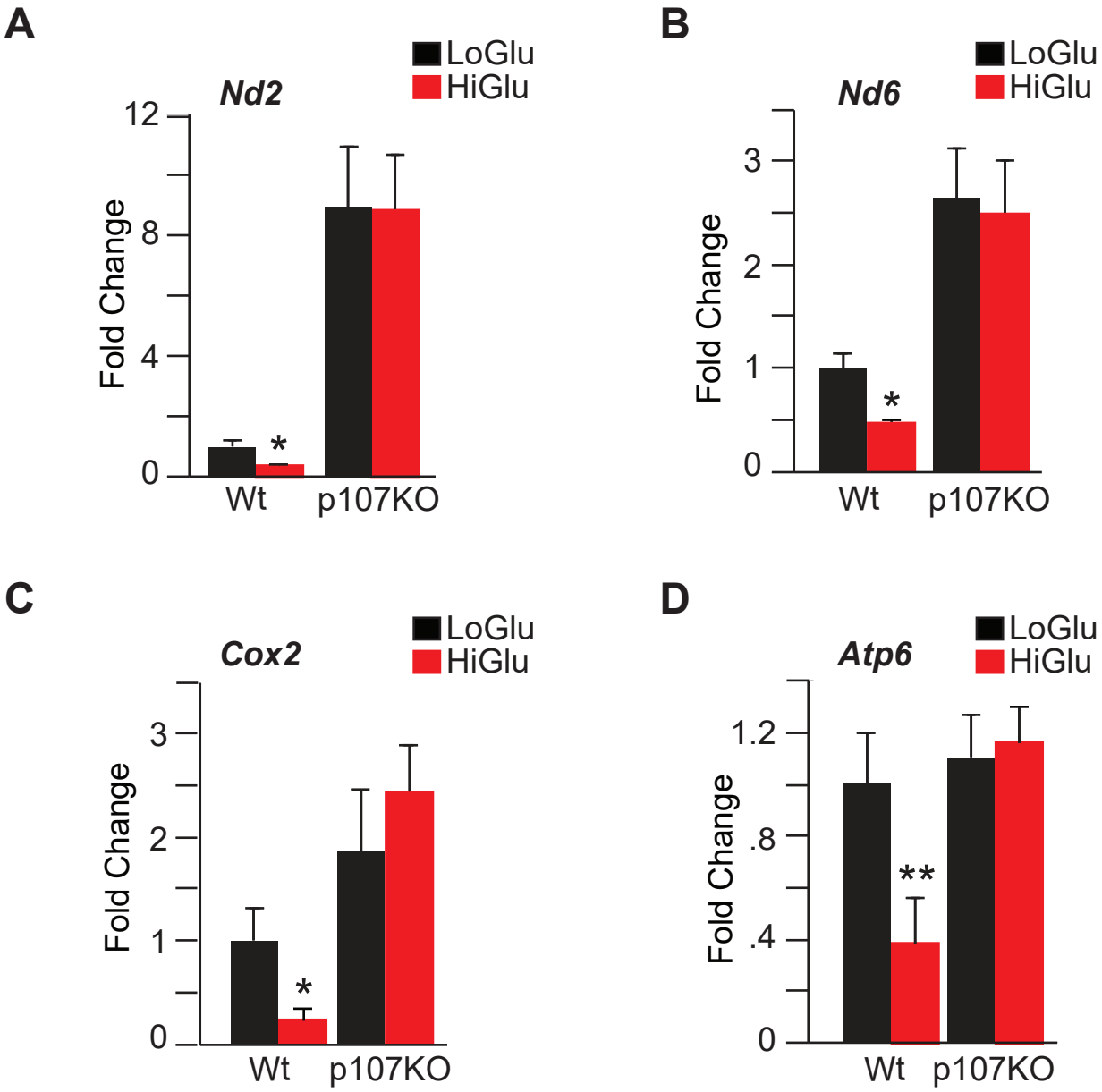

Figure 5.3. p107 reduces mitochondrial gene expression of prMPs in high glucose. Gene expression analysis by qPCR of mitochondrial encoded genes **(A)** *Nd2*, **(B)** *Nd6*, **(C)** *Cox2* and **(D)** *Atp6* for wild type (Wt) and p107KO prMPs grown in stripped media containing only 5.5mM glucose (LoGlu) or 25mM glucose (HiGlu), n=4, asterisks denote significance, *p<0.05, **p<0.01; two-way Anova with post hoc Tukey test.

Figure 5.4

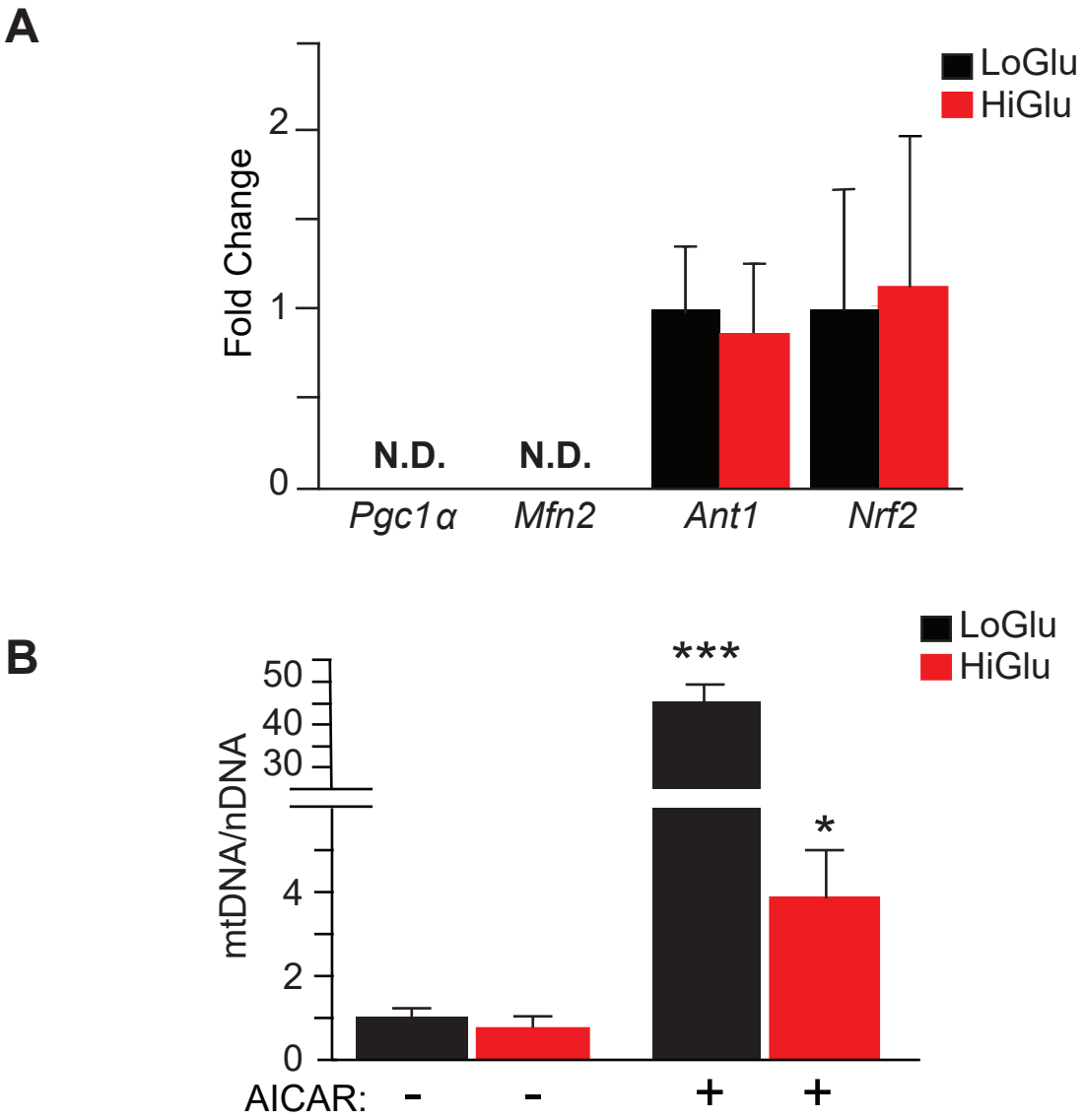

Figure 5.4. High glucose availability does not influence mitochondrial content. (A) Gene expression analysis by qPCR of *Pgc1α*, *Mfn2*, *Ant1* and *Nrf2* for c2c12 cells grown in stripped media (SM) containing 5.5mM glucose (LoGlu) or 25mM glucose (HiGlu), n=3 (N.D. is not detected). **(B)** Mitochondrial DNA (mtDNA) to nuclear DNA (nDNA) ratio for c2c12 cells grown in SM containing LoGlu or HiGlu in the absence or presence of 5-aminoimidazole-4-carboxamide ribonucleotide (AICAR), n=3, asterisks denote significance, *p<0.05, ***p<0.001; two-way Anova with post hoc Tukey test.

Figure 5.5

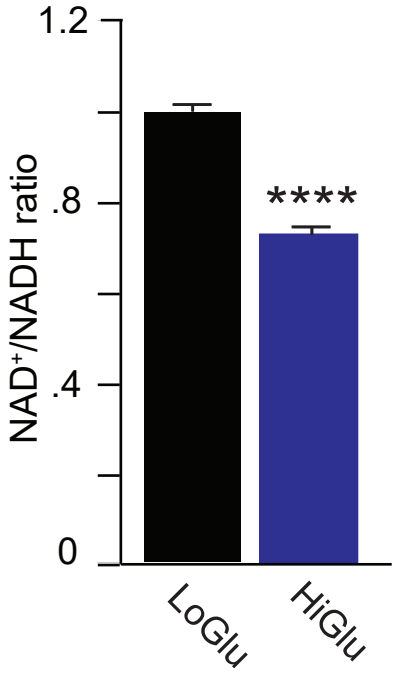

Figure 5.5. High glucose availability decreases NAD⁺/NADH ratio. NAD⁺/NADH ratio for c2c12 cells grown in stripped media containing 5.5mM glucose (LoGlu) or 25mM glucose (HiGlu), n=3, asterisks denote significance, ****p<0.0001; Student T-test.

Figure 5.6

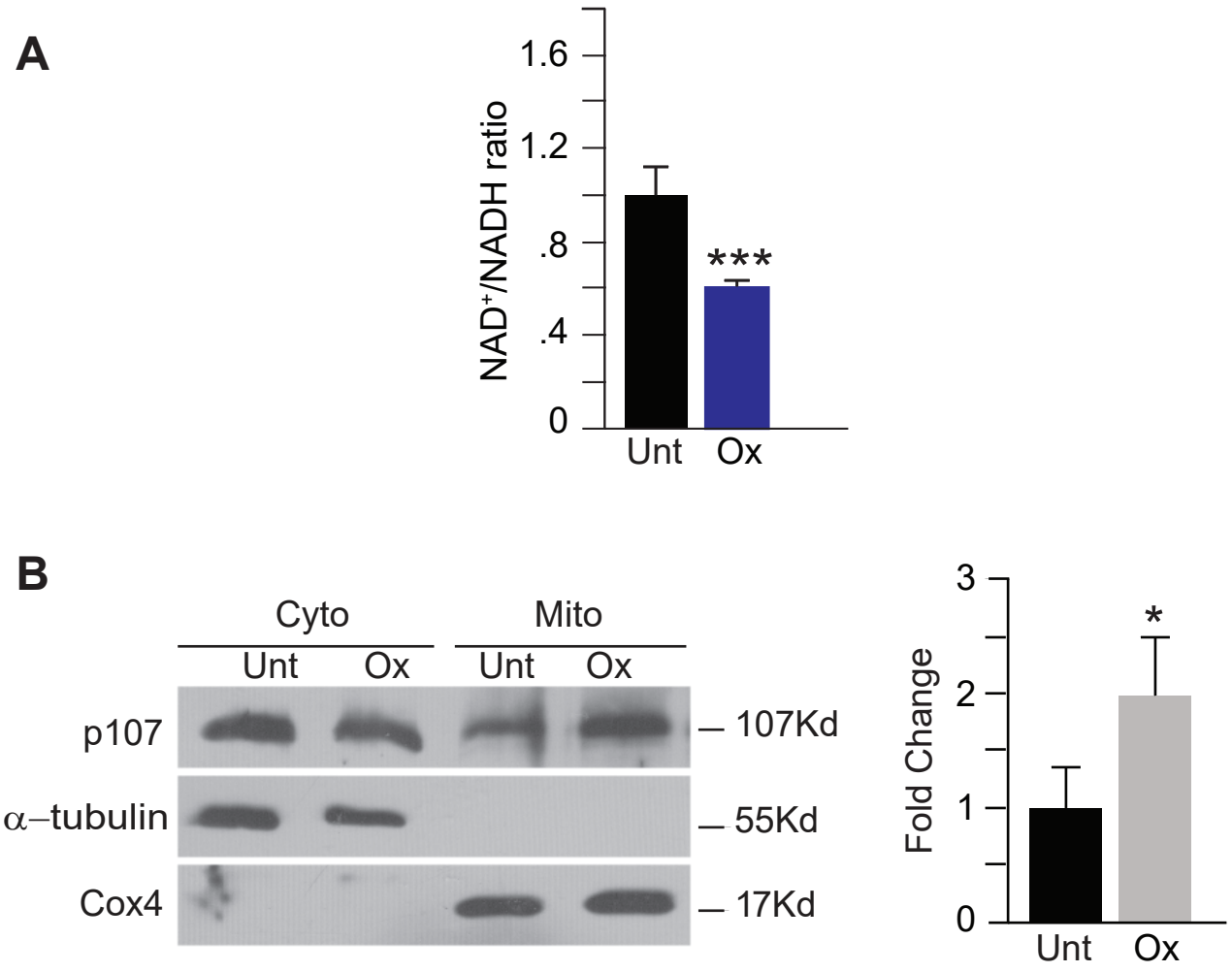

Figure 5.6. Oxamate decreases NAD⁺/NADH ratio and enhances p107 mitochondrial localization. (A) NAD⁺/NADH ratio for c2c12 cells untreated (Unt) or treated with 2.5mM oxamate (Ox), n=4, asterisks denote significance, ***p<0.001; Student T-test. **(B)** Representative Western blots of cytoplasmic (Cyto) and mitochondrial (Mito) fractions for p107, α-tubulin and Cox4 and graphical representaion of Mito fractions of cells in (A), n=3, asterisks denote significance, *p<0.05; Student T-test.

Figure 5.7

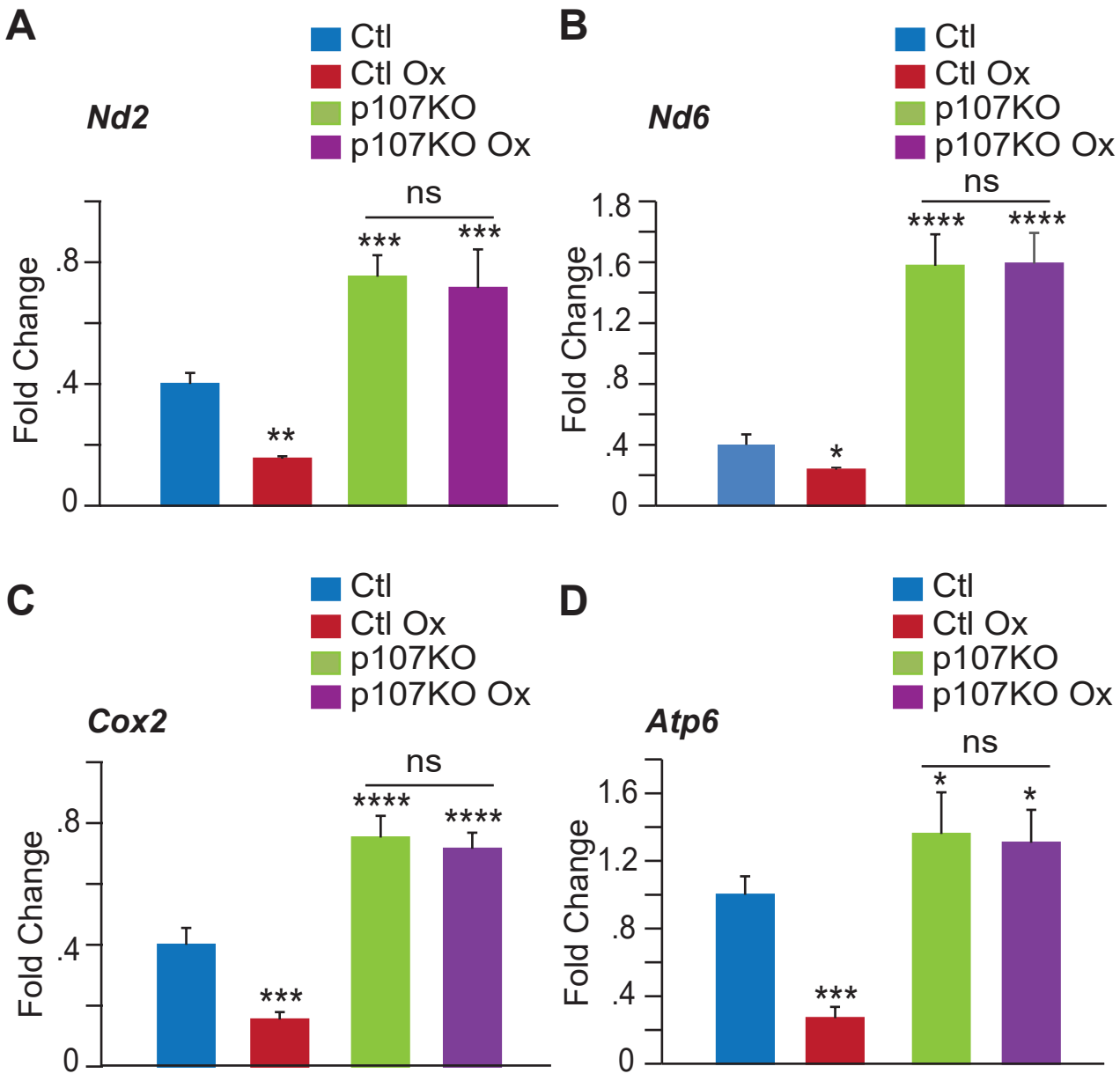

Figure 5.7. p107 decreases mitochondrial encoded gene expression of c2c12 cells treated with oxamate. Gene expression analysis by qPCR of mitochondrial encoded genes **(A)** *Nd2*, **(B)** *Nd6*, **(C)** *Cox2* and **(D)** *Atp6* for control (Ctl) and p107KO c2c12 cells untreated or treated with 2.5mM oxamate (Ox), n=4, difference between p107KO cells treated or untreated with Ox is non-significant (ns), asterisks denote significance, **p*<0.05; ***p*<0.01, ****p*<0.001, *****p*<0.0001; two- way Anova and post hoc Tukey test.

Figure 5.8

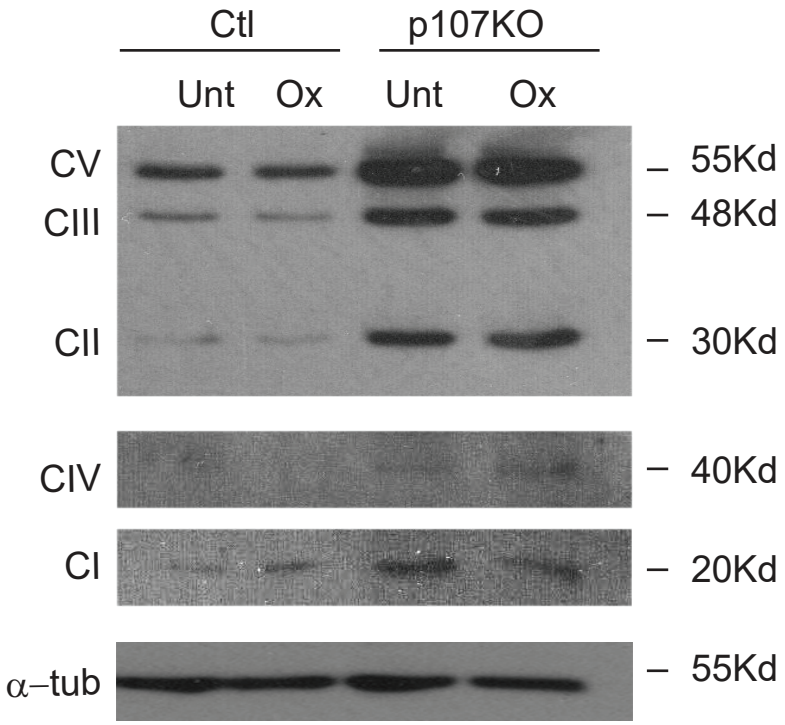

Figure 5.8. Oxamate treatment decreases electron transport chain complex formation in a p107 dependent manner. Representative Western blot for control (Ctl) and p107KO c2c12 cells untreated or treated with 2.5mM oxamate (Ox) for electron transport chain complex (C) subunits, CI (NDUFB8), CII (SDHB), CIII (UQCRC2), CIV (MTCO) and CV (ATP5A).

Figure 5.9

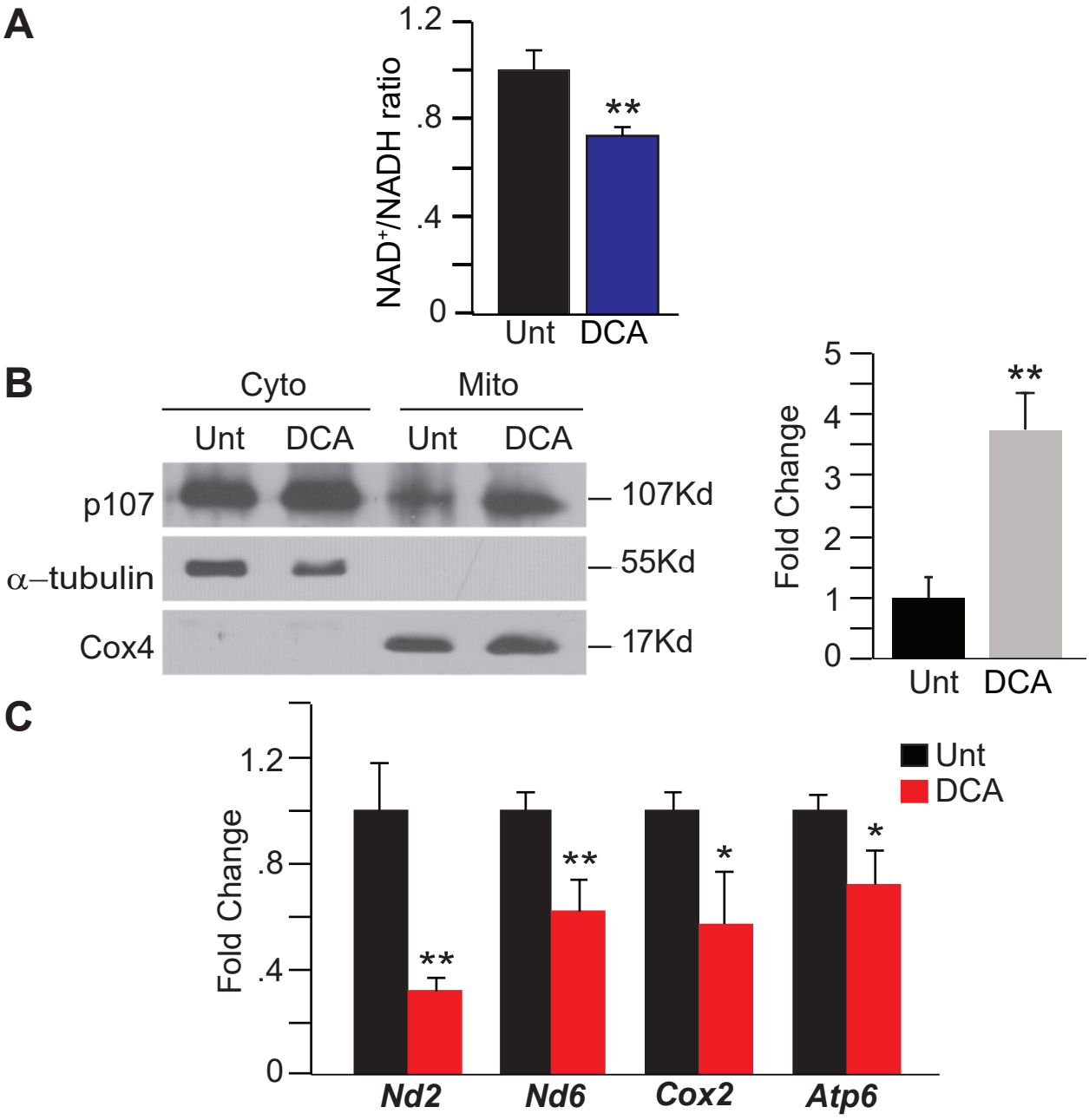

Figure 5.9. Dicholoroacetic acid decreases the NAD⁺/NADH ratio, enhances p107 mitochondrial localization and decreases miochondrial encoded gene expression. **(A)** NAD⁺/NADH ratio for c2c12 cells untreated (Unt) or treated with dichloroacetic acid (DCA), n=4, asterisks denote significance, ***p*<0.01; Student T-test. **(B)** Representative Western blot of cytoplasmic (Cyto) and mitochondrial (Mito) fractions for p107, α-tubulin and Cox4 and graphical representation of p107 in the mito fraction of c2c12 cells in (A), n=3, asterisks denote significance, ***p*<0.01; Student T-test. **(C)** qPCR analysis of cells in (A) for mitochondrial encoded genes *Nd2*, *Nd6*, *Cox2* and *Atp6*, n=3, asterisks denote significance, **p*<0.05, ***p*<0.01; Student T-test.

Figure 5.10

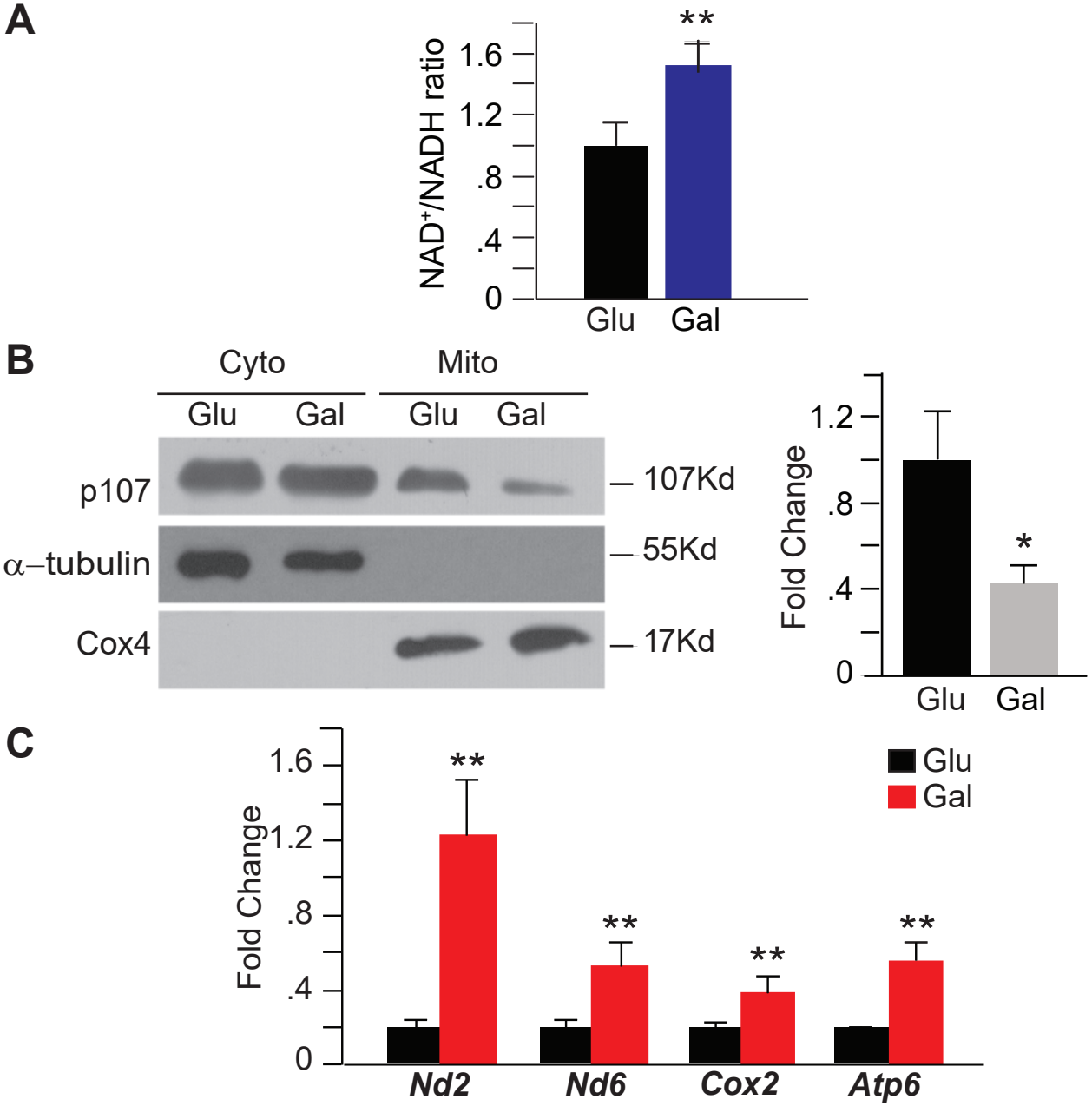

Figure 5.10. Galactose increases the NAD⁺/NADH ratio, decreases p107 mitochondrial localization and enhances miochondrial encoded gene expression.
(A) NAD⁺/NADH ratio for c2c12 cells grown in 25mM glucose (Glu) or 10mM galactose (Gal), n=4, asterisks denote significance, ***p*<0.01; Student T-test. **(B)** Representative Western blot and graphical representation of cytoplasmic (Cyto) and mitochondrial (Mito) fractions for p107, α-tubulin and Cox4 and graphical represntation of mito fractions of c2c12 cells in (A), n=3, asterisks denote significance, **p*<0.05; Student T-test. **(C)** qPCR analysis of cells in (A) for mitochondrial encoded genes *Nd2*, *Nd6*, *Cox2* and *Atp6*, n=3, asterisks denote significance, ***p*<0.01; Student T-test.

Figure 5.11

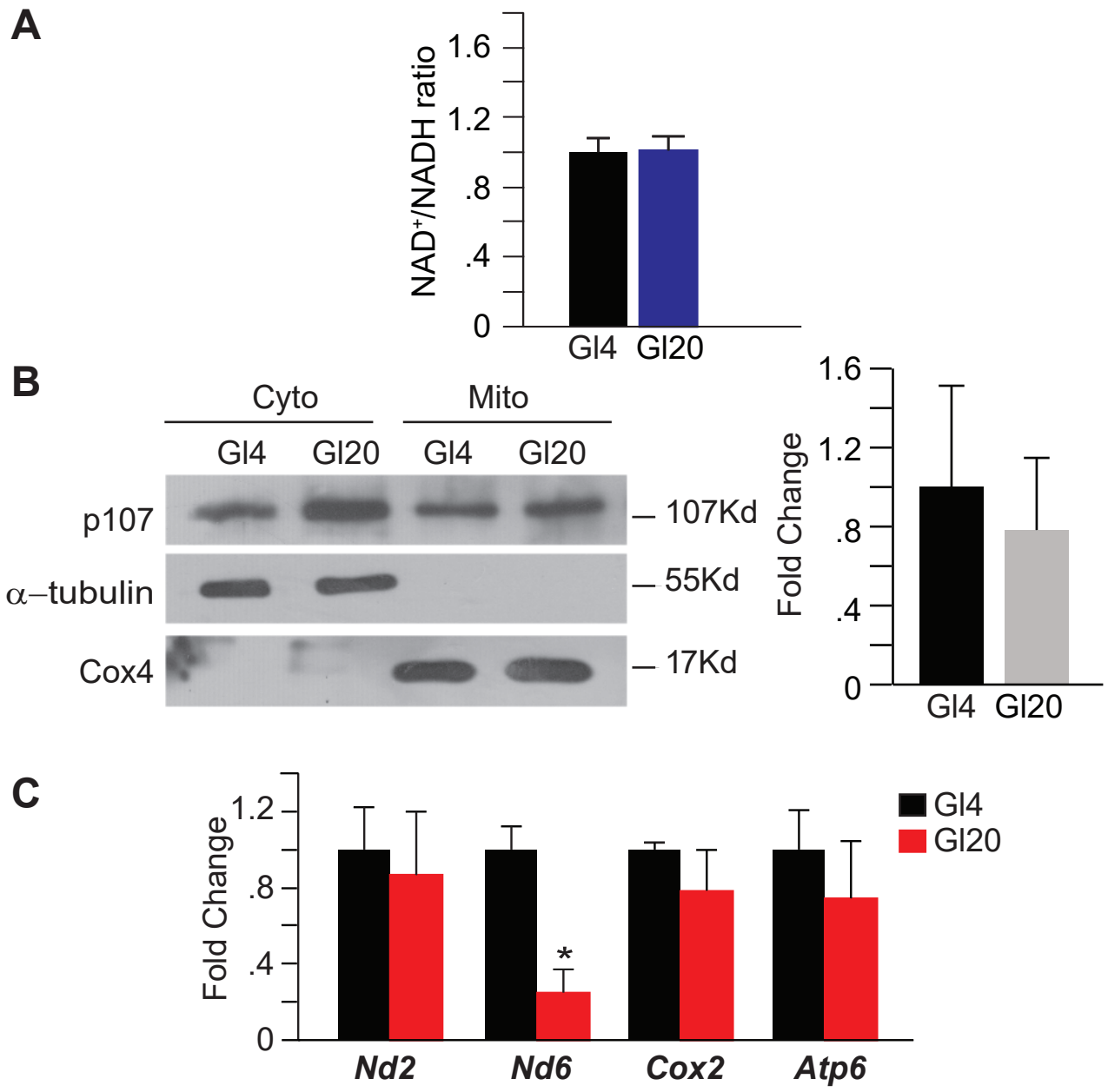

Figure 5.11. Unvarying NAD⁺/NADH ratio by glutamine treatment does not affect p107 mitochondrial localization and function. (A) NAD⁺/NADH ratio for c2c12 cells grown in varying concentrations of glutamine (Gl), 4mM and 20mM, n=4; Student T-test. **(B)** Representative Western blot and graphical representation of cytoplasmic (Cyto) and mitochondrial (Mito) fractions for p107, α-tubulin and Cox4 and graphical represntation of mito fractions of c2c12 cells in (A), n=3. **(C)** qPCR analysis of cells in (A) for mitochondrial encoded genes *Nd2*, *Nd6*, *Cox2* and *Atp6*, n=3, asterisk denote significance, *$p<0.05$; Student T-test.

Figure 5.12

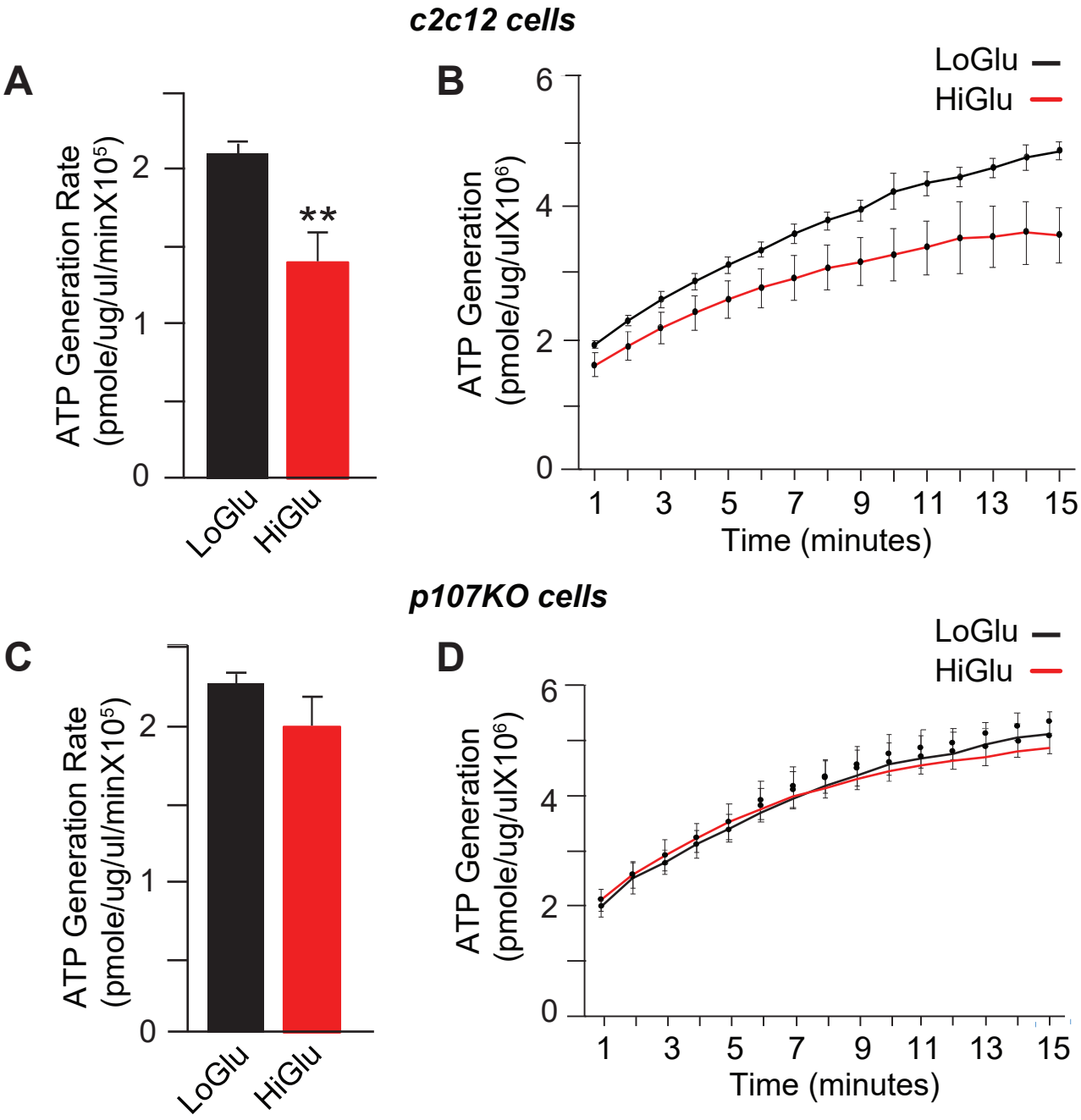

Figure 5.12. p107 is associated with decreased mitochondrial ATP generation in high glucose. ATP generation **(A)** rate and **(B)** capacity over time for isolated mitochondria from c2c12 cells, grown in stripped media containing 5.5mM glucose (LoGlu) or 25mM glucose (HiGlu), n=4. ATP generation **(C)** rate and **(D)** capacity over time for isolated mitochondria from p107KO c2c12 cells, grown in stripped media containing 5.5mM glucose (LoGlu) or 25mM glucose (HiGlu), n=4. For rate, asterisks denote significance, $^{**}p<0.01$; Student T-test. For capacity statistics see Table 3.

Figure 5.13

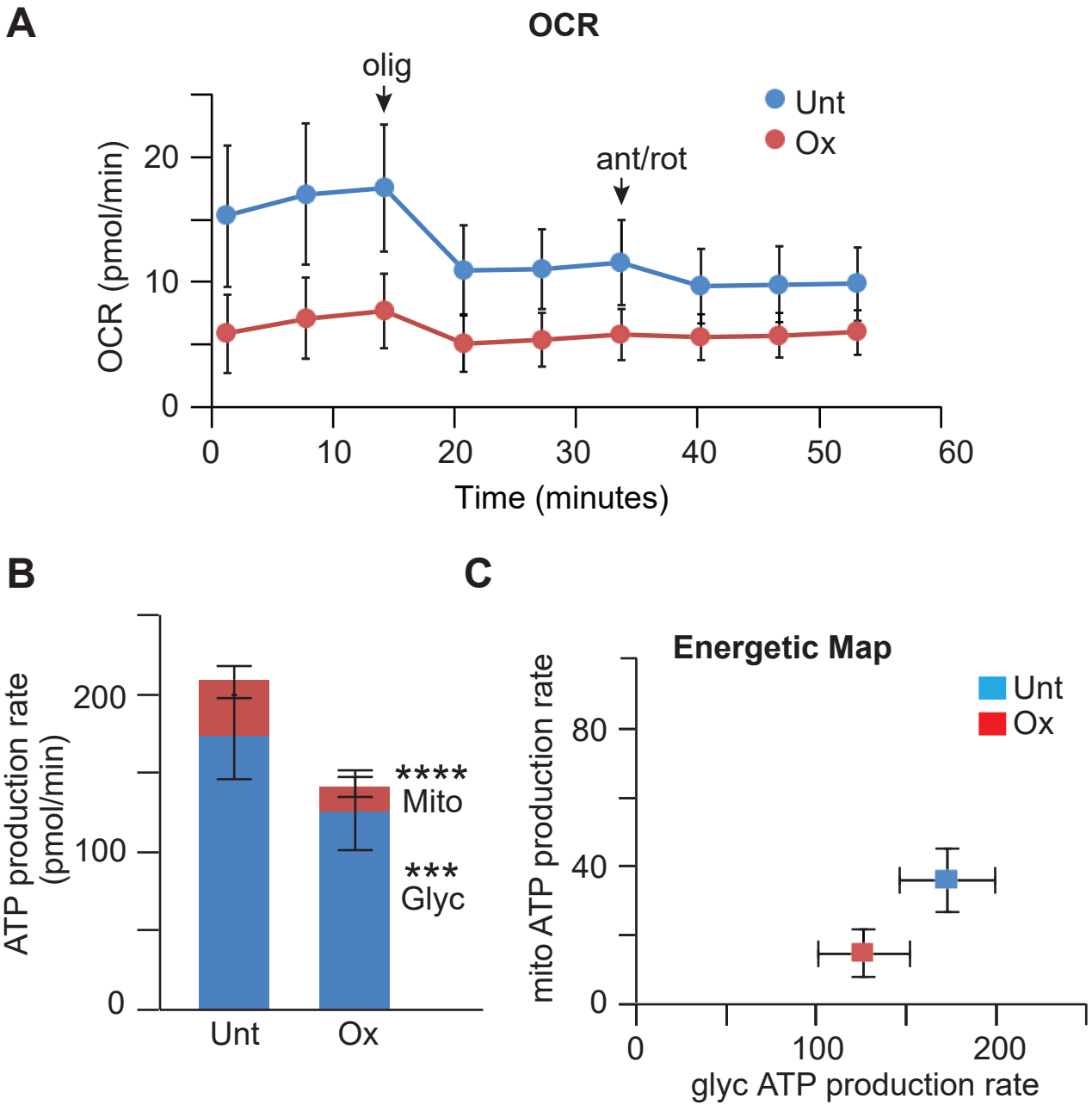

Figure 5.13. Oxamate decreases mitochondrial oxygen consumption and mitochondrial to glycolytic ATP production rates. Live cell metabolic analysis by Seahorse for **(A)** oxygen consumption rate (OCR) over time with addition of oligomycin (olig), antimycin A (ant) and rotenone (rot) **(B)** Glycolytic (Glyc) and mitochondrial (Mito) ATP production rate and **(C)** Energetic map for c2c12 cells untreated (Unt) or treated with oxamate (Ox), n=6-8, ***p<0.001, ****p<0.0001; Student T-test.

Figure 5.14

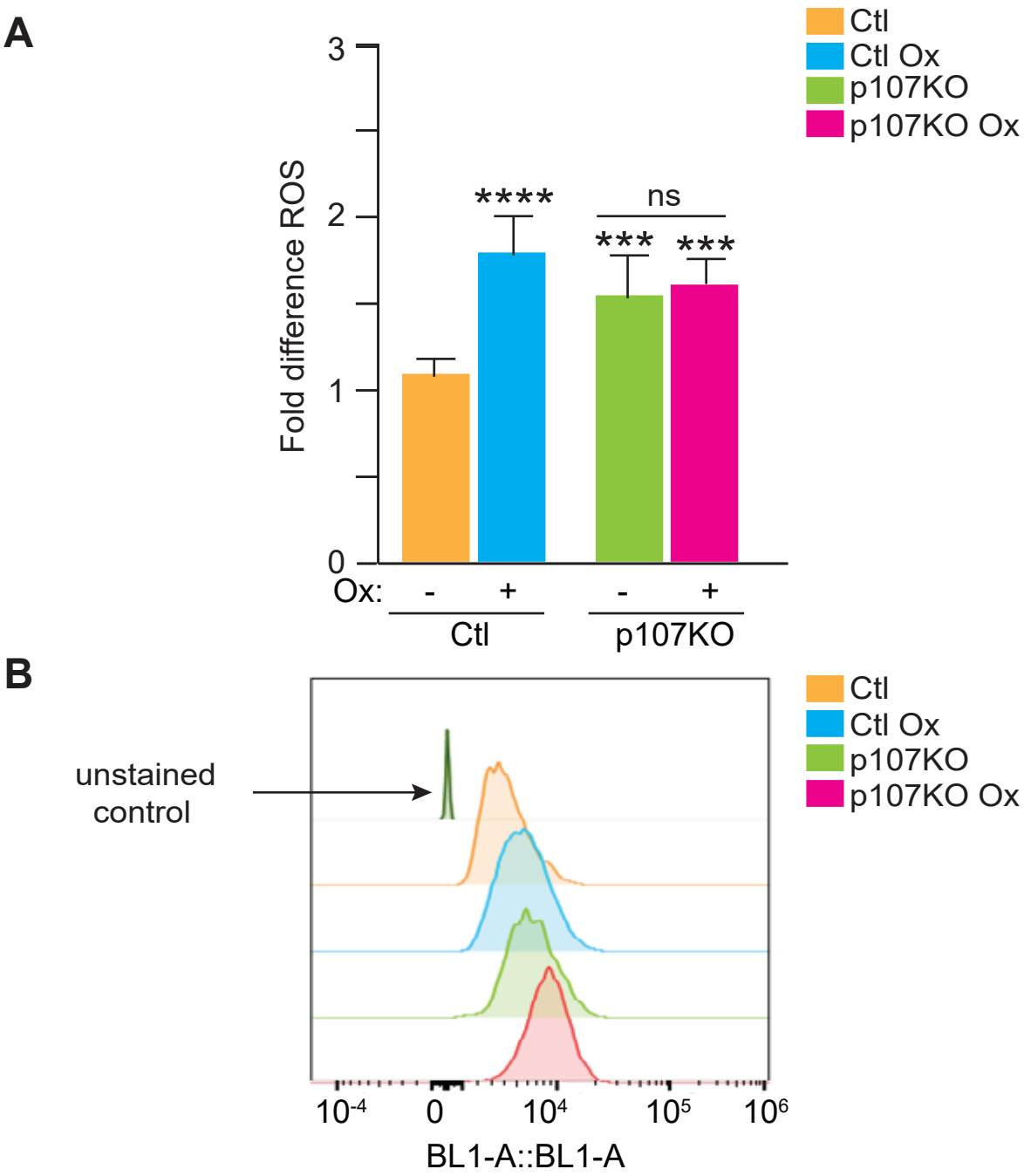

Figure 5.14. p107 mitochondrial function increases mitochondrial ROS production in c2c12 cells treated with oxamate. (A) Graphical representation **(B)** Intensity peaks for mitochondrial ROS generation for control (Ctl) and p107KO c2c12 cells untreated or treated with 2.5mM oxamate (Ox), n=6-8, difference between p107KO cells treated or untreated with Ox is non-significant (ns), asterisks denote significance, ****p*<0.001, *****p*<0.001; two-way Anova with post hoc Tukey test.

Figure 5.15

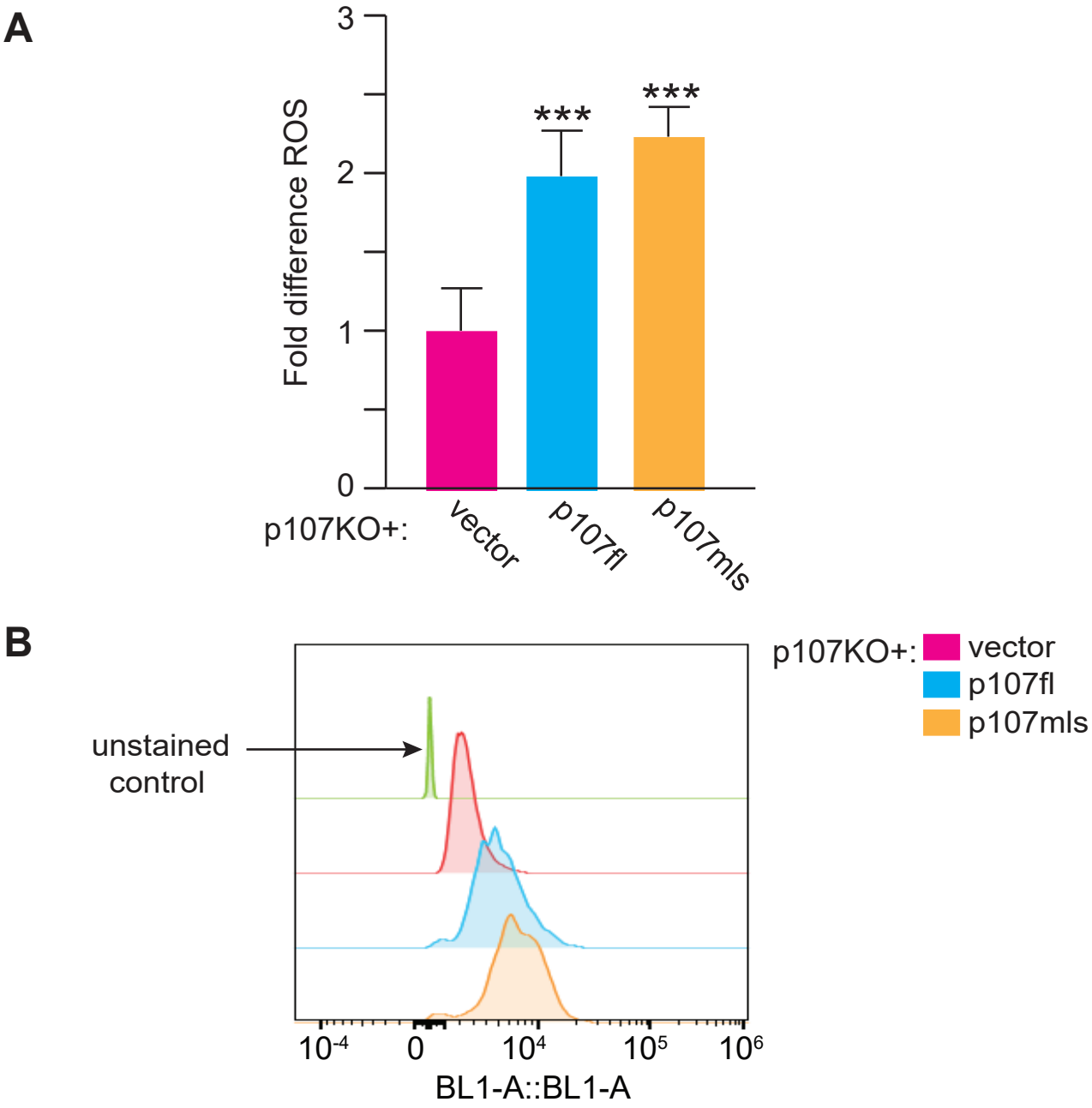

Figure 5.15. p107 overexpression increases mitochondrial ROS production. (A) Graphical representation **(B)** Intensity peaks for mitochondrial ROS generation for p107KO c2c12 cells transfected with either empty vector alone or together with full length p107 (p107fl) or p107 with mitochondrial localization sequence (p107mls), n=6-8, ***p*<0.01, ****p*<0.001; one-way Anova with post hoc Tukey test.

Figure 5.16

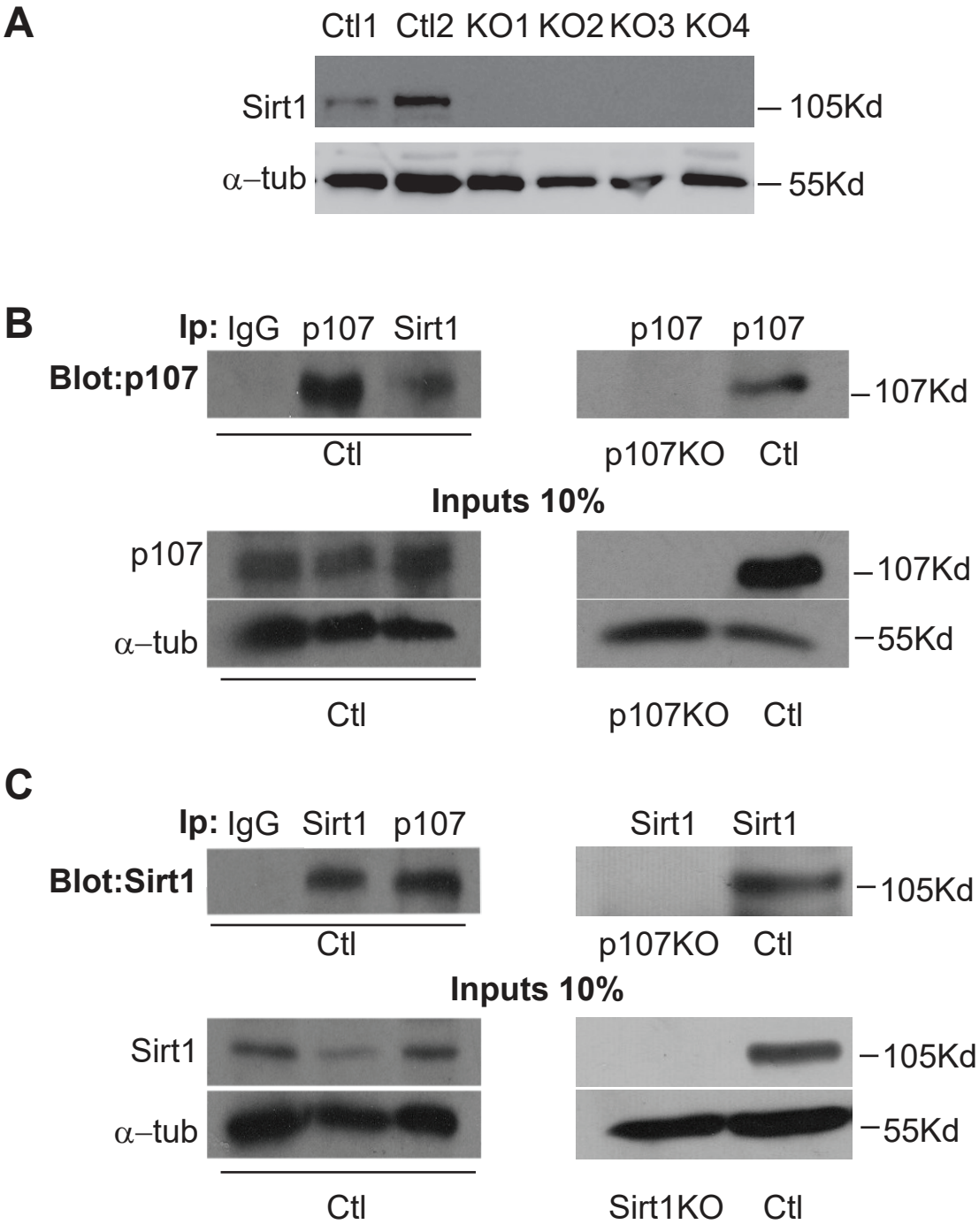

Figure 5.16. p107 interacts with Sirt1 endogenously. (A) Representative Western blot for Sirt1 and α-tubulin (α-tub) of genetically deleted Sirt1 (Sirt1KO) clones generated using Crispr/Cas9 in c2c12 cells. Immunoprecipitation and Western blot for **(B)** p107 and **(C)** Sirt1 of endogenous c2c12 cells. Inputs for analysis of p107KO and Sirt1KO are 10%.

Figure 5.17

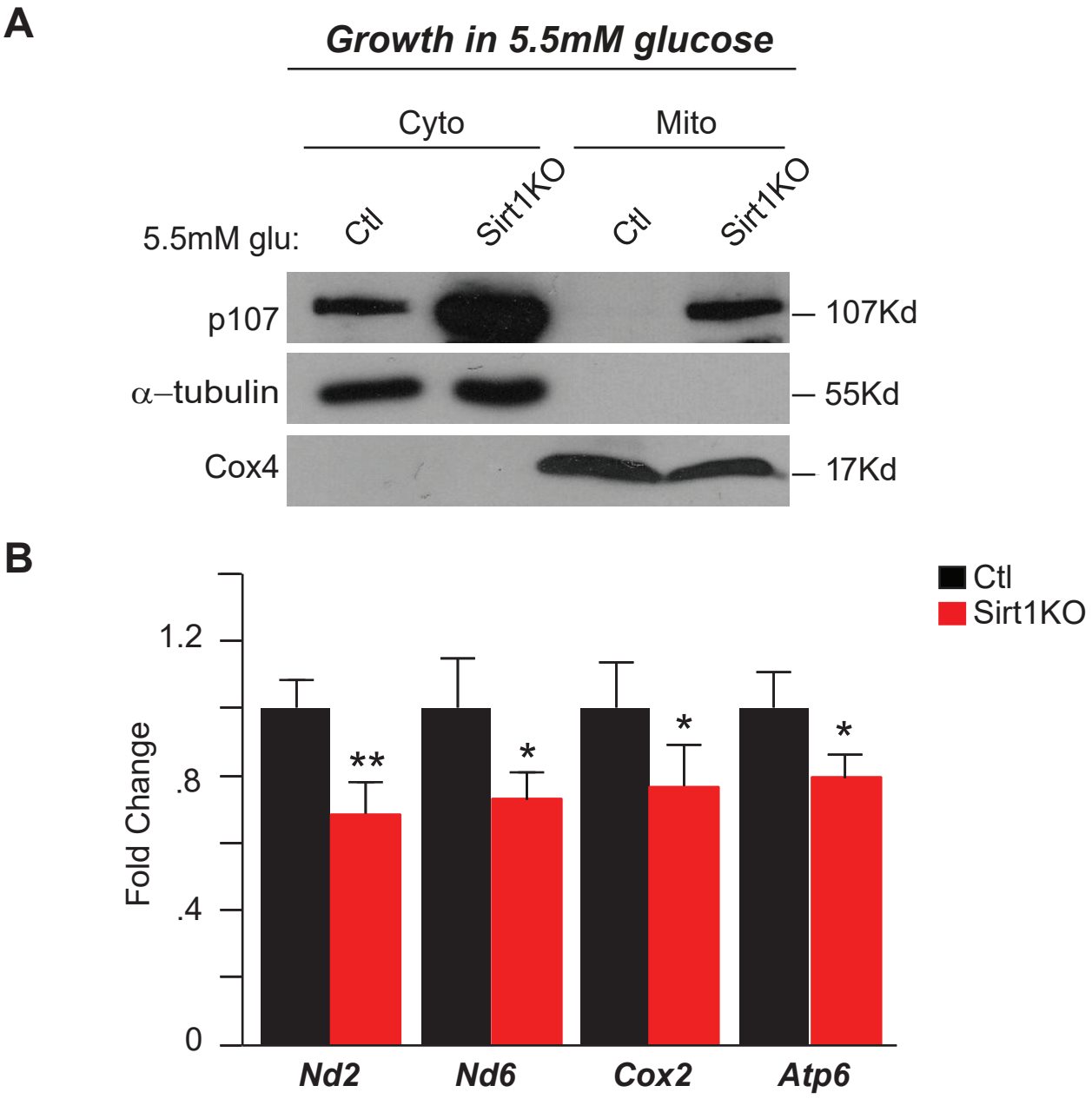

Figure 5.17. p107 mitochondrial localization is not prevented by Sirt1 genetically deleted cells. (A) Representative Western blot of cytoplasmic (Cyto) and mitochondrial (Mito) fractions for p107, α-tubulin and Cox4 and **(B)** qPCR for mitochondrial encoded genes *Nd2*, *Nd6*, *Cox2* and *Atp6* of control **(**Ctl) and Sirt1KO c2c12 cells grown in stripped media containing 5.5mM glucose, n=4, asterisks denote significance, **p*<0.05, ***p*<0.01; Student T-test.

Figure 5.18

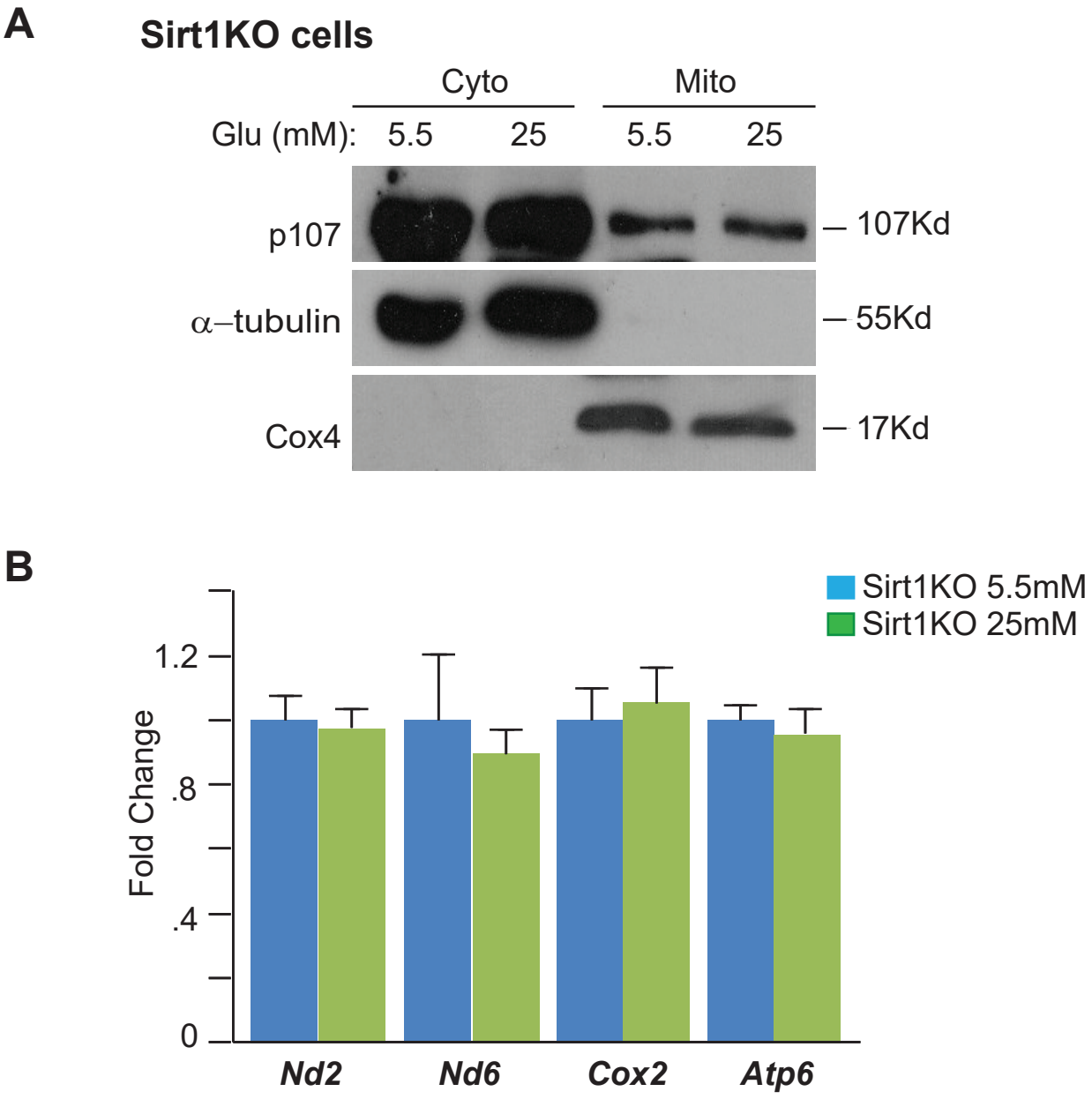

Figure 5.18. Growth in varied glucose conditions do not affect p107 mitochondrial localization and mitochondrial encoded gene expression in Sirt1KO cells. (A) Representative Western blot of cytoplasmic (Cyto) and mitochondrial (Mito) fractions for p107, α-tubulin and Cox4 and **(B)** qPCR for mitochondrial encoded genes *Nd2*, *Nd6*, *Cox2* and *Atp6* of Sirt1KO c2c12 cells grown in stripped media containing 5.5mM and 25mM glucose, n=4; Student T-test.

Figure 5.19

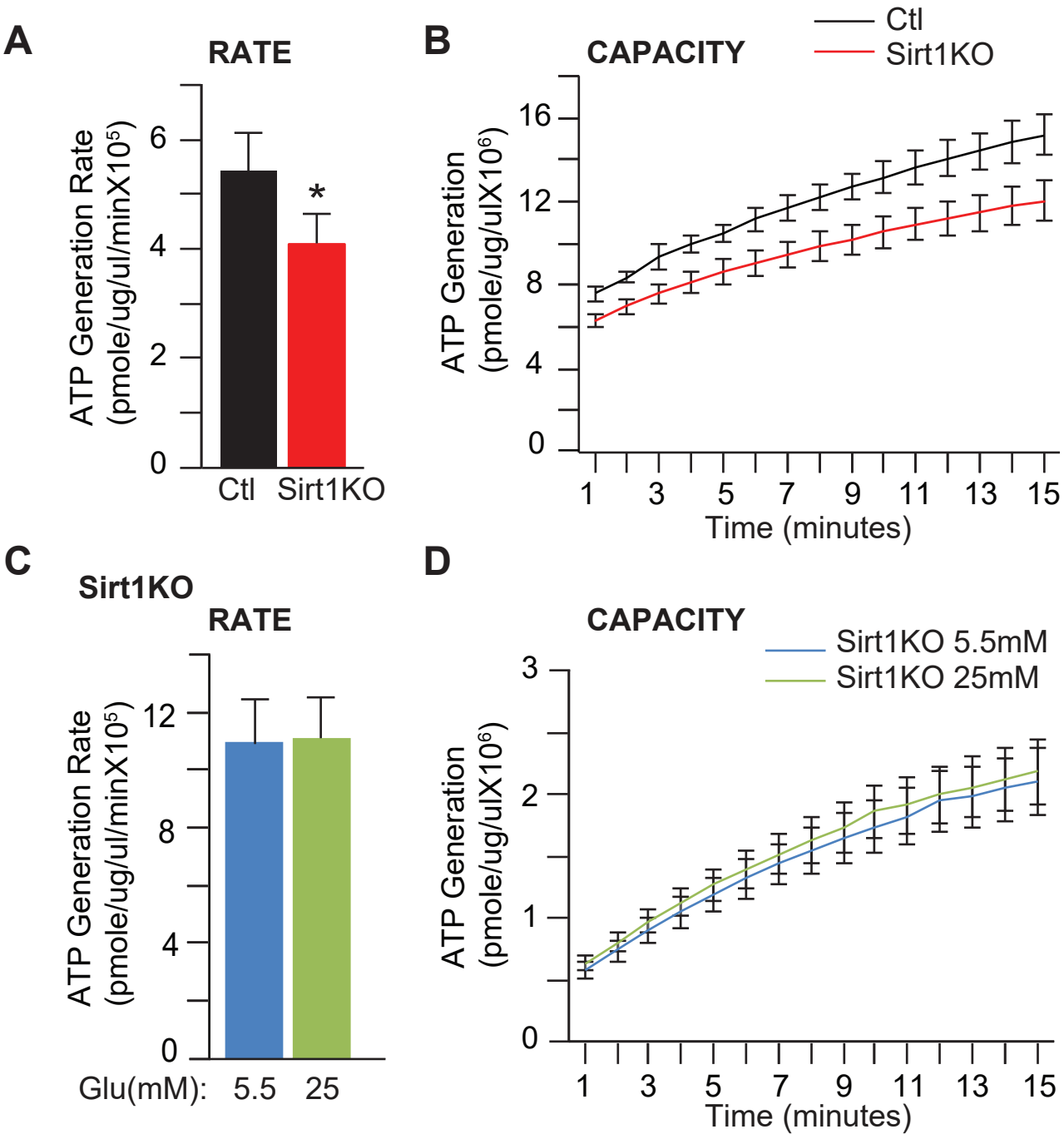

Figure 5.19. Sirt1 genetically deleted cells have dysregulated Oxphos associated with p107 mitochondrial function. (A) ATP generation rate and **(B)** capacity for mitochondria isolated from control (Ctl) and Sirt1KO c2c12 cells grown in stripped media containing 5.5mM glucose. **(C)** ATP generation rate and **(D)** capacity for mitochondria isolated from Sirt1KO c2c12 cells grown in stripped media containing 5.5mM or 25mM glucose, n=4, asterisks denote significance, *p<0.05; Student T-test. For capacity statistics see Table 3.

Figure 5.20

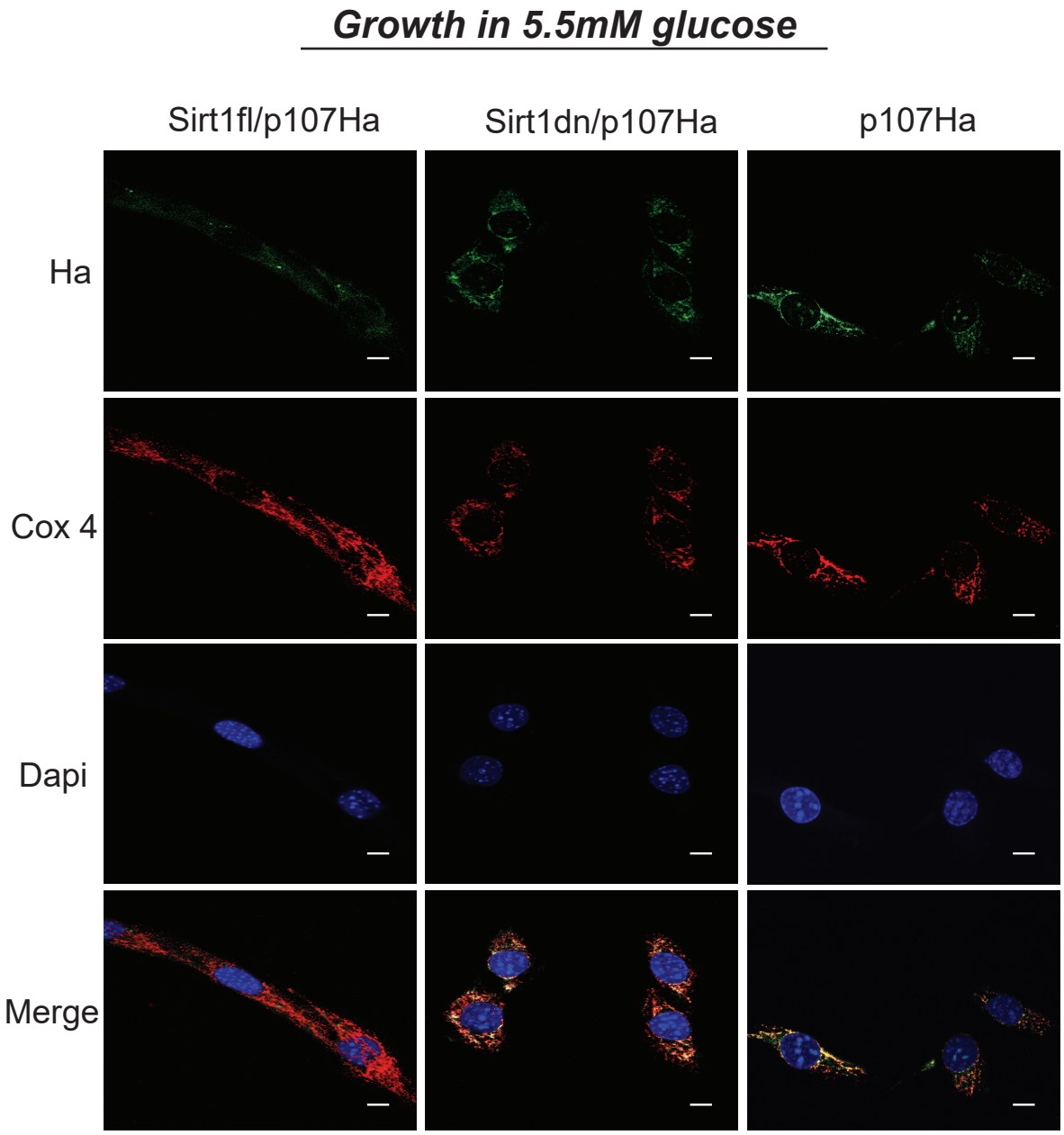

Figure 5.20. Sirt1 enzymatic activity is necessary for p107 mitochondrial localization. Confocal immunofluorescence microscopy and Z-stack (100 nm interval) image using the ZEN program (Zeiss) for Ha (green), Cox4 (red), Dapi (blue) and Merge of c2c12 cells grown in stripped media containing 5.5mM glucose that were transfected with full length Ha-tagged p107 (p107Ha) alone or with full length Sirt1 (Sirt1fl) or dominant negative Sirt1 (Sirt1dn) (scale bar 10μm).

Figure 5.21

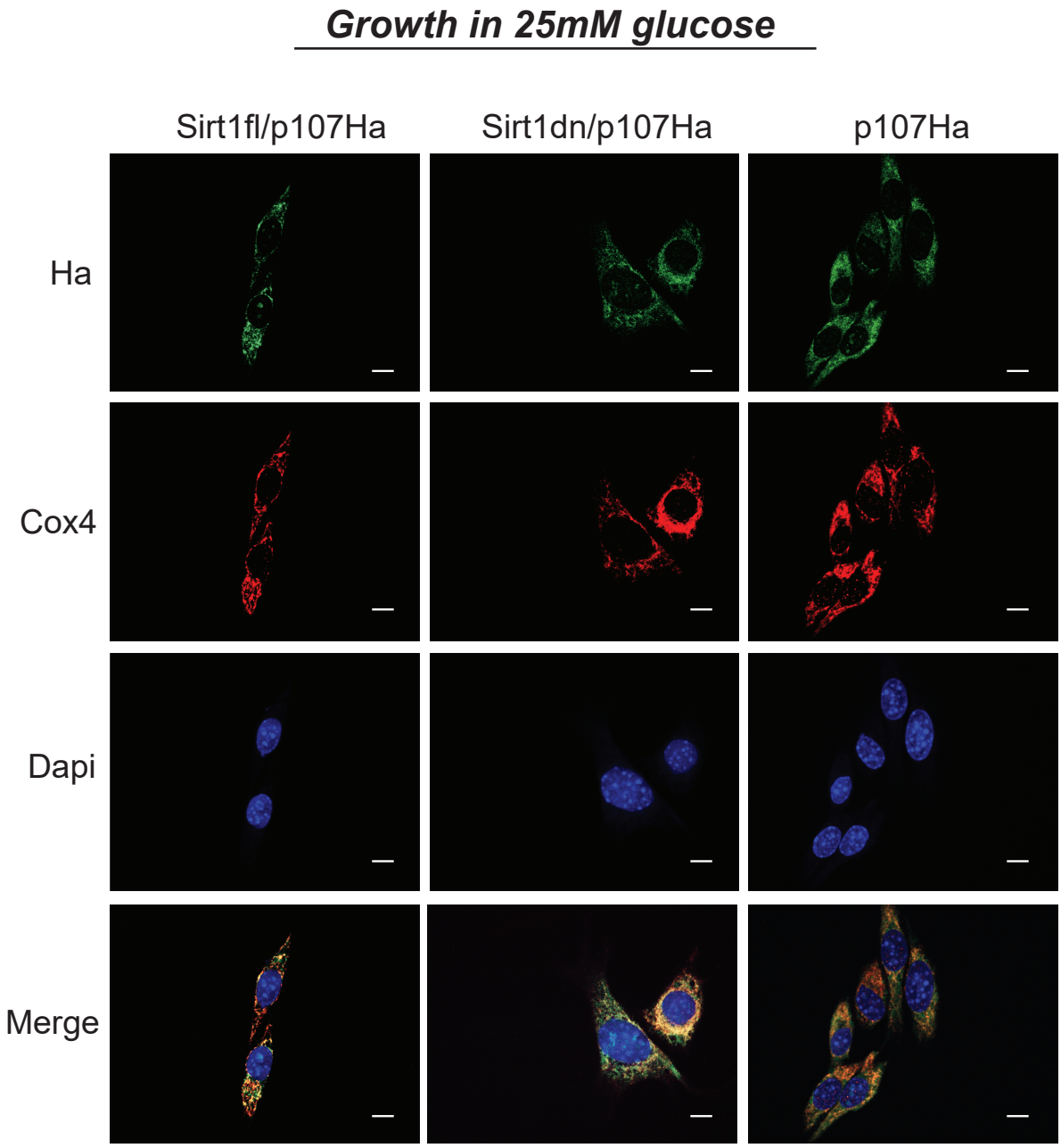

Figure 5.21. Sirt1 enzymatic activity is necessary for p107 mitochondrial localization. Confocal immunofluorescence microscopy and Z-stack (100 nm interval) image using the ZEN program (Zeiss) for Ha (green), Cox4 (red), Dapi (blue) and Merge of c2c12 cells grown in stripped media containing 25mM glucose that were transfected with full length Ha-tagged p107 (p107Ha) alone or with full length Sirt1 (Sirt1fl) or dominant negative Sirt1 (Sirt1dn) (scale bar 10μm).

Figure 5.22

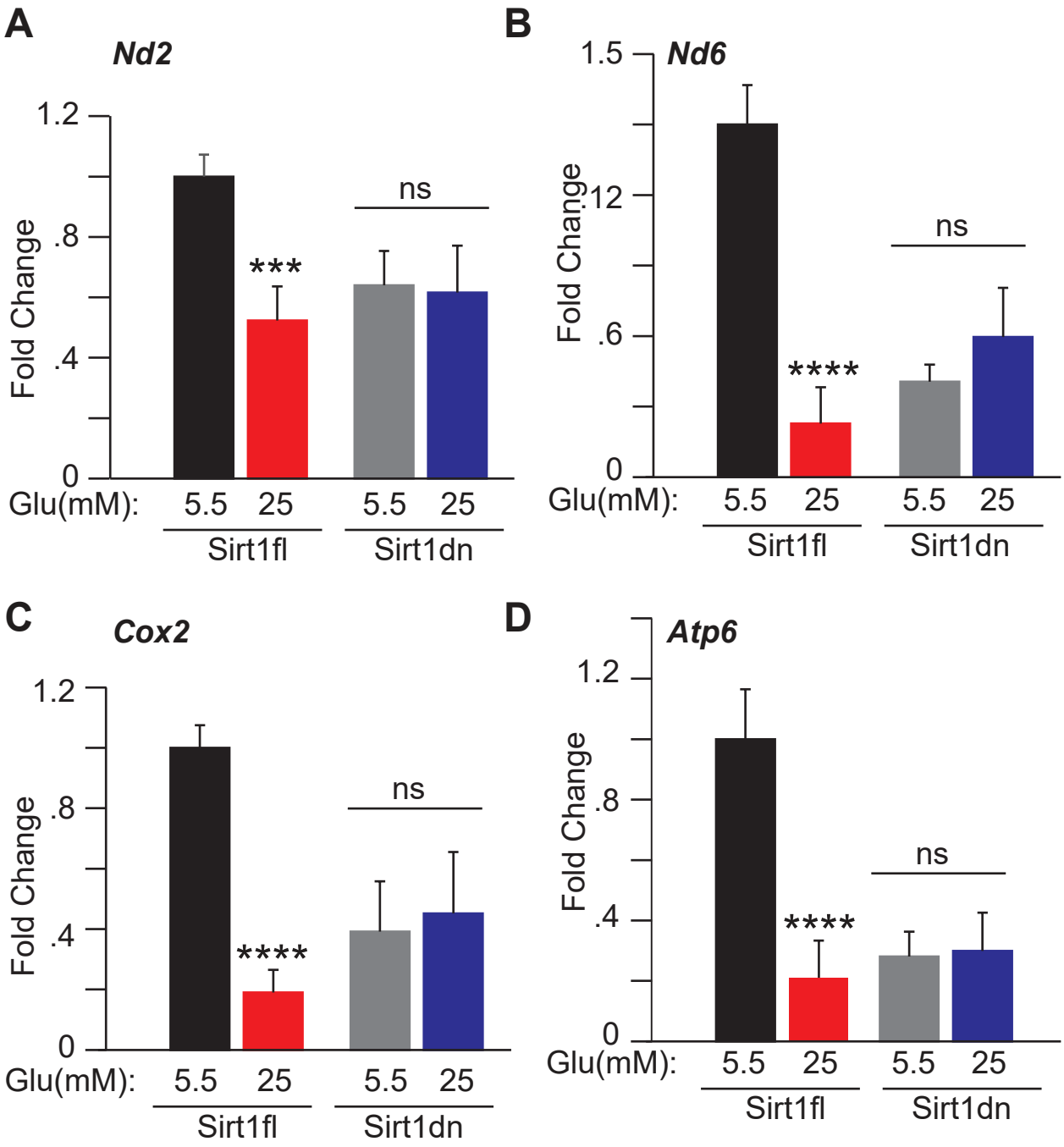

Figure 5.22. Sirt1 enzymatic activity is linked to p107 regulation of mitochondrial encoded gene expression. Gene expression analysis by qPCR of mitochondrial encoded genes **(A)** *Nd2*, **(B)** *Nd6*, **(C)** *Cox2* and **(D)** *Atp6* of c2c12 cells transfected with full length (Sirt1fl) or dominant negative (Sirt1dn) Sirt1 grown in stripped media containing 5.5mM or 25mM glucose, n=4-5, diference between Sirt1dn transfected cells treated with 5.5mM and 25mM glucose is non significant (ns), asterisks denote significance, ***p<0.001, ****p<0.0001; two-way Anova with post hoc Tukey test.

Figure 5.23

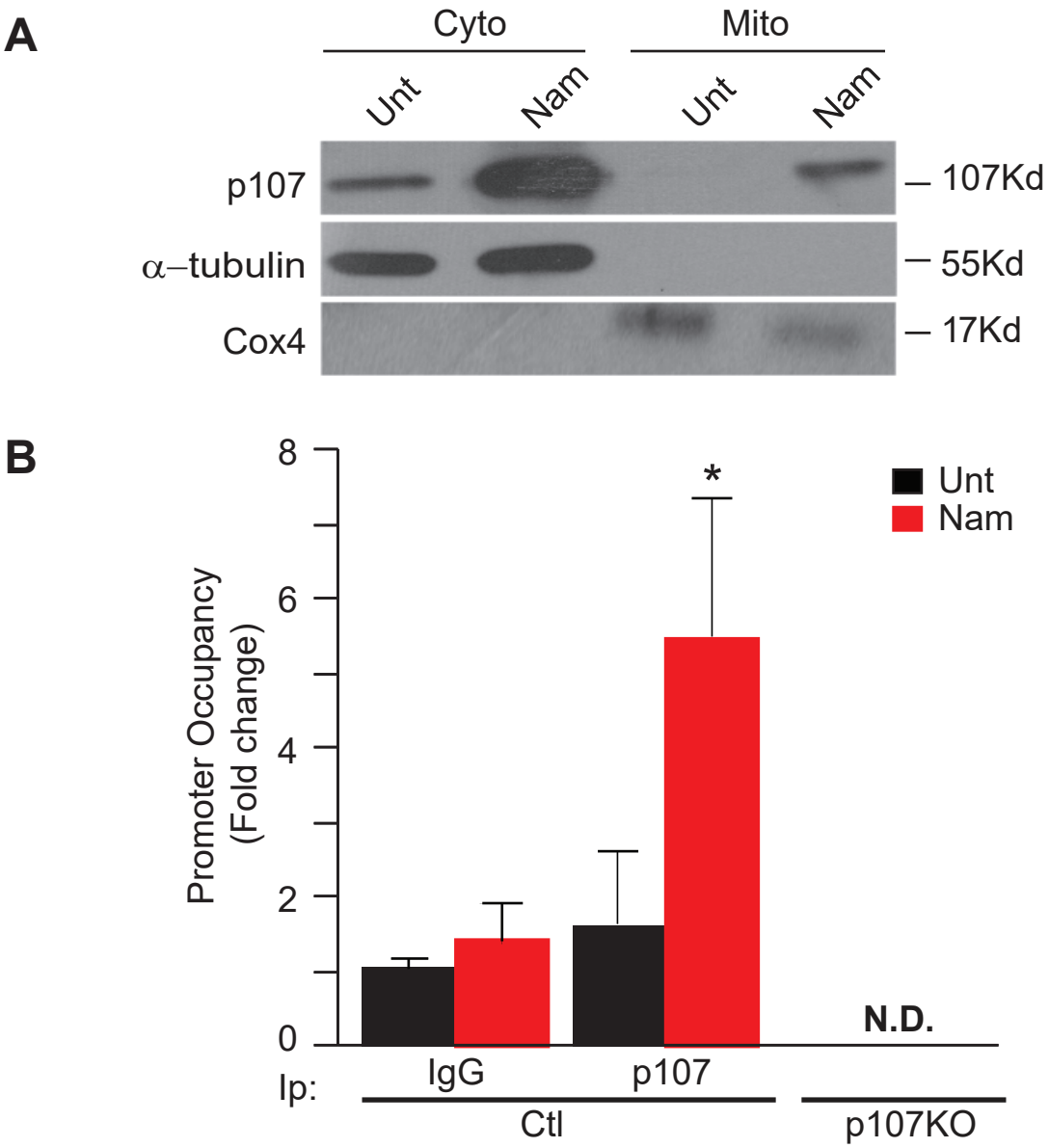

Figure 5.23. Inhibition of Sirt1 activity increases p107 mitochondrial localization and interaction with mtDNA. (A) Representative Western blot for p107, α-tubulin and Cox4 in cytoplasmic (Cyto) and mitochondrial (Mito) fractions from c2c12 cells that were untreated (Unt) or treated (10mM) with Sirt1 inhibitor nicotinamide (Nam). **(B)** Graphical representation of relative p107 and IgG mitochondrial DNA promoter occupancy by qChIP analysis in Ctl and p107KO c2c12 cells untreated (Unt) or treated with 10mM Nam, n=3, asterisks denote significance, *p<0.05; two-way Anova with post hoc Tukey test.

Figure 5.24

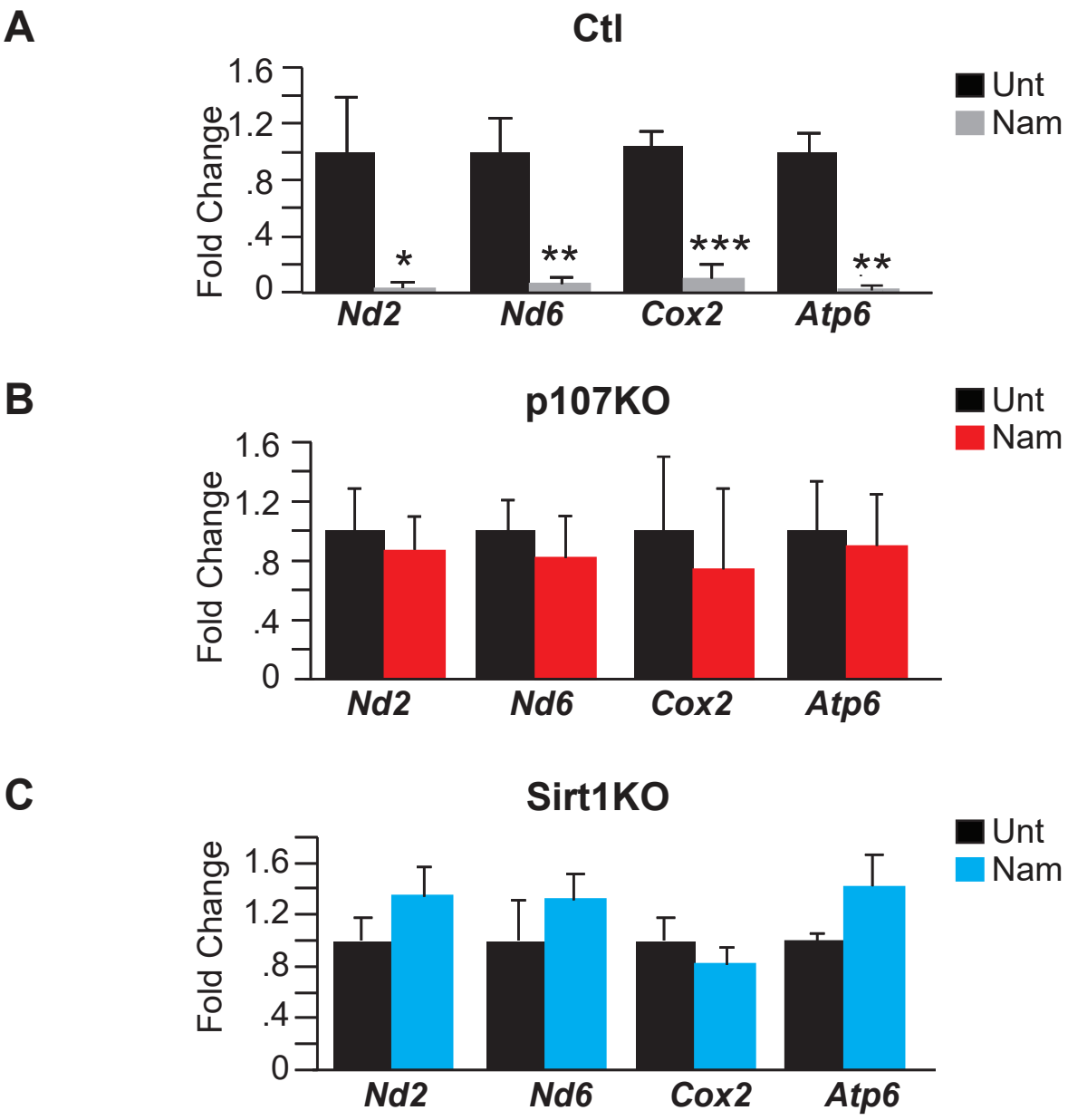

Figure 5.24. Inhibition of Sirt1 activity decreases mitochondrial gene expression via p107. Gene expression analysis by qPCR of mitochondrial encoded genes *Nd2*, *Nd6*, *Cox2* and *Atp6* for **(A)** Ctl, **(B)** p107KO and **(C)** Sirt1KO c2c12 cells untreated (Unt) or treated with 10mM nicotinamide (Nam), n=4, asterisks denote significance, **p*<0.05, ***p*<0.01, ****p*<0.001; Student T-test.

Figure 5.25

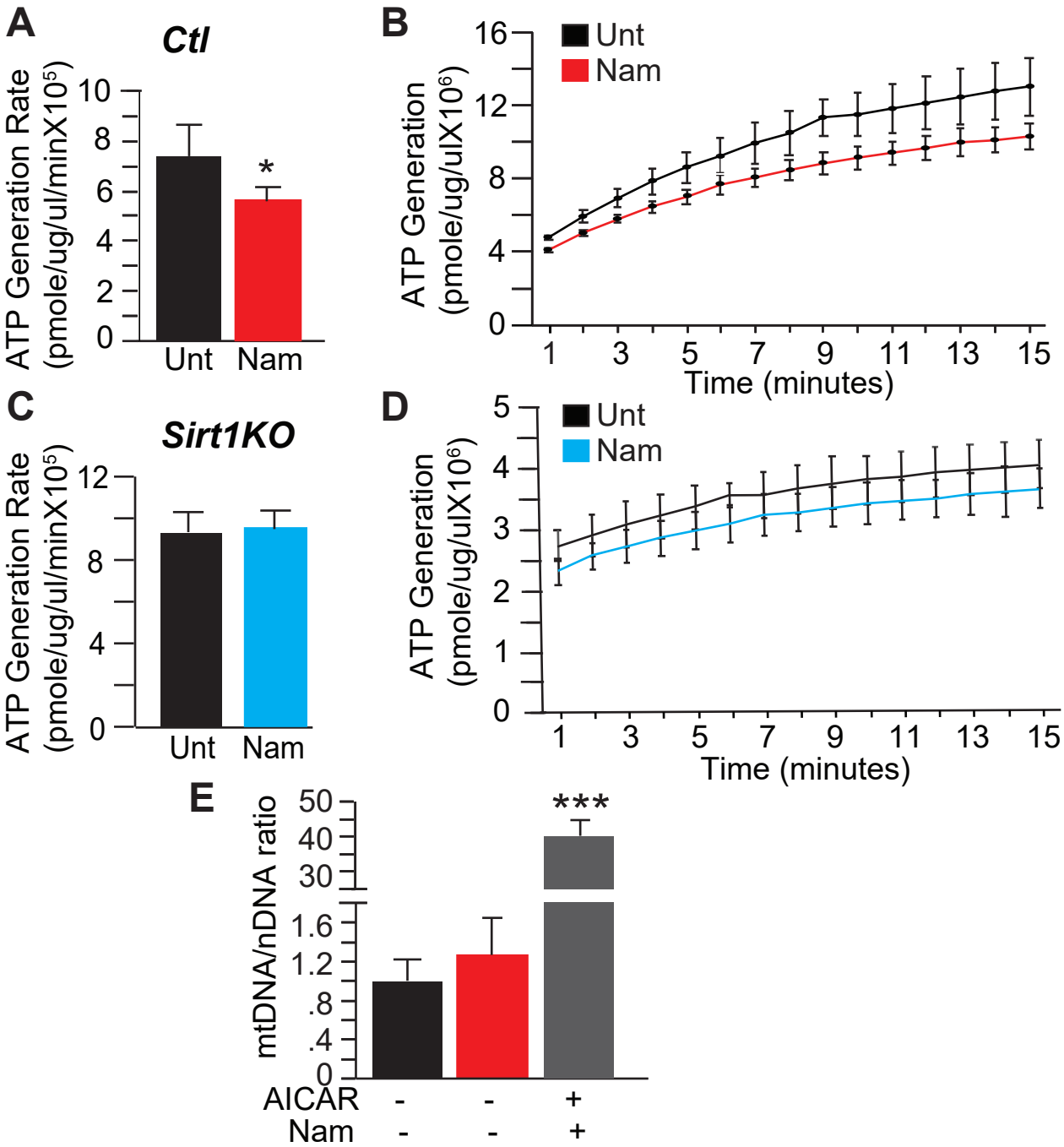

Figure 5.25. Attenuation of Sirt1 activity decreases mitochondrial ATP generation capacity via p107. Isolated mitochondrial ATP generation rate for **(A)** control (Ctl) **(C)** Sirt1KO and capacity for **(B)** Ctl and **(D)** Sirt1KO c2c12 cells treated and untreated (Unt) with 10mM nicotinamide (Nam), n=4. For rate asterisks denote significance, *p<0.05; Student T-test. For capacity statistics see Table 3. **(E)** Mitochondria DNA (mtDNA) to nuclear DNA (nDNA) ratio for c2c12 cells with and without 5-aminoimidazole-4-carboxamide ribonucleotide (AICAR) and Nam, n=4. For rate asterisks denote significance, ***p<0.001; one way Anova and Tukey post hoc test.

Figure 5.26

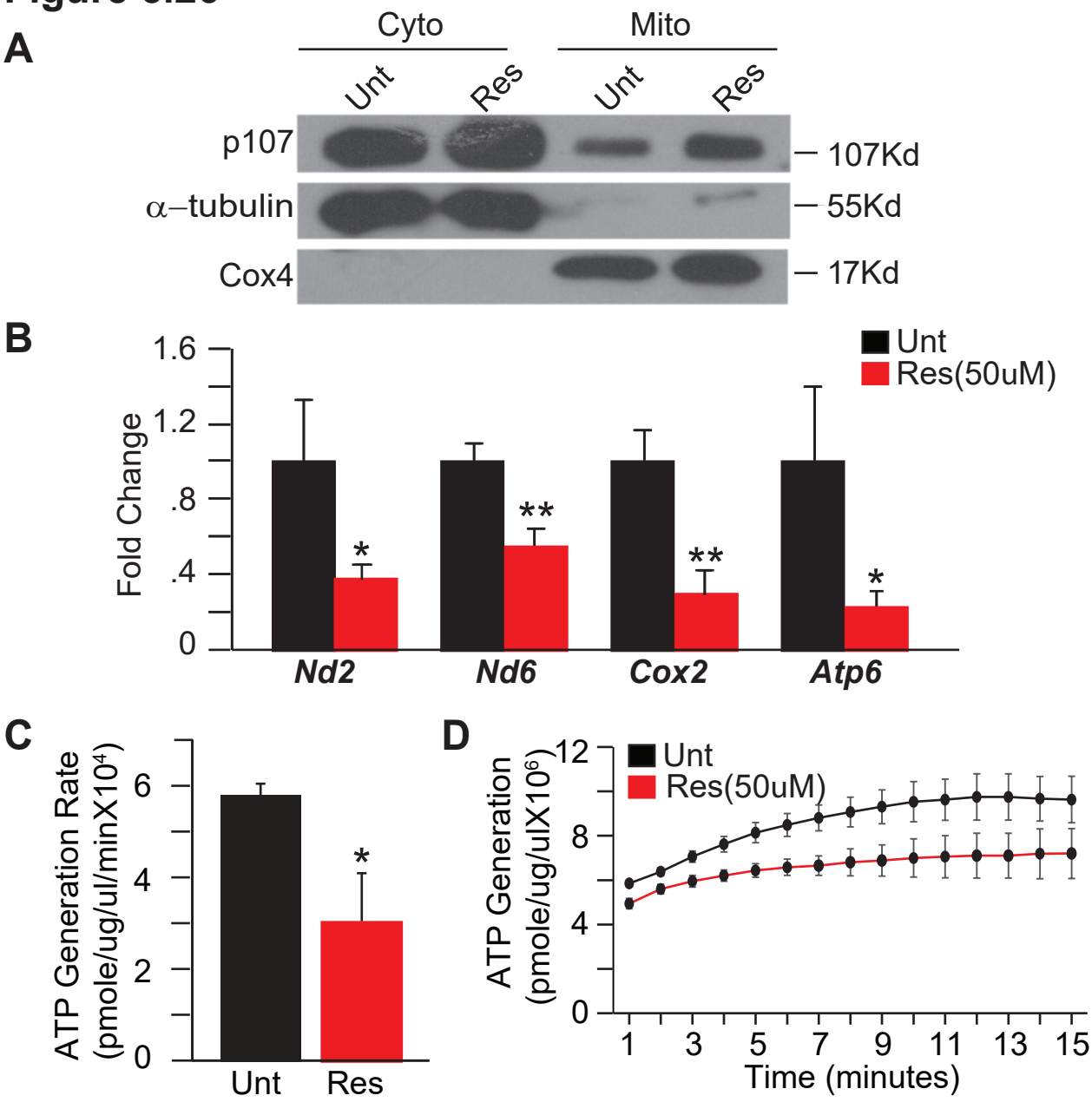

Figure 5.26. High resveratrol concentration that inactivates Sirt1 activity represses p107 mitochondrial function. (A) Representative Western blot of cytoplasmic (Cyto) and mitochondrial (Mito) fractions for p107, α-tubulin and Cox4 of c2c12 cells untreated (Unt) or treated with a concentration (50μM) of resveratrol (Res) that inactivates Sirt1. **(B)** Gene expression analysis by qPCR of mitochondrial encoded genes *Nd2*, *Nd6*, *Cox2* and *Atp6* for c2c12 cells untreated (Unt) or treated with a concentration (50μM) of Res that inactivates Sirt1, n=3-4, asterisks denote significance, *p<0.05, **p<0.01; Student T-test. Isolated mitochondrial ATP generation **(C)** rate and **(D)** capacity over time for c2c12 cells untreated (Unt) or treated with a concentration (50μM) of Res that inactivates Sirt1, asterisks denote significance, *p<0.05, **p<0.01 ***p<0.001; Student T-test. For capacity statistics, see Table 3.

Figure 5.27

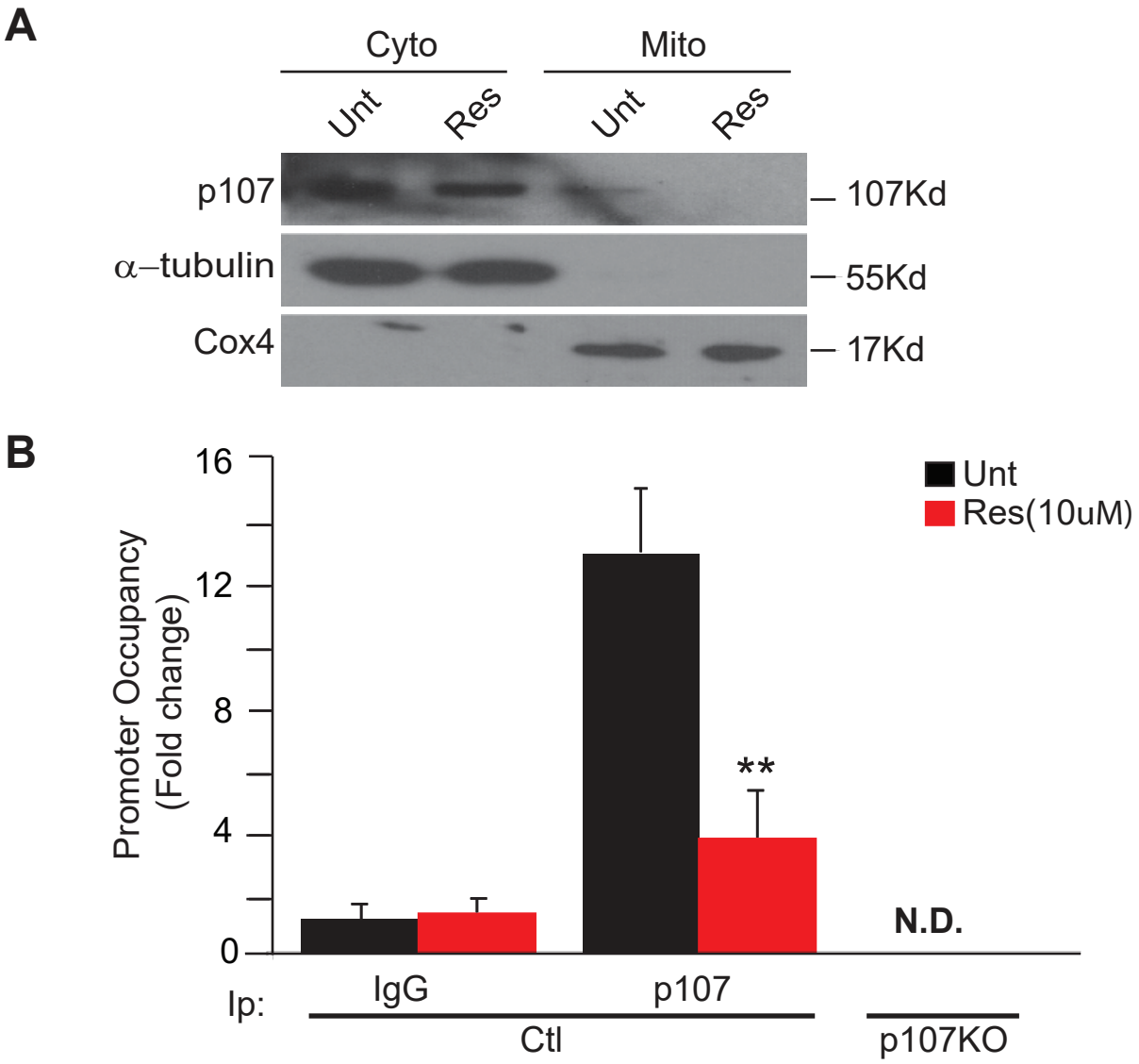

Figure 5.27. Enhancing Sirt1 activity decreases p107 mitochondrial localization and mtDNA interaction. (A) Representative Western blot of cytoplasmic (Cyto) and mitochondrial (Mito) fractions for p107, α-tubulin and Cox4 of c2c12 cells untreated (Unt) or treated (10μM) with a concentration of resveratrol (Res) that activates Sirt1. **(B)** Graphical representation of relative p107 and IgG mitochondrial DNA promoter occupancy by qChIP analysis in control (Ctl) and p107KO c2c12 cells untreated (Unt) or treated with 10μM Res, n=3, asterisks denote significance, $^{**}p<0.01$; two-way Anova with post hoc Tukey test test.

Figure 5.28

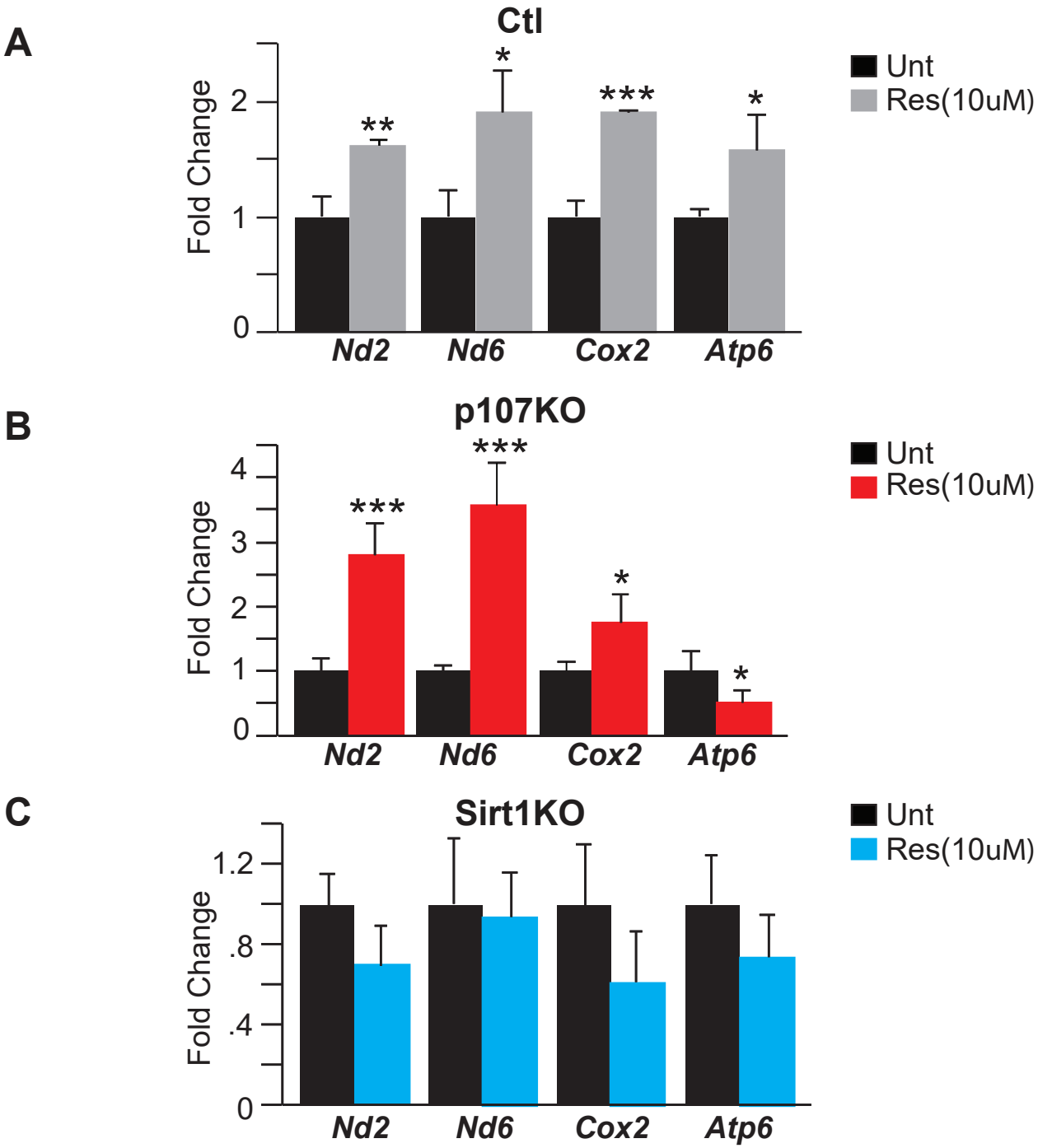

Figure 5.28. Enhancing Sirt1 activity decreases p107 mitochondrial function. Gene expression analysis by qPCR of mitochondrial encoded genes *Nd2*, *Nd6*, *Cox2* and *Atp6* for **(A)** control (Ctl), **(B)** p107KO and **(C)** Sirt1KO c2c12 cells untreated (Unt) or treated (10μM) with a concentration of resveratrol (Res) that activates Sirt1, n=4, asterisks denote significance, *p<0.05, **p<0.01, ***p<0.001; Student T-test.

Figure 5.29

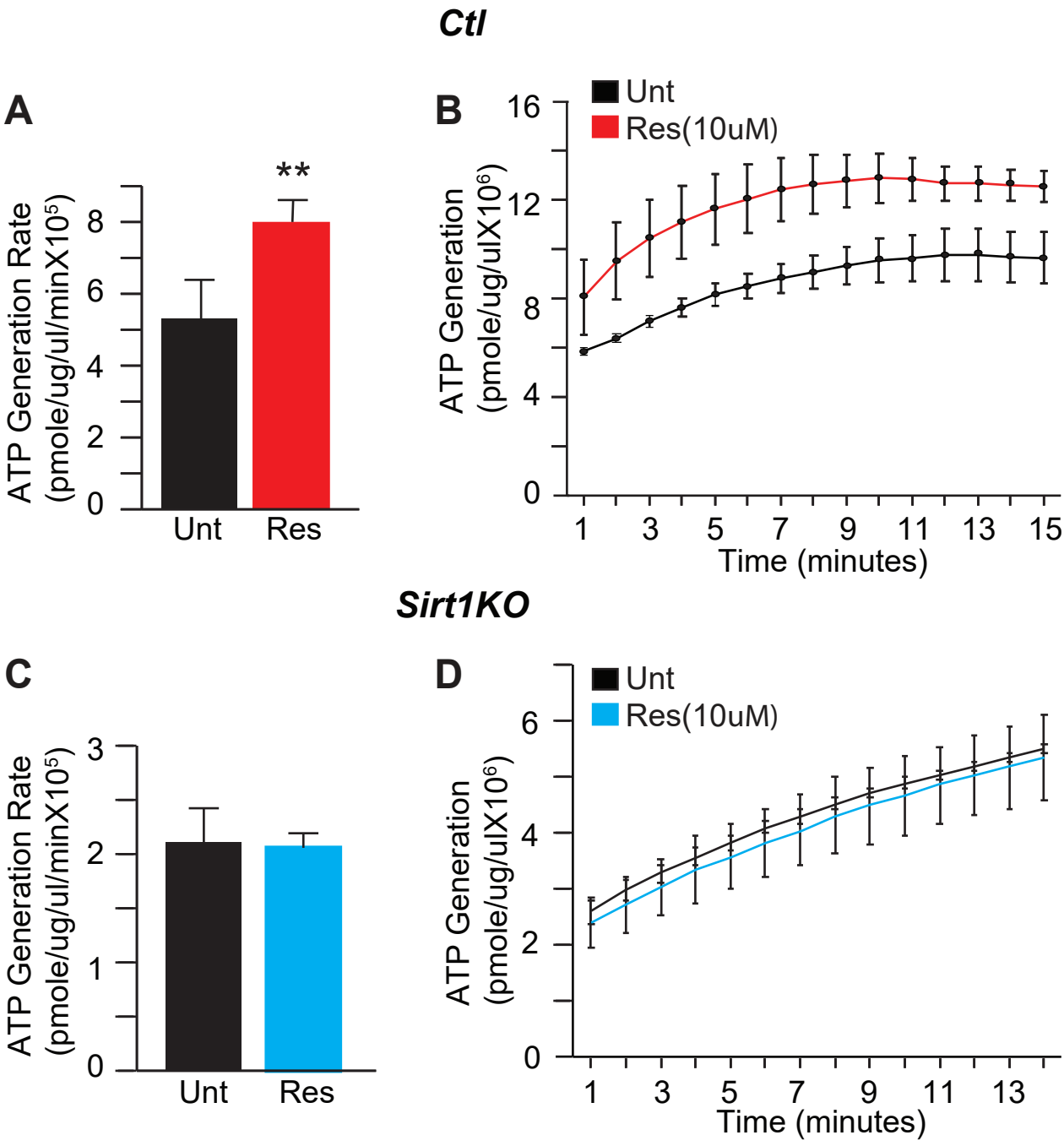

Figure 5.29. Enhncing Sirt1 activity increases mitochondrial ATP generation capacity via p107. Isolated mitochondrial ATP generation rate for **(A)** control (Ctl) **(C)** Sirt1KO and capacity for **(B)** Ctl and **(D)** Sirt1KO c2c12 cells treated and untreated (Unt) with 10uM resveratrol (Res) that activates Sirt1, n=4. For rate asterisks denote significance, ***p*<0.05; Student T-test. For capacity statistics see Table 3.

CHAPTER 6

p107 regulates myogenic progenitor proliferation through management of Oxphos

Abstract

We have shown that p107 can be localized in the mitochondria of proliferating MPs **(Chapter 4)** dependent on the cellular energy status and Sirt1 activity **(Chapter 5).** In the mitochondria p107 reduces ATP generation capacity and rate **(Chapter 4 and 5)** through repression of mitochondrial gene expression, as a consequence of mitochondrial DNA binding **(Chapter 4 and 5).** In this chapter, we have deciphered how this novel mitochondrial role for p107 influences the cellular physiology. We have demonstrated that the amount of ATP generated by the mitochondrial function of p107 is directly associated to the cell cycle rate of MPs both in vitro and in vivo. In vitro, we found that p107KO MPs exhibited a faster cell cycle rate concomitant with increased ATP generation capacity. Alternatively, concentrating p107 to the mitochondria prevented cell cycle progression in conjunction with reduced ATP generation capacity. In vivo, regenerating p107KO mouse skeletal muscle displayed more quiescent SCs and proliferating MPs compared to Wt controls. Hence, corroborating the faster proliferative capacity we found in vitro. These findings highlight a crucial role for p107 linking the regulation of mitochondrial Oxphos and glycolysis, to proliferation dynamics in MPs that is likely to extend to other cell types.

Results

p107KO skeletal muscle have more SCs

Intriguingly, p107 is referred to as a cell cycle regulator because it is known to inhibit cell cycle progression of certain cancer cell types when over expressed (Rodier et al., 2005; Schade et al., 2019; Wirt & Sage, 2010; Zhu et al., 1993). A clue that the p107 mitochondrial function controls cell cycle rate is the quantity of quiescent SCs found in skeletal muscle of p107KO compared to Wt mice. This was ascertained by confocal immunofluorescence that showed p107KO TA muscle had significantly more $Pax7^{+}$ quiescent SCs per myofiber compared to Wt littermates **(Fig. 6.1A and 6.1B).** Pertinently, the increased levels of quiescent SCs in the absence of p107 might suggest that the cells have an inherent capacity to undergo faster cell division and/or self-renewal.

p107KO MPs have a faster proliferation rate following injury

We examined MP proliferation during the early stages of skeletal muscle regeneration that is known to activate and commit SCs to MPs. We injured the TA muscle of Wt and p107KO mice with intramuscular injection of Ctx and introduced the thymidine analog bromodeoxyuridine (Brdu) intraperitoneally on the next day **(Fig. 6.2A)**. Following 2 days post Ctx injury, muscles were isolated, processed and sectioned for confocal immunofluorescence for MP marker MyoD and proliferation indicator Brdu. Quantification of the double positive MyoD and Brdu cells revealed that p107KO TA muscle had significantly more proliferating MPs compared to Wt TA muscle **(Fig. 6.2B and 6.2C)**. This indicates that the p107KO MPs might have a faster cell cycle rate compared to the Wt littermates following injury, which might be due to the lack of p107 mitochondrial function.

We confirmed that the in vivo proliferative differences for MP cells in the p107KO mice was cell autonomous, by considering control and p107KO c2c12 cells. First, we analyzed the cell proliferation rate by plating an equal number of control and p107KO cells and enumerating their number on successive days. We found that p107KO c2c12 cells had almost twice the cell proliferative rate compared to controls **(Fig. 6.3A and 6.3B)**. Second, we evaluated how the cell cycle was affected by the faster proliferation rate in p107KO c2c12 cells. To accomplish this, we performed flow cytometric analysis on cells using propidium iodide (PI) DNA staining. PI is a fluorescent molecule, with excitation and emission at 488/617nm, which binds to DNA by intercalating between nucleotide bases. This allowed quantification of cellular DNA content in G1, S and G2 phases of the cell cycle in presence and absence of p107. We discovered that p107KO c2c12 cells had significantly more cells in S phase compared to controls **(Fig. 6.4)**, which explained p107KO cells having twice the growth rate compared to the control cells **(Fig. 6.3A and 6.3B)**. This finding also corroborated the in vivo findings, where p107KO TA muscle had significantly more proliferating MPs compared to Wt littermates during muscle regeneration **(Fig. 6.2B and 6.2C)** and potentially more SCs in quiescence **(Fig. 6.1A and 6.1B)**. It suggests that the cell cycle differences found in vivo were affected by SC and/or MP specific defects and not due to the influence of other confounding cells. In Sirt1KO cells that had increased levels of p107 in the mitochondria **(Fig. 5.17A)**, along with decreased mitochondrial gene expression **(Fig. 5.17B)** and ATP generation capacity **(Fig. 5.19A and 5.19B)** exhibited significantly decelerated cell cycle progression with significantly fewer cells in S-phase compared to controls **(Fig. 6.5)**. Thus, it suggests that while absence of p107 increases cell cycle progression, presence of p107 in the mitochondria inhibits cell cycle rate, through inhibition of ATP generation as a result of inhibited mitochondrial gene expression.

p107 controls cell cycle rate through management of Oxphos

We evaluated if the enhanced mitochondrial ATP generation potential in p107KO cells **(Fig. 4.12A and 4.12B)** potentially influenced their accelerated cell cycle rate. We surmised if ATP regulated by p107 was essential to cell cycle, then sustaining p107 mitochondrial localization in p107KO c2c12 cells would reduce the proliferative rate. Indeed, we found that sustained p107 expression in the mitochondria of p107KO cells by either p107fl or p107mls, significantly reduced OCR **(Fig. 6.6A)**, decreased Oxphos and glycolysis **(Fig. 6.6B)**, as well as mitochondrial/glycolytic ATP ratio **(Fig. 6.6C)** compared to p107KO cells transfected with empty vector.

Next, we determined the effect of decreased ATP due to p107 mitochondrial localization, on cellular proliferative fates. To accomplish this, we used flow cytometry to assess the cell cycle in the presence or absence of sustained p107 mitochondrial localization. We transfected p107KO cells with an empty vector expressing green fluorescent protein (GFP) in the mitochondria (pCMV6-OCT-HA-eGFP) alone or together with p107mls or p107fl. Twenty-four hours post transfection we stained the cells with PI. Flow cytometry for cell cycle was performed on the GFP positive cells that represented only the transfected fraction of the cells. Compared to cells expressing GFP alone, p107 overexpressed cells had a significant attenuation of cells in S phase with an extensive majority of cells in G1, suggesting that the cells were blocked in G1 phase of the cell cycle **(Fig. 6.7)**. Therefore, the cell cycle block by over expression of p107 in many cell types (Leng et al., 2002; Wirt and Sage, 2010; Zhu et al., 1993) might be due to p107 mitochondrial function, which impedes Oxphos generation capacity by repressing mitochondrial encoded gene expression.

Manipulating p107 affects cell cycle through Oxphos

We further assessed if manipulating p107 mitochondrial function by altering the NAD^+/NADH ratio would affect the proliferative rate of c2c12 cells. Notably, when c2c12 cells were treated with oxamate, they had less ATP generative potential **(Fig. 5.13),** as a consequence of p107 mediated reduction of mitochondrial gene expression **(Fig. 5.7)**. By extension, oxamate treatment should also have an effect on MP proliferation. We assessed this by plating equal numbers of c2c12 cells that were untreated or treated with 2.5mM oxamate, and counted the cells over several days. We found that for the oxamate treated cells, there was a significant decrease in the number and rate of proliferating cells **(Fig. 6.8A and 6.8B)**. Conspicuously, p107KO c2c12 cells that were oxamate untreated and treated, displayed no differences in cell number and proliferation rate over the same period in contrast to the control cells **(Fig. 6.8A and 6.8B)**. We also performed cell cycle analysis by PI staining and flow cytometry on the control and p107KO c2c12 cells with and without oxamate treatment. Oxamate treated c2c12 cells had significantly reduced S phase numbers compared to untreated cells **(Fig. 6.9)**. Contrarily, p107KO cells did not show any changes in cell cycle kinetics when treated with oxamate **(Fig. 6.9)**, which was in congruence with their proliferation potential **(Fig. 6.8A and 6.8B)**. Together, these results suggest ATP generation controls MP proliferation and cell cycle dynamics via an NAD^+/NADH dependent management of p107 mitochondrial function.

Oxamate treatment reduces MP proliferation in vivo

We next tested the effect of oxamate on MPs in vivo during the process of skeletal muscle regeneration following injury. For this, both Wt and p107KO mice were injected with oxamate for 5 days. On day 3, TA muscles were injured by intramuscular injection of Ctx, followed by intraperitoneal injection of Brdu on day 4. MP proliferation was assessed by enumerating cells for

proliferation marker Brdu and MP marker MyoD by immunohistochemistry and confocal microscopy after the TA muscles were isolated on the fifth day **(Fig. 6.10A)**. We found that Wt mice treated with oxamate had significantly fewer proliferating $MyoD^{+}Brdu^{+}$ MPs in their regenerating TA muscle compared to control untreated mice **(Fig. 6.10B and 6.11)**. Importantly, there were no MP proliferative differences for p107KO regenerating TA that were treated for oxamate **(Fig. 6.10B and 6.11**). This result corroborated the in vitro data that showed oxamate treatment decreased MP proliferation in c2c12 cells **(Fig. 6.8A and 6.8B)**, but did not affect proliferation dynamics of p107KO cells **(Fig. 6.8A and 6.8B)**. Together this data suggests that MP proliferation and regeneration capacity might be dependent on a p107 metabolic control mechanism operating in the mitochondria.

Figure 6.1

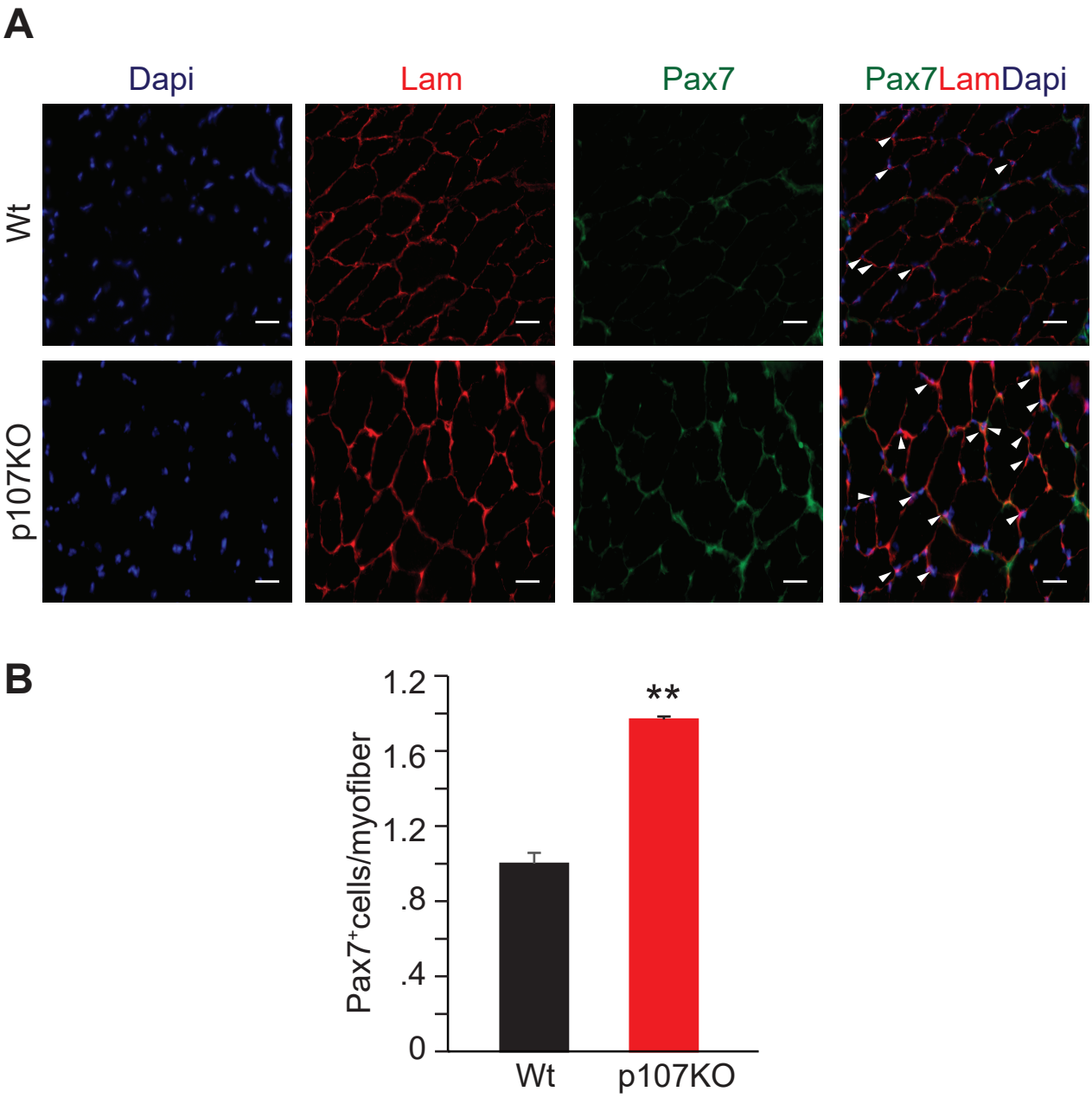

Figure 6.1. p107KO muscle contains significantly more Pax7⁺ quiescent sateliite cells (SCs) indicating a better self-renewal potential. (A) Confocal microscopic immunoflourescence of Dapi (blue), Laminin (Lam) (red), Pax7 (green) and Merge of wild type (Wt) and p107KO tibialis anterior (TA) muscle (scale bar 20um). **(B)** Graph depicting Pax7⁺ quiescent SCs per myofiber of Wt and p107KO TA muscle, n=4, asterisks denote significance, ***p*<0.01; Student T-test.

Figure 6.2

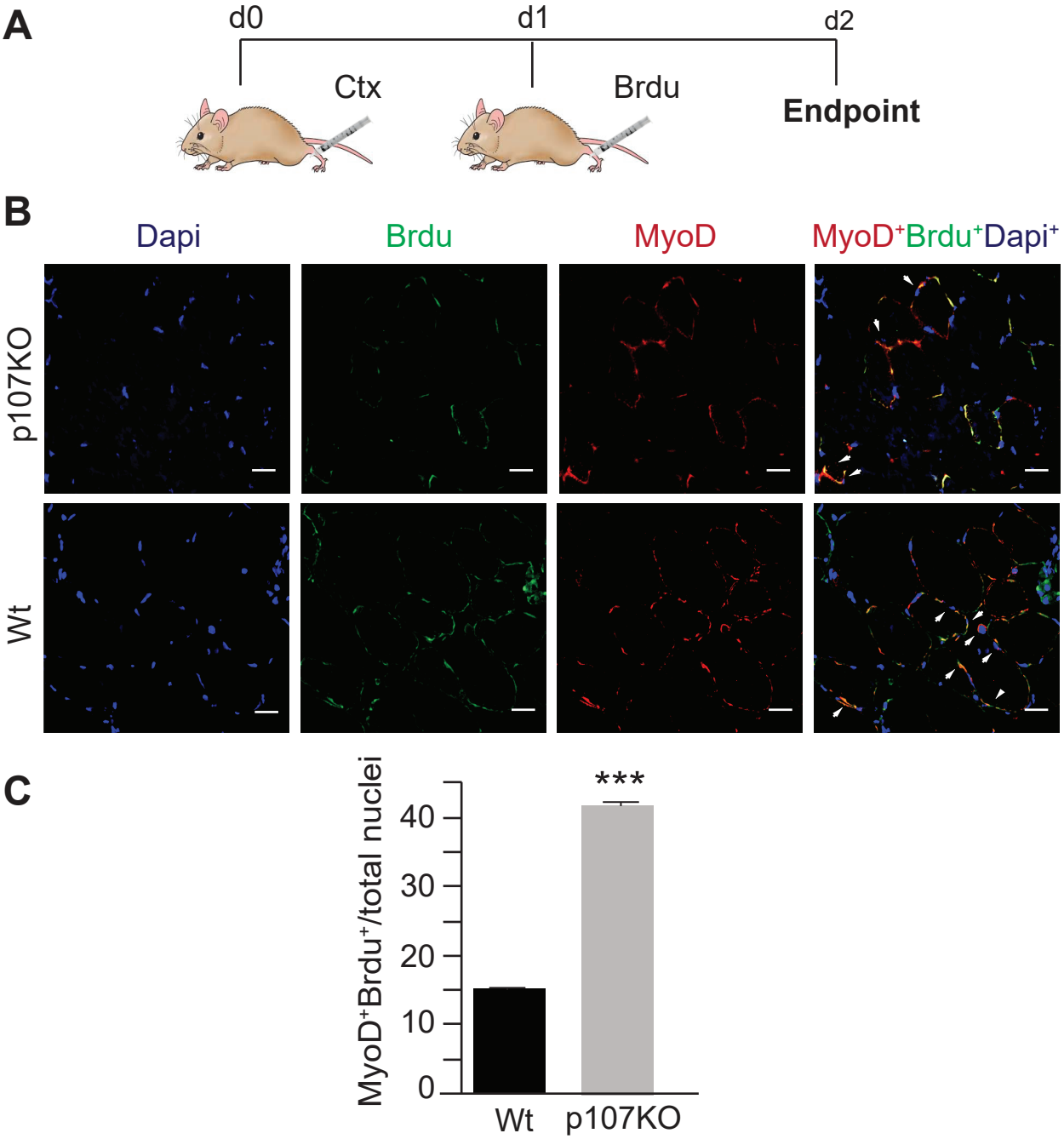

Figure 6.2. p107KO muscle contains significantly more proliferating myogenic progenitors. (A) Time course of treatments for wild type (Wt) and p107KO mice injected with cardiotoxin (Ctx) and bromodeoxyuridine (Brdu). **(B)** Representative confocal microscopic immunofluorescence and Z-stack (100 nm interval) image using the ZEN program (Zeiss) for MyoD (red), Brdu (green), Dapi (blue) and Merged image (scale bar 20um). Arrows denote Brdu and MyoD positive nuclei. **(C)** Graph depicting the percentage of proliferating myogenic progenitors from TA muscle at day 2 post injury, n=4, asterisks denote significance, ***p<0.001; Student T-test.

Figure 6.3

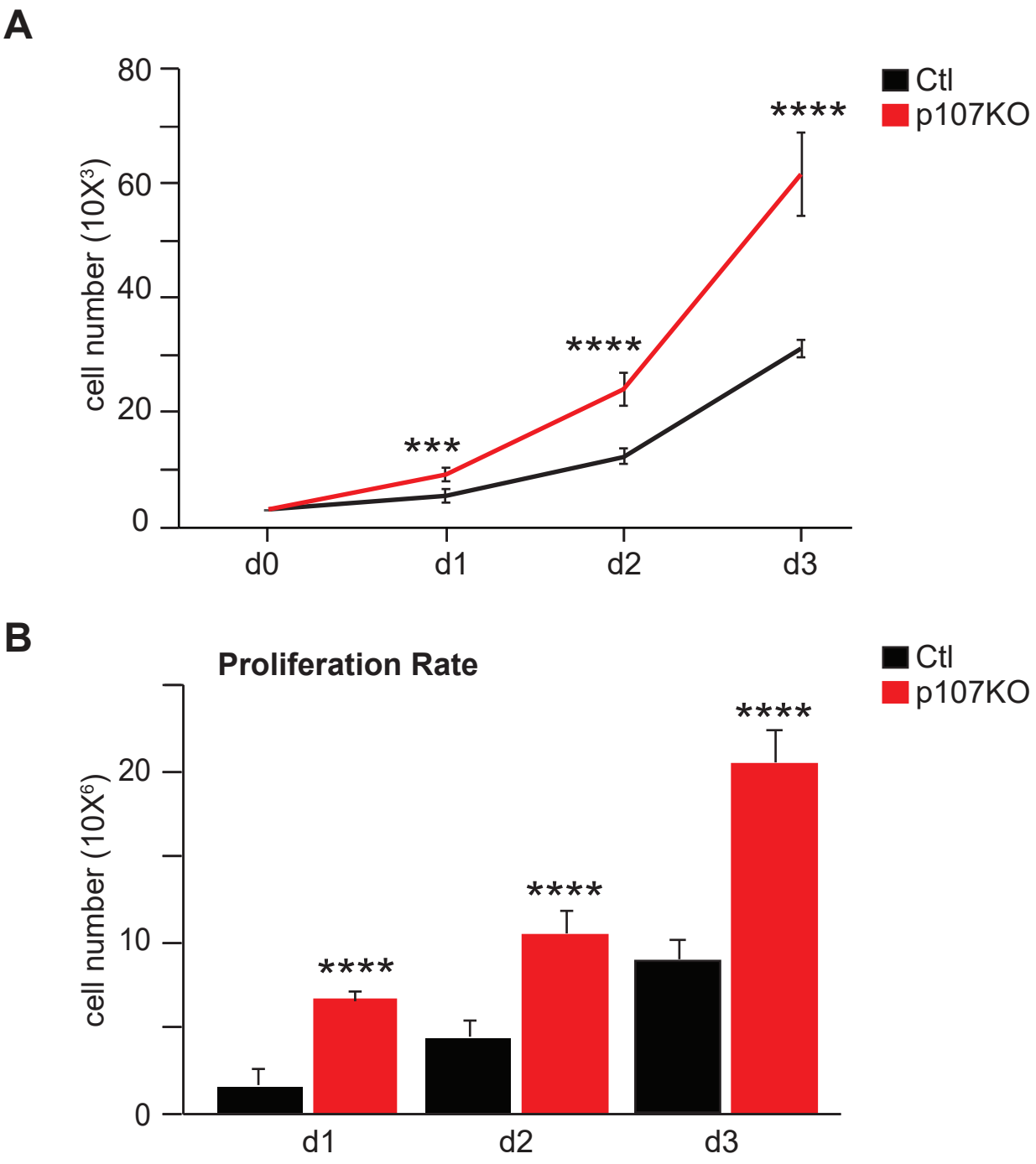

Figure 6.3. p107KO c2c12 cells have a greater proliferation rate. (A) Growth curve and **(B)** proliferation rate for control (Ctl) and p107KO c2c12 cells over 3 days, n=6-8, asterisks denote significance, ***p<0.001, ****p<0.0001; Student T-test.

Figure 6.4

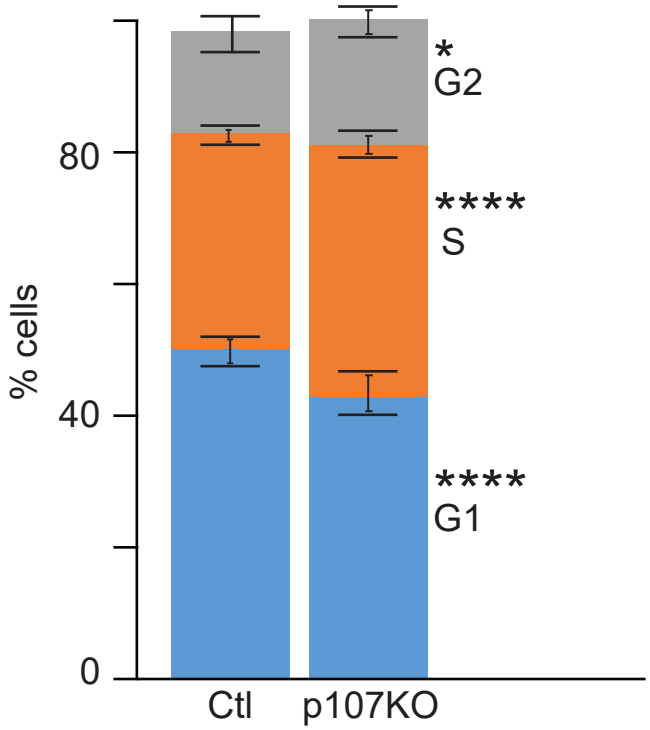

Figure 6.4. p107KO c2c12 cells have a significantly greater S-phase. Cell cycle analysis by flow cytometry for control (Ctl) and p107KO c2c12 cells, n=6-9; asterisks denote significance, *p<0.05, ****p<0.0001; Student T-test.

Figure 6.5

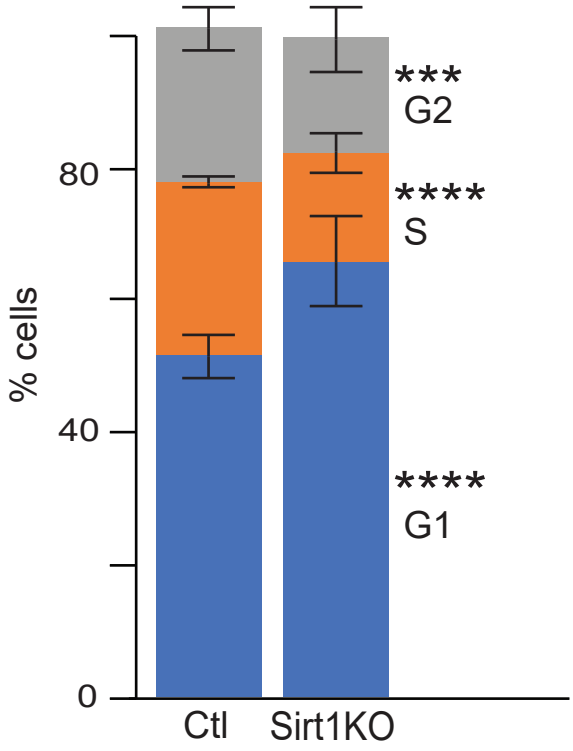

Figure 6.5. Sirt1KO cells have significantly less S-phase. Cell cycle analysis by flow cytometry for control (Ctl) and Sirt1KO c2c12 cells, n=6-9, asterisks denote significance, ***p<0.001; ****p<0.0001; Student T-test.

Figure 6.6

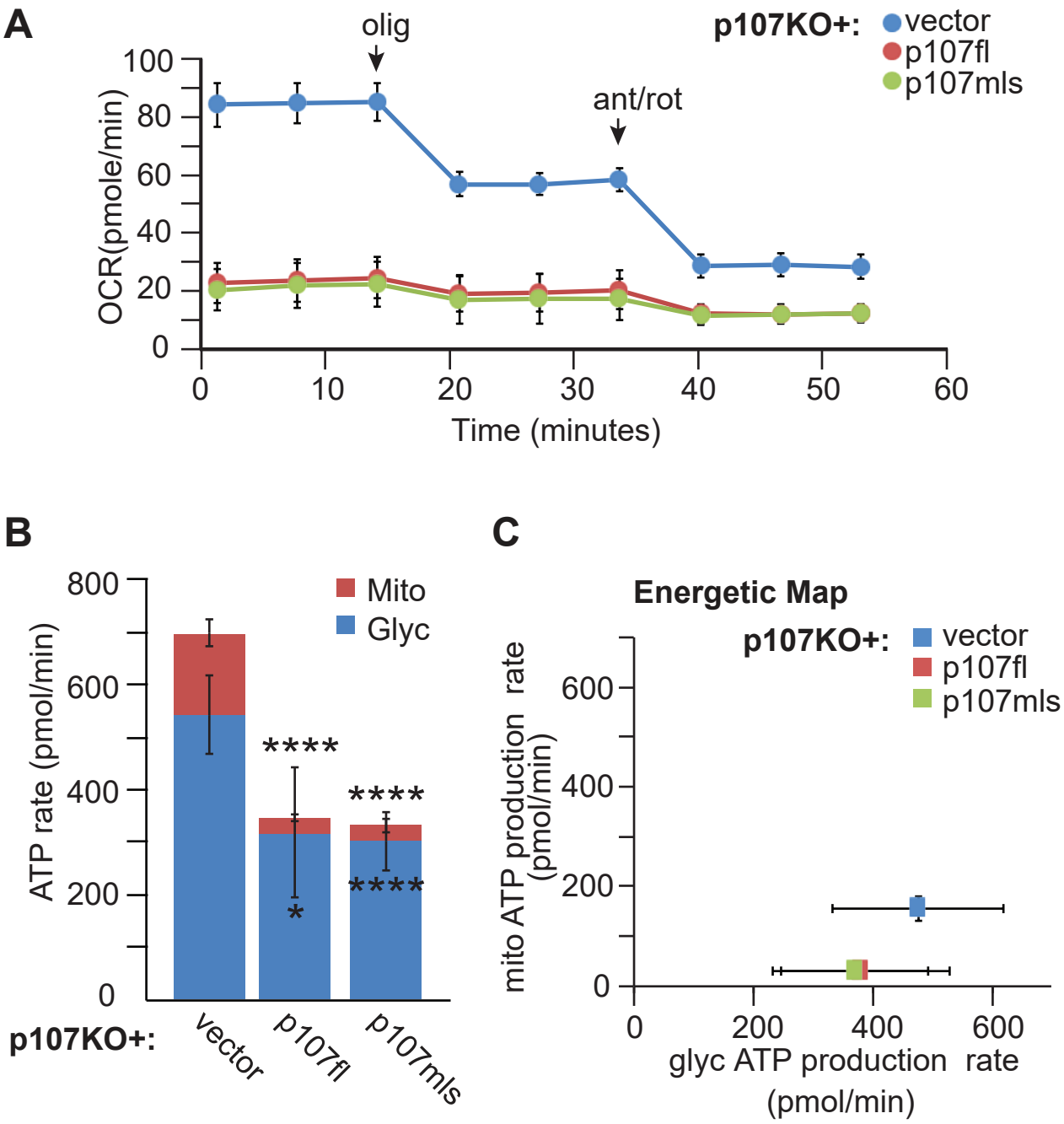

Figure 6.6. Mitochondrial localized p107 significantly decreases ATP generation. Live cell metabolic analysis by Seahorse of **(A)** oxygen consumption rate (OCR) **(B)** ATP production rate from mitochondria (Mito) and glycolysis (Glyc) and **(C)** energetic map for p107KO c2c12 cells transfected with either empty vector alone or together with full length p107 (p107fl) or p107 with mitochondrial localization sequence (p107mls), n=4, asterisks denote significance, ****p<0.001; Student T test.

Figure 6.7

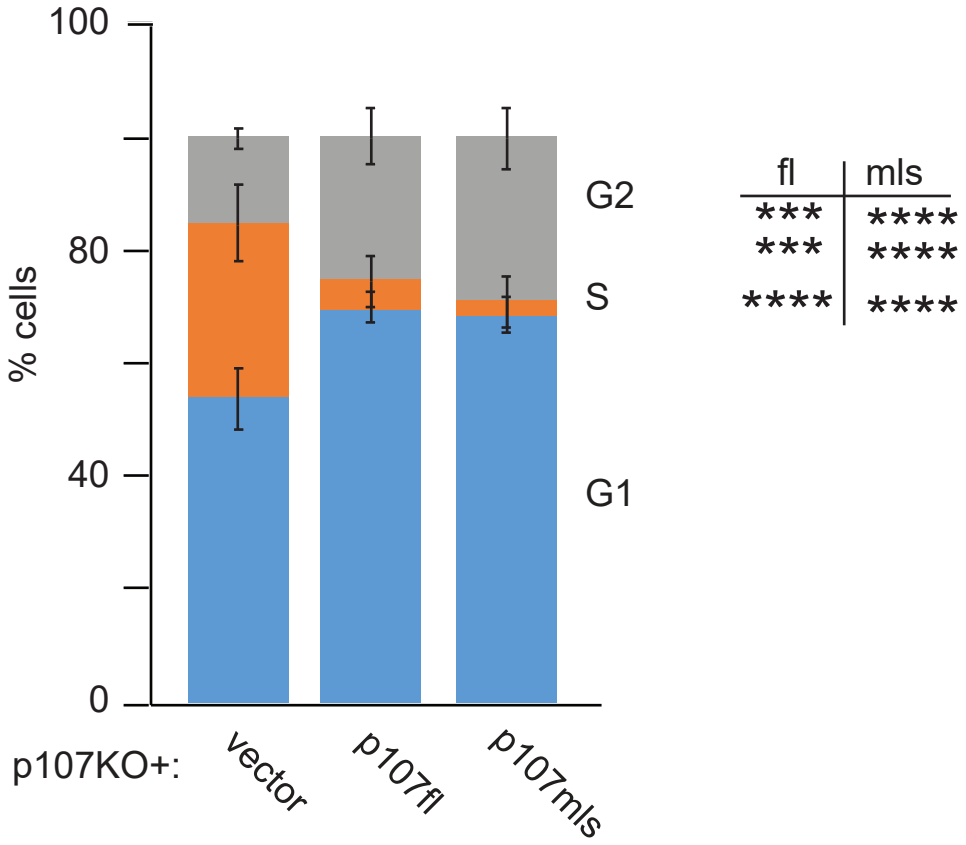

Figure 6.7. Mitochondrial localized p107 significantly decreases S-phase of the cell cycle. Cell cycle analysis by flow cytometry of p107KO c2c12 cells transfected with either empty vector alone or together with full length p107 (p107fl) or p107 with mitochondrial localization sequence (p107mls), n=4; asterisks denote significance, ****p*<0.001, *****p*<0.0001; Student T-test.

Figure 6.8

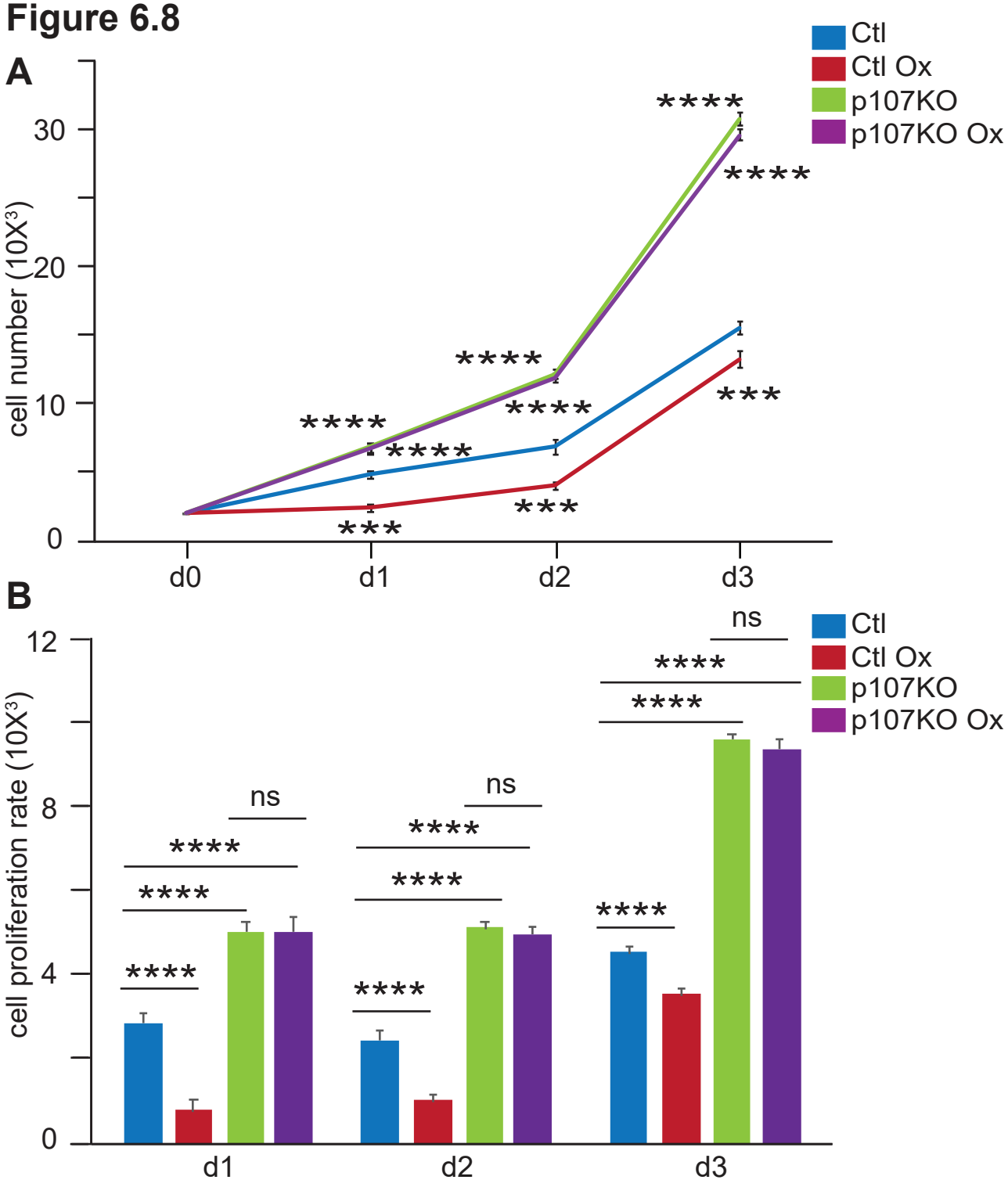

Figure 6.8. p107 decreases proliferation rate of c2c12 cells when treated with oxamate. (A) Growth curve and **(B)** proliferation rate for control (Ctl) and p107KO c2c12 cells untreated or treated with 2.5mM oxamate (Ox), n=6-8, differences between p107KO cells treated or untreated with Ox is non significant (ns), asterisks denote significance, ***p<0.001, ****p<0.001; two-way Anova with post hoc Tukey test.

Figure 6.9

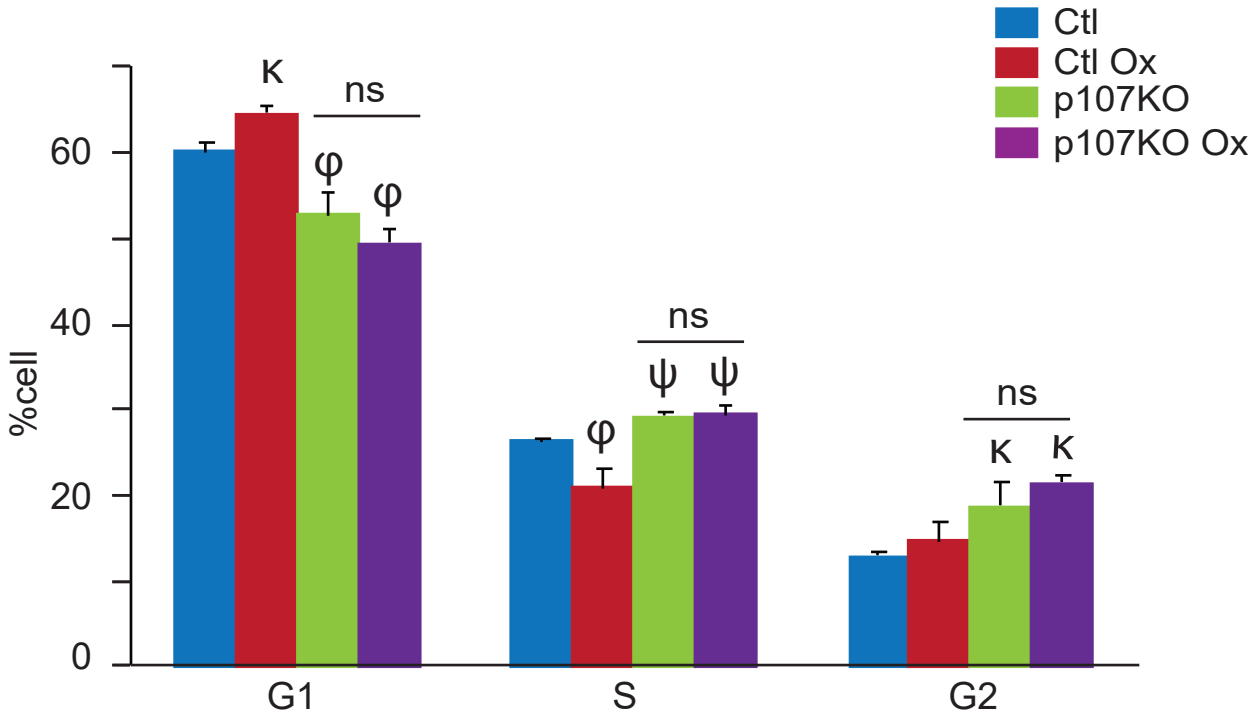

Figure 6.9. p107 decreases S-phase of c2c12 cells when treated with oxamate. Cell cycle analysis using flow cytometry for control (Ctl) and p107KO c2c12 cells untreated or treated with 2.5mM oxamate (Ox), n=6-8, differences between p107KO cells treated and untreated with oxamate in G1, S and G2 phases is non significant (ns), asterisks denote significance, ψ<0.05, κ<0.001, ϕ<0.0001; two-way Anova with post hoc Tukey test.

Figure 6.10

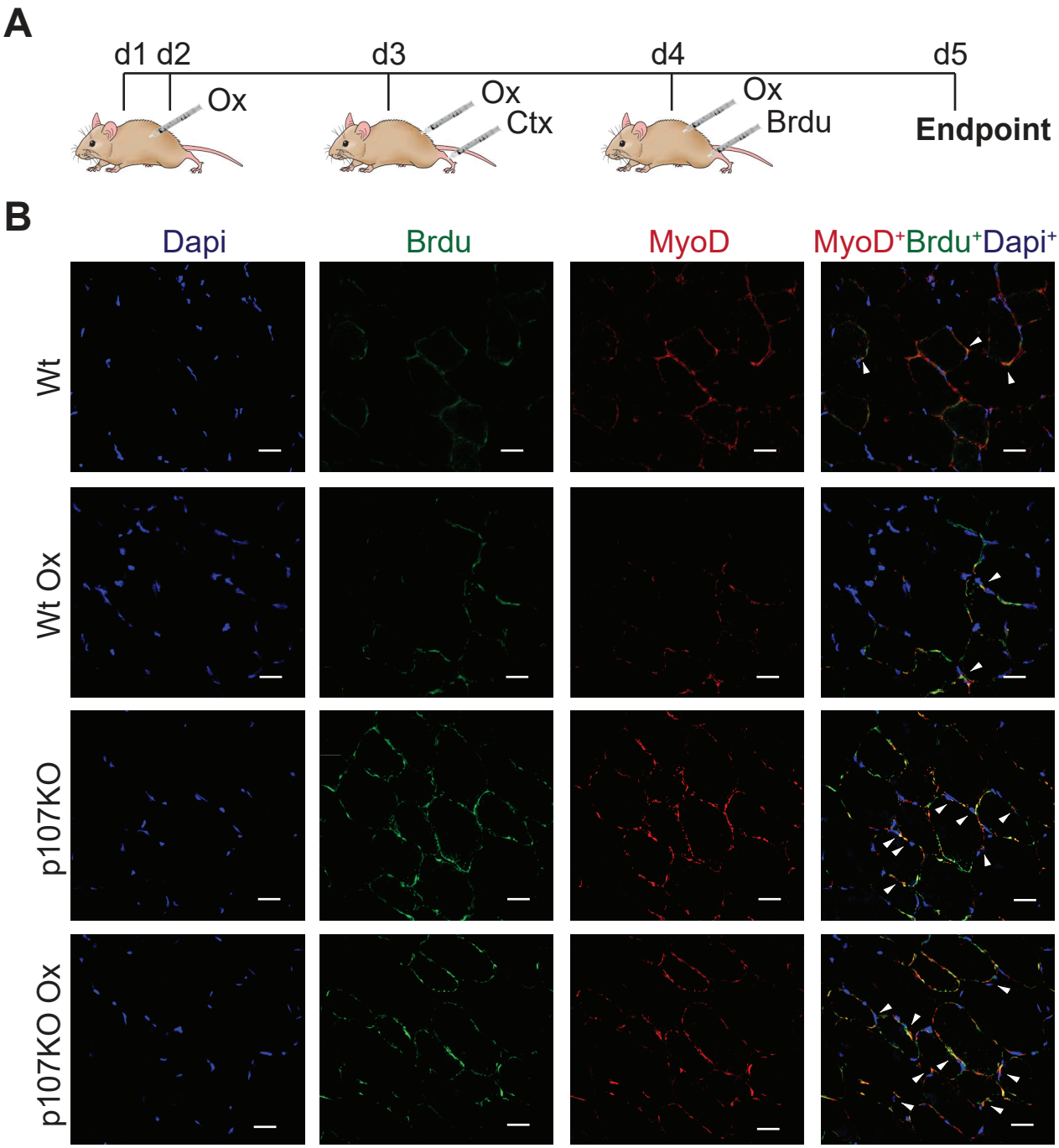

Figure 6.10. Oxamate decreases myogenic progenitor proliferation in regenerating muscle via p107. (A) Time course of treatments for Wt and p107KO mice injected with oxamate (Ox), cardiotoxin (Ctx) and bromodeoxyuridine (Brdu) with Endpoint. **(B)** Representative confocal microscopic immunofluorescence image using the ZEN program (Zeiss) for MyoD (red), Brdu (green), Dapi (blue) and Merged image for proliferating myogenic progenitors (MPs) from tibialis anterior muscle at day 2 post injury (scale bar 20μM), n=5.

Figure 6.11

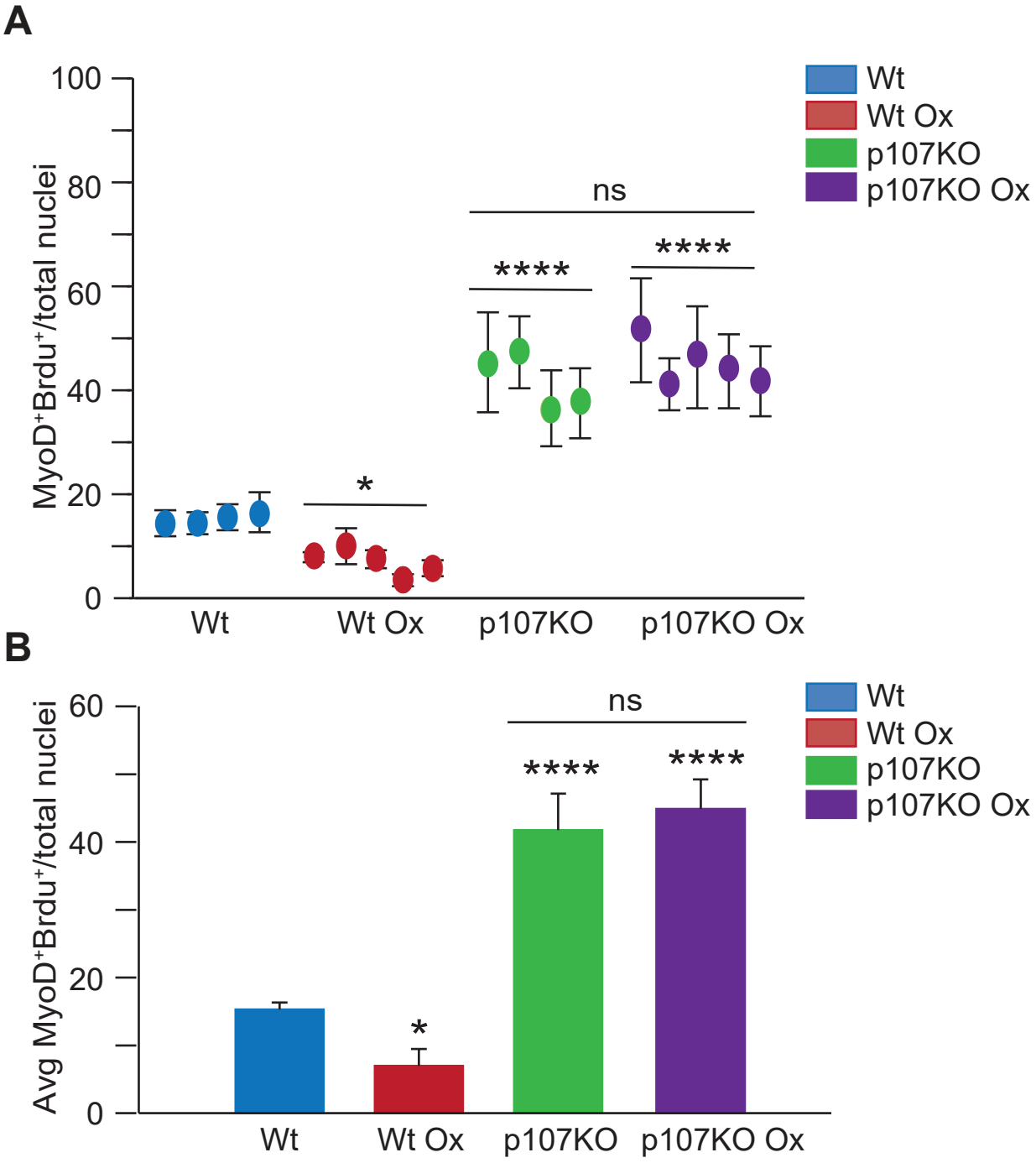

Figure 6.11. Graphical representation of proliferating myogenic progenitor in regenerating muscle with oxamate treatment. (A) Box and whisker plot and **(B)** graphical representation for percentage of proliferating MPs represented by MyoD^{+}Brdu^{+} cells, from tibialis anterior muscle of Wt and p107KO mice, n=4-5, differences between p107KO TA muscle treated or untreated with Ox is non significnat (ns), asterisks denote significance, *p<0.05, ****p<0.001; two-way Anova with post hoc Tukey test.

Table 3. Statistical significance values at each timepoint for various ATP generation capacity graphs.

A) ATP generation capacity for proliferating control (Ctl) and p107KO c2c12 cells, n=4, (Fig. 4.12B)	
Time (min.)	**Significance**
1	0.009 (**)
2	0.008 (**)
3	0.005 (**)
4	0.005 (**)
5	0.004 (**)
6	0.008 (**)
7	0.015 (*)
8	0.045 (*)
9	0.018 (*)
10	0.020 (*)
11	0.018 (*)
12	0.020 (*)
13	0.021 (*)
14	0.021 (*)
15	0.003 (**)

B) ATP generation capacity for proliferation (G) and growth arrest (Ga), n=4, (Fig. 4.13B)	
Time (min.)	**Significance**
1	0.033 (*)
2	0.016 (*)
3	0.011 (*)
4	0.006 (**)
5	0.005 (**)
6	0.005 (**)
7	0.001 (***)
8	0.002 (**)
9	0.001 (**)
10	0.001 (**)
11	0.001 (**)
12	0.001 (**)
13	0.001 (**)
14	0.0009 (***)
15	0.0007 (***)

C) ATP generation capacity for c2c12 cells grown in stripped media containing 5.5mM and 25mM glucose, n=4, (Fig. 5.12B)	
Time (min.)	**Significance**
1	0.035 (*)
2	0.030 (*)
3	0.025 (*)
4	0.024 (*)
5	0.024 (*)
6	0.022 (*)
7	0.021 (*)
8	0.020 (*)
9	0.017 (*)
10	0.009 (**)
11	0.011 (*)
12	0.036 (*)
13	0.016 (*)
14	0.011 (*)
15	0.005 (**)

D) ATP generation capacity for Ctl and Sirt1KO c2c12 cells treated with 5.5mM glucose, n=4, (Fig. 5.19B)	
Time (min.)	**Significance**
1	0.001 (**)
2	0.0004 (***)
3	0.004 (**)
4	0.0007 (***)
5	0.001 (**)
6	0.0008 (***)
7	0.0009 (***)
8	0.001 (**)
9	0.0009 (***)
10	0.001 (**)
11	0.001 (**)
12	0.001 (**)
13	0.001 (**)
14	0.002 (**)
15	0.002 (**)

E) ATP generation capacity for c2c12 cells treated or untreated with 10mM Nam, n=4, (Fig. 5.25B)	
Time (min.)	**Significance**
1	0.0003 (***)
2	0.006 (**)
3	0.014 (*)
4	0.021 (*)
5	0.022 (*)
6	0.032 (*)
7	0.034 (*)
8	0.035 (*)
9	0.007 (**)
10	0.020 (*)
11	0.027 (*)
12	0.032 (*)
13	0.038 (*)
14	0.034 (*)
15	0.032 (*)

F) ATP generation capacity for c2c12 cells treated or untreated with 50µM Res, n=4, (Fig. 5. 26D)	
Time (min.)	**Significance**
1	0.0009 (***)
2	0.001 (**)
3	0.0009 (***)
4	0.0008 (***)
5	0.001 (**)
6	0.001 (**)
7	0.001 (**)
8	0.002 (**)
9	0.003 (**)
10	0.006 (**)
11	0.008 (**)
12	0.010 (*)
13	0.010 (**)
14	0.017 (*)
15	0.019 (*)

G) ATP generation capacity for c2c12 cells treated or untreated with 10µM Res, n=4, (Fig. 5.29B)	
Time (min.)	**Significance**
1	0.064 (*)
2	0.027 (*)
3	0.021 (*)
4	0.016 (*)
5	0.012 (*)
6	0.010 (**)
7	0.006 (**)
8	0.004 (**)
9	0.002 (**)
10	0.002 (**)
11	0.002 (**)
12	0.005 (**)
13	0.005 (**)
14	0.004 (**)
15	0.005 (**)

CHAPTER 7

Decreased transcriptional co-repressor p107 is associated with exercise-induced mitochondrial biogenesis in human skeletal muscle

Debasmita Bhattacharya[1,2,3*], Mia Ydfors[4*], Meghan C. Hughes[2,3], Jessica Norrborn[4], Christopher G. R. Perry[2,3] and Anthony Scimè[1, 2,3,5]

1. Stem Cell Research Group 2. Molecular, Cellular and Integrative Physiology
3. Muscle Health Research Centre Faculty of Health,
York University, Toronto, Canada

4. Department of Physiology and Pharmacology, Karolinska Institutet, Stockholm, Sweden
5. Corresponding author E mail: ascime@yorku.ca
Tel: 1 416 736 2100 ext 33559

* Contributed equally to the manuscript

This manuscript has been published: Bhattacharya D. , Ydfors M. , Hughes M. C. , Norrbom J. , Perry C. G. R. , Scimè A. Decreased transcriptional co-repressor p107 is associated with exercise-induced mitochondrial biogenesis in human skeletal muscle, Physiol Rep, 5 (5), 2017,e13155, doi: 10.14814/phy2.13155

Contributions:

I was involved in the development of conceptual framework of the manuscript. My specific contribution to the experiments included the Western blots (Figure 2), development of all the correlation analysis (Figures 3, 4 and 5). Both Dr. Anthony Scime and I were involved in manuscript writing, editing and revisions. Additional contributions were made by Dr. Christopher Perry and Meghan Hughes, who generously provided us with the samples. Meghan Hughes performed the OXPHOS Westerns previously published but used for the correlation analysis and Mia Ydfors performed the qPCR analysis (Figure 1).

Abstract

Increased mitochondrial content is a hallmark of exercise-induced skeletal muscle remodeling. For this process, considerable evidence underscores the involvement of transcriptional coactivators in mediating mitochondrial biogenesis. However, our knowledge regarding the role of transcriptional corepressors is lacking. In this study, we assessed the association of the transcriptional corepressor Rb family proteins, Rb and p107, with endurance exercise-induced mitochondrial adaptation in human skeletal muscle. We showed that p107, but not Rb, protein levels decrease by 3 weeks of high-intensity interval training. This is associated with significant inverse association between p107 and exercise-induced improved mitochondrial oxidative phosphorylation. Indeed, p107 showed significant reciprocal correlations with the protein contents of representative markers of mitochondrial electron transport chain complexes. These findings in human skeletal muscle suggest that attenuated transcriptional repression through p107 may be a novel mechanism by which exercise stimulates mitochondrial biogenesis following exercise.

Introduction

Skeletal muscle is a highly plastic tissue having the ability to undergo functional adaptations in response to external stimuli including exercise, which is known to improve metabolic health and enhance physical performance (Coffey & Hawley, 2007; Flück & Hoppeler, 2003; Gundersen, 2011). Exercise-induced skeletal muscle adaptations are manifested by changes in metabolic function (Green et al., 1992) that include increases in the content and oxidative capacity of mitochondria (Holloszy, 1967; Holloszy & Coyle, 1984). Ultimately, the enhanced oxidative capacity of skeletal muscle is believed to contribute to more rapid activation of mitochondria oxidative phosphorylation (OXPHOS), improved fat oxidation, and carbohydrate sparing which are hallmarks of greater endurance performance (Holloszy & Coyle, 1984).

Leading models propose that the greater mitochondrial oxidative capacity following chronic exercise result from continual and coordinated stimulation of transcriptional pathways. This process results in a steady state accumulation of mitochondrial proteins manifesting as greater mitochondrial content (Flück & Hoppeler, 2003; Perry et al., 2010; Pilegaard et al., 2000). Indeed, the majority of the literature has focused on the role of transcriptional coactivators and transcription factors required for promoter activation. For example, one model suggests that exercise activates peroxisome proliferator gamma coactivator-1α (Pgc-1α), which coactivates a variety of transcription factors controlling the expression of distinct families of mitochondrial proteins (Kupr & Handschin, 2015). Surprisingly, there is very little knowledge on the role of transcriptional corepressors in mediating mitochondrial biogenesis following exercise. Conceivably, exercise might suppress transcriptional repressors themselves as part of the early stages of mitochondrial biogenesis in the course of training. Receptor interacting protein 140 (RIP140), a transcriptional corepressor of nuclear receptors regulating metabolic genes (Powelka

et al., 2006) and negative regulator of skeletal muscle oxidative capacity (Seth et al., 2007) did not change in content following several weeks of exercise training in rats (Frier et al., 2011; Hoshino et al., 2013). However, in a human study with acute exercise, protein levels of RIP140 were less induced after exercise compared to a time-matched nonexercised control group (Gidlund et al., 2015).

Recent investigations have revealed that the transcriptional corepressors, Rb (Rb1) and p107 (Rbl1) members of the retinoblastoma susceptibility (Rb) family of proteins, may represent a new mechanism by which muscle metabolic capacities are controlled through negative regulation (Fajas, 2013). In addition to their typical role in cell proliferation and cell cycle, Rb was shown to promote mitochondrial integrity by inhibiting autophagy in myotubes to maintain the differentiated state (Ciavarra & Zacksenhaus, 2010). Moreover, oxidative genes in skeletal muscle are repressed by Rb interaction with transcription factor E2F1 (Blanchet et al., 2011). Indeed, skeletal muscle of Rb haploinsufficient mice showed increased fatty acid uptake and oxidation compared to its wild-type littermates (Petrov et al., 2016). In line with this, knockdown of Rb in myotubes showed enhanced mitochondrial to nuclear DNA ratio, increased oxygen consumption, increased basal glucose uptake, and disposal (Petrov et al., 2016). Also, p107 null mice have enhanced whole body lipid utilization, significantly increased levels of Pgc-1α in skeletal muscle, and increased levels of oxidative muscle fiber types (Scimè et al., 2005, 2010).

Despite the role of Rb and p107 in influencing skeletal muscle homeostasis, very few papers have assessed their potential influence during exercise adaptation. Rb null mice showed increased running endurance and enhanced oxidative gene expression (Blanchet et al., 2011). Moreover, after 7 days of acute exercise in mice, Rb is inactivated by phosphorylation, which might be one of the contributing factors to increase mitochondrial oxidative metabolism (Petrov

et al., 2016). For humans, the role of Rb and p107 in exercise-induced muscle adaptation has not been studied until now. Indeed, these corepressors may reveal a novel role for transcriptional de-repression in exercise-induced mitochondrial biogenesis distinct from the well-established concept of transcriptional coactivation. The purpose of this study was to describe the response of Rb and p107 protein expression in human skeletal muscle following repeated intense exercise challenges. We employed a time-course design whereby early changes in markers of skeletal muscle oxidative capacity were related to the expression of Rb and p107 transcriptional corepressors. Our findings reveal that reductions in p107 may be a novel mechanism involved in mitochondrial biogenesis following exercise in human skeletal muscle.

Materials and Methods

Human participants – exercise testing and muscle biopsies

All experimental procedures with human participants were approved by the Research Ethics Board at York University (Toronto, ON, Canada) and conformed to the Declaration of Helsinki. In the participants, exercise testing and muscle biopsy procedure were previously performed and described by Ydfors et al. (2016). The participants were healthy men with: mean ± SEM age of 24.8 ± 1.0 years, height 180.4 ± 1.8 cm, weight 75.5 ± 3.4 kg, body mass index of 23.2 ± 0.8 kg m−2 and peak oxygen uptake peak of 51.9 ± 1.9 mL kg−1 min−1. Over 3 weeks, the subjects performed nine sessions of high-intensity interval training (HIIT) that included 10 × 4 min intervals at 91% maximal heart rate with intermittent 2-min rest between each interval. Before the first exercise session (T1) and preceding exercise session 5 (T5) and session 9 (T9), skeletal muscle sample was collected from vastus lateralis muscle using a percutaneous needle biopsy technique with a 14-gauge Medax Biofeather disposable needle (San Possidonio, MO, Italy) under local

anesthesia. The tissues were frozen in liquid nitrogen and stored for gene and protein expression analysis.

OXPHOS content and individual ETC complex determination

The individual mitochondrial complex determination were previously performed, supplied and determined by Ydfors et al. (2016). The proteins of individual electron transport chain (ETC) complexes were detected by western blot analysis using a human OXPHOS Cocktail (ab110411, Abcam) containing five monoclonal antibodies specific for complex I subunit NDUFB8, complex II subunit SDHB, complex III subunit UQCRC2, complex IV subunit COX II, and complex V subunit ATP5A. The protein levels were quantified by densitometry for three time points including, before the first HIIT session (T1) and pre-session 5 (T5) and pre-session 9 (T9) (Ydfors et al. 2016). The total OXPHOS content for each time point was by determined taking the sum of the protein densities for the five proteins above. The proteins were normalized with the internal control β-tubulin (T8328, Sigma).

qPCR analysis

For quantification of Rb (Rb1) and p107 (Rbl1) mRNA, reverse transcriptase polymerase chain reaction was performed using TaqMan® Fast Universal PCR Master Mix (2X), no AmpErase® UNG (Applied Biosystems) on the CFX384 real-time PCR detection system (Bio-rad). The reaction volume was 10μL, including 2μL of sample cDNA diluted 1:100, 5μL of Master Mix, 0.5μL of target-specific probe for Rb and p107 (Hs01078066_m1 and Hs00765700_m1, Applied Biosystems), and 2.5μL nuclease-free water. GAPDH (4352934E, Applied Biosystems) was used as an endogenous control.

Western blot analysis

An aliquot of 10–30 mg of frozen muscle from each of the biopsies on T1, T5, and T9 were homogenized in ice-cold buffer containing 40 mmol/L Hepes pH 7.1, 120 mmol/L NaCl, 1 mmol/L EDTA, 10 mmol/L NaHP2O7.10H2O pyrophosphate, 10 mmol/L β-glycerophosphate, 10 mmol/L NaF, and 0.3% CHAPS detergent (pH 7.1). Denatured protein lysates (40µg) were loaded on gradient gels (6–15%) and separated by electrophoresis. Proteins were transferred on a 0.45 a polyvinylidene diflouride (PVDF) membrane (Bio-rad) using a wet transfer method. The PVDF membranes were probed with rabbit polyclonal anti-p107 (C18, SantaCruz), validated by LeCouter et al. (1998), mouse monoclonal anti-Rb (G3-245, BD Biosciences) validated by Huh et al. (2004), and monoclonal anti-α-tubulin (T6199, Sigma). Secondary antibodies conjugated with horseradish peroxidase were goat anti-rabbit and anti-mouse (Bio-rad). The membranes were visualized with chemiluminescence on photographic films and evaluated through densitometry using Image J software.

Correlation analysis

Correlation of p107 or Rb protein levels with the total OXPHOS content and individual mitochondrial complexes from Ydfors et al. (2016) on T1, T5, and T9 was done using Pearson correlation and linear regression analysis with Graphpad Prism 5.

Statistical analysis

Statistical analysis was performed by Graphpad Prism 5. One-way ANOVA and Tukey's post hoc tests were used to compare the protein contents of Rb and p107 on T1, T5, and T9. Results were considered to be statistically significant when $P < 0.05$. Associations between variables were investigated using Pearson correlation and linear regression analysis. Statistical significance was accepted at $P < 0.05$.

Results

Exercise decreases p107 protein levels in human skeletal muscle

We assessed the influence of exercise-induced skeletal muscle adaptation on Rb and p107 in human participants from a previous study reporting that markers of mitochondrial content and function increased during training (Ydfors et al., 2016). The participants were engaged in high-intensity interval training (HIIT) over a 3-week period, and muscle samples were obtained pre-exercise at three consecutive time points. Gene expression analysis revealed no changes in the expression patterns of Rb and p107 in skeletal muscle biopsies collected before initiation of the exercise protocol at time point 1 (T1), and pre-exercise at sessions 5 (T5) and 9 (T9) **(Fig. 1A and B)**. As there were no changes for Rb and p107 in gene expression, we determined the protein levels on the biopsied samples by Western blot analysis. Unlike the change in Rb that is seen in mice in 7 days of acute exercise (Petrov et al., 2016), no change was evident in the protein expression level of Rb in the pre-exercise samples over the entire exercise regimen in humans **(Fig. 2A)**. However, Western blot analysis and subsequent quantification of protein levels revealed that p107 was modulated over the 3-week period of the training session **(Fig. 2B)**. Down-regulation of the p107 protein level was observed in the pre-exercise samples on T5 of exercise by 45% compared to T1 before initiating HIIT. The level of p107 decreased significantly ($P < 0.05$) further by T9 in the pre-exercise samples by as much as 61%. Taken together, these results suggest that 3 weeks of HIIT reduced protein expression level of p107, but not Rb in human skeletal muscle.

p107 protein levels are inversely correlated with mitochondrial OXPHOS content

We investigated the potential role of Rb and p107 in muscle metabolic adaptation by assessing their relationship with the total OXPHOS content **(Fig. 3A and B)**. This was determined by quantifying the protein expression of representative markers of the electron transport chain

(ETC) at T1, T5, and T9 of HIIT (Ydfors et al., 2016). Pearson correlation and linear regression analysis revealed that p107 (r = 0.113, $P = 0.711$) and Rb (r = 0.349, $P = 0.496$) protein content did not correlate with OXPHOS content before the initiation of HIIT **(Fig. 3A and B)**. Interestingly, at T9 of HIIT, we found a significantly strong inverse correlation between OXPHOS content and p107 (r = −0.891, $P < 0.05$) **(Fig. 3B)**. On the contrary, Rb failed to show any significant correlation with the total OXPHOS content at T9 **(Fig. 3A)**. These data suggest that the improved mitochondrial oxidative capacity associated with exercise have a strong inverse association with the transcriptional corepressor p107 but not Rb.

p107 and Rb protein levels are inversely correlated with mitochondrial ETC complexes

As a significant association was found between the total OXPHOS content and p107, we evaluated if the mitochondrial ETC complexes separately had correlation with Rb and p107. This was accomplished by comparing the protein content of a representative marker for each of the five mitochondrial ETC complexes with Rb or p107. Before the onset of the HIIT regimen at T1 as well as at T5, we found that neither p107 nor Rb showed correlation with any of the ETC complexes **(Fig. 4 and 5)**. In line with the correlation between the total OXPHOS content and p107 at T9, a very strong negative correlation was also present between every ETC complex and p107 **(Fig. 5)**. Although Rb showed no significant association with the total OXPHOS content on T9, a significant negative correlation was observed only with Complexes III, IV, and V **(Fig. 4)**. This suggests that p107, and to a minor extent Rb, establishes an intricate association with the enhanced mitochondrial content caused by exercise.

Discussion

The adaptation of skeletal muscle in response to exercise has been a matter of extensive research, as considerable evidence exists for the beneficial effects of exercise for improving adverse health conditions (Schenk & Horowitz, 2007). Our study used nine sessions of HIIT over a 3-week period on human subjects as a model for acute endurance exercise to assess its influence on the transcriptional corepressors, Rb and p107. HIIT is a powerful model for investigating muscle plasticity given that it challenges metabolic homeostasis through repetitive intense bursts of contraction.

At present it is not known if p107 targets any of the nuclear or mitochondrial genes promoters associated with OXPHOS. However, the concept of the Rb family interacting with metabolic gene promoters is not atypical as Jones et al. (2016) found that Rb loss in triple-negative breast cancer induces mitochondrial protein translation, concomitant with increased OXPHOS (Jones et al., 2016). Although, others have found that Rb loss has the opposite effect by repressing OXPHOS in noncancerous cells (Nicolay et al., 2015). In addition, an early report, using ChIP-seq, demonstrated the association of E2F4 (a transcription factor binding partner of the RB family) on gene promoters involved with mitochondrial biogenesis (Cam et al., 2004). However, out of more than 10,000 E2F4 binding sites that have been identified through ChIP-seq analysis of E2F4, none has been specifically annotated for mitochondrial biogenesis (Balciunaite et al., 2005; Cam et al., 2004; Lee et al., 2011). Additionally, a large number of E2F4 targets specifically interact without p107 (Balciunaite et al., 2005) and p107 is known to interact with several other transcription factors including Sp1, b-myb, c-myc, and Smad3 (Balciunaite et al., 2005; Wirt & Sage, 2010). A p107-specific ChIP analysis of a DNA microarray (ChIP on ChIP), containing 13,000 human gene promoter regions spanning 700 bp upstream and 200 bp downstream of the

transcription start sites, revealed that p107 was bound to 244 genes, among which some are involved in mitochondrial biogenesis (Balciunaite et al., 2005). To date, none of these promoters involved in mitochondrial biogenesis have been annotated for specific p107 binding using p107 genetically deleted cells as controls. Nonetheless, the increased expression patterns for these genes based on potential p107 de-repression during HIIT might reflect the involvement of another factor(s) that is controlled by p107.

Our data suggest a novel association of p107 with the mitochondrial adaptations that are established after nine sessions of HIIT over 3 weeks. Indeed, the novel findings of this study are that, by the end of the exercise regimen there was (1) a decrease in p107 protein levels, (2) a strong inverse association of p107 with OXPHOS content, and (3) an inverse relation of p107 with each of the five ETC complexes. Therefore, these findings provide a newly discovered association between transcriptional corepressor down-regulation with increased mitochondrial bioenergetics.

Many findings show that p107 levels are normally controlled transcriptionally. Few details are known regarding posttranslational regulation of p107 levels. Two early reports suggest that Ca2+-activated protease calpain and the ubiquitin-proteasome pathway might post-translationally regulate p107 levels (Jang et al., 1999). Intriguingly, during running exercise, total calpain activity is increased and is associated with enhanced rates of protein degradation that is known to occur in skeletal muscle soon after exercise (Belcastro et al., 1998). Future studies investigating if the increase in calpain activity during exercise adaptation would target p107 for degradation are required.

Our findings strongly suggest that Rb might not have a role in influencing skeletal muscle adaptation triggered by exercise at the end of HIIT. Intriguingly, we found there were no changes in the transcriptional and posttranscriptional levels of Rb. Also there were no apparent differences

in posttranslational modification by phosphorylation, as determined by the mobility of Rb through gels, which was unaltered on Western blots. However, p107 showed a significant inverse correlation with each of the five ETC complexes and total OXPHOS content when sum of the complexes were assessed. This is in contrast to Rb that showed negative association with only complexes III, IV, and V and did not show any significant relation when compared to total OXPHOS. In mice, 7 days of acute exercise inactivates Rb in skeletal muscle by its phosphorylation by cyclin-dependent kinases (Petrov et al., 2016). The inactivation of Rb is synonymous with enhanced fatty acid oxidation, glucose uptake, and mitochondrial fusion (Petrov et al., 2016). These metabolic manifestations are the same as observed in human skeletal muscle after exercise training (Cartoni et al., 2005; Holloszy & Coyle, 1984; Neufer & Dohm, 1993; Perry et al., 2008; Richter & Hargreaves, 2013; Talanian et al., 2007). Thus, it remains to be determined if Rb inactivation by phosphorylation or other posttranslational modification(s) is associated with these metabolic improvements following training. In addition, the differences in the mouse and our human study for Rb might be species-specific and/or a disparity with the exercise methodologies used.

In mouse, it was shown that knockdown and knockout of p107 myoblasts resulted in more oxidative fiber types (Scimè et al., 2010). Interestingly, 6 weeks of HIIT also has been shown to induce myoblast activation followed by its differentiation into more metabolically efficient fiber types in humans (Joanisse et al., 2013). However, our human subjects did not show any fiber-type remodeling after nine sessions of HIIT despite a decrease in the p107 levels and an increase in skeletal muscle oxidative capacities, as published previously in these participants (Ydfors et al., 2016). This discrepancy might be explained by the differences in the duration of the HIIT regimen

between the two studies, which might play a crucial role in dictating the fate of myoblasts in humans.

There is strong evidence that inverse association between p107 and the mitochondrial metabolic machinery might be due to a functional role for p107. It has been shown that down-regulation of p107 is associated with oxidative phenotypes such as slow fiber formation (Scimè et al., 2010) and brown fat formation (De Sousa et al., 2014; Scimè et al., 2005) in mice. Indeed, in mouse skeletal muscle, p107 has been shown to suppress the transcriptional levels of Pgc-1α, a master regulator of exercise-induced mitochondrial biogenesis, through direct promoter interaction (Scimè et al., 2010). In humans, several weeks of endurance training (Kuhl et al., 2006; Russell et al., 2003; Short et al., 2003) and acute exercise (Cartoni et al., 2005; Hellsten et al., 2007; Mortensen et al., 2007; Norrbom et al., 2004; Pilegaard et al., 2000; Russell et al., 2005; Watt et al., 2004) are sufficient to increase Pgc-1α mRNA. This suggests that the decrease in p107 levels might release repression on Pgc-1α promoter. Perry et al. (2010) showed that following every session of HIIT, Pgc-1α mRNA increased 4 h post exercise. However, Pgc-1α returned to its pre-exercise levels after 24 h (Perry et al., 2010). We did not test samples for p107 immediately after exercise to assess if its levels were reduced to account for the increased Pgc-1α mRNA immediately post exercise.

In summary, we have found an association between a transcriptional corepressor with improved oxidative capacity after exercise adaptation. Indeed, in human skeletal muscle, p107 protein content is decreased concurrent with increased markers of mitochondrial content during short-term HIIT. This negative relationship suggests that the classic models of regulating mitochondrial biogenesis through positive coactivation should consider the potential role of decreasing transcriptional repression. Moreover, our results highlight that p107 might be more

important than Rb in human skeletal muscle adaptation during exercise. Given the clear relationship between skeletal muscle oxidative capacity and metabolic health, elucidating the role of transcriptional de-repression is of great importance in unraveling the mechanisms by which exercise mediates protection from metabolic disease.

Figure 1

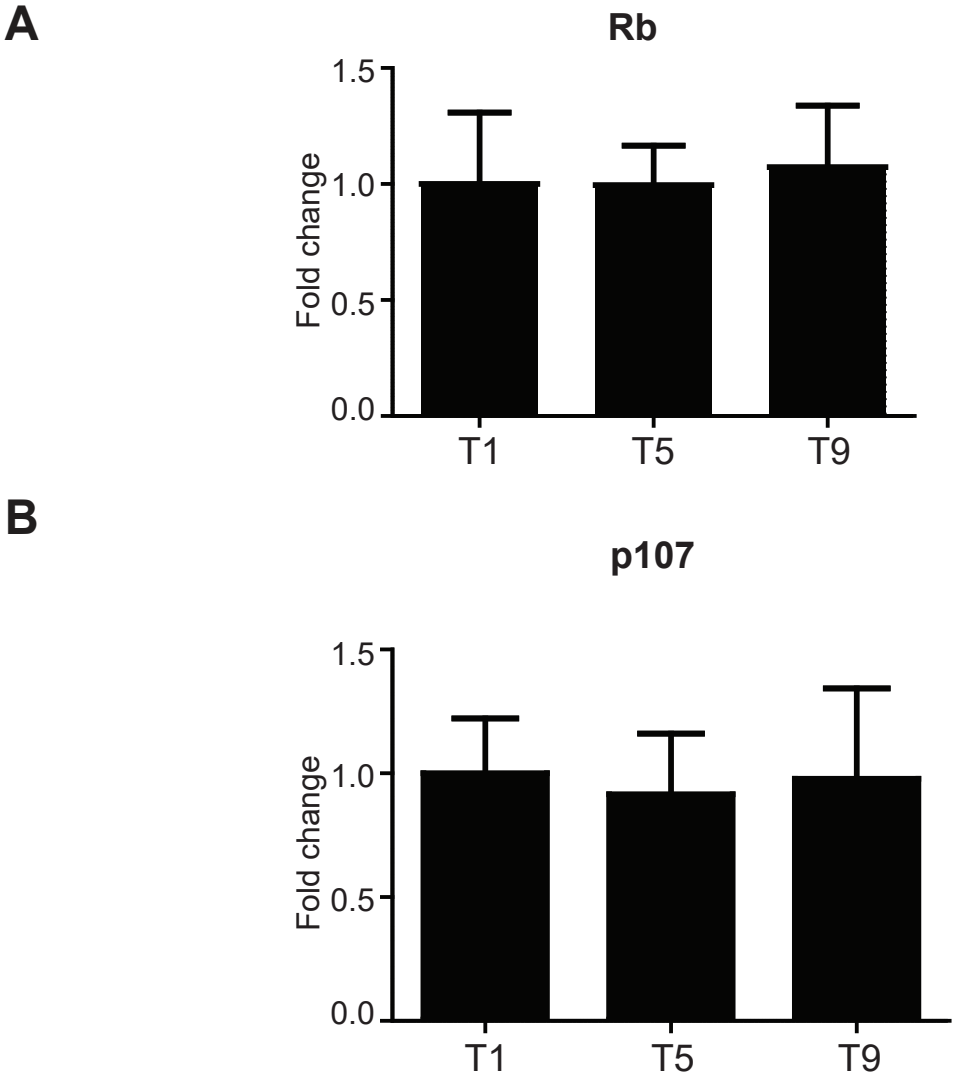

Figure 1. Rb and p107 gene expressions are unaffected after nine sessions of HIIT in human skeletal muscle. (A) qPCR analysis of Rb and **(B)** p107 of vastus lateralis muscle from human subjects engaged in HIIT before the initiation of the exercise protocol at T1 and pre-exercise session 5 (T5) and session (T9). One way ANOVA and Tukey post hoc test analysis were performed to determine the significance, n=10 for Rb and 11 for p107. All data are presented as mean +/- SD.

Figure 2

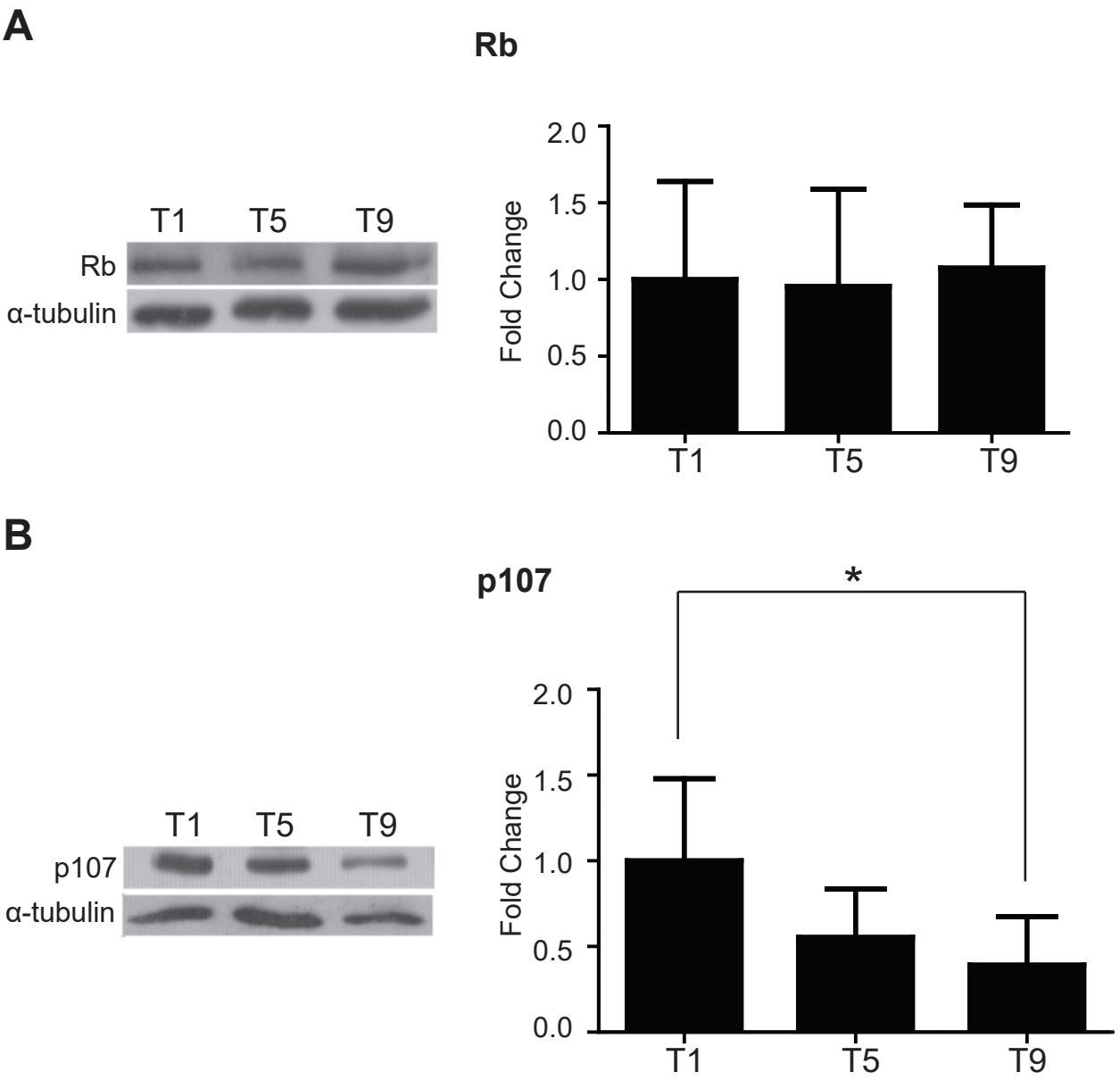

Figure 2: p107 protein levels are significantly decreased over nine sessions of HIIT in human skeletal muscle. (A) Representative Western blot and graphical representation for Rb and α-tubulin **(**control) from vastus lateralis muscle of human subjects engaged in HIIT over nine sessions before the initiation of the exercise protocol on T1 and pre-exercise at T5 and T9. n=8, one way ANOVA and Tukey post hoc test analysis were performed to determine the significance. All data are +/- SD. **(B)** Representative Western blot and graphical representation for p107 and α-tubulin (control) as in (A). n=8 (except n=7 for T5), one-way ANOVA and Tukey post hoc test were performed to determine the significance, asterisks denote significance.*P<0.05. All data are presented as mean +/- SD.

Figure 3

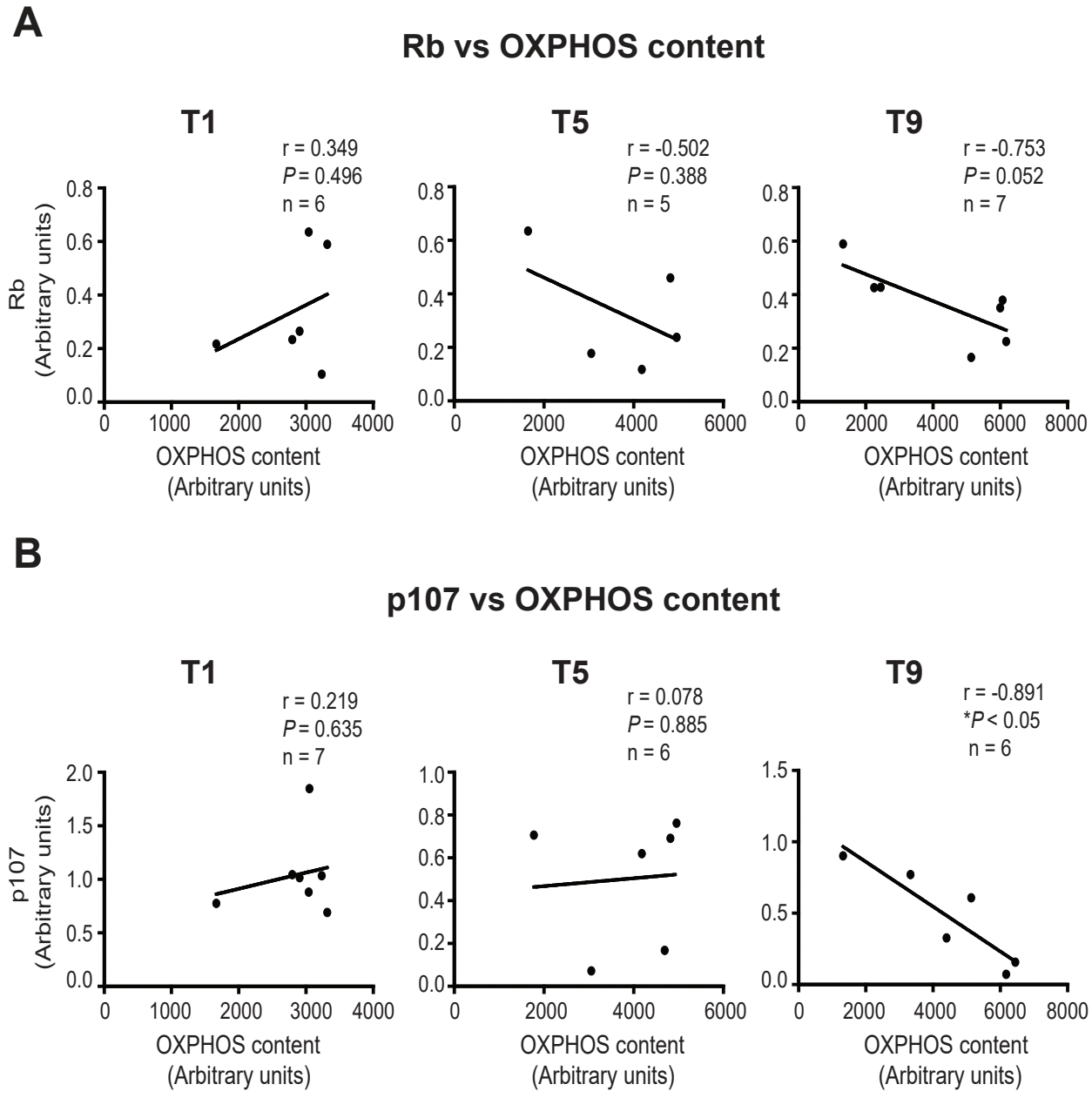

Figure 3: p107 is inversely correlated with total mitochondrial OXPHOS content after nine sessions of HIIT in human skeletal muscle. (A) Correlation and linear regression analysis between the protein levels of Rb and total OXPHOS content at T1 before the inititiation of HIIT and pre-exercise T5 and T9. **(B)** Correlation and linear regression analysis between the protein levels of p107 and total mitochondria OXPHOS content as above. n's are stated on the graph, asterisks denote significance, *P<0.05. r=Pearson correlation coefficient.

Figure 4

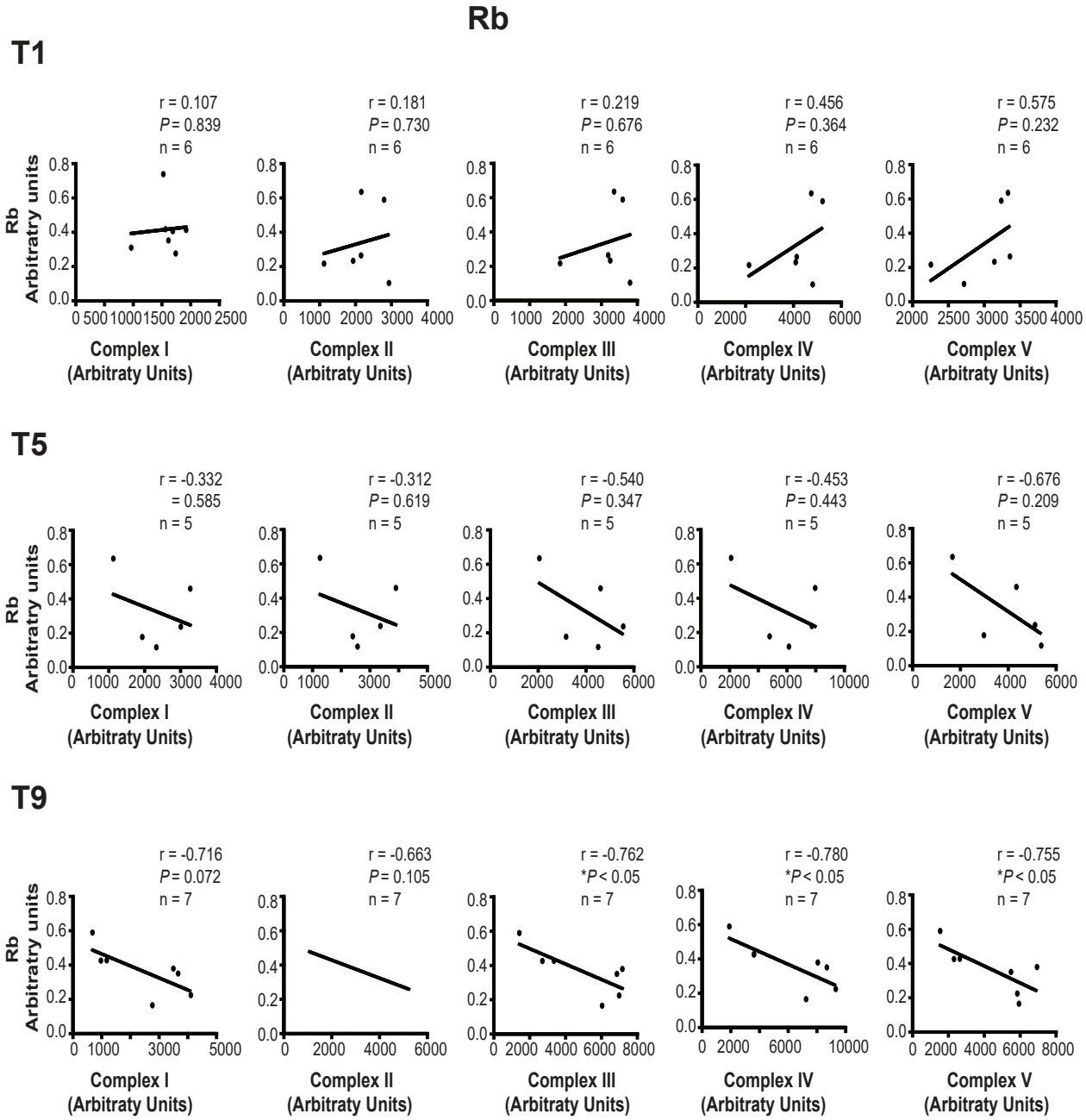

Figure 4: Rb is inversely correlated with ETC complex III, IV and V after nine sessions of HIIT in human skeletal muscle. Correlation and linear regression analysis between the protein levels of **Rb** and complex I, complex II, complex III, complex IV, or complex V of the ETC at T1, T5, and T9 of HIIT**.** n's are stated on the graph, asterisks denote significance *$P < 0.05$. r = Pearson correlation. HIIT, high intensity interval training.

Figure 5

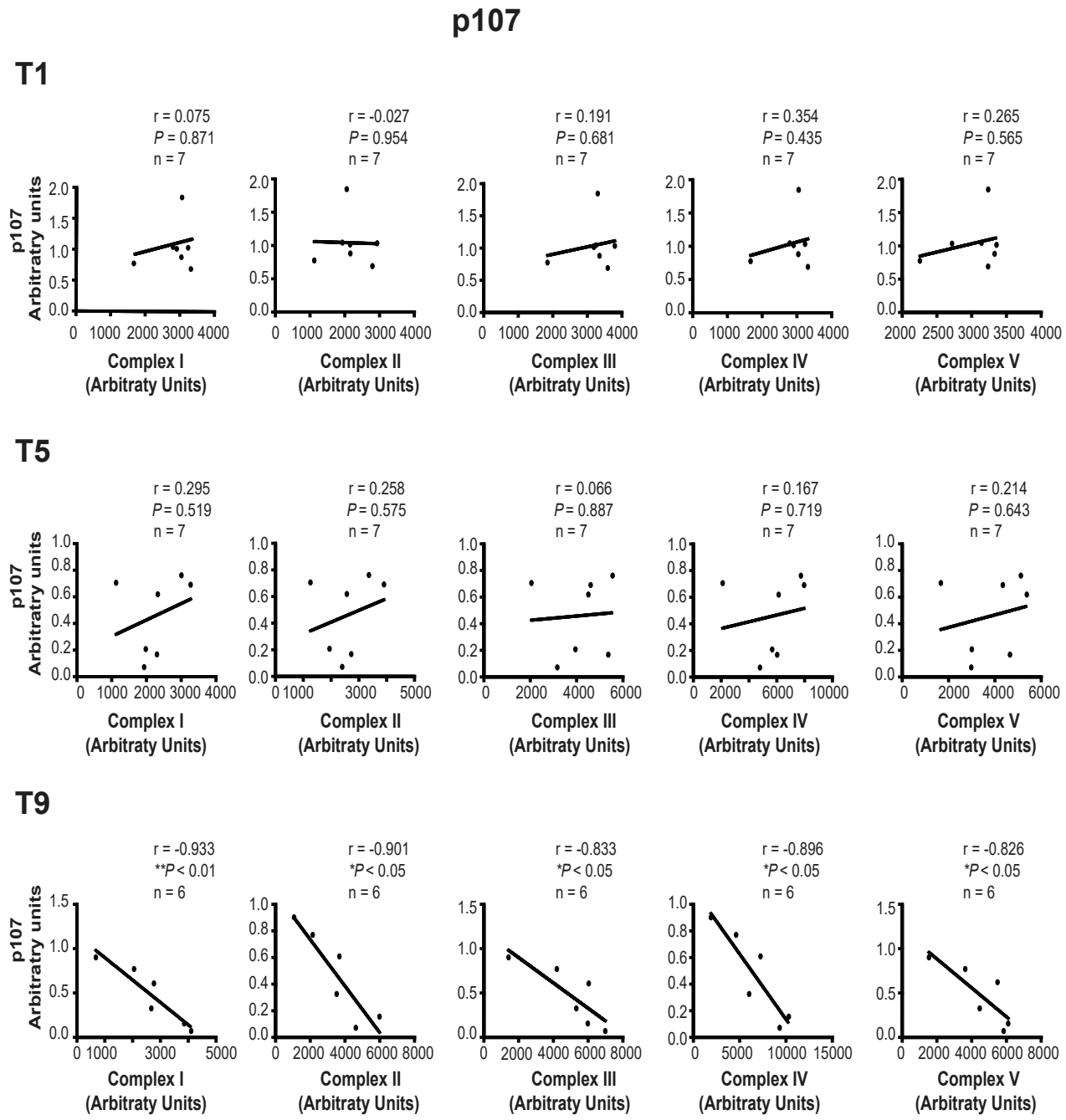

Figure 5: p107 is inversely correlated with individual ETC complexes after nine sessions of HIIT in human skeletal muscle. Correlation and linear regression analysis between the protein levels of p107 and complex I, complex II, complex III, complex IV, or complex V of the ETC at T1, T5, and T9 of HIIT. n's are stated on the graph, asterisks denote significance *$P < 0.05$ and **$P < 0.01$. r = Pearson correlation coefficient. HIIT, high intensity interval training.

References

Balciunaite, E., Spektor, A., Lents, N. H., Cam, H., te Riele, H., Scime, A., Rudnicki, M. A., Young, R., & Dynlacht, B. D. (2005). Pocket Protein Complexes Are Recruited to Distinct Targets in Quiescent and Proliferating Cells. *Molecular and Cellular Biology*, *25*(18), 8166–8178.

Belcastro, A. N., Shewchuk, L. D., & Raj, D. A. (1998). Exercise-induced muscle injury: A calpain hypothesis. In *Molecular and Cellular Biochemistry*, *179*(1–2), 135–145.

Blanchet, E., Annicotte, J. S., Lagarrigue, S., Aguilar, V., Clapé, C., Chavey, C., Fritz, V., Casas, F., Apparailly, F., Auwerx, J., & Fajas, L. (2011). E2F transcription factor-1 regulates oxidative metabolism. *Nature Cell Biology*, *13*(9), 1146–1154.

Cam, H., Balciunaite, E., Blais, A., Spektor, A., Scarpulla, R. C., Young, R., Kluger, Y., & Dynlacht, B. D. (2004). A common set of gene regulatory networks links metabolism and growth inhibition. *Molecular Cell*, *16*(3), 399–411.

Cartoni, R., Léger, B., Hock, M. B., Praz, M., Crettenand, A., Pich, S., Ziltener, J. L., Luthi, F., Dériaz, O., Zorzano, A., Gobelet, C., Kralli, A., & Russell, A. P. (2005). Mitofusins 1/2 and ERRα expression are increased in human skeletal muscle after physical exercise. *Journal of Physiology*, *567*(1), 349–358.

Ciavarra, G., & Zacksenhaus, E. (2010). Rescue of myogenic defects in Rb-deficient cells by inhibition of autophagy or by hypoxia-induced glycolytic shift. *Journal of Cell Biology*, *191*(2), 291–301.

Coffey, V. G., & Hawley, J. A. (2007). The Molecular Bases of Training Adaptation. In *Sports Med*, *37*, 9.

De Sousa, M., Porras, D. P., Perry, C. G. R., Seale, P., & Scimè, A. (2014). p107 Is a Crucial Regulator for Determining the Adipocyte Lineage Fate Choices of Stem Cells. *STEM CELLS*, *32*(5), 1323–1336.

Fajas, L. (2013). Re-thinking cell cycle regulators: The cross-talk with metabolism. In *Frontiers*

in Oncology, *24*(3), 4.

Flück, M., & Hoppeler, H. (2003). Molecular basis of skeletal muscle plasticity--from gene to form and function. In *Reviews of physiology, biochemistry and pharmacology*, *146*, 159–216.

Frier, B. C., Hancock, C. R., Little, J. P., Fillmore, N., Bliss, T. A., Thomson, D. M., Wan, Z., & Wright, D. C. (2011). Reductions in RIP140 are not required for exercise- and AICAR-mediated increases in skeletal muscle mitochondrial content. *Journal of Applied Physiology*, *111*(3), 688–695.

Gidlund, E. K., Ydfors, M., Appel, S., Rundqvist, H., Sundberg, C. J., & Norrbom, J. (2015). Rapidly elevated levels of PGC-1α-b protein in human skeletal muscle after exercise: Exploring regulatory factors in a randomized controlled trial. *Journal of Applied Physiology*, *119*(4), 374–384.

Green, H. J., Helyar, R., Ball-Burnett, M., Kowalchuk, N., Symon, S., & Farrance, B. (1992). Metabolic adaptations to training precede changes in muscle mitochondrial capacity. *Journal of Applied Physiology*, *72*(2), 484–491.

Gundersen, K. (2011). Excitation-transcription coupling in skeletal muscle: The molecular pathways of exercise. *Biological Reviews*, *86*(3), 564–600.

Hellsten, Y., Nielsen, J. J., Lykkesfeldt, J., Bruhn, M., Silveira, L., Pilegaard, H., & Bangsbo, J. (2007). Antioxidant supplementation enhances the exercise-induced increase in mitochondrial uncoupling protein 3 and endothelial nitric oxide synthase mRNA content in human skeletal muscle. *Free Radical Biology and Medicine*, *43*(3), 353–361.

Holloszy, J. O. (1967). Biochemical adaptations in muscle. Effects of exercise on mitochondrial oxygen uptake and respiratory enzyme activity in skeletal muscle. *Journal of Biological Chemistry*, *242*(9), 2278-82.

Holloszy, J. O., & Coyle, E. F. (1984). Adaptations of skeletal muscle to endurance exercise and their metabolic consequences. In *Journal of Applied Physiology Respiratory Environmental and Exercise Physiology*, *56*(4), 831-8.

Hoshino, D., Yoshida, Y., Kitaoka, Y., Hatta, H., & Bonen, A. (2013). High-intensity interval training increases intrinsic rates of mitochondrial fatty acid oxidation in rat red and white skeletal muscle. *Applied Physiology, Nutrition and Metabolism*, *38*(3), 326–333.

Jang, J. S., Lee, S. J., Choi, Y. H., Nguyen, P. M., Lee, J., Hwang, S. G., Wu, M. L., Takano, E., Maki, M., Henkart, P. A., & Trepel, J. B. (1999). Posttranslational regulation of the retinoblastoma gene family member p107 by calpain protease. *Oncogene*, *18*(10), 1789–1796.

Joanisse, S., Gillen, J. B., Bellamy, L. M., McKay, B. R., Tarnopolsky, M. A., Gibala, M. J., & Parise, G. (2013). Evidence for the contribution of muscle stem cells to nonhypertrophic skeletal muscle remodeling in humans. *FASEB Journal*, *27*(11), 4596–4605.

Jones, R. A., Robinson, T. J., Liu, J. C., Shrestha, M., Voisin, V., Ju, Y., Chung, P. E. D., Pellecchia, G., Fell, V. L., Bae, S., Muthuswamy, L., Datti, A., Egan, S. E., Jiang, Z., Leone, G., Bader, G. D., Schimmer, A., & Zacksenhaus, E. (2016). RB1 deficiency in triple-negative breast cancer induces mitochondrial protein translation. *Journal of Clinical Investigation*, *126*(10), 3739–3757.

Kuhl, J. E., Ruderman, N. B., Musi, N., Goodyear, L. J., Patti, M. E., Crunkhorn, S., Dronamraju, D., Thorell, A., Nygren, J., Ljungkvist, O., Degerblad, M., Stahle, A., Brismar, T. B., Andersen, K. L., Saha, A. K., Efendic, S., & Bavenholm, P. N. (2006). Exercise training decreases the concentration of malonyl-CoA and increases the expression and activity of malonyl-CoA decarboxylase in human muscle. *American Journal of Physiology-Endocrinology and Metabolism*, *290*(6), E1296–E1303.

Kupr, B., & Handschin, C. (2015). Complex coordination of cell plasticity by a PGC-1α-controlled transcriptional network in skeletal muscle. In *Frontiers in Physiology*, *6*, 325.

Lee, B. K., Bhinge, A. A., & Iyer, V. R. (2011). Wide-ranging functions of E2F4 in transcriptional activation and repression revealed by genome-wide analysis. *Nucleic Acids Research*, *39*(9), 3558–3573.

Mortensen, O. H., Plomgaard, P., Fischer, C. P., Hansen, A. K., Pilegaard, H., & Pedersen, B. K.

(2007). PGC-1β is downregulated by training in human skeletal muscle: No effect of training twice every second day vs. once daily on expression of the PGC-1 family. *Journal of Applied Physiology*, *103*(5), 1536–1542.

Neufer, P. D., & Dohm, G. L. (1993). Exercise induces a transient increase in transcription of the GLUT-4 gene in skeletal muscle. *American Journal of Physiology - Cell Physiology*, *265*(6 34-6).

Nicolay, B. N., Danielian, P. S., Kottakis, F., Lapek, J. D., Sanidas, I., Miles, W. O., Dehnad, M., Tschöp, K., Gierut, J. J., Manning, A. L., Morris, R., Haigis, K., Bardeesy, N., Lees, J. A., Haas, W., & Dyson, N. J. (2015). Proteomic analysis of pRb loss highlights a signature of decreased mitochondrial oxidative phosphorylation. *Genes and Development*, *29*(17), 1875–1889.

Norrbom, J., Sundberg, C. J., Ameln, H., Kraus, W. E., Jansson, E., & Gustafsson, T. (2004). PGC-1α mRNA expression is influenced by metabolic perturbation in exercising human skeletal muscle. *Journal of Applied Physiology*, *96*(1), 189–194.

Perry, C. G. R., Heigenhauser, G. J. F., Bonen, A., & Spriet, L. L. (2008). High-intensity aerobic interval training increases fat and carbohydrate metabolic capacities in human skeletal muscle. *Applied Physiology, Nutrition and Metabolism*, *33*(6), 1112–1123.

Perry, C. G. R., Lally, J., Holloway, G. P., Heigenhauser, G. J. F., Bonen, A., & Spriet, L. L. (2010). Repeated transient mRNA bursts precede increases in transcriptional and mitochondrial proteins during training in human skeletal muscle. *Journal of Physiology*, *588*(23), 4795–4810.

Petrov, P. D., Ribot, J., López-Mejía, I. C., Fajas, L., Palou, A., & Bonet, M. L. (2016). Retinoblastoma Protein Knockdown Favors Oxidative Metabolism and Glucose and Fatty Acid Disposal in Muscle Cells. *Journal of Cellular Physiology*, *231*(3), 708–718.

Pilegaard, H., Ordway, G. A., Saltin, B., & Neufer, P. D. (2000). Transcriptional regulation of gene expression in human skeletal muscle during recovery from exercise. *American Journal of Physiology - Endocrinology and Metabolism*, *279*(4 42-4).

Powelka, A. M., Seth, A., Virbasius, J. V., Kiskinis, E., Nicoloro, S. M., Guilherme, A., Tang, X., Straubhaar, J., Cherniack, A. D., Parker, M. G., & Czech, M. P. (2006). Suppression of oxidative metabolism and mitochondrial biogenesis by the transcriptional corepressor RIP140 in mouse adipocytes. *Journal of Clinical Investigation*, *116*(1), 125–136.

Richter, E. A., & Hargreaves, M. (2013). Exercise, GLUT4, and skeletal muscle glucose uptake. *Physiological Reviews*, *93*(3), 993–1017.

Russell, A. P., Feilchenfeldt, J., Schreiber, S., Praz, M., Crettenand, A., Gobelet, C., Meier, C. A., Bell, D. R., Kralli, A., Giacobino, J. P., & Dériaz, O. (2003). Endurance Training in Humans Leads to Fiber Type-Specific Increases in Levels of Peroxisome Proliferator-Activated Receptor-γ Coactivator-1 and Peroxisome Proliferator-Activated Receptor-α in Skeletal Muscle. *Diabetes*, *52*(12), 2874–2881.

Russell, A. P., Hesselink, M. K. C., Lo, S. K., & Schrauwen, P. (2005). Regulation of metabolic transcriptional co-activators and transcription factors with acute exercise. *The FASEB Journal*, *19*(8), 986–988.

Schenk, S., & Horowitz, J. F. (2007). Acute exercise increases triglyceride synthesis in skeletal muscle and prevents fatty acid-induced insulin resistance. *Journal of Clinical Investigation*, *117*(6), 1690–1698.

Scimè, A., Grenier, G., Huh, M. S., Gillespie, M. A., Bevilacqua, L., Harper, M. E., & Rudnicki, M. A. (2005). Rb and p107 regulate preadipocyte differentiation into white versus brown fat through repression of PGC-1α. *Cell Metabolism*, *2*(5), 283–295.

Scimè, A., Soleimani, V. D., Bentzinger, C. F., Gillespie, M. A., Le Grand, F., Grenier, G., Bevilacqua, L., Harper, M. E., & Rudnicki, M. A. (2010). Oxidative status of muscle is determined by p107 regulation of PGC-1α. *Journal of Cell Biology*, *190*(4), 651–662.

Seth, A., Steel, J. H., Nichol, D., Pocock, V., Kumaran, M. K., Fritah, A., Mobberley, M., Ryder, T. A., Rowlerson, A., Scott, J., Poutanen, M., White, R., & Parker, M. (2007). The Transcriptional Corepressor RIP140 Regulates Oxidative Metabolism in Skeletal Muscle. *Cell Metabolism*, *6*(3), 236–245.

Short, K. R., Vittone, J. L., Bigelow, M. L., Proctor, D. N., Rizza, R. A., Coenen-Schimke, J. M., & Nair, K. S. (2003). Impact of aerobic exercise training on age-related changes in insulin sensitivity and muscle oxidative capacity. *Diabetes*, *52*(8), 1888–1896.

Talanian, J. L., Galloway, S. D. R., Heigenhauser, G. J. F., Bonen, A., & Spriet, L. L. (2007). Two weeks of high-intensity aerobic interval training increases the capacity for fat oxidation during exercise in women. *Journal of Applied Physiology*, *102*(4), 1439–1447.

Watt, M. J., Southgate, R. J., Holmes, A. G., & Febbraio, M. A. (2004). Suppression of plasma free fatty acids upregulates peroxisome proliferator-activated receptor (PPAR) α and δ and PPAR coactivator 1α in human skeletal muscle, but not lipid regulatory genes. *Journal of Molecular Endocrinology*, *33*(2), 533–544.

Wirt, S. E., & Sage, J. (2010). P107 in the public eye: An Rb understudy and more. *Cell Division*, *5*, 1–13.

Ydfors, M., Hughes, M. C., Laham, R., Schlattner, U., Norrbom, J., & Perry, C. G. R. (2016). Modelling in vivo creatine/phosphocreatine in vitro reveals divergent adaptations in human muscle mitochondrial respiratory control by ADP after acute and chronic exercise. *Journal of Physiology*, *594*(11), 3127–3140.

CHAPTER 8
DISCUSSION

Our results for the first time unveil a potential mechanism for how SCs and their progenitors, MPs, might make fate decisions through p107 mediated control of mitochondrial function. Over many years, prior studies have largely focused on p107 nuclear function in the context of its transcriptional repressor role and ability to repress cell cycle in transient transfection assays (Lindeman et al., 1997; Rodier et al., 2005; Verona et al., 1997; Zini et al., 2001).

Though for decades, it has been known to localize in the cytoplasm up to late G1 and G1/S phase of the cell cycle; its cytoplasmic role was never fully elucidated. (Lindeman et al., 1997; Rodier et al., 2005; Verona et al., 1997; Wirt & Sage, 2010; Zini et al., 2001). Now, our novel results shed light on a new paradigm for p107 function, as a metabolic regulator for cell cycle control. Notably, this is through sensing energy requirement in the cytoplasm that is translated to energy generation in mitochondria, via NAD^+ dependent deacetylase Sirt1. Using a series of complimentary approaches, we found that p107 was located in the mitochondrial matrix, where it interacted at the mtDNA to repress mitochondrial encoded gene expression. By controlling gene expression in this manner, we found p107 directly impacted the Oxphos capacity of MP cells, ultimately restricting their proliferation rate **(Fig. 8.1)**.

In recent years, there has been an emerging realization that cellular metabolism governs how stem cells and their progenitors behave (Ghosh-Choudhary et al., 2020; Khacho et al., 2017; Ochocki & Simon, 2013; Porras et al., 2017). However, the molecular mechanism(s) underlying the metabolic regulation of SCs and their progenitors' fate, is still not completely understood. In this context, glycolysis and Oxphos play a crucial role in SC activation, proliferation, self-renewal

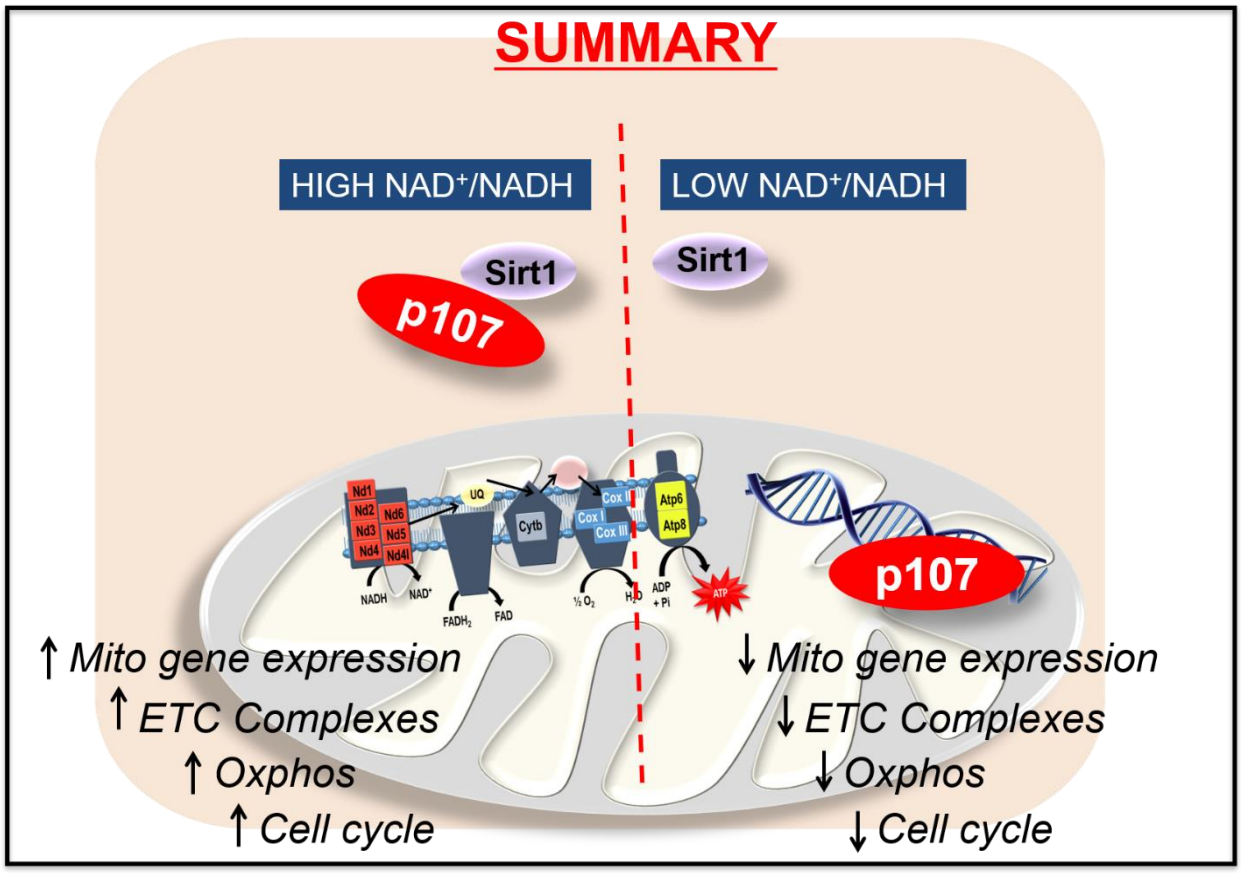

Figure 8.1: p107 controls MP proliferation through its mitochondrial function. In the presence of high NAD^+/NADH ratio, p107 interacts with Sirt1, that prevents its mitochondrial translocation. This causes de-repression of the mitochondrial DNA promoter, increased mitochondrial encoded gene expression, enhanced ATP generation and a faster MP cell cycle rate. When NAD^+/NADH is reduced and Sirt1 inactivated, p107 is localized in the mitochondria. Here it interacts at the mitochondrial DNA promoter causing repression of mitochondrial encoded genes, decreased ATP generation and MP cell cycle rate.

and differentiation (Bhattacharya & Scimè, 2020). Crucially, mitochondria are important for dynamic metabolic reprogramming of SCs and their progenitors during different stages of the differentiation process (Bhattacharya & Scimè, 2020; Folmes et al., 2012; Hori et al., 2019; Lyons et al., 2004; Ryall et al., 2015). Indeed, impaired SC regeneration capacity associated with health complications such as ageing and muscular dystrophies is often attributed to reduced mitochondrial function exhibited by low mtDNA copy number and attenuated Oxphos (Bollinger

et al., 2015; García-Prat et al., 2016a; Minet & Gaster, 2011; Pant et al., 2015; Rocheteau et al., 2015; Vila et al., 2017).

Our results underscore an unanticipated role of p107 in controlling SC and MP fate through regulation of mitochondrial gene expression and ATP generation. Till date the Rb family members, Rb and p130, have not been shown to be involved in regulating mitochondrial ATP generation capacity. A mitochondrial presence for p130 has not been published, but Rb has been shown to be located on the outer mitochondrial membrane, but not in the matrix or inner membrane where mtDNA and ETC complexes are located (Hilgendorf et al., 2013). In the mitochondria Rb directly interacts with the apoptosis regulator BAX, which induces mitochondrial outer membrane permeabilization and release of cytochrome c to initiate the apoptosis cascade (Hilgendorf et al., 2013). Furthermore, overexpression of Rb in the mitochondria of genetically deleted Rb and p53 (which is also a known tumour suppressor protein) mice, hindered tumour development by inducing apoptosis (Hilgendorf et al., 2013). p107 might also have an apoptotic role in the mitochondria, as we found that its sustained presence in the mitochondria enhanced ROS that might cause apoptosis **(Fig. 5.14 and 5.15)**. This mechanism might be separate from its function in normally proliferating cells.

By using a series of complimentary approaches, we found that p107 was localized in the mitochondria of actively proliferating c2c12 cells and prMPs **(Fig. 4.1, 4.3 and 4.5)**. In vivo, p107 was also found to co-localize in the mitochondria with Cox4 of activated and proliferating MPs of Ctx injured TA muscle **(Fig. 4.4)**. Biochemical mitochondrial fractionation showed that it was located in the mitochondrial matrix that is known to harbour mtDNA **(Fig. 4.2)**. At this time, how p107 is shuttled across the outer and inner mitochondrial membranes remains a mystery. It might be a consequence of post-translational modification by acetylation and/or phosphorylation

(Garriga et al., 2004; Leng et al., 2002; Wirt & Sage, 2010). There is evidence for this potentiality, as p107 translocates from the cytoplasm to the nucleus via phosphorylation by cyclin E/cdk2 at G1/S phase (Lindeman et al., 1997; Müller et al., 1997; Rodier et al., 2005; Verona et al., 1997; Zini et al., 2001).

Normally, mitochondrial targeted proteins are imported through specialized mitochondrial import machineries (Chacinska et al., 2009; Lucero et al., 2019; Neupert & Herrmann, 2007). The main mitochondrial protein import machinery consists of a series of complex channels that facilitate protein transport from the cytoplasm (Wiedemann & Pfanner, 2017). Located in the outer mitochondrial membrane is translocase of the outer membrane (Tom) complex, which is composed of various receptors including Tom20 and Tom70. The inner membrane contains two translocase of the inner membrane (Tim) complexes, namely Tim23 and Tim22, constituting several subunits (Hood et al., 2019). Proteins having cleavable mitochondrial targeting amino acid pre-sequences located at the N-terminal are directed to the mitochondrial matrix by Tom20, Tim23 and mitochondrial heat shock protein (Hsp)70, utilizing ATP. Once inside the matrix, mitochondrial processing peptidase cleaves the pre-sequences (Calvo et al., 2017; Wiedemann & Pfanner, 2017). However, Western blotting for both cytoplasmic and mitochondrial fractions of p107, did not show any differences in molecular size, suggesting that p107 might lack a cleavable N-terminal pre-sequence. This suggests that p107 mitochondrial ingress is facilitated by alternate mechanism. In this regard, another pathway dedicated to the mitochondrial import of proteins recognizes internal hydrophobic amino acid domains (Pfanner et al., 2019). This is the case for solute carrier group of membrane transport proteins that contain internal mitochondrial targeting signals made up of hydrophobic elements, in lieu of cleavable N-terminal pre-sequence (Pfanner et al., 2019; Ruprecht & Kunji, 2020). These proteins are recognized by cytosolic chaperones, Hsp70 and Hsp90 which

bind the hydrophobic residues of the proteins in the cytosol, prevent their aggregation and deliver them to Tom70. Although both the chaperones help in mitochondrial protein import, Hsp90 is considered crucial for docking hydrophobic proteins to Tom70 by virtue of their similar structural domain (Yano et al., 2004; Young et al., 2003). The proteins are then transported to Tim22 for mitochondrial import (Wiedemann & Pfanner, 2017; Young et al., 2003b). It is plausible, that p107 via its hydrophobic internal structure might be targeted and imported into the mitochondria (Backes et al., 2018). Indeed, using the Expasy Protscale software, we found that p107 has internal hydrophobic amino acids in the N-terminal (amino acid residues 202-213, 248-253 with maximum hydrophobicity at amino acid 205) and pocket domain (amino acid residues 504-512 and 842-80) which might be necessary for its mitochondrial translocation.

A method to determine p107 mitochondrial import through hydrophobic internal targeting signals, is to test its interaction with Hsp90, which is important for recognizing hydrophobic cytosolic proteins. IP/Western analysis would determine if p107 possibly interacts with Hsp90. Another possible way to determine if Hsp90 is involved in p107 mitochondrial import is by generating genetically deleted Hsp90 cell lines by a Crispr/Cas9 approach (Young et al., 2003b), or using inhibitors such as geldanamycin that decreases Hsp90 activity (Backes & Herrmann, 2017; Barksdale & Bijur, 2009). In this case, we would expect that mitochondrial p107 import would be decreased in absence of Hsp90 and/or diminution of its activity. Alternatively, by performing affinity purification and mass spectrometry, it can be evaluated if Hsp90 is one of the interacting partners of p107 (Meyer & Selbach, 2015). To accomplish this, lysates from c2c12 cells transfected with Flag-tagged p107 can be pre-cleared with protein A/G beads, incubated with anti-Flag agarose beads to pull down the Flag-tagged p107. Following incubation, the beads can be washed to remove non-specific protein interaction, transferred to a spin column with 3XFlag

peptides to separate Flag-tagged p107 from the beads. The eluted purified proteins can then be sent for mass spectrometry to identify the binding partners for p107 involved in protein import pathway (Gerace & Moazed, 2015). This approach would also be useful to find mitochondrial interacting proteins especially the mtDNA binding partner by assessing mitochondrial specific lysates.

Control of cellular metabolism by Rb family members, albeit in a mitochondria independent manner, have been published (De Sousa et al., 2014; Nicolay et al., 2015; Petrov et al., 2016; Porras et al., 2017). Rb was shown to control expression of oxidative genes in skeletal muscle through interaction with the E2f1 transcription factor (Blanchet et al., 2011). Moreover, skeletal muscle of Rb haploinsufficient mice demonstrated increased fatty acid uptake and oxidation compared to its Wt littermates (Petrov et al., 2016). In line with this, knockdown of Rb in myotubes showed enhanced mitochondrial to nuclear DNA ratio, increased oxygen consumption, increased basal glucose uptake and disposal (Petrov et al., 2016). Conversely, another study showed that ablation of Rb reduced mitochondrial ETC complex activity and Oxphos in retinal pigment epithelial and fibroblast cell lines (Nicolay et al., 2015). Similar to many studies on Rb, an inverse relation of p107 with oxidative metabolism, in a mitochondria independent manner, has also been reported (De Sousa et al., 2014; Porras et al., 2017; Scimè et al., 2010). p107 depleted adipose progenitors were shown to be primed for pro-thermogenic adipocyte lineages owing to their reliance on aerobic glycolysis (Porras et al., 2017). Additionally, p107 deficient mice had higher levels of oxidative type I and type IIA muscle fibers with enhanced metabolism (Scimè et al., 2010). Differentiation of p107KO prMPs resulted in formation of oxidative myotubes (Scimè et al., 2010). These studies suggest a negative association between p107 and oxidative function.

Relative to nuclear gene expression, regulation of mitochondrial gene expression is poorly understood. Mitochondria have their own distinctive mechanism of gene expression relying on the transcriptional factors TFB2M and TFAM. Additionally, multiple reports have suggested that transcription factors and co-transcriptional regulators that are typically functional in the nucleus, also have regulatory functions in the mitochondria. Some of the nuclear transcription factors that are characterized as direct regulators of mitochondrial gene expression in mammals are the glucocorticoid receptor (Demonacos et al., 1993; Koufali et al., 2003), thyroid hormone T3 receptor p43 (Enríquez et al., 1999; Wrutniak-Cabello et al., 2001), cyclic-AMP response element binding protein (Cammarota et al., 1999; Ryu et al., 2005), the tumor suppressor p53 (Heyne et al., 2004; Saleem & Hood, 2013), interferon regulatory factor 3 (Liu et al., 2010) estrogen receptors (Chen et al., 2004a), activator protein 1 (Ogita et al., 2002), peroxisome proliferator-activated receptor γ2 (Casas et al., 2000), nuclear factor κB and inhibitor of nuclear factor κB α (Cogswell et al., 2003), signal transducer and activator of transcription 3 (Stat3) (Yang & Rincon, 2016), MOF acetyl transferase (Chatterjee et al., 2017), nuclear factor of activated T cells complex 1 (Lambertini et al., 2015) and myocyte specific enhancer factor 2D (Brusco & Haas, 2015). All these transcription factors have role in mitochondrial gene expression and functions, albeit their prominent nuclear role. Apart from the transcription factors that directly regulate mitochondrial gene expression, transcriptional co-activator Pgc1a has also been shown to interact at the mtDNA promoter in complex with TFAM (Aquilano et al., 2010; Safdar et al., 2011).

Although, there is evidence of mitochondrial gene expression by transcriptional activators, the influence of transcriptional repressors on mitochondrial transcription remains elusive. To date, the only transcriptional repressor found in mammalian mitochondria is MTERF3, which has been shown to repress mitochondrial transcription initiation by binding at the mtDNA promoter (Park

et al., 2007). Absence of MTERF3, caused uncontrolled activation of mtDNA encoded transcription leading to an imbalance between mitochondrial and nuclear ETC complex subunit transcripts (Wredenberg et al., 2013). We propose that p107 is another transcriptional repressor that directly interacts at the D-loop regulatory region of the mtDNA to repress mitochondrial encoded gene expression **(Fig. 4.6B)**. Indeed, an imbalance between mitochondrial ETC complex subunits is associated with p107KO primary MPs and c2c12 cells displaying significant increased expression of the mitochondrial genes encoded for complexes I, III and IV of ETC **(Fig. 4.8A and 4.8B)**.

Our finding renders an important cellular role for p107 pertaining to cell cycle repression, which for many years, has been vague and confusing (Wirt & Sage, 2010). Unlike family member Rb that has been characterized as a bonafide G0/G1 phase restriction check point factor (Giacinti & Giordano, 2006). Over expression of p107 inhibited cell proliferation and arrested cell cycle at G1 in many cell types (Leng et al., 2002; Wirt & Sage, 2010; Zhu et al., 1993) and delayed the G1 to S phase entry in rat fibroblast cell lines (Rodier et al., 2005). Our data showcases an important regulatory mechanism that might govern this function. We revealed that p107 controls cellular proliferation by influencing ATP output through regulation of mitochondrial gene expression. Indeed, forced p107 expression in the mitochondria drastically limits mtDNA gene expression **(Fig. 4.10A, 4.10B, 4.10C and 4.10D)** and ATP generation **(Fig. 6.6A. 6.6B and 6.6C)** that inhibits the cell cycle rate both in vitro and in vivo **(Fig 6.7 and 6.10)**. This is consistent with the finding that showed depletion of mtDNA resulted in impaired cell proliferation due to reduced Oxphos (Martínez-Reyes et al., 2016). Thus, the decreased proliferative capacity and cell cycle dynamics of p107 over-expressing cells found in many reports might now be ascribed to its

mitochondrial role in repressing mitochondrial gene expression, which is required for G1 cell cycle progression.

Thus, the high rate of mitochondrial gene expression accompanied with elevated ATP levels generated by Oxphos and glycolysis, due to absence of p107, can explain the accelerated G1/S phase of cell cycle and proliferation rate in p107KO c2c12 cells **(Fig. 6.3 and 6.4)**. It also supports the significantly greater number of proliferating MPs observed in regenerating skeletal muscle isolated from Ctx injured p107KO mice **(Fig. 6.2B and 6.2C)**. These results now provide the rationale for the higher proliferative and cell cycle rate evidenced in p107KO mouse embryonic fibroblasts and prMPs (Lecouter et al., 1998). This control mechanism for p107 might ensure that ATP levels remain compatible with the demands of the proliferating cells. Moreover, by down regulating ATP generation capacity, p107 might act as a mechanism to provide macromolecules to the proliferating cells by diverting TCA cycle from producing reducing equivalents for the ETC (Vander Heiden & Deberardinis, 2017).

Similar to our study, other reports also disclosed that mitochondrial Oxphos is essential for cell cycle progression (Da Veiga Moreira et al., 2015; McBride et al., 2006). Mitochondrial ATP was shown to increase cyclin E levels that was necessary for Cdk2 activation and G1/S progression (Mitra et al., 2009). Importantly, during G1/S transition of the cell cycle, a glycolytic to Oxphos switch occurs (Kalucka et al., 2015; Mandal et al., 2005). This is the period (late G1 or G1/S phase of the cell cycle) when p107 has been shown to re-locate from the cytoplasm to nucleus (Lindeman et al., 1997; Müller et al., 1997; Rodier et al., 2005; Verona et al., 1997). Moreover, crucial to p107 nuclear translocation during G1/S phase is its phosphorylation by cyclin E/Cdk2 (Kolupaeva & Basilico, 2012; Reshetnikova et al., 2000; Zini et al., 2001). Notably, downregulation of Cdk2 activity prevents p107 translocation to the nucleus, thereby arresting cell

cycle progression (Reshetnikova et al., 2000). In this scenario, we believe the cells might be held in G1 because p107 accumulates in the mitochondria, causing repression of Oxphos. On the other hand, we had showed that for adipocyte progenitors, p107 cytoplasmic to nuclear translocation is associated with silencing Ldha and Pdk2 gene expression on nuclear promoters, thus promoting an increase in Oxphos capacity (Porras et al., 2017). Thus, these results suggest that p107 dynamically modulates cell metabolism during the cell cycle through promoter repression in two different organelles. Through inhibiting Oxphos in G1 (mitochondrial function), dependent on the nutrient load, and increasing Oxphos in S phase (nuclear function), p107 is able to exert dual influences on cell cycle progression.

An important partner of Rb family members in mediating repression of cell cycle genes in the nucleus is the DREAM complex (Fischer & Müller, 2017). A functional role during the cell cycle for this interaction has been shown for Rb at the G0/G1 restriction point and p130 in G0 (Litovchick et al., 2011; Uxa et al., 2019). However, a cell cycle role for p107 is not obvious owing to its ubiquitous expression in proliferating cells when an interaction with DREAM would halt the cell cycle. It suggests that the p107 interaction with the DREAM complex is a unique role independent of normal cell cycle progression. This was showcased by a recent publication that found it had a role in DNA damage response (Schade et al., 2019b). In this case following DNA damage, p107 inhibited gene expression at the G1/S phase of the cell cycle by interacting with the DREAM complex, to mediate cell cycle arrest. Thus, adding more evidence for p107 nuclear functionality only during G1/S phase of the cell cycle. Till date, it is not clear if p107 represses mtDNA transcription by binding with its nuclear transcription factor partner E2f4/E2f5, or the mitochondrial transcription factors TFB2M or TFAM. Co-immunoprecipitation studies between p107 and these transcription factors will determine if this is the case.

Imaging studies of cultured cells have indicated that mitochondrial energy generation causes changes in mitochondrial morphology, which is commensurate with cell cycle progression (Margineantu et al., 2002; Mitra et al., 2009; Taguchi et al., 2007). One of the more prominent features is mitochondrial fusion that causes elongation during the G1/S phase transition that is associated with higher ATP production (Mishra & Chan, 2014; Mitra et al., 2009; Mandal et al., 2005). Interestingly, p107 is not present in mitochondria during G1/S phase, that would increase the mitochondrial ATP generation capacity **(Fig. 4.13 and 4.15)**. Interestingly, p107KO c2c12 cells display elongated mitochondrial network **(Fig. 4.16)** with significantly higher mitochondrial length compared to the controls **(Fig. 4.17)**. This is associated with increased mitochondrial Oxphos **(Fig. 4.12 and 4.14)** due to de-repression of the mitochondrial genes. Moreover, p107KO c2c12 cells and MPs have accelerated cell cycle rates **(Fig. 6.3 and 6.4)**. This might suggest that cells strategically lose p107 from mitochondria to increase Oxphos that cause mitochondrial elongation due to fusion perpetuating cell cycle progression. It would be of interest to determine if decreased cell cycle due to p107 overexpression might increase mitochondrial fragmentation by fission, as a result of significantly reduced ATP generation. This can be tested by assessing mitochondrial morphology and length in p107KO cells over expressing full length (p107fl) and mitochondrial localized p107 (p107ml).

In order to proliferate, cells rely on both glycolysis and Oxphos for ATP production (Locasale & Cantley, 2010). However, it is unclear how glycolysis and Oxphos collectively operate to regulate the yield of ATP. Our data show a major rationale for the ubiquitous expression of p107 in proliferating cells as part of a mechanism involved in this interconnection. Our results highlight that p107 influences ATP production in the mitochondria based on the energy generated in the cytoplasm. We believe that this system is used to balance total cellular ATP production

based on the needs of the proliferating cell (Locasale & Cantley, 2010). Importantly, p107 acts as a nexus in sensing the NAD^+/NADH ratio driven by availability of substrate, to control ATP generation by Oxphos. Increased glucose accessibility that decreased the cytoplasmic NAD^+/NADH ratio **(Fig. 5.5)**, attenuated mitochondrial potential for ATP generation **(Fig. 5.12A and 5.12B)**. This in part due to increasing levels of p107 interacting at the mtDNA **(Fig. 5.1B)** where it repressed gene expression **(Fig. 5.2A, 5.2B, 5.2C and 5.2D)**. Similarly, oxamate that increased p107 mitochondrial levels **(Fig. 5.6B)** by sensing the cytoplasmic NAD^+/NADH ratio **(Fig. 5.6A)**, reduced ATP generation **(Fig. 5.13)**, due to repressed mitochondrial gene expression **(Fig. 5.7)** limiting ETC complex formation **(Fig. 5.8).** On the other hand, increasing the cytoplasmic NAD^+/NADH ratio **(Fig. 5.10A)** by galactose that decreased p107 mitochondrial levels **(Fig. 5.10B)**, decreased mitochondrial gene expression **(Fig. 5.10C)**. Importantly, these findings suggest that p107 acts as a metabolic sensor for the energy produced in the cytoplasm to mediate energy generation in the mitochondria.

Our data strongly support that p107 controls mitochondrial ATP generation by acting as an energy sensor of NAD^+/NADH in conjunction with Sirt1, which is activated by NAD^+. Importantly, we found that p107 interacted with Sirt1 directly by IP/Westerns, using endogenous lysates, which did not contain over expressed proteins **(Fig. 5.16B and 5.16C)**. Moreover, by inhibiting or activating Sirt1 we found that it affected p107 mitochondrial localization, mtDNA promoter binding, mitochondrial gene expression and ATP generation levels. Significantly, Sirt1 regulation of MP cell cycle was also dependent on p107 mitochondrial function **(Fig. 6.5)**. Previous findings have shown that Sirt1 promotes SC activation and MP proliferation with greater SC self-renewal and more proliferative MPs (Rathbone et al., 2009; Zhang et al., 2016). Consistent with this idea, mice with activated Sirt1, due to caloric restriction or NAD^+ repletion exhibited

greater self-renewal and proliferative capacity (Cerletti et al., 2012; Zhang et al., 2016). In this context, primary activated SCs isolated from Sirt1KO mice, showed significantly attenuated cell cycle, as measured by the incorporation of nucleotide base analogs into DNA (Myers et al., 2019; Tang & Rando, 2014). In relation to our finding, this might be suggestive of p107 mitochondrial localization without Sirt1 control that impedes cell cycle through inhibition of ATP generation **(Fig. 6.5, 5.19A and 5.19B)**. Though the use of Sirt1KO cells confirmed that p107 functions through a Sirt1 dependent mechanism in proliferating MPs, it is unlikely that the functional interaction between p107 and Sirt1 is maintained during myogenic differentiation, as Sirt1 has a non-metabolic role during differentiation (Fulco et al., 2008; Ryall et al., 2015). Nonetheless, these findings set the stage for future evaluation of the mitochondrial function of p107 and Sirt1 during SC activation, self-renewal and commitment.

As p107 mitochondrial localization, reduces Oxphos capacity, cell cycle rate and proliferation of MPs, in conjunction with Sirt1, it is crucial to identify the potential structural and functional domains of p107 that regulate the mechanism. For this, truncated and mutated HA-tagged versions of p107 for E2f4, E2f5, cyclin D/Cdk4 and cyclin E/Cdk2 binding sites and point mutations for post translational modification sites could be produced. By transient transfection of these deletion mutant plasmids, mitochondrial localization of p107 can be assessed. Furthermore, the functional consequences of transfecting these mutant plasmids for mtDNA encoded gene expression, ATP generation capacity, cell cycle dynamics, ROS generation and Sirt1 interaction can be investigated**.** Similarly, truncated HA-tagged Sirt1 plasmids, such as N-terminal deletion mutant that normally binds acetylated protein substrates and catalytic domain deletion that binds acetyl-lysine targeted substrates can be assessed for binding to p107. The functional consequences

of the Sirt1 interacting domains can be investigated for mitochondrial encoded gene expression, ATP generation capacity and cell proliferation analysis.

Despite the importance of Sirt1 regulation, the acetylation target(s) of p107 is unknown. It is possible that Sirt1 deacetylates similar amino acid residues found in p130 (Schwarze et al., 2010), its homologous family member **(Fig. 1.9A)**. p130 has been shown to be acetylated in-vitro at a major site K1079, and minor sites at K1068 and K1111 in the C-terminus and K128 and K130 at the N-terminus (Schwarze et al., 2010). A BLAST search between p107 and p130 to evaluate the sequence homology at these acetylation sites was compared to potential p107 acetylated lysine residues obtained using the prediction software, Prediction of Acetylation on Internal Lysines (PAIL). We found K104 and K106 at the N terminus of p107 is highly homologous with K128 and K130 of p130 and at the C terminus, K1007 and K1039 of p107 corresponds to K1079 and

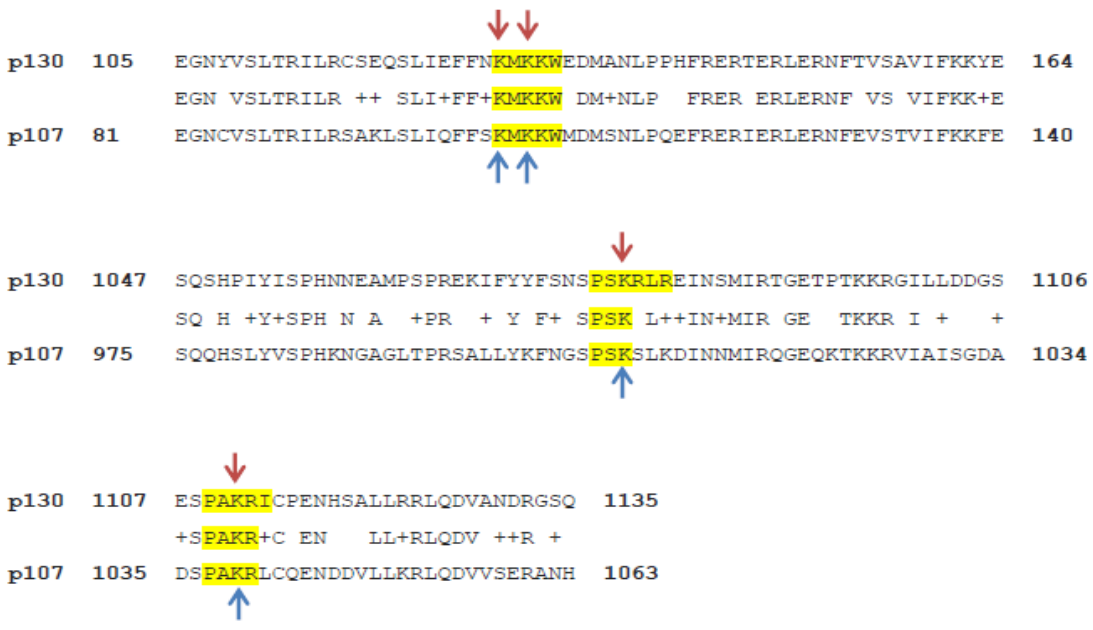

Figure 8.2: Sequence Homology of p107 and p130. BLAST software describes sequence homology of lysine (K) residues, K104 and K106 at N terminus of p107 with K128 and K130 of p130 and at the C terminus K1007 and K1039 of p107 with K1079 and K1111 of p130.

K1111 of p130 **(Fig. 8.2)**. Site directed mutagenesis of p107 for the above-mentioned lysine residues, singly and in combination could be performed. Their cDNA over expressed in cells as a means to evaluate their mitochondrial localization with and without Sirt1 activation. If acetylation in the aforementioned sites is not found, other structural/functional domains of p107 might be taken in consideration to find possible acetylation sites.

Apart from acetylation, other post translational modifications, such as phosphorylation might also influence p107 mitochondrial translocation and function in the mitochondria. p107 has seventeen phosphorylation sites that have been mapped (Iwahori & Kalejta, 2017) **(Fig 1.9B)** and cyclin E/Cdk2 activity is important for p107 translocation into the nucleus at G1/S phase, signifying the importance of phosphorylation in p107 sub-cellular translocation. Therefore, it can be presumed that mutation of cyclin E/Cdk2 binding domain would prevent p107 phosphorylation, impeding its migration into the nucleus, thereby localizing it in the cytoplasm and perhaps in the mitochondria. This can be assessed by Western blot analysis for p107 mitochondrial localization, mitochondrial encoded gene expression and ATP generation capacity.

Another important regulator that phosphorylates p107 in early G1 is cyclin D/Cdk4 (Leng et al., 2002). Cyclin D/Cdk4 has been shown to abrogate the binding between p107 and E2f. This is thought to promote cell cycle progression, although there is no direct link of p107 and E2f4 dissociation in early G1 when cyclin D/Cdk4 is active (Beijersbeigen et al., 1995; Hitomi & Stacey, 1999), a time point when p107 is not found in the nucleus (Lindeman et al., 1997; Rodier et al., 2005; Verona et al., 1997; Wirt & Sage, 2010; Zini et al., 2001). Therefore, suggesting that the role of cyclin D/Cdk4 phosphorylation of p107 might have some other role that could be related to mitochondrial metabolic functions rather than nuclear de-repression. On the other hand, Cdk4

might simply be preparing p107 for nuclear translocation in G1/S phase by promoting subsequent phosphorylation by Cdk2 (Cobrinik, 2005).

Recently, cyclin D/Cdk4 has also been shown to phosphorylate and inactivate different metabolic factors. It was shown that in mice, while fasting decreased cyclin D/Cdk4 activity, feeding increased its activity (Lee et al., 2014). This increase in cyclin D/Cdk4 activity with feeding was shown to phosphorylate and promote GCN5 acetyltransferase function. GCN5 acetylated Pgc1a, which downregulated its mitochondrial function to enhance Oxphos (Lee et al., 2014). Moreover, cyclin D/Cdk4 was also shown to phosphorylate and inactivate Pgc1a directly (Bhalla et al., 2014). This scenario might mirror high glucose conditions (low NAD^+/NADH ratio) when p107 is in the mitochondria **(Fig. 5.1A)** repressing mitochondrial encoded gene expression **(Fig. 5.2)** and ATP generation capacity **(Fig. 5.12A and 5.12B)**. Thus, suggesting that Cdk4 mediated phosphorylation of p107 might promote its mitochondrial localization.

Another possible role for p107 mitochondrial localization might be its ability to control ROS production. Importantly, accumulation of NADH at complex I, caused by low NAD^+/NADH, is known to trigger ROS production by reductive stress (Pryde & Hirst, 2011; Xiao & Loscalzo, 2020; Yan, 2014). In line with this, we believe that the increased p107 mitochondrial function due to oxamate treatment led to ROS generation **(Fig. 5.14A and 5.14B)**. This is also exemplified by overexpressing p107 in the mitochondria that led to elevated level of ROS **(Fig. 5.15A and 5.15B)** which might be due to significant repression of mitochondrial gene expression and ATP generation capacity. ROS generation might be due to reductive stress at complex I (Xiao & Loscalzo, 2020). It might also be due to a drastic reduction of available ETC complexes **(Fig. 5.8)** by an increase in p107 mitochondrial function leading to RET triggering reductive stress. Contrarily, in p107KO cells, the increase of ETC complexes **(Fig. 5.8)** would perhaps allow electrons to move more

efficiently reducing the potential for RET. Using mitochondrial targeted fluorophores that specifically measure superoxides will help to confirm if p107 causes mitochondrial specific ROS generation. Furthermore, to determine if ROS is produced by complex I due to reductive stress, a complex I inhibitor, rotenone can be used. Rotenone stimulates forward electron transfer and inhibits reverse electron transfer that forms superoxide by complex I (Lopez-Fabuel et al., 2016). Thus, if reductive stress has caused ROS in c2c12 cells treated with oxamate or with overexpressed p107mls, rotenone would decrease its production.

At this point it is not known if p107 might function in SCs at physiological level without the need for induced muscle regeneration. As a first step, we used exercise to promote potential impacts on skeletal muscle SCs and MPs. Interestingly, we found that p107 protein levels decreased after 9 days of high intensity interval training in human skeletal muscle **(Chapter 7)**. Additionally, p107 levels were inversely correlated with exercise induced improvements in mitochondrial Oxphos and ETC complex protein levels **(Chapter 7)**. Importantly, some of these alterations within skeletal muscle with exercise, might also include their SCs and MPs. Interestingly, following acute exercise one report described an increased Pgc1α interaction at the mtDNA in complex with Tfam (Safdar et al., 2011). This interaction was shown to enhance mitochondrial encoded gene expression that was thought to play a part in Pgc1α pro-oxidative metabolic function (Safdar et al., 2011). As p107 has been shown to negatively regulate Pgc1α gene expression (Scimè et al., 2005, 2010), it might be possible that a decrease in p107 with exercise might increase Pgc1α levels. It also suggests that the mitochondrial role of p107 and Pgc1α in the mitochondria might be mutually exclusive with opposite metabolic outcomes. When p107 is in the mitochondria it functions as a co-repressor for mitochondrial encoded gene expression, whereas Pgc1α has the opposite effect as a co-activator.

Both in humans and mice, there is evidence that SCs obtained from skeletal muscle and cultured in vitro, become activated, proliferating as MPs that eventually differentiate into myotubes retaining the same metabolic phenotype from where they were derived (Al-Khalili et al., 2003; Al-Khalili et al., 2014; Bell et al., 2010; Bollinger et al., 2015; Bourlier et al., 2013; Boyle et al., 2012; Consitt et al., 2010; Lund et al., 2017). Indeed, exercise that causes metabolic changes also affect activation and regeneration potential of quiescent SC pools (Abreu & Kowaltowski, 2020). This was also reflected in ageing where endurance exercise in humans was shown to improve SC regeneration ability that might be due to improved mitochondrial function (Joanisse et al., 2016). In agreement with these findings, our data suggests that the p107 metabolic function might have a role in affecting SC fate decisions related with activation and self-renewal, as well as in proliferating MPs. In p107KO mice, we detected significantly increased SC activation after 2 days post muscle injury **(Fig. 6.2B)**, which was demonstrated by significantly increased MyoD positive cells compared to control injured mice. Furthermore, by enumerating Pax7 positive cells in tissue sections, we found that that p107KO mice had significantly more quiescent SCs per myofiber compared to the controls **(Fig. 6.1)**. This is indicative of an increased rate of self-renewal in p107KO mice. Thus, suggesting that p107 might be one of the targets for intrinsic changes in SC fate decisions that not only influence the proliferation dynamics of their progenitors, but also activation and self-renewal. These changes at the level of SCs and MPs caused by p107 function might occur with exercise adaptation, which is reflected in our findings in skeletal muscle that show inverse association of p107 with enhanced Oxphos capacity **(Chapter 7)**. Physiological adaptations targeting p107 might also benefit ageing and muscular dystrophy which are characterized by a limited number of SCs and impaired regeneration potential (Bernet et al., 2014; Chen et al., 2020).

A shortcoming to this study is the use of p107 whole body genetic deletion to assess SCs and MPs in vivo. Thus, to better elucidate the p107 contribution to SC fate decisions, it would be paramount to eliminate any potential developmental contributions caused by the whole body p107 "knockout". To accomplish this Cre-Lox recombination system can be used for SC specific genetic deletion of p107. Here Cre-recombinase induced excision at LoxP sites flanking p107, in Pax7 CreER expressing cells with tamoxifen administration would result in p107 deletion. Unfortunately, p107LoxP mice do not exist. If they did exist, the mice could be treated with tamoxifen before 5 days to delete p107, prior to Ctx injection into the muscle, as we had done **(Fig. 6.2A)**. Similar to the p107 whole body knockout mice, p107 floxed mice would be expected to have more proliferating $MyoD^{+}$ expressing cells 2 days post Ctx injury.

In summary, our findings establish that a cell cycle regulator, p107, can be an important regulator of SC and its progenitor fate decision. Our study has unveiled a new paradigm in the context of metabolic control of cellular proliferation. Crucially, p107 functions as a key and fundamental component of the cellular metabolism network during cell division of myogenic progenitors. Indeed, it directly manipulates the energy generation capacity of mitochondria by indirectly sensing the glycolytic energy production through Sirt1. These results provide a conceptual advance for how proliferating cells regulate energy generation through the interplay between glycolysis and Oxphos. Importantly because of the ubiquitous p107 protein expression in most dividing cells, the findings identify a potential universal cellular mechanism with immense implications for studies in other dividing cell types including cancer cell proliferation.

CHAPTER 9
REFERENCE

Abbot, E. L., McCormack, J. G., Reynet, C., Hassall, D. G., Buchan, K. W., & Yeaman, S. J. (2005). Diverging regulation of pyruvate dehydrogenase kinase isoform gene expression in cultured human muscle cells. *FEBS Journal*, *272*(12), 3004–3014.

Abreu, P., & Kowaltowski, A. J. (2020). Satellite cell self-renewal in endurance exercise is mediated by inhibition of mitochondrial oxygen consumption. *Journal of Cachexia, Sarcopenia and Muscle*, *11*(6), 1661-1676.

Acharya, S., Peters, A. M., Norton, A. S., Murdoch, G. K., & Hill, R. A. (2013). Change in Nox4 expression is accompanied by changes in myogenic marker expression in differentiating C2C12 myoblasts. *Pflugers Archiv European Journal of Physiology*, *465*(8), 1181–1196.

Adams, G. R., Caiozzo, V. J., Haddad, F., & Baldwin, K. M. (2002). Cellular and molecular responses to increased skeletal muscle loading after irradiation. *American Journal of Physiology - Cell Physiology*, *283*(4 52-4), 1182–1195.

Agaronyan, K., Morozov, Y. I., Anikin, M., & Temiakov, D. (2015). Replication-transcription switch in human mitochondria. *Science*, *347*(6221), 548–551.

Aguer, C., Gambarotta, D., Mailloux, R. J., Moffat, C., Dent, R., McPherson, R., & Harper, M.-E. (2011). Galactose Enhances Oxidative Metabolism and Reveals Mitochondrial Dysfunction in Human Primary Muscle Cells. *PLoS ONE*, *6*(12), e28536.

Al-Khalili, L., Chibalin, A. V., Kannisto, K., Zhang, B. B., Permert, J., Holman, G. D., Ehrenborg, E., Ding, V. D. H., Zierath, J. R., & Krook, A. (2003). Insulin action in cultured human skeletal muscle cells during differentiation: Assessment of cell surface GLUT4 and GLUT1 content. *Cellular and Molecular Life Sciences*, *60*(5), 991–998.

Al-Khalili, Lubna, de Castro Barbosa, T., Östling, J., Massart, J., Cuesta, P. G., Osler, M. E., Katayama, M., Nyström, A. C., Oscarsson, J., & Zierath, J. R. (2014). Proteasome inhibition in skeletal muscle cells unmasks metabolic derangements in type 2 diabetes. *American Journal of Physiology - Cell Physiology*, *307*(9), C774–C787.

Almeida, A., Bolaños, J. P., & Moncada, S. (2010). E3 ubiquitin ligase APC/C-Cdh1 accounts for the Warburg effect by linking glycolysis to cell proliferation. Proceedings of the National Academy of Sciences of the United States of America, *107*(2), 738–741.

Almeida, C. F., Fernandes, S. A., Ribeiro Junior, A. F., Keith Okamoto, O., & Vainzof, M. (2016). Muscle satellite cells: Exploring the basic biology to rule them. *Stem Cells International*, 1078686.

Alway, S. E., Mohamed, J. S., & Myers, M. J. (2017). Mitochondria initiate and regulate sarcopenia. *Exercise and Sport Sciences Reviews*, *45*(2), 58–69.

Anderson, K. A., Madsen, A. S., Olsen, C. A., & Hirschey, M. D. (2017). Metabolic control by sirtuins and other enzymes that sense NAD+, NADH, or their ratio. *Biochimica et Biophysica Acta – Bioenergetics*, *1858*(12), 991–998.

Aquilano, K., Vigilanza, P., Baldelli, S., Pagliei, B., Rotilio, G., & Ciriolo, M. R. (2010). Peroxisome proliferator-activated receptor γ co-activator 1 α (PGC-1α) and sirtuin 1 (SIRT1) reside in mitochondria: Possible direct function in mitochondrial biogenesis. *Journal of Biological Chemistry*, *285*(28), 21590–21599.

Ardite, E., Barbera, J. A., Roca, J., & Fernández-Checa, J. C. (2004). Glutathione depletion impairs myogenic differentiation of murine skeletal muscle C2C12 cells through sustained NF-κB activation. *American Journal of Pathology*, *165*(3), 719–728.

Asin-Cayuela, J., Schwend, T., Farge, G., & Gustafsson, C. M. (2005). The human mitochondrial transcription termination factor (mTERF) is fully active in vitro in the non-phosphorylated form. *Journal of Biological Chemistry*, *280*(27), 25499–25505.

Attwooll, C., Denchi, E. L., & Helin, K. (2004). The E2F family: Specific functions and overlapping interests. *EMBO Journal*, *23*(24), 4709–4716.

Atz, B. K., & Katz, B. (1961). The termination of the afferent nerve fibre in the muscle spindle of the frog. *Philosophical Transactions of the Royal Society of London. Series B, Biological Sciences*, *243*(703), 221–240.

Baar, K., Wende, A. R., Jones, T. E., Marison, M., Nolte, L. A., Chen, M., Kelly, D. P., & Holloszy, J. O. (2002). Adaptations of skeletal muscle to exercise: rapid increase in the transcriptional coactivator PGC-1. *The FASEB Journal*, *16*(14), 1879–1886.

Bach, D., Pich, S., Soriano, F. X., Vega, N., Baumgartner, B., Oriola, J., Daugaard, J. R., Lloberas, J., Camps, M., Zierath, J. R., Rabasa-Lhoret, R., Wallberg-Henriksson, H., Laville, M., Palacín, M., Vidal, H., Rivera, F., Brand, M., & Zorzano, A. (2003). Mitofusin-2 determines mitochondrial network architecture and mitochondrial metabolism: A novel regulatory mechanism altered in obesity. *Journal of Biological Chemistry*, *278*(19), 17190-

7.

Backes, S., & Herrmann, J. M. (2017). Protein translocation into the intermembrane space and matrix of mitochondria: Mechanisms and driving forces. *Frontiers in Molecular Biosciences*, *2017*(4), 83.

Backes, S., Hess, S., Boos, F., Woellhaf, M. W., Gödel, S., Jung, M., Mühlhaus, T., & Herrmann, J. M. (2018). Tom70 enhances mitochondrial preprotein import efficiency by binding to internal targeting sequences. *Journal of Cell Biology*, *217*(4), 1369–1382.

Baeza-Raja, B., & Muñoz-Cánoves, P. (2004). p38 MAPK-induced Nuclear Factor-κB Activity Is Required for Skeletal Muscle Differentiation: Role of Interleukin-6. *Molecular Biology of the Cell*, *15*(4), 2013–2026.

Bakkar, N., Wang, J., Ladner, K. J., Wang, H., Dahlman, J. M., Carathers, M., Acharyya, S., Rudnicki, M. A., Hollenbach, A. D., & Guttridge, D. C. (2008). IKK/NF-κB regulates skeletal myogenesis via a signaling switch to inhibit differentiation and promote mitochondrial biogenesis. *Journal of Cell Biology*, *180*(4), 787–802.

Balciunaite, E., Spektor, A., Lents, N. H., Cam, H., te Riele, H., Scime, A., Rudnicki, M. A., Young, R., & Dynlacht, B. D. (2005). Pocket Protein Complexes Are Recruited to Distinct Targets in Quiescent and Proliferating Cells. *Molecular and Cellular Biology*, *25*(18), 8166–8178.

Baldelli, S., Barbato, D. L., Tatulli, G., Aquilano, K., & Ciriolo, M. R. (2014). The role of nNOS and PGC-1α in skeletal muscle cells. *Journal of Cell Science*, *127*(22), 4813–4820.

Baracca, A., Solaini, G., Sgarbi, G., Lenaz, G., Baruzzi, A., Schapira, A. H. V., Martinuzzi, A., & Carelli, V. (2005). Severe impairment of complex I-driven adenosine triphosphate synthesis in leber hereditary optic neuropathy cybrids. *Archives of Neurology*, *62*(5), 730-6.

Barksdale, K. A., & Bijur, G. N. (2009). The basal flux of Akt in the mitochondria is mediated by heat shock protein 90. *Journal of Neurochemistry*, *108*(5), 1289–1299.

Barnum, K. J., & O'Connell, M. J. (2014). Cell cycle regulation by checkpoints. *Methods in Molecular Biology*, *1170*, 29–40.

Barshad, G., Marom, S., Cohen, T., & Mishmar, D. (2018). Mitochondrial DNA Transcription and Its Regulation: An Evolutionary Perspective. *Trends in Genetics*, *34*(9), 682–692.

Bassel-Duby, R., & Olson, E. N. (2006). Signaling pathways in skeletal muscle remodeling. *Annual Review of Biochemistry*, *75*, 19–37.

Beijersbeigen, R. L., Cariée, L., Kerkhoven, R. M., & Bernards, R. (1995). Regulation of the retinoblastoma protein-related p107 by G1 cyclin complexes. *Genes and Development*, *9*(11), 1340–1353.

Beijersbergen, R. L., Kerkhoven, R. M., Zhu, L., Carlée, L., Voorhoeve, P. M., & Bernards, R. (1994). E2F-4, a new member of the E2F gene family, has oncogenic activity and associates with p107 in vivo. *Genes and Development*, *8*(22), 2680–2690.

Belcastro, A. N., Shewchuk, L. D., & Raj, D. A. (1998). Exercise-induced muscle injury: A calpain hypothesis. *Molecular and Cellular Biochemistry*, *179*(1–2), 135–145.

Bell, J. A., Reed, M. A., Consitt, L. A., Martin, O. J., Haynie, K. R., Hulver, M. W., Muoio, D. M., & Dohm, G. L. (2010). Lipid partitioning, incomplete fatty acid oxidation, and insulin signal transduction in primary human muscle cells: Effects of severe obesity, fatty acid incubation, and fatty acid translocase/CD36 overexpression. *Journal of Clinical Endocrinology and Metabolism*, *95*(7), 3400–3410.

Bernet, J. D., Doles, J. D., Hall, J. K., Kelly Tanaka, K., Carter, T. A., & Olwin, B. B. (2014). P38 MAPK signaling underlies a cell-autonomous loss of stem cell self-renewal in skeletal muscle of aged mice. *Nature Medicine*, *20*(3), 265–271.

Bertoli, C., Skotheim, J. M., & De Bruin, R. A. M. (2013). Control of cell cycle transcription during G1 and S phases. *Nature Reviews Molecular Cell Biology*, *14*(8), 518–528.

Bhalla, K., Liu, W. J., Thompson, K., Anders, L., Devarakonda, S., Dewi, R., Buckley, S., Hwang, B. J., Polster, B., Dorsey, S. G., Sun, Y., Sicinski, P., & Girnun, G. D. (2014). Cyclin D1 represses gluconeogenesis via inhibition of the transcriptional coactivator PGC1α. *Diabetes*, *63*(10), 3266–3278.

Bhattacharya, D., & Scimè, A. (2020). Mitochondrial Function in Muscle Stem Cell Fates. *Frontiers in Cell and Developmental Biology*, *2020*(8), 480.

Bjornson, C. R. R., Cheung, T. H., Liu, L., Tripathi, P. V., Steeper, K. M., & Rando, T. A. (2012). Notch signaling is necessary to maintain quiescence in adult muscle stem cells. *Stem Cells*, *30*(2), 232-42.

Blaauw, B., & Reggiani, C. (2014). The role of satellite cells in muscle hypertrophy. *Journal of Muscle Research and Cell Motility*, *35*(1), 3–10.

Blanchet, E., Annicotte, J. S., Lagarrigue, S., Aguilar, V., Clapé, C., Chavey, C., Fritz, V., Casas, F., Apparailly, F., Auwerx, J., & Fajas, L. (2011). E2F transcription factor-1 regulates

oxidative metabolism. *Nature Cell Biology*, *13*(9), 1146–1154.

Boily, G., He, X. H., Pearce, B., Jardine, K., & McBurney, M. W. (2009). SirT1-null mice develop tumors at normal rates but are poorly protected by resveratrol. *Oncogene*, *28*(32), 2882-93.

Bollinger, L. M., Powell, J. J. S., Houmard, J. A., Witczak, C. A., & Brault, J. J. (2015). Skeletal muscle myotubes in severe obesity exhibit altered ubiquitin-proteasome and autophagic/lysosomal proteolytic flux. *Obesity*, *23*(6), 1185–1193.

Bordone, L., & Guarente, L. (2005). Calorie restriction, SIRT1 and metabolism: Understanding longevity. *Nature Reviews Molecular Cell Biology*, *6*(4), 298–305.

Borra, M. T., Smith, B. C., & Denu, J. M. (2005). Mechanism of human SIRT1 activation by resveratrol. *Journal of Biological Chemistry*, *280*(17), 17187–17195.

Bortoli, S., Renault, V., Mariage-Samson, R., Eveno, E., Auffray, C., Butler-Browne, G., & Piétu, G. (2005). Modifications in the myogenic program induced by in vivo and in vitro aging. *Gene*, *347*(1), 65–72.

Bouda, E., Stapon, A., & Garcia-Diaz, M. (2019). Mechanisms of mammalian mitochondrial transcription. In *Protein Science*, *28*(9), 1594-1605.

Bourlier, V., Saint-Laurent, C., Louche, K., Badin, P.-M., Thalamas, C., de Glisezinski, I., Langin, D., Sengenes, C., & Moro, C. (2013). Enhanced Glucose Metabolism Is Preserved in Cultured Primary Myotubes From Obese Donors in Response to Exercise Training. *The Journal of Clinical Endocrinology & Metabolism*, *98*(9), 3739–3747.

Boutant, M., & Cantó, C. (2014). SIRT1 metabolic actions: Integrating recent advances from mouse models. *Molecular Metabolism*, *3*(1), 5–18.

Boyle, K. E., Zheng, D., Anderson, E. J., Neufer, P. D., & Houmard, J. A. (2012). Mitochondrial lipid oxidation is impaired in cultured myotubes from obese humans. *International Journal of Obesity*, *36*(8), 1025–1031.

Brack, A. S., & Muñoz-Cánoves, P. (2016). The ins and outs of muscle stem cell aging. *Skeletal Muscle*, *18*(6), 1.

Brien, P., Pugazhendhi, D., Woodhouse, S., Oxley, D., & Pell, J. M. (2013). P38α MAPK regulates adult muscle stem cell fate by restricting progenitor proliferation during postnatal growth and repair. *Stem Cells*, *31*(8), 1597–1610.

Bröhl, D., Vasyutina, E., Czajkowski, M. T., Griger, J., Rassek, C., Rahn, H. P., Purfürst, B.,

Wende, H., & Birchmeier, C. (2012). Colonization of the Satellite Cell Niche by Skeletal Muscle Progenitor Cells Depends on Notch Signals. *Developmental Cell*, *23*(3), 469-81.

Brusco, J., & Haas, K. (2015). Interactions between mitochondria and the transcription factor myocyte enhancer factor 2 (MEF2) regulate neuronal structural and functional plasticity and metaplasticity. *Journal of Physiology*, *593*(16), 3471-81.

Bruusgaard, J. C., Johansen, I. B., Egner, I. M., Rana, Z. A., & Gundersen, K. (2010). Myonuclei acquired by overload exercise precede hypertrophy and are not lost on detraining. *Proceedings of the National Academy of Sciences of the United States of America*, *107*(34), 15111–15116.

Buas, M. F., & Kadesch, T. (2010). Regulation of skeletal myogenesis by Notch. *Experimental Cell Research*, *316*(18), 3028-33.

Buono, R., Vantaggiato, C., Pisa, V., Azzoni, E., Bassi, M. T., Brunelli, S., Sciorati, C., & Clementi, E. (2012). Nitric oxide sustains long-term skeletal muscle regeneration by regulating fate of satellite cells via signaling pathways requiring Vangl2 and cyclic GMP. *Stem Cells*, *30*(2), 197–209.

Burgomaster, K. A., Howarth, K. R., Phillips, S. M., Rakobowchuk, M., Macdonald, M. J., Mcgee, S. L., & Gibala, M. J. (2008). Similar metabolic adaptations during exercise after low volume sprint interval and traditional endurance training in humans. *Journal of Physiology*, *586*(1), 151–160.

Burkhart, D. L., & Sage, J. (2008). Cellular mechanisms of tumour suppression by the retinoblastoma gene. *Nature Reviews Cancer*, *8*(9), 671-82.

Bustin, S. A., Benes, V., Garson, J. A., Hellemans, J., Huggett, J., Kubista, M., Mueller, R., Nolan, T., Pfaffl, M. W., Shipley, G. L., Vandesompele, J., & Wittwer, C. T. (2009). The MIQE guidelines: Minimum information for publication of quantitative real-time PCR experiments. *Clin Chem*, *55*(4), 611-22.

Caito, S., Rajendrasozhan, S., Cook, S., Chung, S., Yao, H., Friedman, A. E., Brookes, P. S., & Rahman, I. (2010). SIRT1 is a redox-sensitive deacetylase that is post-translationally modified by oxidants and carbonyl stress. *The FASEB Journal*, *24*(9), 3145–3159.

Calvo, S. E., Julien, O., Clauser, K. R., Shen, H., Kamer, K. J., Wells, J. A., & Mootha, V. K. (2017). Comparative analysis of mitochondrial N-termini from mouse, human, and yeast. *Molecular and Cellular Proteomics*, *16*(4), 512-523.

Cam, H., Balciunaite, E., Blais, A., Spektor, A., Scarpulla, R. C., Young, R., Kluger, Y., & Dynlacht, B. D. (2004). A common set of gene regulatory networks links metabolism and growth inhibition. *Molecular Cell*, *16*(3), 399–411.

Cammarota, M., Paratcha, G., Bevilaqua, L. R. M., De Stein, M. L., Lopez, M., Pellegrino De Iraldi, A., Izquierdo, I., & Medina, J. H. (1999). Cyclic AMP-responsive element binding protein in brain mitochondria. *Journal of Neurochemistry*, *72*(6), 2272-7.

Cantini, G., Di Franco, A., Mannelli, M., Scimè, A., Maggi, M., & Luconi, M. (2020). The Role of Metabolic Changes in Shaping the Fate of Cancer-Associated Adipose Stem Cells. *Frontiers in Cell and Developmental Biology*, *8*, 1–11.

Cantó, C., & Auwerx, J. (2009). PGC-1α, SIRT1 and AMPK, an energy sensing network that controls energy expenditure. *Current Opinion in Lipidology*, *20*(2), 98-105.

Cantó, C., Houtkooper, R. H., Pirinen, E., Youn, D. Y., Oosterveer, M. H., Cen, Y., Fernandez-Marcos, P. J., Yamamoto, H., Andreux, P. A., Cettour-Rose, P., Gademann, K., Rinsch, C., Schoonjans, K., Sauve, A. A., & Auwerx, J. (2012). The NAD+ precursor nicotinamide riboside enhances oxidative metabolism and protects against high-fat diet-induced obesity. *Cell Metabolism*, *15*(6), 838–847.

Cantó, C., Jiang, L. Q., Deshmukh, A. S., Mataki, C., Coste, A., Lagouge, M., Zierath, J. R., & Auwerx, J. (2010). Interdependence of AMPK and SIRT1 for Metabolic Adaptation to Fasting and Exercise in Skeletal Muscle. *Cell Metabolism*, *11*(3), 213–219.

Cantó, C., Menzies, K. J., & Auwerx, J. (2015). NAD+ Metabolism and the Control of Energy Homeostasis: A Balancing Act between Mitochondria and the Nucleus. *Cell Metabolism*, *22*(1), 31–53.

Cao, S., Li, B., Yi, X., Chang, B., Zhu, B., Lian, Z., Zhang, Z., Zhao, G., Liu, H., & Zhang, H. (2012). Effects of Exercise on AMPK Signaling and Downstream Components to PI3K in Rat with Type 2 Diabetes. *PLoS ONE*, *7*(12).

Cao, Y., Zhao, Z., Gruszczynska-Biegala, J., & Zolkiewska, A. (2003). Role of Metalloprotease Disintegrin ADAM12 in Determination of Quiescent Reserve Cells during Myogenic Differentiation In Vitro. *Molecular and Cellular Biology*, *23*(19), 6725-38.

Carelli, V., & Chan, D. C. (2014). Mitochondrial DNA: Impacting central and peripheral nervous systems. *Urology*, *84*(6), 1126–1142.

Cartee, G. D., Hepple, R. T., Bamman, M. M., & Zierath, J. R. (2017). Exercise Promotes

Healthy Aging of Skeletal Muscle Primary versus Secondary Aging: Setting the Stage. *Cell Metabolism*, *23*(6), 1034–1047.

Cartoni, R., Léger, B., Hock, M. B., Praz, M., Crettenand, A., Pich, S., Ziltener, J. L., Luthi, F., Dériaz, O., Zorzano, A., Gobelet, C., Kralli, A., & Russell, A. P. (2005). Mitofusins 1/2 and ERRα expression are increased in human skeletal muscle after physical exercise. *Journal of Physiology*, *567*(1), 349–358.

Carujo, S., Estanyol, J. M., Ejarque, A., Agell, N., Bachs, O., & Pujol, M. J. (2006). Glyceraldehyde 3-phosphate dehydrogenase is a SET-binding protein and regulates cyclin B-cdk1 activity. *Oncogene*, *25*(29), 4033-42.

Casas, F., Domenjoud, L., Rochard, P., Hatier, R., Rodier, A., Daury, L., Bianchi, A., Kremarik-Bouillaud, P., Becuwe, P., Keller, J. M., Schohn, H., Wrutniak-Cabello, C., Cabello, G., & Dauça, M. (2000). A 45 kDa protein related to PPARγ2, induced by peroxisome proliferators, is located in the mitochondrial matrix. *FEBS Letters*, *478*(1-2), 4-8.

Castaño, E., Kleyner, Y., & Dynlacht, B. D. (1998). Dual Cyclin-Binding Domains Are Required for p107 To Function as a Kinase Inhibitor. *Molecular and Cellular Biology*, *18*(9), 5380–5391.

Catani, M. V., Savini, I., Duranti, G., Caporossi, D., Ceci, R., Sabatini, S., & Avigliano, L. (2004). Nuclear factor κB and activating protein 1 are involved in differentiation-related resistance to oxidative stress in skeletal muscle cells. *Free Radical Biology and Medicine*, *37*(7), 1024-36.

Cerletti, M., Jang, Y. C., Finley, L. W. S., Haigis, M. C., & Wagers, A. J. (2012). Short-term calorie restriction enhances skeletal muscle stem cell function. *Cell Stem Cell*, *10*(5), 515-9.

Cermak, N. M., Snijders, T., McKay, B. R., Parise, G., Verdijk, L. B., Tarnopolsky, M. A., Gibala, M. J., & Van Loon, L. J. C. (2013). Eccentric exercise increases satellite cell content in type II muscle fibers. *Medicine and Science in Sports and Exercise*, *45*(2), 230–237.

Cerutti, R., Pirinen, E., Lamperti, C., Marchet, S., Sauve, A. A., Li, W., Leoni, V., Schon, E. A., Dantzer, F., Auwerx, J., Viscomi, C., & Zeviani, M. (2014). NAD+-dependent activation of Sirt1 corrects the phenotype in a mouse model of mitochondrial disease. *Cell Metabolism*, *19*(6), 1042–1049.

Chabi, B., Adhihetty, P. J., O'Leary, M. F. N., Menzies, K. J., & Hood, D. A. (2009).

Relationship between Sirt1 expression and mitochondrial proteins during conditions of chronic muscle use and disuse. *Journal of Applied Physiology*, *107*(6), 1730–1735.

Chacinska, A., Koehler, C. M., Milenkovic, D., Lithgow, T., & Pfanner, N. (2009). Importing Mitochondrial Proteins: Machineries and Mechanisms. *Cell*, *138*(4), 628-44.

Chakkalakal, J. V., Christensen, J., Xiang, W., Tierney, M. T., Boscolo, F. S., Sacco, A., & Brack, A. S. (2014). Early forming label-retaining muscle stem cells require p27kip1 for maintenance of the primitive state. *Development (Cambridge)*, *141*(8), 1649–1659.

Chakkalakal, J. V., Jones, K. M., Basson, M. A., & Brack, A. S. (2012). The aged niche disrupts muscle stem cell quiescence. *Nature*, *490*(7420), 355–360.

Chandel, N. S. (2018). Mitochondria: Back to the future. In *Nature Reviews Molecular Cell Biology*,*19*(2), 76.

Chang, N. C., Sincennes, M. C., Chevalier, F. P., Brun, C. E., Lacaria, M., Segalés, J., Muñoz-Cánoves, P., Ming, H., & Rudnicki, M. A. (2018). The Dystrophin Glycoprotein Complex Regulates the Epigenetic Activation of Muscle Stem Cell Commitment. *Cell Stem Cell*, *22*(5), 755-768.e6.

Chatterjee, A., Seyfferth, J., Lucci, J., Gilsbach, R., Preissl, S., Böttinger, L., Mårtensson, C. U., Panhale, A., Stehle, T., Kretz, O., Sahyoun, A. H., Avilov, S., Eimer, S., Hein, L., Pfanner, N., Becker, T., & Akhtar, A. (2016). MOF Acetyl Transferase Regulates Transcription and Respiration in Mitochondria. *Cell*, *167*(3), P722-738.

Chen, C. R., Kang, Y., Siegel, P. M., & Massagué, J. (2002). E2F4/5 and p107 as Smad cofactors linking the TGFβ receptor to c-myc repression. *Cell*, *110*(1), 19–32.

Chen, Danian, Livne-bar, I., Vanderluit, J. L., Slack, R. S., Agochiya, M., & Bremner, R. (2004b). Cell-specific effects of RB or RB/p107 loss on retinal development implicate an intrinsically death-resistant cell-of-origin in retinoblastoma. *Cancer Cell*, *5*(6), 539–551.

Chen, Danica, Bruno, J., Easlon, E., Lin, S. J., Cheng, H. L., Alt, F. W., & Guarente, L. (2008). Tissue-specific regulation of SIRT1 by calorie restriction. *Genes and Development*, *22*(13), 1753–1757.

Chen, H., Vermulst, M., Wang, Y. E., Chomyn, A., Prolla, T. A., McCaffery, J. M., & Chan, D. C. (2010). Mitochondrial fusion is required for mtdna stability in skeletal muscle and tolerance of mtDNA mutations. *Cell*, *141*(2), 280–289.

Chen, J. Q., Eshete, M., Alworth, W. L., & Yager, J. D. (2004a). Binding of MCF-7 cell

mitochondrial proteins and recombinant human estrogen receptors α and β to human mitochondrial DNA estrogen response elements. *Journal of Cellular Biochemistry*, *286*(6), E1011-22.

Chen, J. Q., Eshete, M., Alworth, W. L., & Yager, J. D. (2004b). Binding of MCF-7 cell mitochondrial proteins and recombinant human estrogen receptors α and β to human mitochondrial DNA estrogen response elements. *Journal of Cellular Biochemistry*, *93*(2), 358-73.

Chen, W., Datzkiw, D., & Rudnicki, M. A. (2020). Satellite cells in ageing: Use it or lose it. *Open Biology*, *10*(5), 200048.

Chen, Y., Liu, Y., & Dorn, G. W. (2011). Mitochondrial fusion is essential for organelle function and cardiac homeostasis. *Circulation Research*, *109*(12), 1327-31.

Chinnam, M., & Goodrich, D. W. (2011). RB1, Development, and Cancer. *Current Topics in Developmental Biology*, *94*, 129–169.

Chinnery, P. F. (2015). Mitochondrial disease in adults: what's old and what's new? *EMBO Molecular Medicine*, *7*(12), 1503–1512.

Chittenden, T., Livingston, D. M., & DeCaprio, J. A. (1993). Cell cycle analysis of E2F in primary human T cells reveals novel E2F complexes and biochemically distinct forms of free E2F. *Molecular and Cellular Biology*, *13*(7), 3975-83.

Chouchani, E. T., Pell, V. R., Gaude, E., Aksentijević, D., Sundier, S. Y., Robb, E. L., Logan, A., Nadtochiy, S. M., Ord, E. N. J., Smith, A. C., Eyassu, F., Shirley, R., Hu, C. H., Dare, A. J., James, A. M., Rogatti, S., Hartley, R. C., Eaton, S., Costa, A. S. H., … Murphy, M. P. (2014). Ischaemic accumulation of succinate controls reperfusion injury through mitochondrial ROS. *Nature*, *515*(7527), 431–435.

Ciavarra, G., & Zacksenhaus, E. (2010). Rescue of myogenic defects in Rb-deficient cells by inhibition of autophagy or by hypoxia-induced glycolytic shift. *Journal of Cell Biology*, *191*(2), 291–301.

Cisterna, B., Giagnacovo, M., Costanzo, M., Fattoretti, P., Zancanaro, C., Pellicciari, C., & Malatesta, M. (2016). Adapted physical exercise enhances activation and differentiation potential of satellite cells in the skeletal muscle of old mice. *Journal of Anatomy*, *228*(5), 771–783.

Classon, M., & Dyson, N. (2001). p107 and p130: Versatile proteins with interesting pockets.

Experimental Cell Research, *264*(1), 135–147.

Claudio, P. P., Tonini, T., & Giordano, A. (2002). The retinoblastoma family: Twins or distant cousins? *Genome Biology*, *3*(9), 1–9.

Clayton, D. A. (2000). Transcription and replication of mitochondrial DNA. *Human Reproduction*, *15*(2), 11–17.

Cliff, T. S., & Dalton, S. (2017). Metabolic switching and cell fate decisions: implications for pluripotency, reprogramming and development. *Current Opinion in Genetics and Development*, *46*, 44–49.

Cobrinik, D. (2005). Pocket proteins and cell cycle control. *Oncogene*, *24*(17), 2796–2809.

Cobrinik, D., Whyte, P., Peeper, D. S., Jacks, T., & Weinberg, R. A. (1993). Cell cycle-specific association of E2F with the p130 E1A-binding protein. *Genes and Development*, *7*(12A), 2392-404.

Coffey, V. G., & Hawley, J. A. (2007). The Molecular Bases of Training Adaptation. *Sports Med* , *37*(9), 737-763.

Cogswell, P. C., Kashatus, D. F., Keifer, J. A., Guttridge, D. C., Reuther, J. Y., Bristow, C., Roy, S., Nicholson, D. W., & Baldwin Jr., A. S. (2003). NF-kappa B and I kappa B alpha are found in the mitochondria. Evidence for regulation of mitochondrial gene expression by NF-kappa B. *J Biol Chem*, *278*(5), 2963-8.

Coller, H. A., Sang, L., & Roberts, J. M. (2006). A new description of cellular quiescence. *PLoS Biology*, *4*(3), 0329–0349.

Colombo, S. L., Palacios-Callender, M., Frakich, N., Carcamo, S., Kovacs, I., Tudzarova., Moncada, S. (2011). Molecular basis for the differential use of glucose and glutamine in cell proliferation as revealed by synchronized HeLa cells. *Proc Natl Acad Sci U S A*, . *108*(52), 21069-74.

Conboy, I. M., & Rando, T. A. (2002). The regulation of Notch signaling controls satellite cell activation and cell fate determination in postnatal myogenesis. *Developmental Cell*, *3*(3), 397–409.

Conejo, R., Valverde, A. M., Benito, M., & Lorenzo, M. (2001). Insulin produces myogenesis in C2C12 myoblasts by induction of NF-κB and downregulation of AP-1 activities. *Journal of Cellular Physiology*, *186*(1), 82–94.

Consitt, L. A., Bell, J. A., Koves, T. R., Muoio, D. M., Hulver, M. W., Haynie, K. R., Dohm, G.

L., & Houmard, J. A. (2010). Peroxisome proliferator-activated receptor-γ coactivator-1α overexpression increases lipid oxidation in myocytes from extremely obese individuals. *Diabetes*, *59*(6), 1407–1415.

Cosgrove, B. D., Gilbert, P. M., Porpiglia, E., Mourkioti, F., Lee, S. P., Corbel, S. Y., Llewellyn, M. E., Delp, S. L., & Blau, H. M. (2014). Rejuvenation of the muscle stem cell population restores strength to injured aged muscles. *Nature Medicine*, *20*(3), 255–264.

Cotney, J., & Shadel, G. S. (2006). Evidence for an early gene duplication event in the evolution of the mitochondrial transcription factor B family and maintenance of rRNA methyltransferase activity in human mtTFB1 and mtTFB2. *Journal of Molecular Evolution*, *63*(5), 707–717.

Csapo, R., Gumpenberger, M., & Wessner, B. (2020). Skeletal Muscle Extracellular Matrix – What Do We Know About Its Composition, Regulation, and Physiological Roles? A Narrative Review. *Frontiers in Physiology*, *19*(11), 253.

D'Souza, A. R., & Minczuk, M. (2018). Mitochondrial transcription and translation: Overview. *Essays in Biochemistry*, *62*(3), 309–320.

Da Veiga Moreira, J., Peres, S., Steyaert, J. M., Bigan, E., Paulevé, L., Nogueira, M. L., & Schwartz, L. (2015). Cell cycle progression is regulated by intertwined redox oscillators. *Theoretical Biology and Medical Modelling*, *29*(12), 10.

Dahlman, J. M., Bakkar, N., He, W., & Guttridge, D. C. (2010). NF-κB functions in stromal fibroblasts to regulate early postnatal muscle development. *Journal of Biological Chemistry*, *285*(8), 5479–5487.

Dairaghi, D. J., Shadel, G. S., & Clayton, D. A. (1995). Addition of a 29 residue carboxyl-terminal tail converts a simple hmg box-containing protein into a transcriptional activator. *Journal of Molecular Biology*, *249*(1), 11–28.

Dali-Youcef, N., Mataki, C., Coste, A., Messaddeq, N., Giroud, S., Blanc, S., Koehl, C., Champy, M. F., Chambon, P., Fajas, L., Metzger, D., Schoonjans, K., & Auwerx, J. (2007). Adipose tissue-specific inactivation of the retinoblastoma protein protects against diabesity because of increased energy expenditure. *Proc Natl Acad Sci U S A*, *104*(25), 10703-8.

De Palma, C., Falcone, S., Pisoni, S., Cipolat, S., Panzeri, C., Pambianco, S., Pisconti, A., Allevi, R., Bassi, M. T., Cossu, G., Pozzan, T., Moncada, S., Scorrano, L., Brunelli, S., & Clementi, E. (2010). Nitric oxide inhibition of Drp1-mediated mitochondrial fission is

critical for myogenic differentiation. *Cell Death and Differentiation*, *17*(11), 1684-96.

De Sousa, M., Porras, D. P., Perry, C. G. R., Seale, P., & Scimè, A. (2014). p107 Is a Crucial Regulator for Determining the Adipocyte Lineage Fate Choices of Stem Cells. *Stem Cells*, *32*(5), 1323–1336.

De Zio, D., Cianfanelli, V., & Cecconi, F. (2013). New insights into the link between DNA damage and apoptosis. *Antioxidants and Redox Signaling*, *19*(6).

DeBerardinis, R. J., Lum, J. J., Hatzivassiliou, G., & Thompson, C. B. (2008). The Biology of Cancer: Metabolic Reprogramming Fuels Cell Growth and Proliferation. *Cell Metabolism*, *7*(1), 11–20.

Dell'Orso, S., Juan, A. H., Ko, K. D., Naz, F., Perovanovic, J., Gutierrez-Cruz, G., Feng, X., & Sartorelli, V. (2019). Single cell analysis of adult mouse skeletal muscle stem cells in homeostatic and regenerative conditions. *Development (Cambridge)*, *146*(12), 174177.

Demonacos, C., Tsawdaroglou, N. C., Djordjevic-Markovic, R., Papalopoulou, M., Galanopoulos, V., Papadogeorgaki, S., & Sekeris, C. E. (1993). Import of the glucocorticoid receptor into rat liver mitochondria in vivo and in vitro. *Journal of Steroid Biochemistry and Molecular Biology*, *46*(3), 401-13.

de Padua, M. C., Delodi, G., Vučetić, M., Durivault, J., Vial, V., Bayer, P., Noleto, G. R., Mazure, N. M., Ždralević, M., & Pouysségur, J. (2017). Disrupting glucose-6-phosphate isomerase fully suppresses the "Warburg effect" and activates OXPHOS with minimal impact on tumor growth except in hypoxia. *Oncotarget*, *8*(50), 87623–87637.

Díaz-Vegas, A., Eisner, V., & Jaimovich, E. (2019). Skeletal muscle excitation-metabolism coupling. *Archives of Biochemistry and Biophysics*, *664*, 89–94.

Dinulovic, I., Furrer, R., Beer, M., Ferry, A., Cardel, B., & Handschin, C. (2016). Muscle PGC-1α modulates satellite cell number and proliferation by remodeling the stem cell niche. *Skeletal Muscle*, *6*(1), 39.

Doughan, A. K., Harrison, D. G., & Dikalov, S. I. (2008). Molecular mechanisms of angiotensin II-mediated mitochondrial dysfunction: Linking mitochondrial oxidative damage and vascular endothelial dysfunction. *Circulation Research*, *102*(4), 488–496.

Dumont, N. A., Bentzinger, C. F., Sincennes, M. C., & Rudnicki, M. A. (2015a). Satellite cells and skeletal muscle regeneration. *Comprehensive Physiology*, *5*(3), 1027-59.

Dumont, N. A., Wang, Y. X., Maltzahn, J. von, Pasut, A., Bentzinger, C. F., Brun, C. E., &

Rudnicki, M. A. (2015b). Dystrophin expression in muscle stem cells regulates their polarity and asymmetric division. *Nature Medicine*, *21*(12), 1455–1464.

Dunaief, J. L., Strober, B. E., Guha, S., Khavari, P. A., Ålin, K., Luban, J., Begemann, M., Crabtree, G. R., & Goff, S. P. (1994). The retinoblastoma protein and BRG1 form a complex and cooperate to induce cell cycle arrest. *Cell*, *79*(1), 119–130.

Eales, K. L., Hollinshead, K. E. R., & Tennant, D. A. (2016). Hypoxia and metabolic adaptation of cancer cells. *Oncogenesis*, 5(1), e190.

Enríquez, J. A., Fernández-Silva, P., Garrido-Pérez, N., López-Pérez, M. J., Pérez-Martos, A., & Montoya, J. (1999). Direct Regulation of Mitochondrial RNA Synthesis by Thyroid Hormone. *Molecular and Cellular Biology*, *19*(1), 657-70.

Ewen, M. E., Faha, B., Harlow, E., & Livingston, D. M. (1992). Interaction of p107 with cyclin A independent of complex formation with viral oncoproteins. *Science*, *255*(5040), 85–87.

Faha, B., Ewen, M. E., Tsai, L.-H., Livingston, D. M., & Harlow, E. (1992). Interaction between human cyclin A and adenovirus E1A-associated p107 protein. *Science*, *255*(5040), 87–91.

Fajas, L. (2013). Re-thinking cell cycle regulators: The cross-talk with metabolism. *Frontiers in Oncology*, *24*(3), 4.

Falkenberg, M., Gaspari, M., Rantanen, A., Trifunovic, A., Larsson, N. G., & Gustafsson, C. M. (2002). Mitochondrial transcription factors B1 and B2 activate transcription of human mtDNA. *Nature Genetics*, *31*(3), 289–294.

Farge, G. É. R., & Falkenberg, M. (2019). Organization of DNA in mammalian mitochondria. *International Journal of Molecular Sciences*, *20*(11), 1–14.

Farup, J., Rahbek, S. K., Riis, S., Vendelbo, M. H., De Paoli, F., & Vissing, K. (2014). Influence of exercise contraction mode and protein supplementation on human skeletal muscle satellite cell content and muscle fiber growth. *Journal of Applied Physiology*, *117*(8), 898–909.

Ferreira, R., Magnaghi-Jaulin, L., Robin, P., Harel-Bellan, A., & Trouche, D. (1998). The three members of the pocket proteins family share the ability to repress E2F activity through recruitment of a histone deacetylase. *Proceedings of the National Academy of Sciences of the United States of America*, *95*(18), 10493–10498.

Ferreira, R., Naguibneva, I., Pritchard, L. L., Ait-Si-Ali, S., & Harel-Bellan, A. (2001). The Rb/chromatin connection and epigenetic control: Opinion. *Oncogene*, *20*(3), 3128–3133.

Fischer, M., & Müller, G. A. (2017). Cell cycle transcription control: DREAM/MuvB and RB-E2F complexes. *Critical Reviews in Biochemistry and Molecular Biology*, *52*(6), 638–662.

Fisher-Wellman, K. H., Lin, C. Te, Ryan, T. E., Reese, L. R., Gilliam, L. A. A., Cathey, B. L., Lark, D. S., Smith, C. D., Muoio, D. M., & Neufer, P. D. (2015). Pyruvate dehydrogenase complex and nicotinamide nucleotide transhydrogenase constitute an energy-consuming redox circuit. *Biochemical Journal*. *467*(2), 271-80.

Flück, M., & Hoppeler, H. (2003). Molecular basis of skeletal muscle plasticity--from gene to form and function. *Reviews of physiology, biochemistry and pharmacology*, *146*, 159–216.

Folmes, C. D. L., Dzeja, P. P., Nelson, T. J., & Terzic, A. (2012). Metabolic plasticity in stem cell homeostasis and differentiation. *Cell Stem Cell*, *11*(5), 596–606.

Folmes, C. D. L., Nelson, T. J., Martinez-Fernandez, A., Arrell, D. K., Lindor, J. Z., Dzeja, P. P., Ikeda, Y., Perez-Terzic, C., & Terzic, A. (2011). Somatic oxidative bioenergetics transitions into pluripotency-dependent glycolysis to facilitate nuclear reprogramming. *Cell Metabolism*, *14*(2), 264–271.

Forristal, C., Henley, S. A., MacDonald, J. I., Bush, J. R., Ort, C., Passos, D. T., Talluri, S., Ishak, C. A., Thwaites, M. J., Norley, C. J., Litovchick, L., DeCaprio, J. A., DiMattia, G., Holdsworth, D. W., Beier, F., & Dick, F. A. (2014). Loss of the Mammalian DREAM Complex Deregulates Chondrocyte Proliferation. *Molecular and Cellular Biology*, *34*(12), 2221–2234.

Foster, D. A., Yellen, P., Xu, L., & Saqcena, M. (2010). Regulation of G1 cell cycle progression: Distinguishing the restriction point from a nutrient-sensing cell growth checkpoint(s). *Genes and Cancer*, *1*(11), 1124–1131.

Frier, B. C., Hancock, C. R., Little, J. P., Fillmore, N., Bliss, T. A., Thomson, D. M., Wan, Z., & Wright, D. C. (2011). Reductions in RIP140 are not required for exercise- and AICAR-mediated increases in skeletal muscle mitochondrial content. *Journal of Applied Physiology*, *111*(3), 688–695.

Fry, C. S., Lee, J. D., Jackson, J. R., Kirby, T. J., Stasko, S. A., Liu, H., Dupont-Versteegden, E. E., McCarthy, J. J., & Peterson, C. A. (2014a). Regulation of the muscle fiber microenvironment by activated satellite cells during hypertrophy. *28*(4), 1654-65.

Fry, C. S., Noehren, B., Mula, J., Ubele, M. F., Westgate, P. M., Kern, P. A., & Peterson, C. A. (2014b). Fibre type-specific satellite cell response to aerobic training in sedentary adults.

Journal of Physiology, *592*(12), 2625–2635.

Fujimaki, S., Hidaka, R., Asashima, M., Takemasa, T., & Kuwabara, T. (2014). Wnt protein-mediated satellite cell conversion in adult and aged mice following voluntary wheel running. *Journal of Biological Chemistry*, *289*(11), 7399–7412.

Fujimaki, S., Machida, M., Wakabayashi, T., Asashima, M., Takemasa, T., & Kuwabara, T. (2016). Functional overload enhances satellite cell properties in skeletal muscle. *Stem Cells International*, *2016*, 7619418.

Fukada, S., Uezumi, A., Ikemoto, M., Masuda, S., Segawa, M., Tanimura, N., Yamamoto, H., Miyagoe-Suzuki, Y., & Takeda, S. (2007). Molecular Signature of Quiescent Satellite Cells in Adult Skeletal Muscle. *Stem Cells*, *25*(10), 2448–2459.

Fulco, M., Cen, Y., Zhao, P., Hoffman, E. P., McBurney, M. W., Sauve, A. A., & Sartorelli, V. (2008). Glucose Restriction Inhibits Skeletal Myoblast Differentiation by Activating SIRT1 through AMPK-Mediated Regulation of Nampt. *Developmental Cell*, *14*(5), 661–673.

Fulco, M., Schiltz, R. L., Iezzi, S., King, M. T., Zhao, P., Kashiwaya, Y., Hoffman, E., Veech, R. L., & Sartorelli, V. (2003). Sir2 regulates skeletal muscle differentiation as a potential sensor of the redox state. *Molecular Cell*, *12*(1), 51–62.

García-Prat, L., Martínez-Vicente, M., & Muñoz-Cánoves, P. (2016a). Methods for mitochondria and mitophagy flux analyses in stem cells of resting and regenerating skeletal muscle. *Methods in Molecular Biology*, *1460*, 223–240.

García-Prat, L., Martínez-Vicente, M., Perdiguero, E., Ortet, L., Rodríguez-Ubreva, J., Rebollo, E., Ruiz-Bonilla, V., Gutarra, S., Ballestar, E., Serrano, A. L., Sandri, M., & Muñoz-Cánoves, P. (2016b). Autophagy maintains stemness by preventing senescence. *Nature*, *529*(7584), 37–42.

Garriga, J., Jayaraman, A. L., Limón, A., Jayadeva, G., Sotillo, E., Truongcao, M., Patsialou, A., Wadzinski, B. E., & Graña, X. (2004). A dynamic equilibrium between CDKs and PP2A modulates phosphorylation of pRB, p107 and p130. *Cell Cycle*, *3*(10), 1320–1330.

Garriga, J., Limón, A., Mayol, X., Rane, S. G., Albrecht, J. H., Reddy, E. P., Andrés, V., & Graña, X. (1998). Differential regulation of the retinoblastoma family of proteins during cell proliferation and differentiation. *Biochemical Journal*, *333*(3), 645–654.

Gaspari, M., Larsson, N. G., & Gustafsson, C. M. (2004). The transcription machinery in mammalian mitochondria. *Biochimica et Biophysica Acta - Bioenergetics*, *1659*(2–3), 148–

152.

Gerace, E., & Moazed, D. (2015). Affinity Pull-Down of Proteins Using Anti-FLAG M2 Agarose Beads. *Methods in Enzymology*, *2015*(559), 99-110.

Gerhart-Hines, Z., Rodgers, J. T., Bare, O., Lerin, C., Kim, S. H., Mostoslavsky, R., Alt, F. W., Wu, Z., & Puigserver, P. (2007). Metabolic control of muscle mitochondrial function and fatty acid oxidation through SIRT1/PGC-1α. *EMBO Journal*, *26*(7), 1913–1923.

Ghisays, F., Brace, C. S., Yackly, S. M., Kwon, H. J., Kathryn, F., Kashentseva, E., Dimitriev, I. P., Curiel, D. T., & Imai, S. (2016). The N-terminal Domain of SIRT1 Is a Positive Regulator of Endogenous SIRT1-dependent Deacetylation and Transcriptional Outputs. *Cell Rep*, *10*(10), 1665–1673.

Ghosh-Choudhary, S., Liu, J., & Finkel, T. (2020). Metabolic Regulation of Cell Fate and Function. *Trends in Cell Biology*, *30*(3), 201-212.

Giacinti, C., & Giordano, A. (2006). RB and cell cycle progression. *Oncogene*, 25, 5220–5227.

Gidlund, E. K., Ydfors, M., Appel, S., Rundqvist, H., Sundberg, C. J., & Norrbom, J. (2015). Rapidly elevated levels of PGC-1α-b protein in human skeletal muscle after exercise: Exploring regulatory factors in a randomized controlled trial. *Journal of Applied Physiology*, *119*(4), 374–384.

Goh, Q., & Millay, D. P. (2017). Requirement of myomaker-mediated stem cell fusion for skeletal muscle hypertrophy. *ELife*, *10*(6), e20007.

Goh, Q., Song, T., Petrany, M. J., Cramer, A. A., Sun, C., Sadayappan, S., Lee, S. J., & Millay, D. P. (2019). Myonuclear accretion is a determinant of exercise-induced remodeling in skeletal muscle. *ELife*, *23*(8), e44876.

Gopinath, S. D., Webb, A. E., Brunet, A., & Rando, T. A. (2014). FOXO3 promotes quiescence in adult muscle stem cells during the process of self-renewal. *Stem Cell Reports*, *2*(4), 414-26.

Gorbsky, G. J. (2015). The spindle checkpoint and chromosome segregation in meiosis. *FEBS Journal*, *282*(13), 2471-87.

Gorman, G. S., Chinnery, P. F., DiMauro, S., Hirano, M., Koga, Y., McFarland, R., Suomalainen, A., Thorburn, D. R., Zeviani, M., & Turnbull, D. M. (2016). Mitochondrial diseases. *Nature Reviews Disease Primers*, *20*(2), 16080.

Green, H. J., Helyar, R., Ball-Burnett, M., Kowalchuk, N., Symon, S., & Farrance, B. (1992).

Metabolic adaptations to training precede changes in muscle mitochondrial capacity. *Journal of Applied Physiology*, *72*(2), 484–491.

Grounds, M. D., Garrett, K. L., Lai, M. C., Wright, W. E., & Beilharz, M. W. (1992). Identification of skeletal muscle precursor cells in vivo by use of MyoD1 and myogenin probes. *Cell & Tissue Research*, *267*(1), 99–104.

Guardiola, O., Andolfi, G., Tirone, M., Iavarone, F., Brunelli, S., & Minchiotti, G. (2017). Induction of acute skeletal muscle regeneration by cardiotoxin injection. *Journal of Visualized Experiments*, *2017*(119), 54515.

Guarente, L. (2000). Sir2 links chromatin silencing, metabolism, and aging. *Genes and Development*, *14*(9), 1021–1026.

Guerci, A., Lahoute, C., Hébrard, S., Collard, L., Graindorge, D., Favier, M., Cagnard, N., Batonnet-Pichon, S., Précigout, G., Garcia, L., Tuil, D., Daegelen, D., & Sotiropoulos, A. (2012). Srf-dependent paracrine signals produced by myofibers control satellite cell-mediated skeletal muscle hypertrophy. *Cell Metabolism*, *15*(1), 25-37.

Guiley, K. Z., Liban, T. J., Felthousen, J. G., Ramanan, P., Litovchick, L., & Rubin, S. M. (2015). Structural mechanisms of DREAM complex assembly and regulation. *Genes and Development*, *29*(9), 961–974.

Guja, K. E., & Garcia-Diaz, M. (2012). Hitting the brakes: Termination of mitochondrial transcription. *Biochimica et Biophysica Acta - Gene Regulatory Mechanisms*, *1819*(9–10), 939–947.

Gundersen, K. (2011). Excitation-transcription coupling in skeletal muscle: The molecular pathways of exercise. *Biological Reviews*, *86*(3), 564–600.

Gureev, A. P., Shaforostova, E. A., & Popov, V. N. (2019). Regulation of mitochondrial biogenesis as a way for active longevity: Interaction between the Nrf2 and PGC-1α signaling pathways. *Frontiers in Genetics*, *10*, 1–12.

Gustafsson, C. M., Falkenberg, M., & Larsson, N. G. (2016). Maintenance and Expression of Mammalian Mitochondrial DNA. *Annual Review of Biochemistry*, *85*, 133–160.

Guttridge, D. C., Mayo, M. W., Madrid, L. V., Wang, C. Y., & Baldwin, J. (2000). NF-κB-induced loss of MyoD messenger RNA: Possible role in muscle decay and cachexia. *Science*, *289*(5488), 2363–2365.

Gwinn, D. M., Shackelford, D. B., Egan, D. F., Mihaylova, M. M., Mery, A., Vasquez, D. S.,

Turk, B. E., & Shaw, R. J. (2008). AMPK Phosphorylation of Raptor Mediates a Metabolic Checkpoint. *Molecular Cell*, *30*(2), 214-26.

Handschin, C., & Spiegelman, B. M. (2006). Peroxisome proliferator-activated receptor γ coactivator 1 coactivators, energy homeostasis, and metabolism. *Endocrine Reviews*, *27*(7), 728–735.

Hannon, G. J., Demetrick, D., & Beach, D. (1993). Isolation of the Rb-related p130 through its interaction with CDK2 and cyclins. *Genes and Development*, *7*(12A), 2378-91.

Haralampieva, D., Salemi, S., Dinulovic, I., Sulser, T., Ametamey, S. M., Handschin, C., & Eberli, D. (2017). Human muscle precursor cells overexpressing PGC-1α enhance early skeletal muscle tissue formation. *Cell Transplantation*, *26*(6), 1103–1114.

Harrison, M. M., Ceol, C. J., Lu, X., & Horvitz, H. R. (2006). Some C. elegans class B synthetic multivulva proteins encode a conserved LIN-35 Rb-containing complex distinct from a NuRD-like complex. *Proceedings of the National Academy of Sciences of the United States of America*, *103*(45), 16782–16787.

Heiden, M. G. Vander, Cantley, L. C., Thompson, C. B., Mammalian, P., Exhibit, C., & Metabolism, A. (2009). Understanding the Warburg Effect : Cell Proliferation. *Science*, *324*(5930), 1029-33.

Hellsten, Y., Nielsen, J. J., Lykkesfeldt, J., Bruhn, M., Silveira, L., Pilegaard, H., & Bangsbo, J. (2007). Antioxidant supplementation enhances the exercise-induced increase in mitochondrial uncoupling protein 3 and endothelial nitric oxide synthase mRNA content in human skeletal muscle. *Free Radical Biology and Medicine*, *43*(3), 353–361.

Henley, S. A., & Dick, F. A. (2012). The retinoblastoma family of proteins and their regulatory functions in the mammalian cell division cycle. *Cell division*, *7*(1), 10.

Henriksen, T. I., Wigge, L. V., Nielsen, J., Pedersen, B. K., Sandri, M., & Scheele, C. (2019). Dysregulated autophagy in muscle precursor cells from humans with type 2 diabetes. *Scientific Reports*, *9*(1), 1–11.

Heyne, K., Mannebach, S., Wuertz, E., Knaup, K. X., Mahyar-Roemer, M., & Roemer, K. (2004). Identification of a putative p53 binding sequence within the human mitochondrial genome. *FEBS Letters*, *578*(1-2), 198-202.

Hilgendorf, K. I., Leshchiner, E. S., Nedelcu, S., Maynard, M. A., Calo, E., Ianari, A., Walensky, L. D., & Lees, J. A. (2013). The retinoblastoma protein induces apoptosis directly at the

mitochondria. *Genes and Development*, *27*(9), 1003-15.

Hillen, H. S., Morozov, Y. I., Sarfallah, A., Temiakov, D., & Cramer, P. (2017). Structural Basis of Mitochondrial Transcription Initiation. *Cell*. *171*(5), 1072-1081.e10.

Hitomi, M., & Stacey, D. W. (1999). Cyclin D1 production in cycling cells depends on Ras in a cell-cycle-specific manner. *Current Biology*, *9*(19), 1075-84.

Hoffmann, C., Höckele, S., Kappler, L., Hrabě De Angelis, M., Häring, H. U., & Weigert, C. (2018). The effect of differentiation and TGFβ on mitochondrial respiration and mitochondrial enzyme abundance in cultured primary human skeletal muscle cells. *Scientific Reports*, *8*(1), 1–12.

Holloszy, J. O. (1967). Biochemical adaptations in muscle. Effects of exercise on mitochondrial oxygen uptake and respiratory enzyme activity in skeletal muscle. *Journal of Biological Chemistry*, *242*(9), 2278-82.

Holloszy, J. O., & Coyle, E. F. (1984). Adaptations of skeletal muscle to endurance exercise and their metabolic consequences. *Journal of Applied Physiology Respiratory Environmental and Exercise Physiology*, *56*(4), 831-8.

Hood, D. A., Irrcher, I., Ljubicic, V., & Joseph, A. M. (2006). Coordination of metabolic plasticity in skeletal muscle. *Journal of Experimental Biology*, *209*(12), 2265–2275.

Hood, D. A., Memme, J. M., Oliveira, A. N., & Triolo, M. (2019). Maintenance of Skeletal Muscle Mitochondria in Health, Exercise, and Aging. *Annual Review of Physiology*, *81*, 19–41.

Hoppeler, H., Baum, O., Lurman, G., & Mueller, M. (2011). Molecular mechanisms of muscle plasticity with exercise. *Comprehensive Physiology*, *1*(3), 1383–1412.

Hoppins, S., Collins, S. R., Cassidy-Stone, A., Hummel, E., DeVay, R. M., Lackner, L. L., Westermann, B., Schuldiner, M., Weissman, J. S., & Nunnari, J. (2011). A mitochondrial-focused genetic interaction map reveals a scaffold-like complex required for inner membrane organization in mitochondria. *Journal of Cell Biology*, *195*(2), 323–340.

Hori, S., Hiramuki, Y., Nishimura, D., Sato, F., & Sehara-Fujisawa, A. (2019). PDH-mediated metabolic flow is critical for skeletal muscle stem cell differentiation and myotube formation during regeneration in mice. *FASEB Journal*, *33*(7), 8094–8109.

Hoshino, D., Yoshida, Y., Kitaoka, Y., Hatta, H., & Bonen, A. (2013). High-intensity interval training increases intrinsic rates of mitochondrial fatty acid oxidation in rat red and white

skeletal muscle. *Applied Physiology, Nutrition and Metabolism*, *38*(3), 326–333.

Hosoyama, T., Nishijo, K., Prajapati, S. I., Li, G., & Keller, C. (2011). Rb1 gene inactivation expands satellite cell and postnatal myoblast pools. *Journal of Biological Chemistry*, *286*(22), 19556–19564.

Houštěk, J., Pícková, A., Vojtíšková, A., Mráček, T., Pecina, P., & Ješina, P. (2006). Mitochondrial diseases and genetic defects of ATP synthase. *Biochimica et Biophysica Acta - Bioenergetics*, *1757*(9–10), 1400–1405.

Hsieh, H. J., Zhang, W., Lin, S. H., Yang, W. H., Wang, J. Z., Shen, J., Zhang, Y., Lu, Y., Wang, H., Yu, J., Mills, G. B., & Peng, G. (2018). Systems biology approach reveals a link between mTORC1 and G2/M DNA damage checkpoint recovery. *Nature Communications*, *9*(1).

Huh, M. S., Parker, M. H., Scimè, A., Parks, R., & Rudnicki, M. A. (2004). Rb is required for progression through myogenic differentiation but not maintenance of terminal differentiation. *Journal of Cell Biology*, *166*(6), 865–876.

Hurford, R. K., Cobrinik, D., Lee, M. H., & Dyson, N. (1997). pRB and p107/p130 are required for the regulated expression of different sets of E2F responsive genes. *Genes and Development*, *11*(11), 1447–1463.

Hwang, H. C., & Clurman, B. E. (2005). Cyclin E in normal and neoplastic cell cycles. *Oncogene*, *24*(17), 2776-86.

Iavarone, A., & Massagué, J. (1999). E2F and Histone Deacetylase Mediate Transforming Growth Factor β Repression of cdc25A during Keratinocyte Cell Cycle Arrest. *Molecular and Cellular Biology*, *19*(1), 916–922.

Imai, S. I., Armstrong, C. M., Kaeberlein, M., & Guarente, L. (2000). Transcriptional silencing and longevity protein Sir2 is an NAD-dependent histone deacetylase. *Nature*, *403*(6771), 795–800.

Imamura, K., Ogura, T., Kishimoto, A., Kaminishi, M., & Esumi, H. (2001). Cell cycle regulation via p53 phosphorylation by a 5′-AMP activated protein kinase activator, 5-aminoimidazole-4-carboxamide-1-β-D-ribofuranoside, in a human hepatocellular carcinoma cell line. *Biochemical and Biophysical Research Communications*, *287*(2):562-7.

Inoue-Yamauchi, A., & Oda, H. (2012). Depletion of mitochondrial fission factor DRP1 causes increased apoptosis in human colon cancer cells. *Biochemical and Biophysical Research*

Communications, *421*(1), 81–85.

Ito, K., & Ito, K. (2016). Metabolism and the Control of Cell Fate Decisions and Stem Cell Renewal. *Annual Review of Cell and Developmental Biology*, *32*, 399-409.

Iwahori, S., & Kalejta, R. F. (2017). Phosphorylation of transcriptional regulators in the retinoblastoma protein pathway by UL97, the viral cyclin-dependent kinase encoded by human cytomegalovirus. *Virology*, 12, 95-103.

Jackson, J. R., Kirby, T. J., Fry, C. S., Cooper, R. L., McCarthy, J. J., Peterson, C. A., & Dupont-Versteegden, E. E. (2015). Reduced voluntary running performance is associated with impaired coordination as a result of muscle satellite cell depletion in adult mice. *Skeletal Muscle*, *5*(1), 1–17.

Jacobs, R. A., Flück, D., Bonne, T. C., Bürgi, S., Christensen, P. M., Toigo, M., & Lundby, C. (2013). Improvements in exercise performance with high-intensity interval training coincide with an increase in skeletal muscle mitochondrial content and function. *Journal of Applied Physiology*, *115*(6), 785–793.

Jang, J. S., Lee, S. J., Choi, Y. H., Nguyen, P. M., Lee, J., Hwang, S. G., Wu, M. L., Takano, E., Maki, M., Henkart, P. A., & Trepel, J. B. (1999). Posttranslational regulation of the retinoblastoma gene family member p107 by calpain protease. *Oncogene*, *18*(10), 1789–1796.

Jeong, J., Conboy, M. J., & Conboy, I. M. (2013). Pharmacological inhibition of myostatin/TGF-β receptor/pSmad3 signaling rescues muscle regenerative responses in mouse model of type 1 diabetes. *Acta Pharmacologica Sinica*, *34*(8), 1052–1060.

Jheng, H.-F., Tsai, P.-J., Guo, S.-M., Kuo, L.-H., Chang, C.-S., Su, I.-J., Chang, C.-R., & Tsai, Y.-S. (2012). Mitochondrial Fission Contributes to Mitochondrial Dysfunction and Insulin Resistance in Skeletal Muscle. *Molecular and Cellular Biology*, *32*(2), 309–319.

Ji, G., Liu, D., Liu, J., Gao, H., Yuan, X., & Shen, G. (2010). p38 mitogen-activated protein kinase up-regulates NF-κB transcriptional activation through RelA phosphorylation during stretch-induced myogenesis. *Biochemical and Biophysical Research Communications*, *391*(1), 547–551.

Jiang, H., Karnezis, A. N., Tao, M., Guida, P. M., & Zhu, L. (2000). pRB and p107 have distinct effects when expressed in pRB-deficient tumor cells at physiologically relevant levels. *Oncogene*, *19*(34), 3878-87.

Joanisse, S., Gillen, J. B., Bellamy, L. M., McKay, B. R., Tarnopolsky, M. A., Gibala, M. J., & Parise, G. (2013). Evidence for the contribution of muscle stem cells to nonhypertrophic skeletal muscle remodeling in humans. *FASEB Journal*, *27*(11), 4596–4605.

Joanisse, S., McKay, B. R., Nederveen, J. P., Scribbans, T. D., Gurd, B. J., Gillen, J. B., Gibala, M. J., Tarnopolsky, M., & Parise, G. (2015). Satellite cell activity, without expansion, after nonhypertrophic stimuli. *American Journal of Physiology - Regulatory Integrative and Comparative Physiology*, *309*(9), R1101–R1111.

Joanisse, S., Nederveen, J. P., Baker, J. M., Snijders, T., Iacono, C., & Parise, G. (2016). Exercise conditioning in old mice improves skeletal muscle regeneration. *FASEB Journal*, *30*(9), 3256-68.

Jones, N. C., Tyner, K. J., Nibarger, L., Stanley, H. M., Cornelison, D. D. W., Fedorov, Y. V., & Olwin, B. B. (2005b). The p38α/β MAPK functions as a molecular switch to activate the quiescent satellite cell. *Journal of Cell Biology*, *169*(1), 105–116.

Jones, R. A., Robinson, T. J., Liu, J. C., Shrestha, M., Voisin, V., Ju, Y., Chung, P. E. D., Pellecchia, G., Fell, V. L., Bae, S., Muthuswamy, L., Datti, A., Egan, S. E., Jiang, Z., Leone, G., Bader, G. D., Schimmer, A., & Zacksenhaus, E. (2016). RB1 deficiency in triple-negative breast cancer induces mitochondrial protein translation. *Journal of Clinical Investigation*, *126*(10), 3739–3757.

Jones, R. G., Plas, D. R., Kubek, S., Buzzai, M., Mu, J., Xu, Y., Birnbaum, M. J., & Thompson, C. B. (2005a). AMP-activated protein kinase induces a p53-dependent metabolic checkpoint. *Molecular Cell*, *18*(3), 283-93.

Kadi, F., & Thornell, L. E. (2000). Concomitant increases in myonuclear and satellite cell content in female trapezius muscle following strength training. *Histochemistry and Cell Biology*, *113*(2), 99–103.

Kadi, F., Schjerling, P., Andersen, L. L., Charifi, N., Madsen, J. L., Christensen, L. R., & Andersen, J. L. (2004). The effects of heavy resistance training and detraining on satellite cells in human skeletal muscles. *Journal of Physiology*, *558*(3), 1005–1012.

Kalucka, J., Missiaen, R., Georgiadou, M., Schoors, S., Lange, C., De Bock, K., Dewerchin, M., & Carmeliet, P. (2015). Metabolic control of the cell cycle. *Cell Cycle*, *14*(21), 3379-88.

Kane, D. A. (2014). Lactate oxidation at the mitochondria: A lactate-malate-aspartate shuttle at work. *Frontiers in Neuroscience*, *25*(8), 366.

Kaplon, J., van Dam, L., & Peeper, D. (2015). Two-way communication between the metabolic and cell cycle machineries: the molecular basis. *Cell Cycle*, *14*(13):2022-32.

Khacho, M & Slack, R. S. (2017). Mitochondrial activity in the regulation of stem cell self-renewal and differentiation. *Current Opinion in Cell Biology*, *49*, 1-8.

Khacho, M., Clark, A., Svoboda, D. S., Azzi, J., MacLaurin, J. G., Meghaizel, C., Sesaki, H., Lagace, D. C., Germain, M., Harper, M. E., Park, D. S., & Slack, R. S. (2016). Mitochondrial Dynamics Impacts Stem Cell Identity and Fate Decisions by Regulating a Nuclear Transcriptional Program. *Cell Stem Cell*, *19*(2), 232–247.

Kim, B., Kim, J. S., Yoon, Y., Santiago, M. C., Brown, M. D., & Park, J. Y. (2013). Inhibition of Drp1-dependent mitochondrial division impairs myogenic differentiation. *American Journal of Physiology - Regulatory Integrative and Comparative Physiology*, *305*(8).

Knight, J. R. P., & Milner, J. (2012). SIRT1, metabolism and cancer. *Current opinion in oncology*, 24(1), 68–75.

Kolupaeva, V., & Basilico, C. (2012). Overexpression of cyclin E/CDK2 complexes overcomes FGF-induced cell cycle arrest in the presence of hypophosphorylated Rb proteins. *Cell Cycle*, *11*(13), 2557–2566.

Kolupaeva, V., Laplantine, E., & Basilico, C. (2008). PP2A-mediated dephosphorylation of p107 plays a critical role in chondrocyte cell cycle arrest by FGF. *PLoS ONE*, *3*(10), e3447.

Kondoh, K., Sunadome, K., & Nishida, E. (2007). Notch signaling suppresses p38 MAPK activity via induction of MKP-1 in myogenesis. *Journal of Biological Chemistry*, *282*(5), 3058-65.

Korenjak, M., Taylor-Harding, B., Binné, U. K., Satterlee, J. S., Stevaux, O., Aasland, R., White-Cooper, H., Dyson, N., & Brehm, A. (2004). Native E2F/RBF complexes contain Myb-interacting proteins and repress transcription of developmentally controlled E2F target genes. *Cell*, *119*(2), 181–193.

Koufali, M. M., Moutsatsou, P., Sekeris, C. E., & Breen, K. C. (2003). The dynamic localization of the glucocorticoid receptor in rat C6 glioma cell mitochondria. *Molecular and Cellular Endocrinology*, *209*(1-2), 51-60.

Kozakowska, M., Pietraszek-Gremplewicz, K., Jozkowicz, A., & Dulak, J. (2015). The role of oxidative stress in skeletal muscle injury and regeneration: focus on antioxidant enzymes. *Journal of Muscle Research and Cell Motility*, *36*(6), 377–393.

Kraft, C. S., LeMoine, C. M. R., Lyons, C. N., Michaud, D., Mueller, C. R., & Moyes, C. D. (2006). Control of mitochondrial biogenesis during myogenesis. *American Journal of Physiology - Cell Physiology*, *290*(4).

Kuang, S., Kuroda, K., Le Grand, F., & Rudnicki, M. A. (2007). Asymmetric Self-Renewal and Commitment of Satellite Stem Cells in Muscle. *Cell*, *129*(5), 999–1010.

Kuhl, J. E., Ruderman, N. B., Musi, N., Goodyear, L. J., Patti, M. E., Crunkhorn, S., Dronamraju, D., Thorell, A., Nygren, J., Ljungkvist, O., Degerblad, M., Stahle, A., Brismar, T. B., Andersen, K. L., Saha, A. K., Efendic, S., & Bavenholm, P. N. (2006). Exercise training decreases the concentration of malonyl-CoA and increases the expression and activity of malonyl-CoA decarboxylase in human muscle. *American Journal of Physiology-Endocrinology and Metabolism*, *290*(6), E1296–E1303.

Kukat, C., Davies, K. M., Wurm, C. A., Spåhr, H., Bonekamp, N. A., Kühl, I., Joos, F., Polosa, P. L., Park, C. B., Posse, V., Falkenberg, M., Jakobs, S., Kühlbrandt, W., & Larsson, N. G. (2015). Cross-strand binding of TFAM to a single mtDNA molecule forms the mitochondrial nucleoid. *Proceedings of the National Academy of Sciences of the United States of America*, *112*(36), 11288–11293.

Kupr, B., & Handschin, C. (2015). Complex coordination of cell plasticity by a PGC-1α-controlled transcriptional network in skeletal muscle. *Frontiers in Physiology*, 6, 325.

Kurosaka, M., Naito, H., Ogura, Y., Kojima, A., Goto, K., & Katamoto, S. (2009). Effects of voluntary wheel running on satellite cells in the rat plantaris muscle. *Journal of Sports Science and Medicine*, *8*(1), 51-7.

L'Honoré, A., Commère, P. H., Negroni, E., Pallafacchina, G., Friguet, B., Drouin, J., Buckingham, M., & Montarras, D. (2018). The role of Pitx2 and Pitx3 in muscle 1 stem cells gives new insights into P38α MAP kinase and redox regulation of muscle regeneration. *ELife*, *14*(7), e32991.

Lagouge, M., Argmann, C., Gerhart-Hines, Z., Meziane, H., Lerin, C., Daussin, F., Messadeq, N., Milne, J., Lambert, P., Elliott, P., Geny, B., Laakso, M., Puigserver, P., & Auwerx, J. (2006). Resveratrol Improves Mitochondrial Function and Protects against Metabolic Disease by Activating SIRT1 and PGC-1α. *Cell*, *127*(6), 1109–1122.

Lambertini, E., Penolazzi, L., Morganti, C., Lisignoli, G., Zini, N., Angelozzi, M., Bonora, M., Ferroni, L., Pinton, P., Zavan, B., & Piva, R. (2015). Osteogenic differentiation of human

MSCs: Specific occupancy of the mitochondrial DNA by NFATc1 transcription factor. *International Journal of Biochemistry and Cell Biology*, *64*, 212-219.

Latil, M., Rocheteau, P., Châtre, L., Sanulli, S., Mémet, S., Ricchetti, M., Tajbakhsh, S., & Chrétien, F. (2012). Skeletal muscle stem cells adopt a dormant cell state post mortem and retain regenerative capacity. *Nature Communications*, *3*(1), 1–12.

Le Grand, F., Jones, A. E., Seale, V., Scimè, A., & Rudnicki, M. A. (2009). Wnt7a Activates the Planar Cell Polarity Pathway to Drive the Symmetric Expansion of Satellite Stem Cells. *Cell Stem Cell*, *4*(6), 535–547.

Le Moal, E., Pialoux, V., Juban, G., Groussard, C., Zouhal, H., Chazaud, B., & Mounier, R. (2017). Redox Control of Skeletal Muscle Regeneration. *Antioxidants and Redox Signaling*, *27*(5), 276–310.

LeCouter, J. E., Kablar, B., Hardy, W. R., Ying, C., Megeney, L. A., May, L. L., & Rudnicki, M. A. (1998). Strain-Dependent Myeloid Hyperplasia, Growth Deficiency, and Accelerated Cell Cycle in Mice Lacking the Rb-Related p107 Gene. *Molecular and Cellular Biology*, *18*(12), 7455–7465.

Lee, B. K., Bhinge, A. A., & Iyer, V. R. (2011). Wide-ranging functions of E2F4 in transcriptional activation and repression revealed by genome-wide analysis. *Nucleic Acids Research*, *39*(9), 3558–3573.

Lee, C., Chang, J. H., Lee, H. S., & Cho, Y. (2002). Structural basis for the recognition of the E2F transactivation domain by the retinoblastoma tumor suppressor. *Genes and Development*, *16*(24), 3199–3212.

Lee, J. O., Russo, A. A., & Pavletich, N. P. (1998). Structure of the retinoblastoma tumour-suppressor pocket domain bound to a peptide from HPV E7. *Nature*, *391*(6670), 859–865.

Lee, S., Shin, H. S., Shireman, P. K., Vasilaki, A., Van Remmen, H., & Csete, M. E. (2006). Glutathione-peroxidase-1 null muscle progenitor cells are globally defective. *Free Radical Biology and Medicine*, *41*(7), 1174–1184.

Lee, W. H., Shew, J. Y., Hong, F. D., Sery, T. W., Donoso, L. A., Young, L. J., Bookstein, R., & Lee, E. Y. H. P. (1987). The retinoblastoma susceptibility gene encodes a nuclear phosphoprotein associated with DNA binding activity. *Nature*, *329*(6140), 642–645.

Lee, W. T., Sun, X., Tsai, T. S., Johnson, J. L., Gould, J. A., Garama, D. J., Gough, D. J., McKenzie, M., Trounce, I. A., & St. John, J. C. (2017). Mitochondrial DNA haplotypes

induce differential patterns of DNA methylation that result in differential chromosomal gene expression patterns. *Cell Death Discovery*, *3*, 27–31.

Lee, Y., Dominy, J. E., Choi, Y. J., Jurczak, M., Tolliday, N., Camporez, J. P., Chim, H., Lim, J. H., Ruan, H. Bin, Yang, X., Vazquez, F., Sicinski, P., Shulman, G. I., & Puigserver, P. (2014). Cyclin D1-Cdk4 controls glucose metabolism independently of cell cycle progression. *Nature*, *510* (7506), 547-51.

Lee, Y., Lee, H. Y., Hanna, R. A., & Gustafsson, A. B. (2011). Mitochondrial autophagy by bnip3 involves drp1-mediated mitochondrial fission and recruitment of parkin in cardiac myocytes. *American Journal of Physiology - Heart and Circulatory Physiology*, *301*(5), H1924.

Leenders, M., Verdijk, L. B., Van Der Hoeven, L., Van Kranenburg, J., Nilwik, R., & Van Loon, L. J. C. (2013). Elderly men and women benefit equally from prolonged resistance-type exercise training. *Journals of Gerontology - Series A Biological Sciences and Medical Sciences*, *68*(7), 769–779.

Lees, E., Faha, B., Dulic, V., Reed, S. I., & Harlow, E. (1992). Cyclin E/cdk2 and cyclin A/cdk2 kinases associate with p107 and E2F in a temporally distinct manner. *Genes and Development*, *6*(10), 1874–1885.

Legesse-Miller, A., Raitman, I., Haley, E. M., Liao, A., Sun, L. L., Wang, D. J., Krishnan, N., Lemons, J. M. S., Suh, E. J., Johnson, E. L., Lund, B. A., & Coller, H. A. (2012). Quiescent fibroblasts are protected from proteasome inhibition-mediated toxicity. *Molecular Biology of the Cell*, *23*(18), 3566–3581.

Lemons, J. M. S., Coller, H. A., Feng, X. J., Bennett, B. D., Legesse-Miller, A., Johnson, E. L., Raitman, I., Pollina, E. A., Rabitz, H. A., & Rabinowitz, J. D. (2010). Quiescent fibroblasts exhibit high metabolic activity. *PLoS Biology*, *8*(10), e1000514.

Leng, X., Noble, M., Adams, P. D., Qin, J., & Harper, J. W. (2002). Reversal of Growth Suppression by p107 via Direct Phosphorylation by Cyclin D1/Cyclin-Dependent Kinase 4. *Molecular and Cellular Biology*, *22*(7), 2242–2254.

Lewis, P. W., Beall, E. L., Fleischer, T. C., Georlette, D., Link, A. J., & Botchan, M. R. (2004). Identification of a Drosophila Myb-E2F2/RBF transcriptional repressor complex. *Genes and Development*, *18*(23), 2929–2940.

Li, X. (2013). SIRT1 and energy metabolism SIRT1 is a Cellular Metabolic Sensor. *Acta*

Biochim Biophys Sin, *45*, 51–60.

Li, Y., Graham, C., Lacy, S., Duncan, A. M. V., & Whyte, P. (1993). The adenovirus E1A-associated 130-kD protein is encoded by a member of the retinoblastoma gene family and physically interacts with cyclins A and E. *Genes and Development*, *7*(12 A), 2366–2377.

Lim, S., & Kaldis, P. (2013). Cdks, cyclins and CKIs: Roles beyond cell cycle regulation. *Development (Cambridge)*, *140*(15), 3079–3093.

Lin, Y., Zhao, Y., Li, R., Gong, J., Zheng, Y., & Wang, Y. (2014). PGC-1α is associated with C2C12 Myoblast differentiation. *Central European Journal of Biology*, *9*, 1030–1036.

Lindeman, G. J., Gaubatz, S., Livingston, D. M., & Ginsberg, D. (1997). The subcellular localization of E2F-4 is cell-cycle dependent, *PNAS*, *94*(10), 5095-5100

Litonin, D., Sologub, M., Shi, Y., Savkina, M., Anikin, M., Falkenberg, M., Gustafsson, C. M., & Temiakov, D. (2010). Human mitochondrial transcription revisited: Only TFAM and TFB2M are required for transcription of the mitochondrial genes in vitro. *Journal of Biological Chemistry*, *285*(24), 18129–18133.

Litovchick, L., Florens, L. A., Swanson, S. K., Washburn, M. P., & Decaprio, J. A. (2011). DYRK1A protein kinase promotes quiescence and senescence through DREAM complex assembly. *Genes and Development*, *25*(8), 801–813.

Litovchick, L., Sadasivam, S., Florens, L., Zhu, X., Swanson, S. K., Velmurugan, S., Chen, R., Washburn, M. P., Liu, X. S., & DeCaprio, J. A. (2007). Evolutionarily Conserved Multisubunit RBL2/p130 and E2F4 Protein Complex Represses Human Cell Cycle-Dependent Genes in Quiescence. *Molecular Cell*, *26*(4), 539–551.

Liu, L., Cheung, T. H., Charville, G. W., Hurgo, B. M. C., Leavitt, T., Shih, J., Brunet, A., & Rando, T. A. (2013). Chromatin Modifications as Determinants of Muscle Stem Cell Quiescence and Chronological Aging. *Cell Reports*, *4*(1), 189–204.

Liu, W., Wen, Y., Bi, P., Lai, X., Liu, X. S., Liu, X., & Kuang, S. (2012). Hypoxia promotes satellite cell self-renewal and enhances the efficiency of myoblast transplantation. *Development (Cambridge)*, *139*(16), 2857–2865.

Liu, X. Y., Wei, B., Shi, H. X., Shan, Y. F., & Wang, C. (2010). Tom70 mediates activation of interferon regulatory factor 3 on mitochondria. *Cell Research*, *20*(9), 994-1011.

Locasale, J. W., & Cantley, L. C. (2010). Altered metabolism in cancer. *BMC Biol*, *8*(10).

Lodeiro, M. F., Uchida, A. U., Arnold, J. J., Reynolds, S. L., Moustafa, I. M., & Cameron, C. E.

(2010). Identification of multiple rate-limiting steps during the human mitochondrial transcription cycle in vitro. *Journal of Biological Chemistry*, *285*(21), 16387–16402.

Lodeiro, M. F., Uchida, A., Bestwick, M., Moustafa, I. M., Arnold, J. J., Shadel, G. S., & Cameron, C. E. (2012). Transcription from the second heavy-strand promoter of human mtDNA is repressed by transcription factor A in vitro. *Proceedings of the National Academy of Sciences of the United States of America*, *109*(17), 6513–6518.

Lopez-Fabuel, I., Le Douce, J., Logan, A., James, A. M., Bonvento, G., Murphy, M. P., Almeida, A., & Bolaños, J. P. (2016). Complex I assembly into supercomplexes determines differential mitochondrial ROS production in neurons and astrocytes, *Proc Natl Acad Sci U S A*, *113*(46), 13063-13068.

Lu, G., Sun, H., Korge, P., Koehler, C. M., Weiss, J. N., & Wang, Y. (2009). Chapter 14 Functional Characterization of a Mitochondrial Ser/Thr Protein Phosphatase in Cell Death Regulation. *Methods in Enzymology*, *457*(B), 255–273.

Lubischer, J. L. (2007). The Cell Cycle, Principles of Control. David O. Morgan. *Integrative and Comparative Biology*, 13, 98-0199206100.

Lucero, M., Suarez, A. E., & Chambers, J. W. (2019). Phosphoregulation on mitochondria: Integration of cell and organelle responses. *CNS Neuroscience and Therapeutics*, *25*(7), 837–858.

Lund, J., Rustan, A. C., Løvsletten, N. G., Mudry, J. M., Langleite, T. M., Feng, Y. Z., Stensrud, C., Brubak, M. G., Drevon, C. A., Birkeland, K. I., Kolnes, K. J., Johansen, E. I., Tangen, D. S., Stadheim, H. K., Gulseth, H. L., Krook, A., Kase, E. T., Jensen, J., & Thoresen, G. H. (2017). Exercise in vivo marks human myotubes in vitro: Training-induced increase in lipid metabolism. *PLoS ONE*, *12*(4), e0175441.

Lundberg, A. S., & Weinberg, R. A. (1998). Functional Inactivation of the Retinoblastoma Protein Requires Sequential Modification by at Least Two Distinct Cyclin-cdk Complexes. *Molecular and Cellular Biology*, *18*(2), 753–761.

Lunt, S. Y., & Vander Heiden, M. G. (2011). Aerobic glycolysis: Meeting the metabolic requirements of cell proliferation. *Annual Review of Cell and Developmental Biology*, *27*, 441–464.

Lunt, S. Y., Muralidhar, V., Hosios, A. M., Israelsen, W. J., Gui, D. Y., Newhouse, L., Ogrodzinski, M., Hecht, V., Xu, K., Acevedo, P. N. M., Hollern, D. P., Bellinger, G.,

Dayton, T. L., Christen, S., Elia, I., Dinh, A. T., Stephanopoulos, G., Manalis, S. R., Yaffe, M. B., … Vander Heiden, M. G. (2015). Pyruvate kinase isoform expression alters nucleotide synthesis to impact cell proliferation. *Molecular Cell*, *57*(1), 95–107.

Lyons, C. N., Leary, S. C., & Moyes, C. D. (2004). Bioenergetic remodeling during cellular differentiation: changes in cytochrome *c* oxidase regulation do not affect the metabolic phenotype. *Biochemistry and Cell Biology*, *82*(3), 391–399.

Mackey, A. L., Esmarck, B., Kadi, F., Koskinen, S. O. A., Kongsgaard, M., Sylvestersen, A., Hansen, J. J., Larsen, G., & Kjaer, M. (2007). Enhanced satellite cell proliferation with resistance training in elderly men and women. *Scandinavian Journal of Medicine and Science in Sports*, *17*(1), 34–42.

Mackey, A. L., Holm, L., Reitelseder, S., Pedersen, T. G., Doessing, S., Kadi, F., & Kjaer, M. (2011a). Myogenic response of human skeletal muscle to 12 weeks of resistance training at light loading intensity. *Scandinavian Journal of Medicine and Science in Sports*, *21*(6), 773-82.

Mackey, Abigail L., Andersen, L. L., Frandsen, U., & Sjøgaard, G. (2011b). Strength training increases the size of the satellite cell pool in type I and II fibres of chronically painful trapezius muscle in females. *Journal of Physiology*, *589*(22), 5503–5515.

Mackey, Abigail L., Kjaer, M., Charifi, N., Henriksson, J., Bojsen-Moller, J., Holm, L., & Kadi, F. (2009). Assessment of satellite cell number and activity status in human skeletal muscle biopsies. *Muscle and Nerve*, *40*(3), 455–465.

Mackey, Abigail L., Kjaer, M., Dandanell, S., Mikkelsen, K. H., Holm, L., Døssing, S., Kadi, F., Koskinen, S. O., Jensen, C. H., Schrøder, H. D., & Langberg, H. (2007). The influence of anti-inflammatory medication on exercise-induced myogenic precursor cell responses in humans. *Journal of Applied Physiology*, *103*(2), 425–431.

Mages, C. F. S., Wintsche, A., Bernhart, S. H., & Müller, G. A. (2017). The DREAM complex through its subunit Lin37 cooperates with Rb to initiate quiescence. *ELife*, *6*, 1–23.

Majmundar, A. J., Lee, D. S. M., Skuli, N., Mesquita, R. C., Kim, M. N., Yodh, A. G., Nguyen-McCarty, M., Li, B., & Simon, M. C. (2015). HIF modulation of wnt signaling regulates skeletal myogenesis in vivo. *Development (Cambridge)*, *142*(14), 2405–2412.

Mandal, S., Guptan, P., Owusu-Ansah, E., & Banerjee, U. (2005). Mitochondrial regulation of cell cycle progression during development as revealed by the tenured mutation in

Drosophila. *Developmental Cell*, *9*(6), 843-54.

Mann, C. J., Perdiguero, E., Kharraz, Y., Aguilar, S., Pessina, P., Serrano, A. L., & Muñoz-Cánoves, P. (2011). Aberrant repair and fibrosis development in skeletal muscle. *Skeletal Muscle*, *1*(1), 1–20.

Manning, A. L., & Dyson, N. J. (2011). pRB, a tumor suppressor with a stabilizing presence. *Trends in Cell Biology*, *21*(8), 433-41.

Manzanares, G., Brito-Da-Silva, G., & Gandra, P. G. (2019). Voluntary wheel running: Patterns and physiological effects in mice. *Brazilian Journal of Medical and Biological Research*, *52*(1), 1–9.

Manzano, R., Toivonen, J. M., Calvo, A. C., Oliván, S., Zaragoza, P., Rodellar, C., Montarras, D., & Osta, R. (2013). Altered in vitro proliferation of mouse SOD1-G93A skeletal muscle satellite cells. *Neurodegenerative Diseases*, *11*(3), 153–164.

Maples, J. M., Brault, J. J., Shewchuk, B. M., Witczak, C. A., Zou, K., Rowland, N., Hubal, M. J., Weber, T. M., & Houmard, J. A. (2015). Lipid exposure elicits differential responses in gene expression and DNA methylation in primary human skeletal muscle cells from severely obese women. *Physiological Genomics*, *47*(5), 139–146.

Margineantu, D. H., Gregory Cox, W., Sundell, L., Sherwood, S. W., Beechem, J. M., & Capaldi, R. A. (2002). Cell cycle dependent morphology changes and associated mitochondrial DNA redistribution in mitochondria of human cell lines. *Mitochondrion*, *1*(5):425-35.

Martínez-Reyes, I., & Chandel, N. S. (2020). Mitochondrial TCA cycle metabolites control physiology and. disease. *Nature Communications*, *11*(1), 1–11.

Martínez-Reyes, I., Diebold, L. P., Kong, H., Schieber, M., Huang, H., Hensley, C. T., Mehta, M. M., Wang, T., Santos, J. H., Woychik, R., Dufour, E., Spelbrink, J. N., Weinberg, S. E., Zhao, Y., DeBerardinis, R. J., & Chandel, N. S. (2016). TCA Cycle and Mitochondrial Membrane Potential Are Necessary for Diverse Biological Functions. *Molecular Cell*, *61*(2), 199-209.

Masschelein, E., D'Hulst, G., Zvick, J., Hinte, L., Soro-Arnaiz, I., Gorski, T., Von Meyenn, F., Bar-Nur, O., & De Bock, K. (2020). Exercise promotes satellite cell contribution to myofibers in a load-dependent manner. *Skeletal Muscle*, *10*(1), 1–15.

Matre, P. R., Mu, X., Wu, J., Danila, D., Hall, M. A., Kolonin, M. G., Darabi, R., & Huard, J.

(2019). CRISPR/Cas9-Based Dystrophin Restoration Reveals a Novel Role for Dystrophin in Bioenergetics and Stress Resistance of Muscle Progenitors. *Stem Cells*, *37*(12), 1615–1628.

Mauro, A. (1961). Satellite cell of skeletal muscle fibers. *The Journal of Biophysical and Biochemical Cytology*, *9*(2), 493–495.

Mazurek, S. (2011). Pyruvate kinase type M2: A key regulator of the metabolic budget system in tumor cells. *International Journal of Biochemistry and Cell Biology*, *43*(7), 969-80.

McBride, H. M., Neuspiel, M., & Wasiak, S. (2006). Mitochondria: More Than Just a Powerhouse. *Current Biology*, *16*(14), R551-60.

McBurney, M. W., Clark-Knowles, K. V., Caron, A. Z., & Gray, D. A. (2013). SIRT1 is a Highly Networked Protein That Mediates the Adaptation to Chronic Physiological Stress. *Genes and Cancer*, *4*(3–4), 125–134.

Mccarthy, J. J., Mula, J., Miyazaki, M., Erfani, R., Garrison, K., Farooqui, A. B., Srikuea, R., Lawson, B. A., Grimes, B., Keller, C., Van Zant, G., Campbell, K. S., Esser, K. A., Dupont-Versteegden, E. E., & Peterson, C. A. (2011). Effective fiber hypertrophy in satellite cell-depleted skeletal muscle. *Development*, *138*(17), 3657–3666.

McCulloch, V., & Shadel, G. S. (2003). Human Mitochondrial Transcription Factor B1 Interacts with the C-Terminal Activation Region of h-mtTFA and Stimulates Transcription Independently of Its RNA Methyltransferase Activity. *Molecular and Cellular Biology*, *23*(16), 5816–5824.

McCulloch, V., Seidel-Rogol, B. L., & Shadel, G. S. (2002). A Human Mitochondrial Transcription Factor Is Related to RNA Adenine Methyltransferases and Binds S-Adenosylmethionine. *Molecular and Cellular Biology*, *22*(4), 1116–1125.

McKay, B. R., Ogborn, D. I., Bellamy, L. M., Tarnopolsky, M. A., & Parise, G. (2012). Myostatin is associated with age-related human muscle stem cell dysfunction. *The FASEB Journal*, *26*(6), 2509–2521.

McKinnell, I. W., Ishibashi, J., Le Grand, F., Punch, V. G. J., Addicks, G. C., Greenblatt, J. F., Dilworth, F. J., & Rudnicki, M. A. (2008). Pax7 activates myogenic genes by recruitment of a histone methyltransferase complex. *Nature Cell Biology*, *10*(1), 77-84.

Meeusen, S., McCaffery, J. M., & Nunnari, J. (2004). Mitochondrial fusion intermediates revealed in vitro. *Science*, *305*(5691), 1747–1752.

Mendelsohn, B. A., Bennett, N. K., Darch, M. A., Yu, K., Nguyen, M. K., Pucciarelli, D., Nelson, M., Horlbeck, M. A., Gilbert, L. A., Hyun, W., Kampmann, M., Nakamura, J. L., & Nakamura, K. (2018). A high-throughput screen of real-time ATP levels in individual cells reveals mechanisms of energy failure. *PLoS Biology*, *16*(8).

Menon, M. K., Houchen, L., Singh, S. J., Morgan, M. D., Bradding, P., & Steiner, M. C. (2012). Inflammatory and satellite cells in the quadriceps of patients with COPD and response to resistance training. *Chest*, *142*(5), 1134–1142.

Menshikova, E. V., Ritov, V. B., Fairfull, L., Ferrell, R. E., Kelley, D. E., & Goodpaster, B. H. (2006). Effects of exercise on mitochondrial content and function in aging human skeletal muscle. *Journals of Gerontology - Series A Biological Sciences and Medical Sciences*, *61*(6), 534–540.

Menzies, K. J., & Auwerx, J. (2015). Review NAD + Metabolism and the Control of Energy Homeostasis : A Balancing Act between Mitochondria and the Nucleus. *Cell Metab*, *22*(1), 31-53.

Meyer, K., & Selbach, M. (2015). Quantitative affinity purification mass spectrometry: A versatile technology to study protein-protein interactions. *Frontiers in Genetics*, *14*(6), 237.

Michan, S., & Sinclair, D. (2007). Sirtuins in mammals: Insights into their biological function. *Biochemical Journal*, *404*(1), 1–13.

Mikkelsen, U. R., Langberg, H., Helmark, I. C., Skovgaard, D., Andersen, L. L., Kjær, M., & Mackey, A. L. (2009). Local NSAID infusion inhibits satellite cell proliferation in human skeletal muscle after eccentric exercise. *Journal of Applied Physiology*, *107*(5), 1600–1611.

Mills, E. L., Kelly, B., Logan, A., Costa, A. S. H., Varma, M., Bryant, C. E., Tourlomousis, P., Däbritz, J. H. M., Gottlieb, E., Latorre, I., Corr, S. C., McManus, G., Ryan, D., Jacobs, H. T., Szibor, M., Xavier, R. J., Braun, T., Frezza, C., Murphy, M. P., & O'Neill, L. A. (2016). Repurposing mitochondria from ATP production to ROS generation drives a pro-inflammatory phenotype in macrophages that depends on succinate oxidation by complex II. *Cell*, *167*(2), 457-470.e13.

Minczuk, M., He, J., Duch, A. M., Ettema, T. J., Chlebowski, A., Dzionek, K., Nijtmans, L. G. J., Huynen, M. A., & Holt, I. J. (2011). TEFM (c17orf42) is necessary for transcription of human mtDNA. *Nucleic Acids Research*, *39*(10), 4284–4299.

Minet, A. D., & Gaster, M. (2011). The dynamic equilibrium between ATP synthesis and ATP

consumption is lower in isolated mitochondria from myotubes established from type 2 diabetic subjects compared to lean control. *Biochemical and Biophysical Research Communications*, *409*(4), 591–595.

Mishra, P., & Chan, D. C. (2014). Mitochondrial dynamics and inheritance during cell division, development and disease. *Nature Reviews Molecular Cell Biology*, *15*(10), 634–646.

Mishra, P., & Chan, D. C. (2016). Metabolic regulation of mitochondrial dynamics. *Journal of Cell Biology*, *212*(4), 379–387.

Mishra, P., Varuzhanyan, G., Pham, A. H., & Chan, D. C. (2015). Mitochondrial Dynamics Is a Distinguishing Feature of Skeletal Muscle Fiber Types and Regulates Organellar Compartmentalization. *Cell Metabolism*, *22*(6), 1033-44.

Mitra, K., Wunder, C., Roysam, B., Lin, G., & Lippincott-Schwartz, J. (2009). A hyperfused mitochondrial state achieved at G1-S regulates cyclin E buildup and entry into S phase. *Proceedings of the National Academy of Sciences of the United States of America*, *106*(29), 11960–11965.

Mokranjac, D., & Neupert, W. (2005). Protein import into mitochondria. *Biochemical Society Transactions*, *33*(5), 1019–1023.

Montoya, J., Christianson, T., Levens, D., Rabinowitz, M., & Attardi, G. (1982). Identification of initiation sites for heavy-strand and light-strand transcription in human mitochondrial DNA. *Proc Natl Acad Sci U S A*, *79*(23 I), 7195–7199.

Morozov, Y. I., Agaronyan, K., Cheung, A. C. M., Anikin, M., Cramer, P., & Temiakov, D. (2014). A novel intermediate in transcription initiation by human mitochondrial RNA polymerase. *Nucleic Acids Research*, *42*(6), 3884–3893.

Morozov, Y. I., Parshin, A. V., Agaronyan, K., Cheung, A. C. M., Anikin, M., Cramer, P., & Temiakov, D. (2015). A model for transcription initiation in human mitochondria. *Nucleic Acids Research*, *43*(7), 3726–3735.

Mortensen, O. H., Plomgaard, P., Fischer, C. P., Hansen, A. K., Pilegaard, H., & Pedersen, B. K. (2007). PGC-1β is downregulated by training in human skeletal muscle: No effect of training twice every second day vs. once daily on expression of the PGC-1 family. *Journal of Applied Physiology*, *103*(5), 1536–1542.

Mourkioti, F., Kratsios, P., Luedde, T., Song, Y. H., Delafontaine, P., Adami, R., Parente, V., Bottinelli, R., Pasparakis, M., & Rosenthal, N. (2006). Targeted ablation of IKK2 improves

skeletal muscle strength, maintains mass, and promotes regeneration. *Journal of Clinical Investigation*, *116*(11), 2945–2954.

Müller, H, Moroni, M. C., Vigo, E., Petersen, B. O., Bartek, J., & Helin, K. (1997). Induction of S-phase entry by E2F transcription factors depends on their nuclear localization. *Molecular and Cellular Biology*, *17*(9), 5508-20.

Müller, Heiko, Bracken, A. P., Vernell, R., Moroni, M. C., Christians, F., Grassilli, E., Prosperini, E., Vigo, E., Oliner, J. D., & Helin, K. (2001). E2Fs regulate the expression of genes involved in differentiation, development, proliferation, and apoptosis. *Genes and Development*, *15*(3), 267–285.

Mulligan, G., & Jacks, T. (1998). The retinoblastoma gene family: Cousins with overlapping interests. *Trends in Genetics*, *14*(6), 223–229.

Murach, K. A., Englund, D. A., Dupont-Versteegden, E. E., McCarthy, J. J., & Peterson, C. A. (2018a). Myonuclear domain flexibility challenges rigid assumptions on satellite cell contribution to skeletal muscle fiber hypertrophy. *Frontiers in Physiology*, *9*, 1–7.

Murach, K. A., Fry, C. S., Kirby, T. J., Jackson, J. R., Lee, J. D., White, S. H., Dupont-Versteegden, E. E., McCarthy, J. J., & Peterson, C. A. (2018b). Starring or supporting role? Satellite cells and skeletal muscle fiber size regulation. *Physiology*, *33*(1), 26–38.

Murphy, M. M., Keefe, A. C., Lawson, J. A., Flygare, S. D., Yandell, M., & Kardon, G. (2014). Transiently active wnt/β-catenin signaling is not required but must be silenced for stem cell function during muscle regeneration. *Stem Cell Reports*, *3*(3), 475–488.

Myers, M. J., Shepherd, D. L., Durr, A. J., Stanton, D. S., Mohamed, J. S., Hollander, J. M., & Alway, S. E. (2019). The role of SIRT1 in skeletal muscle function and repair of older mice. *Journal of Cachexia, Sarcopenia and Muscle*, *10*(4), 929-949.

Neufer, P. D., & Dohm, G. L. (1993). Exercise induces a transient increase in transcription of the GLUT-4 gene in skeletal muscle. *American Journal of Physiology - Cell Physiology*, *265*(6 34-6).

Neupert, W., & Herrmann, J. M. (2007). Translocation of proteins into mitochondria. *Annual Review of Biochemistry*, 76, 723-49.

Newman, L. E., Schiavon, C., & Kahn, R. A. (2016). Plasmids for variable expression of proteins targeted to the mitochondrial matrix or intermembrane space. *Cellular Logistics*, *6*(4), e1247939.

Ngo, H. B., Kaiser, J. T., & Chan, D. C. (2011). The mitochondrial transcription and packaging factor Tfam imposes a U-turn on mitochondrial DNA. *Nature Structural and Molecular Biology*, *18*(11), 1290-6.

Ngo, H. B., Lovely, G. A., Phillips, R., & Chan, D. C. (2014). Distinct structural features of TFAM drive mitochondrial DNA packaging versus transcriptional activation. *Nature Communications*, *5*, 1–12.

Nguyen, J. H., Chung, J. D., Lynch, G. S., & Ryall, J. G. (2019). The Microenvironment Is a Critical Regulator of Muscle Stem Cell Activation and Proliferation. *Frontiers in Cell and Developmental Biology*, *29*(7), 254.

Nguyen, M. H., Cheng, M., & Koh, T. J. (2011). Impaired muscle regeneration in Ob/ob and Db/db mice. *The Scientific World Journal*, *11*, 1525–1535.

Nicolay, B. N., Danielian, P. S., Kottakis, F., Lapek, J. D., Sanidas, I., Miles, W. O., Dehnad, M., Tschöp, K., Gierut, J. J., Manning, A. L., Morris, R., Haigis, K., Bardeesy, N., Lees, J. A., Haas, W., & Dyson, N. J. (2015). Proteomic analysis of pRb loss highlights a signature of decreased mitochondrial oxidative phosphorylation. *Genes and Development*, *29*(17), 1875–1889.

Norrbom, J., Sundberg, C. J., Ameln, H., Kraus, W. E., Jansson, E., & Gustafsson, T. (2004). PGC-1α mRNA expression is influenced by metabolic perturbation in exercising human skeletal muscle. *Journal of Applied Physiology*, *96*(1), 189–194.

O'Connell, M., McClure, N., & Lewis, S. E. M. (2002). The effects of cryopreservation on sperm morphology, motility and mitochondrial function. *Human Reproduction*, *17*(3), 704-9.

O'Reilly, C., McKay, B., Phillips, S., Tarnopolsky, M., & Parise, G. (2008). Hepatocyte growth factor (HGF) and the satellite cell response following muscle lengthening contractions in humans. *Muscle and Nerve*, *38*(5), 1434–1442.

Ochocki, J. D., & Simon, M. C. (2013). Nutrient-sensing pathways and metabolic regulation in stem cells. *Journal of Cell Biology*, *203*(1), 23-33.

Ogita, K., Okuda, H., Kitano, M., Fujinami, Y., Ozaki, K., & Yoneda, Y. (2002). Localization of Activator Protein-1 Complex with DNA Binding Activity in Mitochondria of Murine Brain after in Vivo Treatment with Kainate. *Journal of Neuroscience*, *22*(7), 2561-70.

Oldham, W. M., Clish, C. B., Yang, Y., & Loscalzo, J. (2015). Hypoxia-Mediated Increases in l-

2-hydroxyglutarate Coordinate the Metabolic Response to Reductive Stress. *Cell Metabolism*, *22*(2), 291-303.

Olguin, H. C., Yang, Z., Tapscott, S. J., & Olwin, B. B. (2007). Reciprocal inhibition between Pax7 and muscle regulatory factors modulates myogenic cell fate determination. *Journal of Cell Biology*, *177*(5), 769–779.

Olsen, S., Aagaard, P., Kadi, F., Tufekovic, G., Verney, J., Olesen, J. L., Suetta, C., & Kjær, M. (2006). Creatine supplementation augments the increase in satellite cell and myonuclei number in human skeletal muscle induced by strength training. *Journal of Physiology*, *573*(2), 525–534.

Onopiuk, M., Brutkowski, W., Wierzbicka, K., Wojciechowska, S., Szczepanowska, J., Fronk, J., Lochmüller, H., Górecki, D. C., & Zabłocki, K. (2009). Mutation in dystrophin-encoding gene affects energy metabolism in mouse myoblasts. *Biochemical and Biophysical Research Communications*, *386*(3), 463–466.

Owusu-Ansah, E., & Banerjee, U. (2009). Reactive oxygen species prime Drosophila haematopoietic progenitors for differentiation. *Nature*, *461*(7263), 537–541.

Oyewole, A. O., & Birch-Machin, M. A. (2015). Mitochondria-targeted antioxidants. *FASEB Journal*, *29*(12), 4766–4771.

Pääsuke, R., Eimre, M., Piirsoo, A., Peet, N., Laada, L., Kadaja, L., Roosimaa, M., Pääsuke, M., Märtson, A., Seppet, E., & Paju, K. (2016). Proliferation of Human Primary Myoblasts Is Associated with Altered Energy Metabolism in Dependence on Ageing in Vivo and in Vitro. *Oxidative Medicine and Cellular Longevity*, *2016*, 8296150.

Pagnotti, G. M., Styner, M., Uzer, G., Patel, V. S., Wright, L. E., Ness, K. K., Guise, T. A., Rubin, J., & Rubin, C. T. (2019). Combating osteoporosis and obesity with exercise: leveraging cell mechanosensitivity. *Nature Reviews Endocrinology*, *15*(6), 339-355.

Pajcini, K. V., Corbel, S. Y., Sage, J., Pomerantz, J. H., & Blau, H. M. (2010). Transient inactivation of Rb and ARF yields regenerative cells from postmitotic mammalian muscle. *Cell Stem Cell*, *7*(2), 198-213.

Pala, F., Di Girolamo, D., Mella, S., Yennek, S., Chatre, L., Ricchetti, M., & Tajbakhsh, S. (2018). Distinct metabolic states govern skeletal muscle stem cell fates during prenatal and postnatal myogenesis. *Journal of Cell Science*, *131*(14).

Pallafacchina, G., François, S., Regnault, B., Czarny, B., Dive, V., Cumano, A., Montarras, D.,

& Buckingham, M. (2010). An adult tissue-specific stem cell in its niche: A gene profiling analysis of in vivo quiescent and activated muscle satellite cells. *Stem Cell Research*, *4*(2), 77–91.

Pan, M., Yuan, H., Brent, M., Ding, E. C., & Marmorsteins, R. (2012). SIRT1 contains N- and C-terminal regions that potentiate deacetylase activity. *Journal of Biological Chemistry*, *287*(4), 2468-76.

Pant, M., Sopariwala, D. H., Bal, N. C., Lowe, J., Delfín, D. A., Rafael-Fortney, J., & Periasamy, M. (2015). Metabolic Dysfunction and Altered Mitochondrial Dynamics in the Utrophin-Dystrophin Deficient Mouse Model of Duchenne Muscular Dystrophy. *PLOS ONE*, *10*(4), e0123875.

Papanicolaou, K. N., Kikuchi, R., Ngoh, G. A., Coughlan, K. A., Dominguez, I., Stanley, W. C., & Walsh, K. (2012). Mitofusins 1 and 2 are essential for postnatal metabolic remodeling in heart. *Circulation Research*, *111*(8), 1012-26.

Pardo, P. S., & Boriek, A. M. (2011). The physiological roles of Sirt1 in skeletal muscle. *Aging*, *3*(4), 430–437.

Park, C. B., Asin-Cayuela, J., Cámara, Y., Shi, Y., Pellegrini, M., Gaspari, M., Wibom, R., Hultenby, K., Erdjument-Bromage, H., Tempst, P., Falkenberg, M., Gustafsson, C. M., & Larsson, N. G. (2007). MTERF3 Is a Negative Regulator of Mammalian mtDNA Transcription. *Cell*, *130*(2), 273–285.

Park, S. J., Ahmad, F., Philp, A., Baar, K., Williams, T., Luo, H., Ke, H., Rehmann, H., Taussig, R., Brown, A. L., Kim, M. K., Beaven, M. A., Burgin, A. B., Manganiello, V., & Chung, J. H. (2012). Resveratrol ameliorates aging-related metabolic phenotypes by inhibiting cAMP phosphodiesterases. *Cell*, *148*(3), 421–433.

Pavlidou, T., Rosina, M., Fuoco, C., Gerini, G., Gargioli, C., Castagnoli, L., & Cesareni, G. (2017). Regulation of myoblast differentiation by metabolic perturbations induced by metformin. *PLoS ONE*, *12*(8).

Pello, R., Martín, M. A., Carelli, V., Nijtmans, L. G., Achilli, A., Pala, M., Torroni, A., Gómez-Durán, A., Ruiz-Pesini, E., Martinuzzi, A., Smeitink, J. A., Arenas, J., & Ugalde, C. (2008). Mitochondrial DNA background modulates the assembly kinetics of OXPHOS complexes in a cellular model of mitochondrial disease. *Human Molecular Genetics*, *17*(24), 4001–4011.

Perdiguero, E., Ruiz-Bonilla, V., Serrano, A. L., & Muñoz-Cánoves, P. (2007). Genetic deficiency of p38α reveals its critical role in myoblast cell cycle exit: The p38α-JNK connection. *Cell Cycle*, *6*(11), 1298–1303.

Perry, C. G. R., Heigenhauser, G. J. F., Bonen, A., & Spriet, L. L. (2008). High-intensity aerobic interval training increases fat and carbohydrate metabolic capacities in human skeletal muscle. *Applied Physiology, Nutrition and Metabolism*, *33*(6), 1112–1123.

Perry, C. G. R., Lally, J., Holloway, G. P., Heigenhauser, G. J. F., Bonen, A., & Spriet, L. L. (2010). Repeated transient mRNA bursts precede increases in transcriptional and mitochondrial proteins during training in human skeletal muscle. *Journal of Physiology*, *588*(23), 4795–4810.

Petrella, J. K., Kim, J. S., Cross, J. M., Kosek, D. J., & Bamman, M. M. (2006). Efficacy of myonuclear addition may explain differential myofiber growth among resistance-trained young and older men and women. *American Journal of Physiology - Endocrinology and Metabolism*, *291*(5), 937–946.

Petrov, P. D., Ribot, J., López-Mejía, I. C., Fajas, L., Palou, A., & Bonet, M. L. (2016). Retinoblastoma Protein Knockdown Favors Oxidative Metabolism and Glucose and Fatty Acid Disposal in Muscle Cells. *Journal of Cellular Physiology*, *231*(3), 708–718.

Pette, D., & Staron, R. S. (2001). Transitions of muscle fiber phenotypic profiles. *Histochemistry and Cell Biology*, *115*(5), 359–372.

Pfanner, N., Warscheid, B., & Wiedemann, N. (2019). Mitochondrial proteins: from biogenesis to functional networks. *Nature Reviews Molecular Cell Biology*, *20*(5), 267-284.

Pfeiffer, T., Schuster, S., & Bonhoeffer, S. (2001). Erratum: Cooperation and competition in the evolution of ATP-producing pathways. *Science*, *293*(5534), 1436.

Philippos, M., Sambasivan, R., Castel, D., Rocheteau, P., Bizzarro, V., & Tajbakhsh, S. (2012). A critical requirement for notch signaling in maintenance of the quiescent skeletal muscle stem cell state. *Stem Cells*, *30*(2), 243-52.

Pilegaard, H., Ordway, G. A., Saltin, B., & Neufer, P. D. (2000). Transcriptional regulation of gene expression in human skeletal muscle during recovery from exercise. *American Journal of Physiology - Endocrinology and Metabolism*, *279*(4 42-4).

Pilkinton, M., Sandoval, R., & Colamonici, O. R. (2007). Mammalian Mip/LIN-9 interacts with either the p107, p130/E2F4 repressor complex or B-Myb in a cell cycle-phase-dependent

context distinct from the Drosophila dREAM complex. *Oncogene*, *26*(54), 7535–7543.

Polyak, K., Kato, J. Y., Solomon, M. J., Sherr, C. J., Massague, J., Roberts, J. M., & Koff, A. (1994). p27(Kip1), a cyclin-Cdk inhibitor, links transforming growth factor-β and contact inhibition to cell cycle arrest. *Genes and Development*, *8*(1), 9–22.

Porras, D. P., Abbaszadeh, M., Bhattacharya, D., D'Souza, N. C., Edjiu, N. R., Perry, C. G. R., & Scimè, A. (2017). p107 Determines a Metabolic Checkpoint Required for Adipocyte Lineage Fates. *Stem Cells*, *35*(5), 1378–1391.

Porter, C., Reidy, P. T., Bhattarai, N., Sidossis, L. S., & Rasmussen, B. B. (2015). Resistance Exercise Training Alters Mitochondrial Function in Human Skeletal Muscle. *Medicine and Science in Sports and Exercise*, *47*(9), 1922–1931.

Posse, V., Hoberg, E., Dierckx, A., Shahzad, S., Koolmeister, C., Larsson, N. G., Wilhelmsson, L. M., Hällberg, B. M., & Gustafsson, C. M. (2014). The amino terminal extension of mammalian mitochondrial RNA polymerase ensures promoter specific transcription initiation. *Nucleic Acids Research*, *42*(6), 3638–3647.

Powelka, A. M., Seth, A., Virbasius, J. V., Kiskinis, E., Nicoloro, S. M., Guilherme, A., Tang, X., Straubhaar, J., Cherniack, A. D., Parker, M. G., & Czech, M. P. (2006). Suppression of oxidative metabolism and mitochondrial biogenesis by the transcriptional corepressor RIP140 in mouse adipocytes. *Journal of Clinical Investigation*, *116*(1), 125–136.

Pryde, K. R., & Hirst, J. (2011). Superoxide is produced by the reduced flavin in mitochondrial complex I: A single, unified mechanism that applies during both forward and reverse electron transfer. *Journal of Biological Chemistry*, *286*(20):18056-65.

Przewoźniak, M., Czaplicka, I., Czerwińska, A. M., Markowska-Zagrajek, A., Moraczewski, J., Stremińska, W., Jańczyk-Ilach, K., Ciemerych, M. A., & Brzoska, E. (2013). Adhesion Proteins - An Impact on Skeletal Myoblast Differentiation. *PLoS ONE*, *8*(5).

Pugh, J. K., Faulkner, S. H., Turner, M. C., & Nimmo, M. A. (2018). Satellite cell response to concurrent resistance exercise and high-intensity interval training in sedentary, overweight/obese, middle-aged individuals. *European Journal of Applied Physiology*, *118*(2), 225–238.

Ramachandran, A., Basu, U., Sultana, S., Nandakumar, D., & Patel, S. S. (2017). Human mitochondrial transcription factors TFAM and TFB2M work synergistically in promoter melting during transcription initiation. *Nucleic Acids Research*, *45*(2), 861–874.

Ramos, E. S., Motori, E., Brüser, C., Kühl, I., Yeroslaviz, A., Ruzzenente, B., Kauppila, J. H. K., Busch, J. D., Hultenby, K., Habermann, B. H., Jakobs, S., Larsson, N. G., & Mourier, A. (2019). Mitochondrial fusion is required for regulation of mitochondrial DNA replication. *PLoS Genetics*, *15*(6).

Rathbone, C. R., Booth, F. W., & Lees, S. J. (2009). Sirt1 increases skeletal muscle precursor cell proliferation. *European Journal of Cell Biology*, *88*(1), 35-44.

Rayman, J. B., Takahashi, Y., Indjeian, V. B., Dannenberg, J. H., Catchpole, S., Watson, R. J., Riele, H., & Dynlacht, B. D. (2002). E2F mediates cell cycle-dependent transcriptional repression in vivo by recruitment of an HDAC1/mSin3B corepressor complex. *Genes and Development*, *16*(8), 933–947.

Reinecke, F., Smeitink, J. A. M., & van der Westhuizen, F. H. (2009). OXPHOS gene expression and control in mitochondrial disorders. *Biochimica et Biophysica Acta - Molecular Basis of Disease*, *1792*(12), 1113-21.

Relaix, F., & Zammit, P. S. (2012). Satellite cells are essential for skeletal muscle regeneration: The cell on the edge returns centre stage. *Development (Cambridge)*, *139*(16), 2845-56.

Remels, A. H. V., Langen, R. C. J., Schrauwen, P., Schaart, G., Schols, A. M. W. J., & Gosker, H. R. (2010). Regulation of mitochondrial biogenesis during myogenesis. *Molecular and Cellular Endocrinology*, *315*(1–2), 113–120.

Reshetnikova, G., Barkan, R., Popov, B., Nikolsky, N., & Chang, L. S. (2000). Disruption of the actin cytoskeleton leads to inhibition of mitogen-induced cyclin E expression, Cdk2 phosphorylation, and nuclear accumulation of the retinoblastoma protein-related p107 protein. *Experimental Cell Research*, *259*(1), 35-53.

Richards, S. A., Muter, J., Ritchie, P., Lattanzi, G., & Hutchison, C. J. (2011). The accumulation of un-repairable DNA damage in laminopathy progeria fibroblasts is caused by ROS generation and is prevented by treatment with N-acetyl cysteine. *Human Molecular Genetics*, *20*(20), 3997–4004.

Richter, E. A., & Hargreaves, M. (2013). Exercise, GLUT4, and skeletal muscle glucose uptake. *Physiological Reviews*, *93*(3), 993–1017.

Rigamonti, E., Touvier, T., Clementi, E., Manfredi, A. A., Brunelli, S., & Rovere-Querini, P. (2013). Requirement of Inducible Nitric Oxide Synthase for Skeletal Muscle Regeneration after Acute Damage. *The Journal of Immunology*, *190*(4), 1767–1777.

Rochard, P., Rodier, A., Casas, F., Cassar-Malek, I., Marchal-Victorion, S., Daury, L., Wrutniak, C., & Cabello, G. (2000). Mitochondrial activity is involved in the regulation of myoblast differentiation through myogenin expression and activity of myogenic factors. *Journal of Biological Chemistry*, *275*(4), 2733–2744.

Rocheteau, P., Chatre, L., Briand, D., Mebarki, M., Jouvion, G., Bardon, J., Crochemore, C., Serrani, P., Lecci, P. P., Latil, M., Matot, B., Carlier, P. G., Latronico, N., Huchet, C., Lafoux, A., Sharshar, T., Ricchetti, M., & Chrétien, F. (2015). Sepsis induces long-term metabolic and mitochondrial muscle stem cell dysfunction amenable by mesenchymal stem cell therapy. *Nature Communications*, *6*, 10145.

Rocheteau, Pierre, Gayraud-Morel, B., Siegl-Cachedenier, I., Blasco, M. A., & Tajbakhsh, S. (2012). A subpopulation of adult skeletal muscle stem cells retains all template DNA strands after cell division. *Cell*, *148*(1–2), 112–125.

Rodgers, J. T., King, K. Y., Brett, J. O., Cromie, M. J., Charville, G. W., Maguire, K. K., Brunson, C., Mastey, N., Liu, L., Tsai, C. R., Goodell, M. A., & Rando, T. A. (2014). MTORC1 controls the adaptive transition of quiescent stem cells from G 0 to GAlert. *Nature*, *510*(7505), 393–396.

Rodgers, J. T., Lerin, C., Haas, W., Gygi, S. P., Spiegelman, B. M., & Puigserver, P. (2005). Nutrient control of glucose homeostasis through a complex of PGC-1α and SIRT1. *Nature*, *434*(7029), 113–118.

Rodier, G., Makris, C., Coulombe, P., Scime, A., Nakayama, K., Nakayama, K. I., & Meloche, S. (2005). p107 inhibits G1 to S phase progression by down-regulating expression of the F-box protein Skp2. *Journal of Cell Biology*, *68*(1), 55-66.

Rodrigues, A. S., Correia, M., Gomes, A., Pereira, S. L., Perestrelo, T., Sousa, M. I., & Ramalho-Santos, J. (2015). Dichloroacetate, the pyruvate dehydrogenase complex and the modulation of mESC pluripotency. *PLoS ONE*, *10*(7), e0131663.

Romero-Pozuelo, J., Figlia, G., Kaya, O., Martin-Villalba, A., & Teleman, A. A. (2020). Cdk4 and Cdk6 Couple the Cell-Cycle Machinery to Cell Growth via mTORC1. *Cell Reports*, *31*(2), 107504.

Rosenblatt, J. D., & Parry, D. J. (1992). Gamma irradiation prevents compensatory hypertrophy of overloaded mouse extensor digitorum longus muscle. *Journal of Applied Physiology*, *73*(6), 2538–2543.

Rossignol, R., Gilkerson, R., Aggeler, R., Yamagata, K., Remington, S.J., & Capaldi, R.A.. (2004). Energy substrate modulates mitochondrial structure and oxidative capacity in cancer cells. *Cancer Res*. *64*:985–993.

Rubio-Cosials, A., Sidow, J. F., Jiménez-Menéndez, N., Fernández-Millán, P., Montoya, J., Jacobs, H. T., Coll, M., Bernadó, P., & Solà, M. (2011). Human mitochondrial transcription factor A induces a U-turn structure in the light strand promoter. *Nature Structural and Molecular Biology*, *18*(11), 1281–1289.

Ruprecht, J. J., & Kunji, E. R. S. (2020). The SLC25 Mitochondrial Carrier Family: Structure and Mechanism. *Trends in Biochemical Sciences*, *45*(3), 244-258.

Russell, A. P., Feilchenfeldt, J., Schreiber, S., Praz, M., Crettenand, A., Gobelet, C., Meier, C. A., Bell, D. R., Kralli, A., Giacobino, J. P., & Dériaz, O. (2003). Endurance Training in Humans Leads to Fiber Type-Specific Increases in Levels of Peroxisome Proliferator-Activated Receptor-γ Coactivator-1 and Peroxisome Proliferator-Activated Receptor-α in Skeletal Muscle. *Diabetes*, *52*(12), 2874–2881.

Russell, A. P., Hesselink, M. K. C., Lo, S. K., & Schrauwen, P. (2005). Regulation of metabolic transcriptional co-activators and transcription factors with acute exercise. *The FASEB Journal*, *19*(8), 986–988.

Ryall, J. G. (2013). Metabolic reprogramming as a novel regulator of skeletal muscle development and regeneration. *FEBS Journal*, *280*(17), 4004–4013.

Ryall, J. G., Dell'Orso, S., Derfoul, A., Juan, A., Zare, H., Feng, X., Clermont, D., Koulnis, M., Gutierrez-Cruz, G., Fulco, M., & Sartorelli, V. (2015). The NAD+-dependent sirt1 deacetylase translates a metabolic switch into regulatory epigenetics in skeletal muscle stem cells. *Cell Stem Cell*, *16*(2), 171–183.

Ryu, H., Lee, J., Impey, S., Ratan, R. R., & Ferrante, R. J. (2005). Antioxidants modulate mitochondrial PKA and increase CREB binding to D-loop DNA of the mitochondrial genome in neurons. *Proc Natl Acad Sci U S A*, *102*(39), 13915-2.

Ryzhkova, A. I., Sazonova, M. A., Sinyov, V. V., Galitsyna, E. V., Chicheva, M. M., Melnichenko, A. A., Grechko, A. V., Postnov, A. Y., Orekhov, A. N., & Shkurat, T. P. (2018). Mitochondrial diseases caused by mtDNA mutations: A mini-review. *Therapeutics and Clinical Risk Management*, *14*, 1933–1942.

Sadasivam, S., Duan, S., & DeCaprio, J. A. (2012). The MuvB complex sequentially recruits B-

Myb and FoxM1 to promote mitotic gene expression. *Genes and Development*, *26*(5), 474–489.

Safdar, A., Little, J. P., Stokl, A. J., Hettinga, B. P., Akhtar, M., & Tarnopolsky, M. A. (2011). Exercise increases mitochondrial PGC-1α content and promotes nuclear-mitochondrial cross-talk to coordinate mitochondrial biogenesis. *Journal of Biological Chemistry*, *286*(12), 10605-17.

Saleem, A., & Hood, D. A. (2013). Acute exercise induces tumour suppressor protein p53 translocation to the mitochondria and promotes a p53-Tfam-mitochondrial DNA complex in skeletal muscle. *Journal of Physiology*, *591*(14), 3625–3636.

Sanchis-Gomar, F., Garcia-Gimenez, J., Gomez-Cabrera, M., & Pallardo, F. (2014). Mitochondrial Biogenesis in Health and Disease. Molecular and Therapeutic Approaches. *Current Pharmaceutical Design*, *20*(35), 5619–5633.

Sandiford, S. De, Kennedy, K. A., Xie, X., Pickering, J. G., & Li, S. S. (2014). Dual Oxidase Maturation factor 1 (DUOXA1) overexpression increases reactive oxygen species production and inhibits murine muscle satellite cell differentiation. *Cell Communication and Signaling*, *12*(1), 5.

Schade, A. E., Fischer, M., & DeCaprio, J. A. (2019b). RB, p130 and p107 differentially repress G1/S and G2/M genes after p53 activation. *Nucleic acids research*, 47(21), 11197–11208.

Schade, A. E., Oser, M. G., Nicholson, H. E., & DeCaprio, J. A. (2019a). Cyclin D–CDK4 relieves cooperative repression of proliferation and cell cycle gene expression by DREAM and RB. *Oncogene*, *38*(25), 4962-4976.

Schauss, A. C., Huang, H., Choi, S. Y., Xu, L., Soubeyrand, S., Bilodeau, P., Zunino, R., Rippstein, P., Frohman, M. A., & McBride, H. M. (2010). A novel cell-free mitochondrial fusion assay amenable for high-throughput screenings of fusion modulators. *BMC Biology*, *26*(8), 100.

Schenk, S., & Horowitz, J. F. (2007). Acute exercise increases triglyceride synthesis in skeletal muscle and prevents fatty acid-induced insulin resistance. *Journal of Clinical Investigation*, *117*(6), 1690–1698.

Schiaffino, S., & Reggiani, C. (2011). Fiber types in Mammalian skeletal muscles. *Physiological Reviews*, *91*(4), 1447–1531.

Schieber, M., & Chandel, N. S. (2014). ROS function in redox signaling and oxidative stress. In

Current Biology, *24*(10), R453.

Schmit, F., Korenjak, M., Mannefeld, M., Schmitt, K., Franke, C., Von Eyss, B., Gagrica, S., Hänel, F., Brehm, A., & Gaubatz, S. (2007). LINC, a human complex that is related to pRB-containing complexes in invertebrates regulates the expression of G2/M genes. *Cell Cycle*, *6*(15), 1903-13.

Schwarz, J. K., Devoto, S. H., Smith, E. J., Chellappan, S. P., Jakoi, L., & Nevins, J. R. (1993). Interactions of the p107 and Rb proteins with E2F during the cell proliferation response. *EMBO Journal*, *12*(3), 1013-20.

Schwarze, F., Meraner, J., Lechner, M., Loidl, A., Stasyk, T., Laich, A., & Loidl, P. (2010). Cell cycle-dependent acetylation of Rb2/p130 in NIH3T3 cells. *Oncogene*, *29*(42), 5755–5760.

Scialò, F., Sriram, A., Fernández-Ayala, D., Gubina, N., Lõhmus, M., Nelson, G., Logan, A., Cooper, H. M., Navas, P., Enríquez, J. A., Murphy, M. P., & Sanz, A. (2016). Mitochondrial ROS Produced via Reverse Electron Transport Extend Animal Lifespan. *Cell Metabolism*, *23*(4), 725–734.

Scimè, A., Grenier, G., Huh, M. S., Gillespie, M. A., Bevilacqua, L., Harper, M. E., & Rudnicki, M. A. (2005). Rb and p107 regulate preadipocyte differentiation into white versus brown fat through repression of PGC-1α. *Cell Metabolism*, *2*(5), 283–295.

Scimè, A., Soleimani, V. D., Bentzinger, C. F., Gillespie, M. A., Le Grand, F., Grenier, G., Bevilacqua, L., Harper, M. E., & Rudnicki, M. A. (2010). Oxidative status of muscle is determined by p107 regulation of PGC-1α. *Journal of Cell Biology*, *190*(4), 651–662.

Sena, L. A., & Chandel, N. S. (2012). Physiological roles of mitochondrial reactive oxygen species. *Molecular Cell*, *48*(2), 158–167.

Sestili, P., Barbieri, E., Martinelli, C., Battistelli, M., Guescini, M., Vallorani, L., Casadei, L., D'Emilio, A., Falcieri, E., Piccoli, G., Agostini, D., Annibalini, G., Paolillo, M., Gioacchini, A. M., & Stocchi, V. (2009). Creatine supplementation prevents the inhibition of myogenic differentiation in oxidatively injured C2C12 murine myoblasts. *Molecular Nutrition and Food Research*, *53*(9), 1187–1204.

Seth, A., Steel, J. H., Nichol, D., Pocock, V., Kumaran, M. K., Fritah, A., Mobberley, M., Ryder, T. A., Rowlerson, A., Scott, J., Poutanen, M., White, R., & Parker, M. (2007). The Transcriptional Corepressor RIP140 Regulates Oxidative Metabolism in Skeletal Muscle. *Cell Metabolism*, *6*(3), 236–245.

Seyer, P., Grandemange, S., Busson, M., Carazo, A., Gamaléri, F., Pessemesse, L., Casas, F., Cabello, G., & Wrutniak-Cabello, C. (2006). Mitochondrial activity regulates myoblast differentiation by control of c-Myc expression. *Journal of Cellular Physiology*, *207*(1), 75–86.

Seyer, P., Grandemange, S., Rochard, P., Busson, M., Pessemesse, L., Casas, F., Cabello, G., & Wrutniak-Cabello, C. (2011). P43-dependent mitochondrial activity regulates myoblast differentiation and slow myosin isoform expression by control of Calcineurin expression. *Experimental Cell Research*, *317*(14), 2059–2071.

Shea, K. L., Xiang, W., LaPorta, V. S., Licht, J. D., Keller, C., Basson, M. A., & Brack, A. S. (2010). Sprouty1 Regulates Reversible Quiescence of a Self-Renewing Adult Muscle Stem Cell Pool during Regeneration. *Cell Stem Cell*, *6*(2), 117-29.

Shefer, G., Rauner, G., Yablonka-Reuveni, Z., & Benayahu, D. (2010). Reduced satellite cell numbers and myogenic capacity in aging can be alleviated by endurance exercise. *PLoS ONE*, *5*(10).

Sherr, C. J., & Roberts, J. M. (1999). CDK inhibitors: Positive and negative regulators of G1-phase progression. *Genes and Development*, *13*(12), 1501–1512.

Shi, Y., Dierckx, A., Wanrooij, P. H., Wanrooij, S., Larsson, N. G., Wilhelmsson, L. M., Falkenberg, M., & Gustafsson, C. M. (2012). Mammalian transcription factor A is a core component of the mitochondrial transcription machinery. *Proceedings of the National Academy of Sciences of the United States of America*, *109*(41), 16510–16515.

Shintaku, J., Peterson, J. M., Talbert, E. E., Gu, J. M., Ladner, K. J., Williams, D. R., Mousavi, K., Wang, R., Sartorelli, V., & Guttridge, D. C. (2016). MyoD Regulates Skeletal Muscle Oxidative Metabolism Cooperatively with Alternative NF-κB. *Cell Reports*, *17*(2), 514–526.

Shiratori, R., Furuichi, K., Yamaguchi, M., Miyazaki, N., Aoki, H., Chibana, H., Ito, K., & Aoki, S. (2019). Glycolytic suppression dramatically changes the intracellular metabolic profile of multiple cancer cell lines in a mitochondrial metabolism-dependent manner. *Scientific reports*, *9*(1), 18699.

Shirodkar, S., Ewen, M., DeCaprio, J. A., Morgan, J., Livingston, D. M., & Chittenden, T. (1992). The transcription factor E2F interacts with the retinoblastoma product and a p107-cyclin A complex in a cell cycle-regulated manner. *Cell*, *68*(1), 157-66.

Shokolenko, I. N., & Alexeyev, M. F. (2017). Mitochondrial transcription in mammalian cells. In *Frontiers in Bioscience – Landmark*, *1*(22), 835-853.

Short, K. R., Bigelow, M. L., Kahl, J., Singh, R., Coenen-Schimke, J., Raghavakaimal, S., & Nair, K. S. (2005). Decline in skeletal muscle mitochondrial function with aging in humans. *Proceedings of the National Academy of Sciences of the United States of America*, *102*(15), 5618–5623.

Short, K. R., Vittone, J. L., Bigelow, M. L., Proctor, D. N., Rizza, R. A., Coenen-Schimke, J. M., & Nair, K. S. (2003). Impact of aerobic exercise training on age-related changes in insulin sensitivity and muscle oxidative capacity. *Diabetes*, *52*(8), 1888–1896.

Shutt, T. E., Lodeiro, M. F., Cotney, J., Cameron, C. E., & Shadel, G. S. (2010). Core human mitochondrial transcription apparatus is a regulated two-component system in vitro. *Proceedings of the National Academy of Sciences of the United States of America*, *107*(27), 12133–12138.

Shyh-Chang, N., & Ng, H. H. (2017). The metabolic programming of stem cells. *Genes and Development*, *31*(4), 336-346.

Shyh-Chang, N., Daley, G. Q., & Cantley, L. C. (2013). Stem cell metabolism in tissue development and aging. *Development (Cambridge)*, *140*(12), 2535-47.

Simsek, T., Kocabas, F., Zheng, J., Deberardinis, R. J., Mahmoud, A. I., Olson, E. N., Schneider, J. W., Zhang, C. C., & Sadek, H. A. (2010). The distinct metabolic profile of hematopoietic stem cells reflects their location in a hypoxic niche. *Cell Stem Cell*, *7*(3), 380–390.

Sin, J., Andres, A. M., Taylo R, D. J. R., Weston, T., Hiraumi, Y., Stotland, A., Kim, B. J., Huang, C., Doran, K. S., & Gottlieb, R. A. (2016). Mitophagy is required for mitochondrial biogenesis and myogenic differentiation of C2C12 myoblasts. *Autophagy*, *12*(2), 369–380.

Snezhkina, A. V., Kudryavtseva, A. V., Kardymon, O. L., Savvateeva, M. V., Melnikova, N. V., Krasnov, G. S., & Dmitriev, A. A. (2020). ROS generation and antioxidant defense systems in normal and malignant cells. *Oxidative Medicine and Cellular Longevity*, 2019, 6175804.

Snijders, T., Verdijk, L. B., Smeets, J. S. J., McKay, B. R., Senden, J. M. G., Hartgens, F., Parise, G., Greenhaff, P., & van Loon, L. J. C. (2014). The skeletal muscle satellite cell response to a single bout of resistance-type exercise is delayed with aging in men. *Age*, *36*(4).

Song, S., & Hwang, E. (2018). A Rise in ATP, ROS, and Mitochondrial Content upon Glucose

Withdrawal Correlates with a Dysregulated Mitochondria Turnover Mediated by the Activation of the Protein Deacetylase SIRT1. *Cells*, *8*(1), 11.

Soufi, A., & Dalton, S. (2016). Cycling through developmental decisions: How cell cycle dynamics control pluripotency, differentiation and reprogramming. *Development (Cambridge)*, *143*(23), 4301–4311.

Sperber, H., Mathieu, J., Wang, Y., Ferreccio, A., Hesson, J., Xu, Z., Fischer, K. A., Devi, A., Detraux, D., Gu, H., Battle, S. L., Showalter, M., Valensisi, C., Bielas, J. H., Ericson, N. G., Margaretha, L., Robitaille, A. M., Margineantu, D., Fiehn, O., … Ruohola-Baker, H. (2015). The metabolome regulates the epigenetic landscape during naive-to-primed human embryonic stem cell transition. *Nature Cell Biology*, *17*(12), 1523–1535.

Stiegler, P., De Luca, A., Bagella, L., & Giordano, A. (1998). The COOH-terminal Region of pRb2/p130 Binds to Histone Deacetylase 1 (HDAC1), Enhancing Transcriptional Repression of the E2F-dependent Cyclin A Promoter. *Cancer Research*, *58*(22).

Suetta, C., Frandsen, U., Mackey, A. L., Jensen, L., Hvid, L. G., Bayer, M. L., Petersson, S. J., Schrøder, H. D., Andersen, J. L., Aagaard, P., Schjerling, P., & Kjaer, M. (2013). Ageing is associated with diminished muscle re-growth and myogenic precursor cell expansion early after immobility-induced atrophy in human skeletal muscle. *Journal of Physiology*, *591*(15), 3789–3804.

Sun, F., Dai, C., Xie, J., & Hu, X. (2012). Biochemical issues in estimation of cytosolic free NAD/NADH ratio. *PloS one*, *7*(5), e34525.

Taguchi, N., Ishihara, N., Jofuku, A., Oka, T., & Mihara, K. (2007). Mitotic phosphorylation of dynamin-related GTPase Drp1 participates in mitochondrial fission. *Journal of Biological Chemistry*, *282*(15), 11521-9.

Takubo, K., Nagamatsu, G., Kobayashi, C. I., Nakamura-Ishizu, A., Kobayashi, H., Ikeda, E., Goda, N., Rahimi, Y., Johnson, R. S., Soga, T., Hirao, A., Suematsu, M., & Suda, T. (2013). Regulation of glycolysis by Pdk functions as a metabolic checkpoint for cell cycle quiescence in hematopoietic stem cells. *Cell Stem Cell*, *12*(1), 49–61.

Talanian, J. L., Galloway, S. D. R., Heigenhauser, G. J. F., Bonen, A., & Spriet, L. L. (2007). Two weeks of high-intensity aerobic interval training increases the capacity for fat oxidation during exercise in women. *Journal of Applied Physiology*, *102*(4), 1439–1447.

Tang, A. H., & Rando, T. A. (2014). Induction of autophagy supports the bioenergetic demands

of quiescent muscle stem cell activation. *The EMBO Journal*, *33*(23), 2782–2797.

Tang, B. L. (2016). Sirt1 and the mitochondria. *Molecules and Cells*, *39*(2), 87-95.

Tatsumi, R., Liu, X., Pulido, A., Morales, M., Sakata, T., Dial, S., Hattori, A., Ikeuchi, Y., & Allen, R. E. (2006). Satellite cell activation in stretched skeletal muscle and the role of nitric oxide and hepatocyte growth factor. *American Journal of Physiology - Cell Physiology*, *290*(6).

Taubert, S., Gorrini, C., Frank, S. R., Parisi, T., Fuchs, M., Chan, H.-M., Livingston, D. M., & Amati, B. (2004). E2F-Dependent Histone Acetylation and Recruitment of the Tip60 Acetyltransferase Complex to Chromatin in Late G1. *Molecular and Cellular Biology*, *24*(10), 4546–4556.

Taylor, C. T., & Moncada, S. (2010). Nitric oxide, cytochrome c oxidase, and the cellular response to hypoxia. *Arteriosclerosis, Thrombosis, and Vascular Biology*, *30*(4), 643–647.

Taylor, R. W., & Turnbull, D. M. (2007). Mitochondrial DNA Transcription: Regulating the Power Supply. *Cell*, *130*(2), 211-3.

Tezze, C., Romanello, V., Desbats, M. A., Fadini, G. P., Albiero, M., Favaro, G., Ciciliot, S., Soriano, M. E., Morbidoni, V., Cerqua, C., Loefler, S., Kern, H., Franceschi, C., Salvioli, S., Conte, M., Blaauw, B., Zampieri, S., Salviati, L., Scorrano, L., & Sandri, M. (2017). Age-Associated Loss of OPA1 in Muscle Impacts Muscle Mass, Metabolic Homeostasis, Systemic Inflammation, and Epithelial Senescence. *Cell Metabolism*, *25*(6), 1374-1389.e6.

Toth, K. G., McKay, B. R., de Lisio, M., Little, J. P., Tarnopolsky, M. A., & Parise, G. (2011). IL-6 induced STAT3 signalling is associated with the proliferation of human muscle satellite cells following acute muscle damage. *PLoS ONE*, *6*(3).

Tothova, Z., Kollipara, R., Huntly, B. J., Lee, B. H., Castrillon, D. H., Cullen, D. E., McDowell, E. P., Lazo-Kallanian, S., Williams, I. R., Sears, C., Armstrong, S. A., Passegué, E., DePinho, R. A., & Gilliland, D. G. (2007). FoxOs Are Critical Mediators of Hematopoietic Stem Cell Resistance to Physiologic Oxidative Stress. *Cell*, *128*(2), 325–339.

Touvier, T., De Palma, C., Rigamonti, E., Scagliola, A., Incerti, E., Mazelin, L., Thomas, J. L., D'Antonio, M., Politi, L., Schaeffer, L., Clementi, E., & Brunelli, S. (2015). Muscle-specific Drp1 overexpression impairs skeletal muscle growth via translational attenuation. *Cell Death and Disease*, *6*(2), 1–11.

Treberg, J. R., Quinlan, C. L., & Brand, M. D. (2011). Evidence for two sites of superoxide

production by mitochondrial NADH-ubiquinone oxidoreductase (complex I). *Journal of Biological Chemistry*, *286*(31), 27103-10.

Trouche, D., Le Chalony, C., Muchardt, C., Yaniv, M., & Kouzarides, T. (1997). RB and hbrm cooperate to repress the activation functions of E2F1. *Proceedings of the National Academy of Sciences of the United States of America*, *94*(21), 11268–11273.

Tudzarova, S., Colombo, S. L., Stoeber, K., Carcamo, S., Williams, G. H., & Moncada, S. (2011). Two ubiquitin ligases, APC/C-Cdh1 and SKP1-CUL1-F (SCF)-β-TrCP, sequentially regulate glycolysis during the cell cycle. *Proceedings of the National Academy of Sciences of the United States of America*, *108*(13), 5278–5283.

Uxa, S., Bernhart, S. H., Mages, C. F. S., Fischer, M., Kohler, R., Hoffmann, S., Stadler, P. F., Engeland, K., & Müller, G. A. (2019). DREAM and RB cooperate to induce gene repression and cell-cycle arrest in response to p53 activation. *Nucleic Acids Research*, *47*(17), 9087-9103.

Valvona, C. J., Fillmore, H. L., Nunn, P. B., & Pilkington, G. J. (2016). The Regulation and Function of Lactate Dehydrogenase A: Therapeutic Potential in Brain Tumor. *Brain Pathology*, *26*(1), 3-17.

Van Den Heuvel, S., & Dyson, N. J. (2008). Conserved functions of the pRB and E2F families. *Nature Reviews Molecular Cell Biology*, *9*(9), 713–724.

Vander Heiden, M. G., & Deberardinis, R. J. (2017). Understanding the intersections between metabolism and cancer biology. *Cell*, *168*(4), 657–669.

Vaziri, H., Dessain, S. K., Eaton, E. N., Imai, S. I., Frye, R. A., Pandita, T. K., Guarente, L., & Weinberg, R. A. (2001). hSIR2SIRT1 functions as an NAD-dependent p53 deacetylase. *Cell*, *107*(2), 149-59.

Vazquez, A., Liu, J., Zhou, Y., & Oltvai, Z. N. (2010). Catabolic efficiency of aerobic glycolysis : The Warburg effect revisited. *BMC Syst Biol*, *6*(4), 58.

Verdijk, L. B., Gleeson, B. G., Jonkers, R. A. M., Meijer, K., Savelberg, H. H. C. M., Dendale, P., & Van Loon, L. J. C. (2009). Skeletal muscle hypertrophy following resistance training is accompanied by a fiber type-specific increase in satellite cell content in elderly men. *Journals of Gerontology - Series A Biological Sciences and Medical Sciences*, *64*(3), 332–339.

Verona, R., Moberg, K., Estes, S., Starz, M., Vernon, J. P., & Lees, J. A. (1997). E2F activity is

regulated by cell cycle-dependent changes in subcellular localization. *Molecular and Cellular Biology*, *17*(12), 7268-82.

Vila, M. C., Rayavarapu, S., Hogarth, M. W., Van Der Meulen, J. H., Horn, A., Defour, A., Takeda, S., Brown, K. J., Hathout, Y., Nagaraju, K., & Jaiswal, J. K. (2017). Mitochondria mediate cell membrane repair and contribute to Duchenne muscular dystrophy. *Cell Death and Differentiation*, *24*(2), 330–342.

Wade Harper, J., Adami, G. R., Wei, N., Keyomarsi, K., & Elledge, S. J. (1993). The p21 Cdk-interacting protein Cip1 is a potent inhibitor of G1 cyclin-dependent kinases. *Cell*, *75*(4), 805–816.

Walker, D. K., Fry, C. S., Drummond, M. J., Dickinson, J. M., Timmerman, K. L., Gundermann, D. M., Jennings, K., Volpi, E., & Rasmussen, B. B. (2012). PAX7+ satellite cells in young and older adults following resistance exercise. *Muscle and Nerve*, *46*(1), 51-9.

Wang, H., Hertlein, E., Bakkar, N., Sun, H., Acharyya, S., Wang, J., Carathers, M., Davuluri, R., & Guttridge, D. C. (2007). NF-κB Regulation of YY1 Inhibits Skeletal Myogenesis through Transcriptional Silencing of Myofibrillar Genes. *Molecular and Cellular Biology*, *27*(12), 4374–4387.

Wang, Y., Bi, Y., Chen, X., Li, C., Li, Y., Zhang, Z., Wang, J., Lu, Y., Yu, Q., Su, H., Yang, H., & Liu, G. (2016). Histone Deacetylase SIRT1 Negatively Regulates the Differentiation of Interleukin-9-Producing CD4+ T Cells. *Immunity*, *44*(6), 1337-49.

Watt, M. J., Southgate, R. J., Holmes, A. G., & Febbraio, M. A. (2004). Suppression of plasma free fatty acids upregulates peroxisome proliferator-activated receptor (PPAR) α and δ and PPAR coactivator 1α in human skeletal muscle, but not lipid regulatory genes. *Journal of Molecular Endocrinology*, *33*(2), 533–544.

Wen, Y., Bi, P., Liu, W., Asakura, A., Keller, C., & Kuang, S. (2012). Constitutive Notch Activation Upregulates Pax7 and Promotes the Self-Renewal of Skeletal Muscle Satellite Cells. *Molecular and Cellular Biology*, *32*(12), 2300-11.

Wernbom, M., Apro, W., Paulsen, G., Nilsen, T. S., Blomstrand, E., & Raastad, T. (2013). Acute low-load resistance exercise with and without blood flow restriction increased protein signalling and number of satellite cells in human skeletal muscle. *European Journal of Applied Physiology*, *113*(12), 2953–2965.

White, R. B., Biérinx, A. S., Gnocchi, V. F., & Zammit, P. S. (2010). Dynamics of muscle fibre

growth during postnatal mouse development. *BMC Developmental Biology*, *10*(1), 21.

Wiedemann, N., & Pfanner, N. (2017). Mitochondrial machineries for protein import and assembly. *Annual Review of Biochemistry*, *86*, 685-714.

Wirt, S. E., & Sage, J. (2010). p107 in the public eye: An Rb understudy and more. *Cell Division*, *5*, 1–13.

Woo, M. S., Sánchez, I., & Dynlacht, B. D. (1997). P130 and P107 Use a Conserved Domain To Inhibit Cellular Cyclin-Dependent Kinase Activity. *Molecular and Cellular Biology*, *17*(7), 3566–3579.

Wredenberg, A., Lagouge, M., Bratic, A., Metodiev, M. D., Spåhr, H., Mourier, A., Freyer, C., Ruzzenente, B., Tain, L., Grönke, S., Baggio, F., Kukat, C., Kremmer, E., Wibom, R., Polosa, P. L., Habermann, B., Partridge, L., Park, C. B., & Larsson, N. G. (2013). MTERF3 Regulates Mitochondrial Ribosome Biogenesis in Invertebrates and Mammals. *PLoS Genetics*, *9*(1), e1003178.

Wrutniak-Cabello, C., Casas, F., & Cabello, G. (2001). Thyroid hormone action in mitochondria. *Journal of Molecular Endocrinology*, *26*(1), 67-77.

Wu, Z., Puigserver, P., Andersson, U., Zhang, C., Adelmant, G., Mootha, V., Troy, A., Cinti, S., Lowell, B., Scarpulla, R. C., & Spiegelman, B. M. (1999). Mechanisms controlling mitochondrial biogenesis and respiration through the thermogenic coactivator PGC-1. *Cell*, *98*(1), 115–124.

Xiao, W., & Loscalzo, J. (2020). Metabolic Responses to Reductive Stress. *Antioxidants and Redox Signaling*, *32*(18), 1330-1347.

Xiao, W., Wang, R. S., Handy, D. E., & Loscalzo, J. (2018). NAD(H) and NADP(H) Redox Couples and Cellular Energy Metabolism. *Antioxidants and Redox Signaling*, 28(3), 251–272.

Xiao, Z. X., Ginsberg, D., Ewen, M., & Livingston, D. M. (1996). Regulation of the retinoblastoma protein-related protein p107 by G1 cyclin-associated kinases. *Proceedings of the National Academy of Sciences of the United States of America*, *93*(10), 4633–4637.

Yablonka-Reuveni, Z. (2011). The Skeletal Muscle Satellite Cell: Still Young and Fascinating at 50. *Journal of Histochemistry and Cytochemistry*, *59*(12), 1041-59.

Yablonka-Reuveni, Z., & Rivera, A. J. (1994). Temporal expression of regulatory and structural muscle proteins during myogenesis of satellite cells on isolated adult rat fibers.

Developmental Biology, *164*(2), 588–603.

Yakubovskaya, E., Guja, K. E., Eng, E. T., Choi, W. S., Mejia, E., Beglov, D., Lukin, M., Kozakov, D., & Garcia-Diaz, M. (2014). Organization of the human mitochondrial transcription initiation complex. *Nucleic Acids Research*, *42*(6), 4100-12.

Yakubovskaya, E., Mejia, E., Byrnes, J., Hambardjieva, E., & Garcia-Diaz, M. (2010). Helix unwinding and base flipping enable human MTERF1 to terminate mitochondrial transcription. *Cell*, *141*(6), 982-93.

Yalcin, A., Clem, B. F., Simmons, A., Lane, A., Nelson, K., Clem, A. L., Brock, E., Siow, D., Wattenberg, B., Telang, S., & Chesney, J. (2009). Nuclear targeting of 6-phosphofructo-2-kinase (PFKFB3) increases proliferation via cyclin-dependent kinases. *Journal of Biological Chemistry*, *284*(36), 24223-32.

Yan, L. J. (2014). Pathogenesis of chronic hyperglycemia: From reductive stress to oxidative stress. *Journal of Diabetes Research*, 2014, 137919.

Yang, R., & Rincon, M. (2016). Mitochondrial Stat3, the need for design thinking. *International Journal of Biological Sciences*, *12*(5), 532-44.

Yang, W., Xia, Y., Hawke, D., Li, X., Liang, J., Xing, D., Aldape, K., Hunter, T., Alfred Yung, W. K., & Lu, Z. (2012). PKM2 phosphorylates histone H3 and promotes gene transcription and tumorigenesis. *Cell*, *50*(4), 685-96.

Yang, X., Yang, S., Wang, C., & Kuang, S. (2017). The hypoxia-inducible factors HIF1α and HIF2α are dispensable for embryonic muscle development but essential for postnatal muscle regeneration. *Journal of Biological Chemistry*, *292*(14), 5981–5991.

Yano, M., Terada, K., & Mori, M. (2004). Mitochondrial Import Receptors Tom20 and Tom22 Have Chaperone-like Activity. *Journal of Biological Chemistry*, *279*(11), 10808-13.

Ydfors, M., Hughes, M. C., Laham, R., Schlattner, U., Norrbom, J., & Perry, C. G. R. (2016). Modelling in vivo creatine/phosphocreatine in vitro reveals divergent adaptations in human muscle mitochondrial respiratory control by ADP after acute and chronic exercise. *Journal of Physiology*, *594*(11), 3127–3140.

Yin, H., Price, F., & Rudnicki, M. A. (2013). Satellite cells and the muscle stem cell niche. *Physiological Reviews*, *93*(1), 23–67.

Young, A. P., Nagarajan, R., & Longmore, G. D. (2003a). Mechanisms of transcriptional regulation by Rb-E2F segregate by biological pathway. *Oncogene*, *22*(46), 7209–7217.

Young, J. C., Hoogenraad, N. J., & Hartl, F. U. (2003b). Molecular chaperones Hsp90 and Hsp70 deliver preproteins to the mitochondrial import receptor Tom70. In *Cell*. *112*(1), 41-50.

Yu, L., Chen, X., Wang, L., & Chen, S. (2016). The sweet trap in tumors: Aerobic glycolysis and potential targets for therapy. *Oncotarget*, *7*(25), 38908–38926.

Zacksenhaus, E., Shrestha, M., Liu, J. C., Vorobieva, I., Chung, P. E. D., Ju, Y. J., Nir, U., & Jiang, Z. (2017). Mitochondrial OXPHOS Induced by RB1 Deficiency in Breast Cancer: Implications for Anabolic Metabolism, Stemness, and Metastasis. *Trends in Cancer*, *3*(11), 768-779.

Zammit, P. S., Golding, J. P., Nagata, Y., Hudon, V., Partridge, T. A., & Beauchamp, J. R. (2004). Muscle satellite cells adopt divergent fates: A mechanism for self-renewal? *Journal of Cell Biology*, *166*(3), 347–357.

Zammit, P. S., Relaix, F., Nagata, Y., Ruiz, A. P., Collins, C. A., Partridge, T. A., & Beauchamp, J. R. (2006). Pax7 and myogenic progression in skeletal muscle satellite cells. *Journal of Cell Science*, *119*(9), 1824–1832.

Zhang, D. X., Chen, Y. F., Campbell, W. B., Zou, A. P., Gross, G. J., & Li, P. L. (2001). Characteristics and superoxide-induced activation of reconstituted myocardial mitochondrial ATP-sensitive potassium channels. *Circulation Research*, *89*(12), 1177-83.

Zhang, H., Ryu, D., Wu, Y., Gariani, K., Wang, X., Luan, P., D'Amico, D., Ropelle, E. R., Lutolf, M. P., Aebersold, R., Schoonjans, K., Menzies, K. J., & Auwerx, J. (2016). NAD+ repletion improves mitochondrial and stem cell function and enhances life span in mice. *Science*. *352*(6292), 1436-43.

Zhang, S., Hulver, M. W., McMillan, R. P., Cline, M. A., & Gilbert, E. R. (2014). The pivotal role of pyruvate dehydrogenase kinases in metabolic flexibility. *Nutrition and Metabolism*, *11*(1), 10.

Zhou, W., Choi, M., Margineantu, D., Margaretha, L., Hesson, J., Cavanaugh, C., Blau, C. A., Horwitz, M. S., Hockenbery, D., Ware, C., & Ruohola-Baker, H. (2012). HIF1α induced switch from bivalent to exclusively glycolytic metabolism during ESC-to-EpiSC/hESC transition. *EMBO Journal*, *31*(9), 2103–2116.

Zhu, L., Van den Heuvel, S., Helin, K., Fattaey, A., Ewen, M., Livingston, D., Dyson, N., & Harlow, E. (1993). Inhibition of cell proliferation by p107, a relative of the retinoblastoma

protein. *Genes and Development*, *7*(7 A), 1111–1125.

Zhu, Liang, Harlow, E., & Dynlacht, B. D. (1995). p107 uses a p21CIP1-related domain to bind cyclin/cdk2 and regulate interactions with E2F. *Genes and Development*, *9*(14), 1740–1752.

Zierath, J. R., & Hawley, J. A. (2004). Skeletal muscle fiber type: Influence on contractile and metabolic properties. *PLoS Biology*, *2*(10).

Zini, N., Trimarchi, C., Claudio, P. P., Stiegler, P., Marinelli, F., Maltarello, M. C., La Sala, D., De Falco, G., Russo, G., Ammirati, G., Maraldi, N. M., Giordano, A., & Cinti, C. (2001). pRb2/p130 and p107 control cell growth by multiple strategies and in association with different compartments within the nucleus. *Journal of Cellular Physiology*, *189*(1), 34–44.

Zollo, O., Tiranti, V., & Sondheimer, N. (2012). Transcriptional requirements of the distal heavy-strand promoter of mtDNA. *Proceedings of the National Academy of Sciences of the United States of America*, *109*(17), 6508–6512.